

ABSTRACT

WIND LOAD INTERACTION ON AN ADJACENT BUILDING

In recent years, wind loading on buildings has been an area of active investigation by many authors. A review of this literature indicates that little is known about the effect of an adjacent building on the pressure distribution, mean force and moment coefficients and the probability density function of the peak pressures acting on a structure. Especially important is the need for a possible area of research.

WIND LOAD INTERACTION ON AN  
ADJACENT BUILDING

by

T. G. Zambrano\* and J. A. Peterka\*\*

The purpose of this paper is to give a detailed picture of these effects for a structures and relative positions. The results show that shielding and channeling effects can be of significant effect in some wind loading and local pressure distributions. It is shown to predict local peak pressures resulting from wind-turbine interaction using the statistical characteristics of wind.

National Science Foundation  
Grant ENG 76-03135

Fluid Mechanics and Wind Engineering Program  
Fluid Dynamics and Diffusion Laboratory  
Department of Civil Engineering  
Colorado State University  
Fort Collins, Colorado 80523

March 1978

\*Graduate Research Assistant  
\*\*Associate Professor

CER77-78TGZ-JAP26



U18401 0074865

Engineering Sciences

MAY 15 '78

Branch Library

FOLIO  
TA7  
C6  
CFR 77/79 -26

ABSTRACT

WIND LOAD INTERACTION ON AN ADJACENT BUILDING

In recent years, wind loading on buildings has been an area of active investigation by many authors. A review of this literature indicates that little information is available on the effect of an adjacent building on the pressure distribution, mean force and moment coefficients and the probability density function of the peak pressures acting on a structure. Especially evident is the need for defining possible areas of augmented high wind loading. The purpose of this paper is to give a detailed picture of these effects for a set of upwind structures and relative positions. The results show where shielding and channeling effects can be of significant effect in mean-wind loading and local pressure distribution. Also, an attempt is made to predict local peak pressures resulting from building interaction using the statistical characteristics of wind.

## TABLE OF CONTENTS

<u>Chapter</u>		<u>Page</u>
	LIST OF TABLES . . . . .	vi
	LIST OF FIGURES. . . . .	vii
	LIST OF SYMBOLS. . . . .	xi
1	INTRODUCTION . . . . .	1
2	BACKGROUND . . . . .	4
3	SCALING REQUIREMENTS . . . . .	10
	General. . . . .	10
	Neglected Parameters . . . . .	11
	Relevant Parameters. . . . .	12
	Time Scaling . . . . .	13
4	EXPERIMENTAL PROCEDURE . . . . .	16
	General. . . . .	16
	The Wind Tunnel. . . . .	17
	The Models . . . . .	19
	The Principal Building . . . . .	19
	Obstructing Buildings. . . . .	20
	Measurements . . . . .	21
	Data Acquisition . . . . .	21
	Data Reduction . . . . .	23
	Pressure Measurements. . . . .	23
5	RESULTS AND DISCUSSION . . . . .	26
	General. . . . .	26
	Set A: Side 1 . . . . .	26
	Set A: Side 2 . . . . .	30
	Set A: Side 3 . . . . .	33
	Set A: Side 4 . . . . .	34
	Set B: Variation of Height of Obstructing Building . . . . .	35
	Set B: Side 1 . . . . .	35
	Set B: Side 2 . . . . .	36
	Set C: Change in Direction of Approach Wind . . . . .	37
	Summary of Pressure Contour Results. . . . .	39
	Forces and Moments . . . . .	40
	Peak Surface Pressures--Probability Densities. . . . .	42
6	CONCLUSIONS AND RECOMMENDATIONS FOR FURTHER STUDY. . .	48
	Conclusions. . . . .	48
	Recommendations for Further Study. . . . .	49

<u>Chapter</u>	<u>Page</u>
REFERENCES . . . . .	51
TABLES . . . . .	53
FIGURES. . . . .	57

LIST OF TABLES

<u>Table</u>		<u>Page</u>
1	Summary of Properties--Boundary Layer 2 (Akins, 1976). . . . .	54
2	Geometric Scaling--Wind Tunnel to Full-Scale (Akins, 1976). . . . .	55
3	Building Details . . . . .	56

## LIST OF FIGURES

<u>Figure</u>		<u>Page</u>
2.1	Flow Pattern around a Rectangular Block (Woo, 1976). . .	58
2.2	Streamlines in the Flow on the Centerline for a Rectangular Block (Woo, 1976). . . . .	59
3.1	Ratio of Probable Maximum Speed Averaged over Period (t) to that Averaged over One Hour (Vellozzi and Cohen, 1968) . . . . .	60
4.1	Building Configurations. . . . .	61
4.2	Industrial Aerodynamics Wind Tunnel, Fluid Dynamics and Diffusion Laboratory, Colorado State University. .	62
4.3	Spire Geometry . . . . .	63
4.4	Wind Tunnel Arrangement. . . . .	64
4.5	Roughness Configurations . . . . .	65
4.6	Mean Velocity Profile (B. L. "2," Akins, 1976) . . . .	66
4.7	Lateral Variation of Mean Velocity Profile (B. L. "2," Akins, 1976). . . . .	67
4.8a	Local Longitudinal Turbulence Intensity. . . . .	68
4.8b	Local Lateral Turbulence Intensity . . . . .	69
4.8c	Local Vertical Turbulence Intensity. . . . .	70
4.9	Pressure Tap Spacing . . . . .	71
4.10	Principal Building Showing Pressure Valve and Transducers. . . . .	72
4.11	Obstructing Buildings and Principal Building . . . . .	72
4.12	Schematic of Data Acquisition System . . . . .	73
4.13	Forces and Moments . . . . .	74
5.1	Effect of Varying Obstructing Building Placement in the Lateral Direction (Streamlines in the Flow). . . .	75
5.2	Effect of Varying Obstructing Building Placement in the Longitudinal Direction (Streamlines in the Flow). . . . .	76
5.3	Pressure Coefficients for Side 4 . . . . .	77

<u>Figure</u>		<u>Page</u>
5.4	Effect of Varying Obstructing Building Height (Streamlines in the Flow and Smoke Visualization). . .	78
5.5	RMS Pressure Distribution for Small Changes in Approach Wind Configurations . . . . .	79
5.6a	Mean Pressure Coefficients, Set A, Side 1. . . . .	80
5.6b	Mean Pressure Effects, Set A, Side 1 . . . . .	82
5.6c	RMS Pressure Coefficients, Set A, Side 1 . . . . .	84
5.6d	RMS Pressure Effects, Set A, Side 1. . . . .	86
5.6e	Peak Pressure Coefficients, Set A, Side 1. . . . .	88
5.6f	Peak Pressure Effects, Set A, Side 1 . . . . .	90
5.7a	Mean Pressure Coefficients, Set A, Side 2. . . . .	92
5.7b	Mean Pressure Effects, Set A, Side 2 . . . . .	94
5.7c	RMS Pressure Coefficients, Set A, Side 2 . . . . .	96
5.7d	RMS Pressure Effects, Set A, Side 2. . . . .	98
5.7e	Peak Pressure Coefficients, Set A, Side 2. . . . .	100
5.7f	Peak Pressure Effects, Set A, Side 2 . . . . .	102
5.8a	Mean Pressure Coefficients, Set A, Side 3. . . . .	104
5.8b	Mean Pressure Effects, Set A, Side 3 . . . . .	106
5.8c	RMS Pressure Coefficients, Set A, Side 3 . . . . .	108
5.8d	RMS Pressure Effects, Set A, Side 3. . . . .	110
5.8e	Peak Pressure Coefficients, Set A, Side 3. . . . .	112
5.8f	Peak Pressure Effects, Set A, Side 3 . . . . .	114
5.9a	Mean Pressure Coefficients, Set B, Side 1. . . . .	116
5.9b	Mean Pressure Effects, Set B, Side 1 . . . . .	118
5.9c	RMS Pressure Coefficients, Set B, Side 1 . . . . .	120
5.9d	RMS Pressure Effects, Set B, Side 1. . . . .	122
5.9e	Peak Pressure Coefficients, Set B, Side 1. . . . .	124
5.9f	Peak Pressure Effects, Set B, Side 1 . . . . .	126

<u>Figure</u>		<u>Page</u>
5.10a	Mean Pressure Coefficients, Set B, Side 2 . . . . .	128
5.10b	Mean Pressure Effects, Set B, Side 2 . . . . .	130
5.10c	RMS Pressure Coefficients, Set B, Side 2 . . . . .	132
5.10d	RMS Pressure Effects, Set B, Side 2. . . . .	134
5.10e	Peak Pressure Coefficients, Set B, Side 2. . . . .	136
5.10f	Peak Pressure Effects, Set B, Side 2 . . . . .	138
5.11a	Mean Pressure Coefficients, Set C. . . . .	140
5.11b	Mean Pressure Effects, Set C . . . . .	142
5.11c	RMS Pressure Coefficients, Set C . . . . .	144
5.11d	RMS Pressure Effects, Set C. . . . .	146
5.11e	Peak Pressure Coefficients, Set C. . . . .	148
5.11f	Peak Pressure Effects, Set C . . . . .	150
5.12a	$C_{\text{DRAG-FORCE}}$ : Set A. . . . .	152
5.12b	$C_{\text{DRAG-MOMENT}}$ : Set A . . . . .	153
5.12c	$C_{\text{LIFT-FORCE}}$ : Set A. . . . .	154
5.12d	$C_{\text{LIFT-MOMENT}}$ : Set A . . . . .	155
5.12e	$C_{\text{MOMENT-TWIST}}$ : Set A. . . . .	156
5.13a	$C_{\text{DRAG-FORCE}}$ : Set C. . . . .	157
5.13b	$C_{\text{DRAG-MOMENT}}$ : Set C . . . . .	158
5.13c	$C_{\text{LIFT-FORCE}}$ : Set C. . . . .	159
5.13d	$C_{\text{LIFT-MOMENT}}$ : Set C . . . . .	160
5.14a	$C_{\text{DRAG-FORCE}}$ : Set B. . . . .	161
5.14b	$C_{\text{DRAG-MOMENT}}$ : Set B . . . . .	162
5.15	Probability Distribution of Peak Positive Pressure, Tap 244. . . . .	163
5.16	Probability Distribution of Peak Negative Pressure, Tap 141--350 Points. . . . .	164

<u>Figure</u>		<u>Page</u>
5.17	Probability Distribution of Peak Negative Pressure, Tap 144. . . . .	165
5.18	One Second Continuous Pressure Samples, Taps 141, 144, 244 . . . . .	166
5.19	$(\eta/\eta_{\infty})$ versus Distance between Buildings . . . . .	167

## LIST OF SYMBOLS

### General

$C_D$	drag coefficient
$C_{Dm}$	drag-moment coefficient
$C_L$	lift coefficient
$C_{Lm}$	lift-moment coefficient
$C_{P_{max}}$	peak maximum pressure coefficient
$C_{P_{mean}}$	mean pressure coefficient
$C_{P_{min}}$	peak minimum coefficient
$C_{P_{rms}}$	root-mean-square pressure coefficient
$C_T$	coefficient of twisting moment
$d$	size of cubic roughness elements
$f$	general function used in data analysis
$H$	building height
$n$	frequency
$P_d$	dynamic pressure
$P$	pressure
$q$	reference pressure
$T$	time or return period
$U$	longitudinal velocity
$u, v, z$	coordinates, Fig. 4.4
$X$	crosswind distance between buildings
$Y$	alongwind distance between buildings
$\alpha$	power-law exponent
$\delta$	boundary layer thickness
$\theta$	wind direction
$\eta$	pressure gust factor (reduced variate)

### General

$\Lambda$	integral thickness
$v$	average effective fluctuation rate
$\rho$	density of air

### Symbols for Eq. (3.1-3)

$C_{po}$	specific heat at constant pressure	(-)
$g$	gravitational constant	(L/T <sup>2</sup> )
$L$	length scale	(L)
$P$	pressure	(F/L <sup>2</sup> )
$t$	time	(T)
$T$	temperature	( $\theta$ )
$\nu$	kinematic viscosity	(L <sup>2</sup> /T)
$\rho$	density*	(m/L <sup>3</sup> )
$\delta$	Kronecker delta	(-)
$\epsilon_{ijk}$	tensor permutation symbol	(-)
$\Omega$	angular velocity	(T <sup>-1</sup> )
$\phi$	dissipation of heat due to viscosity	(-)
$\theta'$	potential temperature	(°K)

## Chapter 1

### INTRODUCTION

A tall building by its very nature is an obstacle to the wind. The pattern of airflow around a building depends on the characteristics of the approaching wind, on the immediate surroundings and on the size and shape of the building itself.

There is a general outline for estimating wind loads and patterns on buildings. One initially assumes a certain design life for the building, and determines the mean hourly wind speed, gust factor and roughness category for the site based on local meteorological data and the American National Standard Institute building code requirements. A first estimate of forces and moments on various areas of the building is then obtained using basic shape factors with this building information. When possible high wind loading situations are likely, wind tunnel tests are usually justified to quantify the wind loading. A rigid model is made and placed in the modeled area, with a suitable modeled approach wind. Local measurements of fluctuating pressure are made at numerous points on the building for many wind directions. From this data and from a knowledge of the statistics of the atmospheric wind magnitude and direction at the structure site, the wind loads to be expected at various locations on the building during the design life of the structure may be determined.

When a nearby structure is included in the consideration of loading effects, wind analysis becomes more complex. A dramatic instance of adverse wind loading induced by adjacent structures occurred at Ferry bridge in England in 1965 with the collapse of three cooling towers in an array of eight. The cause was determined to be increased loading on

the towers due to adjacent towers (see Sachs, 1972). Adverse wind effects due to adjacent structures were encountered during pre-erection wind-tunnel studies on the five-building Renaissance Center Complex in Detroit, Michigan (see Peterka and Cermak, 1976). The general interference problem resulted from the center tower being exposed to accelerated flow from the upwind buildings. Slight changes in the approach wind direction caused large variations in mean loading on the center structure in addition to the local loading effects.

Guidance from wind-tunnel tests can provide the designer with quantitative indications of situations in which a nearby building may cause increased or decreased loading.

In recent years, wind loading on buildings has been an area of active investigation by many authors. A review of this literature indicates that little information is available on the effect of an adjacent building on the pressure distribution, mean force and moment coefficients and the probability density function of the peak pressures. A few studies have been performed to determine the structure of mean winds about groups of buildings but these are of minor use in assessing wind loads. Especially evident is the need for defining possible areas of augmented high wind loading.

The objective of this research is to present a general set of guidelines for adverse and beneficial wind loadings resulting from building interaction.

Two buildings are used. The first, named the principal building, is instrumented and set at a fixed position. On this all measurements are made. The second building is set at an upstream position to create a flow interference on the principal building. Wind tunnel measurements

are made to establish the effect of the obstructing building in various positions in relation to the principal building. Height, distance between buildings, angle of approach wind, and aspect ratio (H/W) are variables which are investigated.

Reported are local pressure coefficients, and the force and moment coefficients. All coefficients are based upon the velocity profile in the approach flow. Peak pressures described by two probability density functions are used to rationally predict peak pressures.

No attempt was made to define potential interaction leading to dynamic problems such as galloping or buffeting.

## Chapter 2

### BACKGROUND

Two methods can be used to investigate wind load interaction on adjacent buildings. The first way is to examine the flow about an upwind building, especially in the separated and wake regions; and predict how the perturbed flow will respond upon collision with the downwind building. For this type of analysis a detailed picture of flow characteristics about the upwind building is needed. Many investigators have done just this. In 1976, Akins organized pressure measurements for a range of isolated buildings subjected to several planetary boundary layers. Hunt (1969) and Woo, Peterka, and Cermak (1976) investigated the wakes to be found behind a large building in atmosphere wind, and Wise (1971) looked at the regions around a tall building where accelerated flow is likely near the ground. A summary of these investigations shall follow in this chapter.

The second method of investigating wind load interaction on adjacent buildings is by examination of the pressure distribution on the downwind building. Surprisingly, there has been very little written on this subject. Kelnhofner (1971) looked only at the influence of a neighboring building on the flat roof wind loading of a parallel building. His results lose some practicality because the experiments were conducted in uniform flow. It is well accepted now that if an accurate assessment of the wind force is to be obtained, the model must be submerged in a turbulent shear flow that simulates the natural wind. Ishizaki and Sung (1971) investigated the wind speed in the gap between two buildings. They found for certain building orientations, the wind speed may be increased by a factor of 1.4. The critical separation

distance was dependent on building widths and lengths as well as separation distance. There have been numerous studies concerning wind effects on a particular building and building complexes. In examining the wind loading on the Renaissance Center in Detroit, Michigan, Peterka and Cermak (1974) sited adverse and beneficial effects of the neighboring structures on the principal building. Similar observations were made by the same authors in wind studies of the Denver Square Office Complex in Denver, Colorado (1976), and One Houston Center in Houston, Texas (1976). As new buildings are designed with acute angles and lighter materials, Peterka and Cermak concluded that certain isolated wind azimuths peculiar to that urban environment result in hazardous effects on the cladding. Also total wind loading on a building may be either adversely or beneficially affected due to surrounding buildings. The importance of adjacent structures on wind loading and the need for a general study of wind load interaction on adjacent buildings is seen from these reports. The following chapters shall present a quantitative study of the pressure distribution on the downwind building.

Although this report was not designed to study flow characteristics around an isolated building, it is important to present a summary of this phenomena as a preface to investigating wind load interaction between two buildings.

The mean and fluctuating pressures on flat-roofed buildings immersed in a thick boundary layer were reported by Akins (1976). Relevant geometric and atmospheric variables which affect the surface pressure on the buildings were singled out so that regions of severe local pressure could be identified. Mean pressure measurements for different aspect ratios ( $H/W$ ) and different approach flow conditions were condensed to

one set of mean pressure coefficients based upon a local velocity for each side ratio ( $D/W$ ) of the building. This, added to the large selection of building shapes investigated, enabled Akins to predict mean and fluctuating pressure coefficients for a wide range of rectangular shaped buildings. Results showed that a small change in the flow incident upon a building changes the pressure distribution on the building quite significantly. Also, the local pressure coefficients for corresponding locations and wind directions were found to be primarily dependent on the side ratio of the building as a result of differing separation-reattachment characteristics.

Hunt (1969) developed a theory which related the overturning moment on the body to the moment of momentum deficit in the wake. From this the mean velocity in the wake behind the two-dimensional and three-dimensional surface mounted obstacles in a turbulent boundary layer is predicted. Several assumptions were made by Hunt in developing this "momentum wake theory." A basic assumption is that obstacles cause only a small perturbation in the boundary layer and that the height of the obstacle is much less than the thickness of the boundary layer. The zone of separated flow behind the body does not meet this criterion and therefore, the flow in this region cannot be predicted by the theory.

In addition, Hunt related the perturbation shear stress to the local mean velocity gradient by an eddy viscosity, which is constant over most of the wake. Admitting this hypothesis may be an oversimplification, Hunt notes that the usefulness of this assumption is that the equations of motion can then be solved for a first order solution. The comparison between his measured and theoretical mean velocity profiles for flow behind a two-dimensional block is good. In the case

for the three-dimensional wake, the mean velocity results exhibit fair agreement with the observations for the limited data published. The most important limitation to the theory is that it is only valid at a distance of several building heights downwind, which may rule out its usefulness in studying wind interaction between buildings. Hunt concludes that characteristics of a turbulent boundary layer subjected to two-dimensional or three-dimensional obstacles is highly complicated and with the present knowledge about turbulent flow, theoretical developments must rely to a great extent upon experimental observations and measurements.

Woo, Peterka and Cermak (1976) and Hansen and Cermak (1975) showed experimentally that wakes generated by buildings are generally characterized by increased turbulence, mean velocity defect and in certain situations by organized strong vortices with axes parallel to the main flow direction (Fig. 2.1, 2.2). Woo showed that the fluctuating turbulent velocity in the wake of the rectangular block is greatest at a height just above the block. In this region turbulence is convected downstream and diffused in a downward direction. The similar observation was made by Hunt.

It is evident that before building wake characteristics can be predicted with a high degree of confidence, further detailed measurements in the wakes of a wider range of building shapes is needed. From the existing velocity and turbulence measurements we can at best qualitatively estimate the change in mean and fluctuating winds acting on a building placed in the wake of another one. There is the added, and severe, problem of predicting pressure distributions even if the approach flow is defined.

Wise (1971) investigated case studies of air movement around tall buildings. He reports the wind speeds of ground level corner streams and through-flow regions of selected buildings. The results of his study show that a person walking from a sheltered region among low buildings might experience up to a four-fold increase in wind speed on entering an arcade beneath a tall building. Since the force of the wind increases with the square of its speed, this implies a sixteen-fold increase in the force on a person, and illustrates the unpleasantness and possible danger of such a situation. The effect of the dimensions and spacing of two buildings on the wind speed in corner streams were also reported. Wise indicated that the height and width of the tall building are seen to be the most important factors. From flow visualization he observed the distance between the high and low buildings has minor effect, and the height of the low building is unimportant until it is at least one-third of the height of the tall building. The maximum speed in the corner stream is little influenced by the wind angle, although the positions of the corner-streams obviously will change with wind angle. Little attempt was made to relate his velocity measurements to overall effects on adjacent buildings, and although some information is reported on the pressure distribution on the downwind building, the scope was not large enough to make any generalizations concerning wind load interaction on adjacent buildings.

Peterka and Cermak (1976) discussed qualitatively the adverse wind loading induced by adjacent buildings. The largest pressures acting on a structure are negative and act in a region of flow separation. This indicates that pressures in these regions could be increased if the flow in the vicinity of these regions were accelerated by influence of an

adjacent structure. At the stagnation region on the front of a structure where largest positive values occur, any increase in the mean velocity or turbulence approaching this region will result in increased positive pressures. In a like manner, any shielding effects of adjacent buildings acting to reduce the velocities in these regions will have the effects of reducing pressure also. No mention was made of the forces and overturning moments on the building complex examined, although this can be readily derived given the mean-pressure distribution.

The American Standard Building Code Requirement for Minimum Design Loads in Buildings makes little mention of possible hazards or benefits in total loading or cladding design that can result from wind interaction from another building. On shielding and channeling effects of adjacent buildings, the Building Code states:

"Reductions in velocity pressures, due to direct shielding afforded by adjacent buildings or structures or by terrain features are not permitted....For building complexes involving several structures, direct shielding may result in markedly reduced loads for certain wind directions. On the other hand, channeling and buffeting in the wake of upwind obstructions might increase the pressures or suction, and such increases should be allowed for in the design. Wind-tunnel tests in appropriate wind tunnels are recommended for this purpose."

Thus, there is a need for quantitative descriptions of wind loading induced by an adjacent building. It is the purpose of this study to give a detailed picture of these effects for a set of upwind structures and relative positions. It is hoped that this information will be the primary step in formulating a designer's guide to prediction of local peak pressures on a downwind building.

## Chapter 3

### SCALING REQUIREMENTS

#### General

The general requirements for similarity of atmospheric boundary layers may be obtained by inspectional analysis of the equations of mass, momentum and energy. The three governing equations may be expressed in the following form (Cermak, 1971):

$$\frac{\partial \rho^*}{\partial t^*} + \frac{\partial (\rho^* u_i^*)}{\partial x_i^*} = 0, \quad (3.1)$$

$$\begin{aligned} \frac{\partial U_i^*}{\partial t^*} + U_j^* \frac{\partial U_i^*}{\partial x_j^*} + \left[ \frac{L_o \Omega_o}{U_o} \right] 2\epsilon_{ijk} \Omega_j^* U_k^* = - \frac{\partial P^*}{\partial x_i^*} - \left[ \frac{\Delta T_o}{T_o} \frac{L_o g_o}{U_o^2} \right] \Delta T^* g^* \delta_{i3} \\ + \left[ \frac{v_o}{U_o L_o} \right] \frac{\partial^2 U_i^*}{\partial x_k^* \partial x_k^*} + \frac{\partial \overline{-u_i' u_j'}}{\partial x_j^*}, \end{aligned} \quad (3.2)$$

and

$$\begin{aligned} \frac{\partial T^*}{\partial t^*} + U_i^* \frac{\partial T^*}{\partial x_i^*} = \left[ \frac{k_o}{\rho_o C_{po} v_o} \right] \left[ \frac{v_o}{L_o U_o} \right] \frac{\partial^2 T^*}{\partial x_k^* \partial x_k^*} + \frac{\partial \overline{-\theta' u_i'}}{\partial x_i^*} \\ + \left[ \frac{v_o}{U_o L_o} \right] \left[ \frac{U_o^2}{C_{po} (\Delta T)_o} \right] \phi^*. \end{aligned} \quad (3.3)$$

The dependent and independent variables have been made dimensionless (indicated by asterisk) by choosing appropriate reference values.

Cermak (1975) in "Applications of Fluid Mechanics to Wind Engineering--A Freeman Scholar Lecture" details the requirements for exact similarity of the nondimensional coefficients (quantities in brackets) shown in Eqs. (3.1), (3.2) and (3.3) for the physical model and the atmosphere. In summary the requirements may be stated as follows:

1. Undistorted geometry
2. Equal Rosby number:  $Ro = U_o / (L_o \Omega_o)$
3. Equal gross Richardson number:  $Ri = \frac{\Delta T_o g_o L_o}{T_o U_o^2}$
4. Equal Reynolds number:  $Re = \frac{U_o L_o}{\nu_o}$
5. Equal Prandtl number:  $Pr = (\nu_o \rho_o C_{po}) k_o$
6. Equal Eckert number:  $Ec = U_o^2 / [C_{po} (\Delta T)_o]$
7. Similar surface-boundary conditions
8. Similar approach-flow characteristics

Cermak shows that all of the above requirements cannot be simultaneously satisfied in the wind tunnel and atmosphere. However, some of the quantities are not important for the simulation of many flow conditions. The parameters which can be neglected and those which are important to this study will now be discussed.

#### Neglected Parameters

Wind forces on buildings require information on boundary layers during strong winds. Thermal stratification is destroyed by intense mixing of the airflow (neutral stability) hence boundary layers with adiabatic lapse rates are generally used for this type of study. This relaxes Richardson number requirements. Since air is used in the model for simulating the atmospheric boundary, Prandtl numbers are equal. Eckert number differences are insignificant until the flow speed approaches the speed of sound. The Rosby number is a quantity which indicates the effect of the earth's rotation on the flow field. This effect is assumed to insignificant in this study and therefore Rosby number similarity is neglected.

### Relevant Parameters

Geometric scaling, surface-boundary-conditions, and approach-flow characteristics must be similar for the atmosphere and its model. The special design features of the wind tunnel used in this study to meet these requirements will be discussed in detail in the next chapter.

Reynolds number similarity requires that the quantity  $UD/\nu$  be similar for model and prototype. Since  $\nu$ , the kinematic viscosity of air is identical for both, Reynolds numbers cannot be made precisely equal with reasonable wind velocities. Wind velocity in the wind tunnel would have to be the model scale factor times the prototype wind (Peterka and Cermak, 1976). However, for sufficiently high Reynolds number ( $> 2 \times 10^4$ ) a pressure coefficient at any location on the building will essentially be constant with Reynolds number if the model is characterized by sharp corners. This will tend to fix separation points and so fix overall characteristics of the flow.

Templin, Peterka and Cermak (1976) and Roshko (1970) indicated that care must be taken when modeling fine details such as building mullions and architectural features. Roshko conducted a wind tunnel study of a square prism with and without shallow grooves cut along the length of the two upstream faces. Wind was at a  $45^\circ$  angle to both front faces. Pressures on the leeward sides were measured with and without the grooves on the upstream face. A variation in the mean pressure of about five percent was observed for the range of Reynolds number from  $4.3 \times 10^5$  to  $7.8 \times 10^5$ . Although small, this indicated that exact scaling of details from full-scale to model will not automatically give accurate results.

Templin et al. (1976) conducted a series of tests in which small architectural features were exaggerated relative to the true scale.

Although some differences were detected, the effects were small compared to the effects of overall geometry. Templin concluded that no general law for scaling small details can be formulated since there are too many parameters such as building geometry and wind direction that play a significant role in the final process.

### Time Scaling

Time scaling is essential to relate peak pressures observed on the model to that in full-scale. Akins (1976) used the concept of reduced velocity for time scaling. The scaling specified was given by:

$$\left(\frac{\bar{U}}{n_o D}\right)_M = \left(\frac{\bar{U}}{n_o D}\right)_P \quad (3.4)$$

where  $D$  is an appropriate dimension of the building under consideration,  $n_o$  is a characteristic frequency, and  $\bar{U}$  is the mean wind velocity. One may note that the reduced velocity is the reciprocal of the Strouhal number. Since  $n_o = \frac{1}{T}$ , Eq. (3.4) can be rearranged to

$$T_M = \left(\frac{U_P}{U_m}\right) \left(\frac{D_m}{D_p}\right) T_P \quad (3.5)$$

If  $\bar{U}_p = \bar{U}_m$ , only the geometric scale is involved in the time scaling. For a model scale of 1:250, approximately 16 seconds of wind tunnel wind averaging will correspond to a mean hourly wind in full-scale.

The American National Standard Institute (ANSI) building code says that the basic wind speed to be used in the determination of wind load on a building corresponds to the fastest-mile speed for a 100-year mean recurrence interval. This speed is based on observed airflow in open level country at a height of 30 feet above the ground. For city

centers where extreme variations of shielding and channeling prevail more information regarding distribution of extreme winds is needed.

The method given by ANSI for determining an appropriate time reference interval to convert peak pressure coefficients to full-scale loads will now be shown.

1. Vellozzi and Cohen (1968) developed a simple conversion of fastest mile wind speeds to mean hourly averages (see Fig. 3.1). For a period of  $t$  seconds Fig. 3.1 gives,  $F$ , the ratio of the average probably maximum wind speed ( $V_a$ ) to the mean hourly speed. The averaging period,  $t$ , for the fastest mile of wind is determined by

$$t = \left( \frac{3600}{V_f} \right) \quad (3.5)$$

in which  $t$  is in seconds and  $V_f$  is the fastest mile velocity in miles per hour.

2. Vellozzi and Cohen (1968) also gave an approximate method for adjusting the hourly wind speed obtained in Fig. 3.1 from the 1/7 power law velocity profile to a different approach flow condition. It is

$$\bar{V}_z = 1.63 \bar{V}_a \left( \frac{z}{z_g} \right)^\alpha \quad (3.6)$$

in which  $z_g$  is the gradient height,  $\bar{V}_a$  is the hourly speed at 30 feet for the 1/7 power law velocity profile and  $\alpha$  is an experimentally determined value for the approach flow conditions being studied (in this study  $\alpha = .27$ ).

3. The appropriate reference pressure based on the mean velocity at the height of the reference wind tunnel measurement is then given by

$$q = \frac{1}{2} \rho \bar{V}_z^2 \quad (3.7)$$

When this reference pressure is multiplied by the peak pressure coefficients, peak loads are obtained.

## Chapter 4

### EXPERIMENTAL PROCEDURE

#### General

There are many variables to consider in dealing with wind pressures on buildings due to adjacent buildings. Examples are building heights, aspect ratios, relative positions, wind direction, and boundary layer characteristics. In order to present a reasonable amount of systematic experimental data, it was necessary to restrict the study to a limited range of some of these variables. It was decided to establish the effect of one upstream building in various positions on just one downstream building. This downstream building shall be referred to as the "principal building." The dimensions of the principal building were the same for all measurements. The single building upstream is referred to as the "obstructing building." Three series of experiments on wind load interaction on the two buildings were performed. They were:

- A. Obstructing and principal buildings were the same size; wind direction was normal to one side of the obstructing and principal buildings, and the distance between buildings varied laterally and longitudinally.
- B. Height of the obstructing building varied and wind direction was longitudinal to the buildings. Distance between buildings was varied also in the longitudinal direction.
- C. Obstructing and principal buildings were the same size; wind approached at different azimuths with respect to the center of the principal building; the distance between buildings varied longitudinally.

In total 176 different building configurations were examined. The layout of the building configurations used for Series A, B, and C, and associated nomenclature are given in Fig. 4.1a,b,c.

### The Wind Tunnel

All measurements were made in the industrial aerodynamics wind tunnel located in the Fluid Dynamics and Diffusion Laboratory at Colorado State University, Fort Collins, Colorado. A schematic of the wind tunnel is shown in Fig. 4.2. It is a closed-return tunnel powered by a 75 hp constant speed induction motor. A sixteen-blade variable pitch axial fan provides control of the speed of the tunnel. The flow is forced through a 4:1 contraction into a square test section 18.3 m long with a cross-sectional area of  $3.35 \text{ m}^2$ .

In order to obtain a thick turbulent boundary layer in the wind tunnel, spires and roughness elements were used in addition to the length of available test section. The spires used were developed by Peterka and Cermak (1974). The dimensions of the spires are shown in Fig. 4.3 and the positions at which they are located are shown in Fig. 4.4. In addition to the spires, barrier and roughness elements were used. The barrier and roughness elements began at a distance 1.22 m downstream of the spires and extended the length of the test section. The spacing and size of the roughness elements is given in Fig. 4.5.

The turbulent boundary layer in which all tests were conducted was similar to that of Akins' (1976) Boundary Layer 2. The difference was that no roughness elements were used within 2.18 m of the center of the principal building. This is unlikely to effect any characteristics of Boundary Layer 2. Figure 4.6 is the mean velocity profile for this boundary layer. The velocity profile developed had a mean profile

following a power law of the form

$$\frac{\bar{U}(z)}{\bar{U}(\delta)} = \left(\frac{z}{\delta}\right)^\alpha \quad (4.1)$$

where  $\bar{U}(z)$  and  $\bar{U}(\delta)$  are the mean velocities at an arbitrary height,  $z$ , and at the top of the boundary layer,  $\delta$ , respectively. The exponent  $\alpha$  is determined by the boundary roughness. For this study  $\alpha$  had a value of 0.26. The exponent of the power-law profile,  $\alpha$ , in full-scale situations has been reported to range from 0.12 for very smooth surfaces upwind of the measurement location to 0.40 for an upwind terrain with very large and irregular obstacles.

Figure 4.7 is the lateral variation of the mean velocity profile as measured by Akins (1976). The coordinate system used to describe the measurement locations are shown in Fig. 4.4.

The local turbulence intensity as measured by Akins (1976) is plotted in Figs. 4.8a,b,c and listed in Table 1. The local turbulence intensity is defined as the ratio of the velocity fluctuations,  $u'$ ,  $v'$ ,  $w'$ , to the mean velocity,  $\bar{U}(z)$ , at the height of the measurement. The longitudinal RMS velocity is ( $u'$ ), the lateral RMS velocity is ( $v'$ ) and ( $w'$ ) is the vertical RMS velocity. Davenport (1961) showed wind tunnel values are close to full-scale estimates, and the trend of local turbulence intensity with increasing power-law exponent is the same in the wind tunnel as in the full-scale environment.

Geometric scaling of the boundary-layer ranged from 1:200 to 1:300 for a power-law exponent of 0.26. This is determined by comparison of three lengths, the roughness length  $z_0$ , the longitudinal integral scale  $\Lambda_x$  and the boundary-layer thickness  $z_0$ , to full-scale measurements. Table 2 (from Akins, 1976) gives a range of reported values

from which geometric scaling was based. In order to make further comparisons more convenient, a scale of 1:250 is used in the remainder of this report. Table 2 indicates any scale range in the region 1:200 to 1:300 would be equally appropriate.

Comparisons of other properties of the full-scale and wind tunnel boundary layers, such as velocity spectra, autocorrelation function and coherence functions are reported by Akins (1976). The reader is referred to this reference for a complete discussion of scaling boundary layers between the two systems.

### The Models

The Principal Building. All measurements were made on the principal building. The building was made of 0.635 cm thick Plexiglas and instrumented on one surface. The dimensions and the locations of the taps on the principal building are given in Fig. 4.9. The different sides of the building are referenced in Fig. 4.1 as 1 through 4. With the wind being from the north, the west face of the principal building was number 1 and the other sides were numbered clockwise. A photograph of the building is given in Fig. 4.10. The building was centered on a turntable at the downwind edge of the test section. The turntable was supported by a large inertial mass to isolate the building from any vibrations in the wind tunnel. The building was aligned in the wind tunnel using a small laser. The laser was placed at the upstream end of the wind tunnel and reflected off a mirror on the building surface 16 m downstream. The building was rotated so that the reflected beam was within 0.05 m of the incident beam resulting in a maximum error of the building orientation of 0.2 degrees. Other building orientations were then set using a graduated scale (readable to approximately 0.25 degree) located on the base of the turntable.

The wind directions were measured clockwise from true north. Because the principal building is completely symmetrical, taps were located on only one side. Data for the remainder of the building were obtained by rotating the building  $90^\circ$ ,  $180^\circ$ , and  $270^\circ$ . Therefore 76 real taps were used to measure pressures at 304 different locations.

To measure pressures, holes were drilled in the model 1.5 mm in diameter perpendicular to the surface. A brass tube with inside diameter 1.5 mm was connected to each tap and projected into the interior of the building. Flexible "Tygon" tubing (1.5 mm ID, 3.0 mm OD) was used to connect each tap to a pressure selector valve located at the base of the building. Tube lengths were all 0.46 m. Akins (1976) determined the effect of the pressure-selector valve and the lengths of tubing on the frequency response of the entire system. He showed through comparison with a typical pressure spectrum that a maximum error in RMS of 5 percent will result due to amplification of the signal through 0.46 m length of plastic tubing. A second comparison of the probability density functions of the fluctuating pressure measured with different tube lengths showed no significant differences.

Regions near the edge of the roof are subject to local intense pressure as a result of corner vortices being formed for certain wind directions. Due to the limitations of available instrumentation and the large number of taps needed to obtain an overall picture of the character of the surface pressure on the roofs, it was decided to leave effects on the roof for a future study.

Obstructing Buildings. The obstructing building was always placed upwind to the principal building. The thirteen different obstructing building sizes used are shown in Fig. 4.11. The dimensions of these

are listed in Table 3. All buildings were made of wood except for the one which was of identical dimensions as the principal building. It was made of Plexiglas for flow visualization purposes. The use of wood instead of Plexiglas was done for economics and was assumed to make no difference in the flow characteristics.

### Measurements

Data Acquisition. A high-speed digital data-acquisition system was used for pressure measurements. The principal components of the system are a pressure-selector valve and an analog-to-digital converter. A block diagram of the system is given in Fig. 4.12. The instantaneous pressure at a location on the model was transmitted from the taps to the selector valve in the 0.46 lengths of plastic tubing. The selector valve consisted of two flat plates free to rotate relative to one another with an airtight seal between them. The top plate contained 80 holes so that pressures from 80 locations could be connected simultaneously. The lower plate had four holes which could be rotated to monitor any set of four pressures from the top plate simultaneously. The pressures were transmitted through very short tube lengths to the positive side of four differential pressure transducers (Statham Model PM283TC) mounted immediately below the valve. The negative or reference side of each transducer was connected to the static side of a pitot-static tube located above the model at the top of the boundary layer. In this way, the differential pressure measured corresponded to the difference between the external pressure on the building and local atmospheric pressure. When non-dimensionalized with an appropriate dynamic pressure, this gave an external pressure coefficient.

The fluctuating D.C. signal from each transducer was amplified and transmitted to a multi-channel analog-to-digital converter (Digital Data Recording System, Systems Development, Inc., Dallas, Texas). A minicomputer controlled the A-D converter and multiplexor with sample-and-hold circuits which sampled all channels simultaneously and held the information until the A-D converter could read it. An operator controlled the system through a teletype. The number of channels, sample rate, and details of digital tape formatting were all input parameters. In all cases the pressures were measured simultaneously on four channels at a sample rate of 250 samples/sec for 16.3 sec. The reason for this time interval is that after 16 seconds, the mean and RMS were shown experimentally to be within one percent of the values that would represent the mean and RMS for an arbitrarily long record of random signal (see Templin, 1976). As shown in Chapter 3, this 16 second time corresponds to about one hour of record at the assumed 1:250 scale. The digital data were then analyzed using the CDC 6400 at the Computer Center of Colorado State University.

The first four ports of the 80 port selector valve were connected by a manifold to the stagnation side of the Pitot-static tube. When the valve was in the first position, a signal was obtained by all four transducers that was proportional to the free stream dynamic pressure. This is related to the free stream velocity by

$$\bar{P}_d = 1/2 \rho (\bar{U}(\delta))^2 \quad (4.2)$$

where  $\bar{P}_d$  is the mean free stream dynamic pressure,  $\rho$  is the density of air and  $\bar{U}(\delta)$  is the mean free stream velocity.

The pressure measurement system consisting of both the transducers and amplifiers was calibrated in one operation. The gains of the

amplifiers were adjusted so that each pressure transducer/amplifier combination had the same calibration factor. All calibrations were linear and repeatable within 0.5 percent.

Data Reduction. The digital tape generated from the analog-to-digital converter contained a record of a voltage signal  $e(t)$ , in a discrete form, consisting of  $N$  values obtained by sampling at intervals of  $\Delta t$ . The total length of the record was then equal to  $N\Delta T$ , where  $T$  is length of the record in seconds. The basic computation was to convert the voltage signal into physical units of pressure. As shown by Akins (1976), the use of linear pressure transducers makes this a single multiplication. The discrete form of the record in physical units was expressed as  $f(t_i)$  or  $f_i$ . Then:

$$\bar{f} = \frac{1}{N} \sum_{i=1}^N f_i \quad \text{was the mean, and} \quad (4.3)$$

$$\bar{f}^2 = \frac{1}{(n-1)} \sum_{i=1}^N (f_i - \bar{f})^2 \quad \text{was the variance,} \quad (4.4)$$

with RMS being the square root of  $(\bar{f})^2$ . The  $N$  values were searched for the maximum and minimum value. The two quantities were called  $f_{\max}$  and  $f_{\min}$  respectively.

Pressure Measurements. Non-dimensional pressure coefficients,  $C_p$ , were obtained from the surface pressure on the principal building. The coefficients are defined as:

$$C_{p_{\text{mean}}} = \frac{(p-p_{\text{static}})_{\text{mean}}}{0.5\rho\{\bar{U}(\delta)\}^2} \quad (4.5)$$

$$C_{p_{\text{rms}}} = \frac{\{(p-p_{\text{static}}) - (p-p_{\text{static}})_{\text{mean}}\}^2}{0.5\rho\{\bar{U}(\delta)\}^2}^{1/2} \quad (4.6)$$

$$C_{P_{\max}} = \frac{(p-p_{\text{static}})_{\max}}{0.5\rho\{\bar{U}(\delta)\}^2} \quad (\text{maximum in record}) \quad (4.7)$$

$$C_{P_{\min}} = \frac{(p-p_{\text{static}})_{\min}}{0.5\rho\{\bar{U}(\delta)\}^2} \quad (\text{minimum in record}) \quad (4.8)$$

The mean pressure coefficient gives static wind loading. The RMS pressure coefficient is a measure of the amplitude of fluctuation in the pressure signal. The peak pressure coefficient is used to determine the largest loads acting at any point on the building and can be readily converted to full-scale by multiplication with a suitable reference pressure at the field site. Examination of a large number of pressure readings showed that the overall accuracy of the coefficients are  $\pm .03$  for mean pressure,  $\pm .01$  for RMS pressure, and  $\pm .1$  for peak pressure coefficients (see Templin et al., 1976).

Force and moment coefficients can be computed by integrating the mean pressure over each surface of the building. The forces and moments, expressed in coefficient form, are as follows:

$$C_{\text{LIFT}} = \frac{F_{\text{LIFT}}}{0.5\rho\bar{U}_A^2 WH}$$

$$C_{\text{DRAG}} = \frac{F_{\text{DRAG}}}{0.5\rho\bar{U}_A^2 WH}$$

$$C_{\text{DRAG MOMENT}} = \frac{M_{\text{OVERTURNING (DRAG)}}}{0.5\rho\bar{U}_A^2 WH^2}$$

$$C_{\text{LIFT MOMENT}} = \frac{M_{\text{OVERTURNING (LIFT)}}}{0.5\rho\bar{U}_A^2 WH^2}$$

$$C_{\text{TWIST}} = \frac{M_{\text{TWIST}}}{0.5\rho\bar{U}_A^2W^3}$$

$$\bar{U}_A = \frac{1}{H} \int_0^H U(z) dz$$

The coordinate system describing these forces and moments is shown in Fig. 4.13. Note that for comparison with Akins, Peterka, and Cermak (1975), force and moment coefficients were referenced to the mean velocity averaged over the height of the principal building, H. Also, moment coefficients do not include the component of force from the roof. The error resulting in the moment coefficients for the size of principal building used is small (as shown by Akins, Peterka, and Cermak, 1975, the error is approximately 10 percent). However this error can be significant if a principal building with larger side ratios was used. The force and moment coefficients in this study are used for comparison with other building configurations and care should be taken in interpreting these coefficients for overall mean wind loadings.

## Chapter 5

### RESULTS AND DISCUSSION

#### General

This chapter presents the effects on the principal building that result from wind load interaction of over 175 obstructing building configurations. A computer software package was developed to present a graphical display of all the pressure information obtained. This resulted in over 1700 individual contour plots of pressure distribution and pressure effects for the four sides of the principal building.

Because of the large amount of information presented, the building configurations are separated into three sets. The first set are the configurations in which the principal and obstructing buildings are the same size, and the wind azimuth is normal to one side of each building. In the second set the height of the obstructing building is varied. The two buildings are aligned parallel to the north and the wind direction is northerly. The third set is for configurations in which the two buildings are aligned parallel to the north. The wind direction with respect to the center of the principal building is varied and the two buildings are of the same size (see Fig. 4.1).

Also presented in this chapter are the mean force and moments that act on the principal building for different building configurations investigated. The chapter is concluded with preliminary results of a statistical investigation of peak wind loading values on an unobstructed building and the same building subjected to upwind interference.

#### Set A: Side 1

Figure 5.6a shows the mean pressure coefficients for side 1. As the two buildings are separated farther in the along-wind direction ( $y/w$ )

increases. Accordingly as the two buildings are separated farther in the cross-wind direction ( $x/w$ ) increases.

Looking in the ( $y/w$ ) direction for ( $x/w$ ) = 0.0, the mean pressure distribution changes dramatically until ( $y/w$ ) approaches 6.0. For ( $y/w$ ) less than 3.0 there is a small pressure gradient with the average pressure coefficient across the face being -0.1. As ( $y/w$ ) approaches 6.0 the gradient increases. At ( $y/w$ ) of 6.0 and above the mean pressure distribution on side 1 is nearly the same.

It is difficult to assess how far upstream the obstructing building affects the principal building on side 1. For obstructing building coordinates of [ $(x/w), (y/w)$ ] = (0.0, 5.0) the mean pressure at the top of the leading edge of side 1 is slightly lower than that on the unobstructed face (see Fig. 5.6a), whereas the pressure on trailing edge is higher than that seen on the unobstructed face. A simple method was devised to readily show where the placement of the obstructing building adversely or beneficially affected the pressure distribution on the principal building.

For each point on the principal building where a measurement is taken, the absolute value of each pressure coefficient was subtracted from the corresponding absolute value of the pressure coefficient on the unobstructed building. Mathematically it is:

$$|C_{P_i \text{ unobstructed}}| - |C_{P_i \text{ principal}}| = P \quad (5.1)$$

If  $P$  is negative, the pressure coefficient has either undergone an increase in positive pressure or a decrease in negative pressure relative to the unobstructed building. This means the placement of the upwind building has had an adverse effect on that particular point on

the principal building. Likewise, a decrease in positive pressure or increase in negative pressure relative to the unobstructed building will make  $P$  a positive number, therefore resulting in beneficial effects due to obstructing building placement. On the contour maps areas of adverse effects are shaded for emphasis.

Figure 5.6b is the adverse and beneficial wind loading effects for the mean pressure on side 1. Looking at the contour map one can see how the obstructing building has passed the region in which it is affecting side 1 of the principal building. This line which is given by  $[(x/w), (y/w)]$  coordinates of (1.2, 1.5), (1.4, 2.0), (1.4, 3.0), and (1.0, 4.0) shall be referred to as a "safe line" for side 1 of this set of building configurations.

The obstructing building has generally had a beneficial shielding effect for the mean pressures. In the region of  $0.8 \geq (x/w) \geq 0.2$  the obstructing building has shielded the principal building in the middle and trailing edge. However, some hazardous effects occur on the leading edge for  $0.8 \geq (x/w) \geq 0.4$ . This is caused by the flow field accelerating around the corner from side 2 of the principal building. Figure 5.1 depicts how as the value of  $(x/w)$  approaches 0.6 to 0.8 the flow field is distorted to a critical range in which the corner is adversely affected. As  $(x/w)$  approaches 1.2 to 1.4 the adverse effect has diminished since a through-flow condition has developed on both sides 1 and 3 of the principal building.

Examination of Fig. 5.6d emphasizes the flow-through characterized in Fig. 5.1. Figure 5.6d is the adverse and beneficial wind loading effects due to the RMS pressure on side 1. In all configurations up to the "safe line" there are adverse RMS effects occurring on the leading edge of the principal building and beneficial effects on the

trailing edge. Some cases such as (0.8, 2.0) show that as much as a 66 percent improvement occurs on the trailing edge while the same percent worsening occurs on the leading edge. Examining these RMS contour plots (Fig. 5.6c), the indication is that the accelerated flow generated by the obstructing building may attach to the leading edge of side 1 of the principal building for small values of  $(x/w)$ . As  $(x/w)$  increases the combination of the flow accelerating from the obstructing building and the flow accelerating around the corner of the principal building causes a very local instability in that same area. The RMS contour plots provide a good way of measuring the degree of this instability, which is important for cladding design.

An adverse effect is formed on configurations (0.0, 1.5) to (0.0, 6.0) with the worst effects near (0.0, 4.0) (see Fig. 5.6b, 5.6d). This can be explained from the analogy that these building configurations are similar to one long building. There is the indication that for values of  $(y/w)$  less than 6.0 the two buildings are acting in a similar manner to that of a single building with a side ratio of  $1:1 + (y/w)$ . This interpretation is noticed by the approximate position of reattachment of the flow on side 1 in Fig. 5.6c. Akins (1976) presented pressure information for buildings of different side ratios. He showed that reattachment occurs where the RMS pressure coefficient on a particular horizontal line is maximum and that the reattachment location was closer to the leading edge as the side ratio (length of side 2/length of side 1) decreased.

Figure 5.2 is an illustration of this flow phenomena. Reattachment of the separation bubble originating on the obstructing building gives rise to large fluctuations on side 1. As the buildings separate, the

reattachment position moves towards the leading edge of side 1. At  $(y/w) = 6.0$  the reattachment will not reach the sides of the principal building, therefore the large fluctuating pressure region on side 1 diminishes.

For the unobstructed case reattachment does not occur on side 1 for the side ratio of 1.0. This is in agreement with the findings of Akins (1976).

Figure 5.6e is the wind loading for the peak pressures on side 1. It is seen how in the region of  $(0.0, 2.0)$  to  $(0.0, 5.0)$  the peak pressures can be over twice as high as in the unobstructed case. This is not surprising in view of the preceding discussion of the adverse mean and RMS in this region. Also, the "safe line" is seen to be in the same position as that for the mean pressures. Figure 5.6f is the adverse and beneficial wind loading for the peak pressure on side 1. This figure can serve as a unique design guide for local effects, and points out the hazardous conditions which develop along the leading corners. One should note that these are the absolute values of the largest peak positive or negative pressure coefficients.

Set A: Side 2

Figure 5.7a shows the mean pressure coefficients for side 2. As would be expected the pressure distribution for the unobstructed case is the result of the wind deflecting down to the lower level, up over the building and around the sides. The vorticity is concentrated below the stagnation point in front of side 2 and a streamwise component of vorticity (horseshoe vortex) is formed (see Fig. 2.2). The piling up of vortex lines in front of the face induces secondary vortices in the

opposite direction. This results in a small eddy attaching to the lower part of the front face and correspondingly a localized increase in pressure. Because of these effects the pressure distribution on the front face is referred to as being saddle shaped. Woo, Peterka and Cermak (1976) presented a detailed examination of the turbulence characteristics of wake flow, vortex stretching over and around a building and viscous effects encountered at the base of the building in "Wind Tunnel Measurements on the Wakes of Structures." The reader is referred to this for a detailed discussion of these topics.

The effect of the obstructing building is deflection of the horseshoe vortex and breakdown of the secondary vortices. This phenomena coincided with the blockage of the basic stagnation region on the principal building by the obstructing building. The position at which stagnation does occur and the degree to which blocking occurs is dramatically seen in the mean pressure contours for side 2 (Fig. 5.7a).

Figure 5.7b is the adverse and beneficial wind loading effects on the mean pressure for side 2. The obstructing building interferes with the stagnation position as far away upstream as  $(y/w) = 6.0$  and to a lesser degree as far away crosswind as  $(x/w) = 1.4$ . For configurations in which  $(x/w) = 0$ , it is apparent that up to about  $(y/w) = 3.0$  side 2 is subjected to a wake flow from the obstructing building. This is a beneficial effect, especially in the main stagnation region and at the ground level where the attached eddy has disappeared. Along the corner there is a slight adverse effect but the pressure is small ( $C_{P_{\text{mean}}} = -.1$  compared to  $C_{P_{\text{mean}}} = 0.0$  for unobstructed). At  $(0.0, 4.0)$  the characteristic saddle begins to form with a reduced vortex strength and

apparently no secondary vortices being attached to the front face. By (0.0, 6.0) the vortex has gained strength and has the characteristics of the unobstructed case, however, the distance between buildings is still not great enough for the development of the horseshoe vortex to be uneffected from the turbulence created by the wake of the obstructing building. By (0.0, 10.0) the obstructing building wake is sufficiently dissipated that the pressure distribution on side 2 is nearly the same as in the unobstructed case.

The region bounded by  $0.2 \leq (x/w) \leq 1.0$  and  $0.0 \leq (y/w) \leq 4.0$  provides an interesting study of the development of the saddle shaped mean pressure distribution and the stability of the horseshoe vortex. As close as  $(x/w) = 0.4$ , the high acceleration resulting from the separation of flow on the obstructing building creates a local high pressure region on side 2. As  $(x/w)$  increases the position of this pressure region correspondingly shifts. Accordingly, as  $(y/w)$  increases this effect gradually weakens.

Figure 5.7c shows the RMS pressure coefficients for side 2. Up to  $(y/w) = 4.0$  the pressure fluctuations are greater than those of the unobstructing case showing that the obstructing building wake is preventing formation of the stagnation region and horseshoe vortex formation. Figure 5.7d, which is the adverse and beneficial effects on the RMS pressures on side 2, shows the increase in fluctuating pressure is generally widespread for even as far away as  $(y/w) = 10.0$ . However, the increase is very small, especially as the  $(x/w)$  distance increases. By  $(x/w) = 1.2$  the obstructing building for all intents has little influence on side 2 of the principal building.

Figure 5.7e is the peak pressure coefficients for side 2 and Fig. 5.7f is the adverse and beneficial wind loading effects for peak pressures on side 2. The corners of the front face are subjected to hazardous effects as a result of building interaction but to a lesser degree than the adversity seen on side 1. By  $(x/w) = 1.0$  there is only a minimal change in peak pressure on side 2, but there is still an important increment in peak pressure occurring up to  $(y/w)$  of 10.0. This is an indication that the important adverse effects will occur for obstructing building orientations which are longitudinally upwind more so than those at lateral positions.

Set A: Side 3

Figure 5.8a is the mean pressure coefficients for side 3. As expected the flow phenomena about side 3 for configurations of  $(x/w) = 0.0$  exhibit the same characteristics as those about side 1. This was a good check of the symmetry of flow in the wind tunnel.

The region of  $0.2 \leq (x/w) \leq 0.8$  is generally one of a blockage effect. Mean pressures in this area are drastically reduced and as shown in Fig. 5.8b, the effect is very beneficial on side 3. However, examination of Fig. 5.8d, which is the adverse and beneficial wind loading effects on RMS pressure and Fig. 5.8f (which is the corresponding effects on peak pressures) show the top leading edge to be a hazardous wind area. In some cases such as configurations  $(0.4, 2.0)$ ,  $(0.4, 3.0)$  and  $(0.8, 3.0)$  the fluctuating and peak pressures along the top of the leading edge have doubled, whereas at the distance of less than one third the width of the side away from the leading top corner, the fluctuating and peak pressures are about the same as on the unobstructed case. This points out that although the obstructing building may produce

beneficial mean loading effects, the local adverse effects produced can be severe.

In examining the region of  $0.8 \leq (x/w) \leq 1.2$  for side 1, it was pointed out that the wind pattern undergoes a critical change due to deflection off the front face. For side 3, the alignment of the two buildings in this region still provides a basic shielding effect, except to a lesser extent than in the  $0.2 \leq (x/w) \leq 0.8$  range. Figures 5.8e and 5.8f indicate that  $(y/w) = 3.0$  is a critical range for peak pressures. At this distance and  $(x/w)$  around  $(0.8 - 1.0)$  the geometry suggests that a strong localized eddy from the front face might be swept around the sharp corner as a result of the angle of through flow between the two buildings. The effective change in angle of approach flow on the principal building due to the deflection of flow caused by the obstructing building is approximately 10 degrees. Flow visualization of building configurations in this range verified the instability of the flow on the leading edge of side 3 and also the approximate angle of the deflection of flow.

It is interesting to note that as  $(x/w)$  becomes greater than 1.2, there appears to be a situation of gap flow between the two buildings. This may account for the adverse regions of mean pressure effects (see Fig. 5.8b) on side 3, since there is a slight acceleration of flow between the two buildings.

#### Set A: Side 4

Figure 5.3 is a sample of the mean, RMS and peak pressure measurements for side 4. Since this side of the principal building is the wake region, it would not be expected that the obstructing building placed upwind would have major effects. Figure 5.3 justifies this

expectation for the flow conditions and size of buildings used in this study.

#### Set B: Variation of Height of Obstructing Building

The following discussion will concern wind effects on the principal building resulting from the obstructing building being of a different height. Figure 4.1b gives an illustration of the building and wind configuration. It should be noted that because of the results of Set A, no measurements were made for side 4. Also, because of symmetry, the discussion of wind pressures on side 1 also apply to side 3.

#### Set B: Side 1

Figure 5.9a is the mean pressure coefficients for side 1 of Set B. Figure 5.9b is the adverse and beneficial wind loading effects for the mean pressure on side 1. When the obstructing building is of greater height than the principal building, there is virtually a total shielding effect. This can be expected due to the proximity of the two buildings.

For  $(Z/H) = 1.0$  the data from this set can be compared to Fig. 5.1a for  $(x/w) = 0.0$ , and it is seen that the experimental measurements are consistent.

Figure 5.9d is the adverse and beneficial wind loading effects for RMS pressure on side 1. From examination of this plot along with those for the mean pressures, it is apparent that when the obstructing building coordinates are  $((Z/H), (y/w)) = (0.6, 1.5)$ , the adverse effects on side 1 of the principal building are the greatest. As the height increases or decreases the adverse effect gradually lessens. Also as the distance between the two buildings increase, adverse effects decrease but to a lesser degree than that seen by changing the building height.

Figure 5.9e is the peak pressure coefficients for side 1, and Fig. 5.9f is the corresponding plot of the adverse and beneficial wind loading effects. The flow accelerating from the roof of the obstructing building sweeping around the sides of the principal building result in high peak pressures along the leading edge of side 1. Very high peaks (2.0) are seen on the corner of the principal building when the obstructing building is taller. This implies that adverse effects may also be occurring on the roof of the principal building and further research is needed to quantify this phenomena. High peaks are evident for a significant area of side 1 for all obstructing building heights greater than  $(Z/H) = 0.5$ . This leads to the conclusion that changes of building height may have a more pronounced effect on those building configurations in Set A. Further investigation by using an obstructing building of different heights for the configurations in Set A may result in extreme adverse local effects due to the complex flow created by: 1) acceleration from the roof, 2) effective change in angle of approach flow and, 3) acceleration of flow from side 2 of the principal building to side 1.

#### Set B: Side 2

Figure 5.10a quantitatively shows the development of the saddle shaped mean pressure distribution on the windward face of the principal building. As the upwind building decreases in height, the downwash effect begins to increase. At an obstructing building height of  $(Z/H) = 0.5$  the lower level of the principal building begins to experience a significant adverse pressure effect. This is apparent from Fig. 5.10b and 5.10f which are the adverse and beneficial wind loading effects for the means and peak pressure coefficients, respectively. The corresponding map of RMS pressure effects (Fig. 5.10d) illustrates that on the

middle section of the principal building, the stable horseshoe vortex flow has developed at  $(Z/H) = 0.5$ .

Figure 5.4 shows the apparent flow development on side 2. It was already noted that for the unobstructed case, the increase in mean pressure along the lower edge of side 2 was by a secondary eddy from the large horseshoe vortex. In the region of  $0.9 \geq (Z/H) \geq 0.5$ , there is a downwash phenomena from the rooftop of the obstructing building. This downwash causes an adverse effect on the top edge of the principal building. As the obstructing building decreases in this range, the position of the downwash also decreases and the adverse effect on the top edge diminishes. At  $(Z/H) < 0.5$  the accelerated flow from the roof of the obstructing building causes the stagnation region to extend to the lower levels of the principal building. Thus, where the pressure increase on the bottom of side 2 was by secondary eddy effects on the unobstructed case, it is now caused by the strong downdraft caused by the small obstructing building. The extension of the saddle-shape pressure distribution downward as shown in Fig. 5.10a illustrates this flow condition.

#### Set C: Change in Direction of Approach Wind

The results of Set A showed that adverse effects on the principal building are largely caused by a change in the wind direction upon interference with the obstructing building. Also, adverse effects were the most prominent in the RMS pressures and were local in nature. Therefore, the final set of pressure contours attempt to isolate critical angles of approach wind for two building configurations (see Fig. 4.1c).

Figure 5.11a shows the mean pressure coefficients for Set C, and Fig. 5.11b is the adverse and beneficial wind loading for the mean

pressures. For small wind angles, mean adverse effects are located along the edges and are generally small on side 2. For the wind directions reported, side 1 is generally in a wake situation and thus shielded from any mean loading effects. Side 3 is most effected by the change in wind direction reported.

Figure 5.11b shows that for wind directions of 10 and 15 degrees, negative mean pressures reach -0.5 for the unobstructed case on side 3. This is lower than seen for 0 degrees, and indicates that the adverse effects seen for similar angles in Set A are plausible. The obstructing building causes beneficial effects on side 3 for wind directions of 10 and 15 degrees. This is sensible, since using the analogy of the single building with large side ratio, the flow may be reattaching on the principal building thus diminishing high negative pressure separation region.

Adverse effects on mean pressure are seen at wind directions of 35 to 45 degrees for side 3. These are large and cover nearly the entire face. This overall adverse effect is the first one seen of significant value. Another significant overall adverse effect on the mean pressures is seen on side 2 at wind directions 60 and 90 degrees. These wind directions create a gap flow between the two side-by-side buildings. The negative pressure gradient is especially steep (as shown in Fig. 5.11a) for wind direction 90 degrees with values reaching -0.5 for the entire leading edge. For wind direction 60 degrees, the pressure gradient is not as steep but the angle of approach flow causes the leading edge of side 2 to be exposed to highly adverse pressure fluctuations (see Fig. 5.11b).

The results of these overall adverse effects resulting from shielding and channeling effects can lead to the maximum structural

loading occurring for approach winds other than those normal to the face of the unobstructed building. These hazardous conditions can also effect cladding design, and pedestrian levels, and are what were sought after in this investigation. The finding of these adverse areas also direct where future investigations should be concentrated, which was another goal of this study.

Referring to the results of Set A, it was found that when effective change in approach flow on the principal building due to the deflection of flow caused by the obstructing building was approximately 10 degrees, local adverse effects were seen on the leading edges. Results from Fig. 5.11d (which is the adverse and beneficial wind loading for RMS pressures) confirm this to be a critical deflection angle. In order to see if this deflection angle was only sensitive to the building configurations considered, a small experiment was conducted in which the wind was deflected at a  $10^\circ$  angle from different reference points on the principal and obstructing buildings. Figure 5.5 is the RMS pressures for 6 configurations investigated. In all cases the RMS at the corner was higher than the unobstructed case with the wind normal to side 2 (see Fig. 5.1c). The highest local fluctuating pressure is seen in configurations A and F where RMS values reached 0.3 in the corner.

#### Summary of Pressure Contour Results

For the experiments conducted, there was seen no building orientation which would drastically increase the RMS pressure over 0.35, or the peak pressure coefficient greater than 2.75, or mean pressure coefficient greater than 0.60. However, care must be taken when trying to apply results from this study to other buildings. The geometric scaling, approach flow conditions and levels of turbulence intensity

are parameters which can dramatically change the magnitudes and positions of the wind loads. The results presented by these pressure measurements are a useful starting point for locating critical areas and are useful in defining the flow phenomena which will generally affect all adjacent buildings.

An interesting investigation would be to examine the effects on the rooftop of the principal building for obstructing building heights of  $(Z/H) > 1.0$ . Only limited information on this phenomena is in the literature. Kelnhofer investigated rooftop effects on the principal building for obstructing building height of  $(Z/H) < 1.0$ . The largest absolute peak value Kelnhofer found was at wind azimuth  $135^\circ$  and  $Z/H = 0.75$ . Since the obstructing building is in the wake of the taller principal building for this wind direction it is questionable as to whether the obstructing building is the cause of the peak pressure. Woo (1974) determined by observing smoke flow that the roof-corner-vortex pair on an isolated building is strongest at an angle of  $47^\circ$ . This corresponds to  $137^\circ$  on Kelnhofer's directional scale.

#### Forces and Moments

Mean force and moment coefficients for the building configurations examined are presented in graphical form. These coefficients were calculated by integrating the mean pressure measured on the surface of the principal building (see Fig. 4.14). Drag force and moments are directed along the  $y$  direction on the contour plots. Lift forces and moments correspond to the  $x$  direction on the same figures. This directional system allows for clarity and easy calculation of resultant forces and moments. Calculations do not include contributions of skin friction, which are assumed to be relatively small. Also, all force and moment

coefficients use the approach wind speed averaged over the height of the principal building.

Figure 5.12a shows the drag force for building configurations in Set A. For the unobstructed case (or  $C_{D\infty}$ ) the drag force coefficient is 1.4. This corresponds well to the value reported by Akins, Peterka, and Cermak (1976) of 1.44. As expected, the mean drag force decreases considerably when the principal building is in the wake of the obstructing building. The effect of small negative pressures on the windward face is not large enough to reverse the direction of the drag force, although for obstructing building configuration (0, 1.5) the drag is practically zero. A 33 percent decrease in drag force is seen at a  $(y/w)$  distance of 4.0. By  $(y/w) = 10.0$ , there is practically no reduction in drag force. For the  $(y/w)$  range of 2 to 3 the reduction in drag force is considerable (50 percent) up to  $(x/w) = 0.6$ . As the buildings are separated farther in the  $(x/w)$  direction the reduction in drag force diminishes.  $(x/w) = 1.2$  has the same drag force as the unobstructed case. The drag force is never greater than that of the unobstructed case. Figure 5.13a shows the drag force coefficients for Set C. For the unobstructed case reduction in the drag force is insignificant for wind directions less than  $45^\circ$ . Although the drag force for the case of  $(y/w) = 1.5$  is always smaller than that of the unobstructed building, it is of interest to note the shape of this plot. The drag force increases until about 25 degrees, and then tapers down to zero. The shape of this plot suggests that channeling effects will cause an increase in total loading and there can possibly be a building orientation which can cause even greater loading than when the wind is normal to the unobstructed building.

The drag-moment coefficients are shown in Figs. 5.12b and 5.13b and exhibit the same characteristics as the drag force. Akins et al. obtained a drag-moment coefficient of 0.81 compared to the  $C_{Dm}$  of 0.76. The slight difference can be due to the neglect of the rooftop component of force in this study.

Figure 5.12c shows the lift force coefficients for building configurations in Set A. As would be expected, the lift force will increase as the obstructing building deflects flow onto the principal building. In some instances, there is a reversal of lift force direction due to large negative pressures occurring on one side of the principal building. The lift force is at its peak ( $C_L = 0.52$ ) at obstructing building configuration of (0.6, 3.0), which is where high local pressure effects were noticed (see Figs. 5.8b, d).

Figure 5.12d is the lift-moment coefficients for the Set A. The plot shows the lift force is relatively insensitive to the  $(y/w)$  of the obstructing building. Little appreciable difference in lift moment is also seen in Fig. 5.13d which is the corresponding coefficients for Set C. Figure 5.12e is the twist moment for Set A, which is shown to be negligible upon the building placements investigated.

Figures 5.14a and 5.14b clearly show the decrease in drag force and moments as the obstructing building height increases. For the cases in which the obstructing building is taller than the principal building the drag force and moment, although small, reverse in direction.

#### Peak Surface Pressures--Probability Densities

The peak pressure coefficient for a given location and building configuration is a discrete point taken from a random pressure signal. Knowledge of the statistical characteristics of this pressure signal

is required to predict the peak values likely to occur in a given time period.

Techniques for predicting the peak wind loading values on a structure by generating peak probability density functions are available for the positive peaks (Peterka and Cermak, 1975) (Davenport, 1964). The procedure involves the assumption of a Gaussian pressure distribution of local pressures acting on the structure in response to a Gaussian distribution of velocity in the turbulent flow about the structure. Measurements made by Dalgliesh (1976) and Peterka and Cermak (1974, 1977) in the positive pressure region agree well with Davenport's theoretical analysis. For the non-Gaussian fluctuations in the regions of high negative pressure, techniques for predicting peak probability density functions are being developed by Peterka (1977). In all cases, the design procedures are not intended to handle the presence of structures immediately upstream. Preliminary work to account for building interference phenomena on the statistical characteristics of peak pressures is discussed in this section.

The peak probability density function is a function of sample time (Davenport, 1961a). Since climatological records commonly refer to hourly mean wind velocities, the sample duration of frequent interest is one hour. The purpose of Davenport's statistical model is therefore to relate the largest likely instantaneous value of the pressure force occurring during that hour to the mean value, power spectrum, and probability distribution of the peak fluctuations at that point. It has been shown earlier in this study that 16 seconds of wind tunnel sampling corresponded to a mean hourly wind. With this in mind, an experiment was developed to obtain statistical information on peak pressure loading influenced by an upwind building.

Four pressure locations were selected on the principal building for this study. They were tap 44 on side 2 (or 244), taps 41 and 44 on side 1 (141, 144) and, tap 44 on side 4 (444). As seen in Fig. 4.10, all taps were the same height on the building. The four taps were simultaneously sampled for approximately 1 1/2 hours to obtain 350 records of 16 second intervals. The largest negative and largest positive peak for each record was found. These data were used to plot a frequency distribution for the negative peak value and a similar curve for the positive peak value. The experiment was run for three obstructing building configurations (( $\bar{x}/w$ ,  $y/w$ ) of (0,2), (0,3) and (0,6)) and for the case in which no obstructing building was present.

To compare the experimental data from the model with that from Davenport's (1964) theory and Peterka and Cermak's (1975) data, only two pressure regimes are of immediate importance. They are (1) those associated with direct wind impingement on the structure with generally positive mean pressures (tap 244) and (2) those associated with separated regions with negative pressures (taps 141 and 144). Three sets of peak probability density curves are therefore reported. They are:  
 Probability Distribution of Peak Positive Pressure, Tap 244 (Fig. 5.15)  
 Probability Distribution of Peak Negative Pressure, Tap 141 (Fig. 5.16)  
 Probability Distribution of Peak Negative Pressure, Tap 144 (Fig. 5.17).  
 Figure 5.18 shows the random pressure sample for one second of each pressure tap measurement for which a probability density curve is reported.

The theory by Davenport is that given a stationary random function  $x = f(t)$  having a normal probability distribution with mean  $\bar{x}$ , standard

deviation  $\sigma(x)$ , and  $\eta$  defined as  $(x-\bar{x})/\sigma(x)$ , the probability distribution of the function is

$$p(\eta) = \frac{1}{(2\pi)} \exp\left(-\frac{1}{2} \eta^2\right) \quad (5.2)$$

The probability distribution for the largest peak in time  $T$  is

$$p(\eta) = \nu T \exp\left(-\frac{\eta^2}{2}\right) - \nu T \exp\left(-\frac{\eta^2}{2}\right) \quad (5.3)$$

The quantity,  $\nu$ , is interpreted by Davenport to be the frequency at which most of the energy in the spectrum will generally be close to the natural frequency (for application to building motion). In order to obtain this value (called average effective fluctuation rate) the power spectral density for the positive and negative mean data are required. Because of the limited scope of this investigation, an approximate value of  $\nu$  was obtained by best fitting the experimental data with a family of curves generated for different values of  $\nu T$  in Eq. 5.3. For the positive peak probability distribution (Fig. 5.11) with no upwind building ( $y/w = \text{infinity}$ )  $\nu$  was approximately 20, and ranged from approximately 5 for when  $(y/w) = 2.0$  up to approximately 45 for when  $(y/w) = 3.0$ . The value of  $\nu$  agrees with values reported by Akins (1976) ( $\nu$  approximately 20 in both separated and stagnation regions) for the case with no upstream values. Values of  $\nu$  for cases with upstream building interference are original to this study and therefore these values are not available in the literature for comparison. Since  $\nu$  is defined as the average effective fluctuation rate of the random signal in peaks per second, an approximate value can be obtained by obtaining the number of independent peaks on the appropriate time vs. pressure curve. Unfortunately, this involves theoretical

analysis of extreme value statistics based on the power spectrum of the random function at a given frequency. The scope of this investigation did not include measurements for generating a power spectral density with the frequency response needed to carry out the extreme value statistics.

The experimental curves for the negative peak probability densities exhibit the same characteristics as those reported by Peterka and Cermak (1975) in that they do not fit Davenport's theoretical curve well. Also the peaks of the experimental data are displaced to higher values and the larger peaks tail off slowly to values of nine standard deviations from the mean, as seen by Peterka and Cermak.

In light of the preceding information, a design technique suggested by Dalglish (1971) and Akins (1976) for peak surface pressures was examined and expanded to apply for situations in which there is upwind interference by an adjacent building. Akins shows the approach to be based on the knowledge of the spatial distribution of the mean and RMS pressures and the probability distribution of the peak pressures. The peak pressure coefficient can be expressed as

$$C_{p_{\text{peak}}} = C_{p_{\text{mean}}} + \eta C_{p_{\text{rms}}} \quad (5.4)$$

For the four building configurations examined at the three pressure taps considered, the experimental values for  $C_{p_{\text{mean}}}$  and  $C_{p_{\text{rms}}}$  were used with an appropriate value of  $\eta$  to statistically predict a  $C_{p_{\text{peak}}}$ . The  $\eta$  used was the mean value of the corresponding probability density curve given in Figs. 5.15, 5.16, and 5.17. This choice of  $\eta$  meant the probability of occurrence of the predicted peak being greater than or less than the experimental peak was the same. For all cases the

predicted peaks and the peaks found experimentally were within the repeatability of the measuring system.

The predicted values of  $\eta$  were normalized with respect to  $C_{P_{peak}}$  for the corresponding unobstructed building case. This ratio is plotted versus distance between buildings in Fig. 5.19. The results show that for each of the three building distances investigated, the normalized value of  $\eta$  is practically the same for each tap. This finding is new and has not previously been reported in the literature. What makes this finding of particular significance is that  $(\eta/\eta_{\infty})$  is the same for tap locations in either positive or negative pressure regions. Also,  $(\eta/\eta_{\infty})$  does not increase more than 13 percent from the value with no building interference, indicating the sensitivity of the obstructing building to the statistical method used. There is also the possibility that in the limited number of configurations investigated, the maximum value may have been passed over.

A wider ranging investigation is needed to conclude what general effect the obstructing building has on the statistical characteristics of peak pressures. Nevertheless, the results presented are a first step into this phenomena and establish a technique for comparison with future studies.

## Chapter 6

### CONCLUSIONS AND RECOMMENDATIONS FOR FURTHER STUDY

#### Conclusions

The experimental findings of this study are limited to one approach flow condition and geometric scaling, therefore no attempt shall be made to state any generalized conclusions regarding exactly where and in what magnitude does an obstructing building adversely or beneficially effect the principal building. However, the mechanisms which were shown to cause beneficial and adverse wind loading are general in nature. This study presents a detailed picture of these mechanisms for a particular set of upwind buildings and relative positions. With this in mind, conclusions reached by this report are now listed.

1. Local adverse effects occur mainly along the corners and leading edges of the principal building. These effects are most pronounced when an obstructing building is about 3 diameters (center-to-center) upwind and 0.8 to 1.2 diameters crosswind (center-to-center) from the principal building. The effect of these configurations can double the local peak surface pressure. The building configurations stated correspond to an approximately 10 degree deflection of the wind azimuth from true north. Thus in a preliminary investigation of local wind effects, a starting point may be to isolate building configurations and wind directions which produce these small acute angles on the alongwind sides of the principal building under investigation.

2. By 6 diameters upwind or by 1.6 diameters crosswind, an obstructing building of similar or smaller size than the principal building has very little effect on the pressure distribution or mean wind loading on the principal building.

3. Results from both shielding and channeling effects show that at wind azimuths 25-45 degrees from true north (with the two buildings being relatively close) mean wind loading may be greater than that for winds normal to the face of the two buildings. However, mean wind loading is still not greater than if there were no obstructing building upwind of the principal building.

4. Local adverse effects are sometimes very sensitive to wind direction. In some instances a change of 5 degrees in wind azimuth shows a dramatic change in the magnitude and position of these effects.

5. The height of the obstructing building greatly effects positions where local adverse effects occur on the principal building. An obstructing building of 0.9 to 0.5 the height of the principal building will create adverse effects in pressure along the top edge of the windward face. Obstructing building heights lower than this can cause high local pressures near the base. Also, the drag force and moment decreases as the obstructing building height increases.

6. The effect of the obstructing building on statistical prediction of peak surface pressures on the principal building was investigated. Preliminary results indicated that a consistent trend exists in the probability densities for peak pressures as distance between buildings increases.

7. The lift or drag forces and moments are not larger than when the obstructing building is missing.

#### Recommendations for Further Study

Numerous extensions to the work discussed in this study are evident.

1. Extension of the results of this study to different approach flow conditions, and different geometric scalings.
2. Investigation of rooftop effects due to adjacent buildings.
3. Additional studies for obstruction and principal buildings of different aspect ratios, different corner geometry and surface texture. Also further investigation of the effect of changing the relative positions of the buildings used in this study and the number of obstructing buildings.
4. Dynamic analysis of wind load interaction by an adjacent building.
5. Further investigation of statistical techniques for prediction of peak surface loads on a building.
6. Investigation of multiple building interference effects.

## REFERENCES

- Akins, R. E., Peterka, J. A., Cermak, J. E., 1975, "Mean Force and Moment Coefficients for Buildings in Turbulent Boundary Layers," Report CEP75-76REA-JAP-JEC20, Fluid Mechanics Program, Colorado State University, Fort Collins, Colorado.
- Akins, R. E., and Cermak, J. E., 1976, "Wind Pressures on Buildings," Report CER76-77REA-JEC15, Fluid Mechanics Program, Colorado State University, Fort Collins, Colorado.
- Akins, R. E., 1976, Personal Communication.
- American National Standards Institute, 1972, Building Code Requirements for Minimum Design Loads in Buildings and other Structures, ANSI A58.1-1972.
- Cermak, J. E., 1971, "Laboratory Simulation of the Atmospheric Boundary Layer," AIAA Journal, Vol. 9, No. 9, pp. 1746-1754.
- Cermak, J. E., 1975, "Applications of Fluid Mechanics to Wind Engineering--A Freeman Scholar Lecture," ASME Journal of Fluids Engineering, Vol. 97, Ser. 1, No. 1, March, pp. 9-38.
- Cermak, J. E., 1976, "Aerodynamics of Buildings," Annual Review of Fluid Mechanics, Vol. 8, pp. 75-106.
- Cermak, J. E., 1977, Personal Communication.
- Dalgliesh, W. A., 1971, "Statistical Treatment of Peak Gusts on Cladding," Journal of the Structural Division, ASCE, Vol. 97, ST3, pp. 2173-2187.
- Davenport, A. G., 1960, "A Rationale for Determining Design Wind Velocities," Journal of the Structural Division, ASCE, Vol. 86, ST5, pp. 39-68.
- Davenport, A. G., 1961a, "The Application of Statistical Concepts to the Wind Loading of Structures," Proceedings of the Institution of Civil Engineers, Vol. 19, pp. 449-471.
- Davenport, A. G., 1964, "Note on the Distribution of the Largest Value of a Random Function with Application to Gust Loading," Proceedings of the Institution of Civil Engineers, Vol. 28, pp. 187-196.
- Hansen, C. A. and Cermak, J. E., 1975, "Vortex-Containing Wakes of Surface Obstacles," Report CER75-76ACH-JEC16, Fluid Mechanics Program, Colorado State University, Fort Collins, Colorado.
- Hunt, J. C. R. and Smith, G. P., 1969, "A Theory of Wakes behind Buildings and Some Provisional Experimental Results," Report RD/L/N 31/69, Central Electricity Research Laboratories, Leatherhead, England.

- Ishizaki, H. and Sung, I. W., 1971, "Influence of Adjacent Buildings to Wind," 3rd International Conference on Wind Effects on Buildings and Structures, Tokyo, Japan.
- Kelnhofer, W. J., 1971, "Influence of a Neighboring Building on Flat Roof Wind Loading," 3rd International Conference on Wind Effects on Buildings and Structures, Tokyo, Japan.
- Loehrke, R. I., 1977, Personal Communication.
- Peterka, J. A., 1977, Personal Communication.
- Peterka, J. A. and Cermak, J. E., 1974, "Wind Engineering Study of Renaissance Center, Detroit," Report CER74-75JAP-JEC5, Fluid Mechanics Program, Colorado State University, Fort Collins, Colorado.
- Peterka, J. A. and Cermak, J. E., 1974, "Simulation of Atmospheric Flows in Short Wind Tunnel Test Sections," Colorado State University, Fluid Mechanics Program Technical Report CER73-74JAP-JEC32.
- Peterka, J. A. and Cermak, J. E., 1975, "Wind Pressures on Buildings-Probability Densities," Journal of the Structural Division, ASCE, Vol. 101, ST6, June, pp. 1255-1267.
- Peterka, J. A. and Cermak, J. E., 1975, "Adverse Wind Loading Induced by Adjacent Buildings," Journal of Structural Division, ASCE, Vol. 102, No. ST3, March, pp. 533-548.
- Peterka, J. A. and Cermak, J. E., 1976, "Wind Engineering Study of One Houston Center, Houston," Report CER75-76JAP-JEC37, Fluid Mechanics Program, Colorado State University, Fort Collins, Colorado.
- Roshko, A., 1970, "On the Aerodynamic Drag of Cylinders at High Reynolds Numbers," Proc. of Seminar on Wind Loads on Structures, Honolulu, Hawaii, October.
- Sachs, P., 1974, Wind Forces in Engineering, Pergamon Press.
- Templin, J. T. and Cermak, J. E., 1976, "Wind Pressures on Buildings: Effect of Mullions," Report CER76-77JTT-JEC24, Fluid Mechanics Program, Colorado State University, Fort Collins, Colorado.
- Templin, J. T., 1976, Personal Communication.
- Velozzi, J. and Cohen, E., 1968, "Gust Response Factors," Journal of the Structural Division, ASCE, Vol. 94, No. ST6, pp. 1295-1313.
- Wise, A. F. E., 1971, "Effects Due to Groups of Buildings," Phil. Trans. Royal Society, London, A269, 469-485.
- Woo, H. G. C., Peterka, J. A., and Cermak, J. E., 1976, "Wind-Tunnel Measurements in the Wakes of Structures," Report CER75-76HGCV-JAP-JEC40, Fluid Mechanics Program, Colorado State University, Fort Collins, Colorado.

TABLES

Table 1. Summary of Properties--Boundary Layer 2 (Akins, 1976)

$z/\delta$	$\bar{U}(z)/\bar{U}(\delta)$	$u'(z)/\bar{U}(z)$	$v'(z)/\bar{U}(z)$	$w'(z)/\bar{U}(z)$
0.02	0.39	0.245		
0.04	0.46	0.225	0.161	0.129
0.06	0.52	0.210	0.147	0.117
0.10	0.60	0.175	0.120	0.101
0.14	0.66	0.150	0.104	0.081
0.18	0.70	0.133	0.091	0.073
0.20	0.72	0.125	0.088	0.070
0.30	0.80	0.096	0.069	0.087
0.40	0.85	0.075	0.056	0.049
0.50	0.89	0.064	0.048	
0.60	0.92	0.054	0.040	0.035
0.70	0.94	0.044	0.034	0.032
0.80	0.96	0.040		0.030
0.90	0.98			
1.00	1.00			

Table 2. Geometric Scaling--Wind Tunnel to Full-Scale (Akins, 1976)

Boundary Layer	p Power-Law Exponent	$z_0$ m			$\lambda_x$ m			$\delta$ m			Terrain Description
		Full-Scale	Wind Tunnel	Scale	Full-Scale	Wind Tunnel	Scale	Full-Scale	Wind Tunnel	Scale	
1	0.12	0.001-0.01	$1.22 \times 10^{-5}$	82-820	122	0.45	270	270	1.27	210	level surfaces with very small surface obstructions, grassland
2	0.26	0.1-0.5	$2.79 \times 10^{-3}$	36-180	130	0.60	220	360	1.27	280	rolling or level surface broken by numerous obstructions such as trees or small houses
3	0.34	0.5-1.0	$4.9 \times 10^{-3}$	100-204	140	0.50	280	360	1.27	280	heterogenous surface with structures larger than one story
4	0.38	0.7-1.5	$1.1 \times 10^{-2}$	64-140	152	0.50	300	450	1.27	350	heavily built up suburban area, typical of approach flow over a large metropolitan area
Source		ESDU(1972)			Templin(1969)			ANSI A58.1-1972			

Table 3. Building Details

BUILDING DETAILS		
Number	Height (cm)	Sides Squares (cm)
1	2.54	12.7
2	5.08	12.7
3	7.62	12.7
4	10.2	12.7
5	12.7	12.7
6	15.2	12.7
7	17.8	12.7
8	20.3	12.7
9	22.9	12.7
10	25.4	12.7
11	27.9	12.7
12	30.5	12.7
13	33.0	12.7

FIGURES

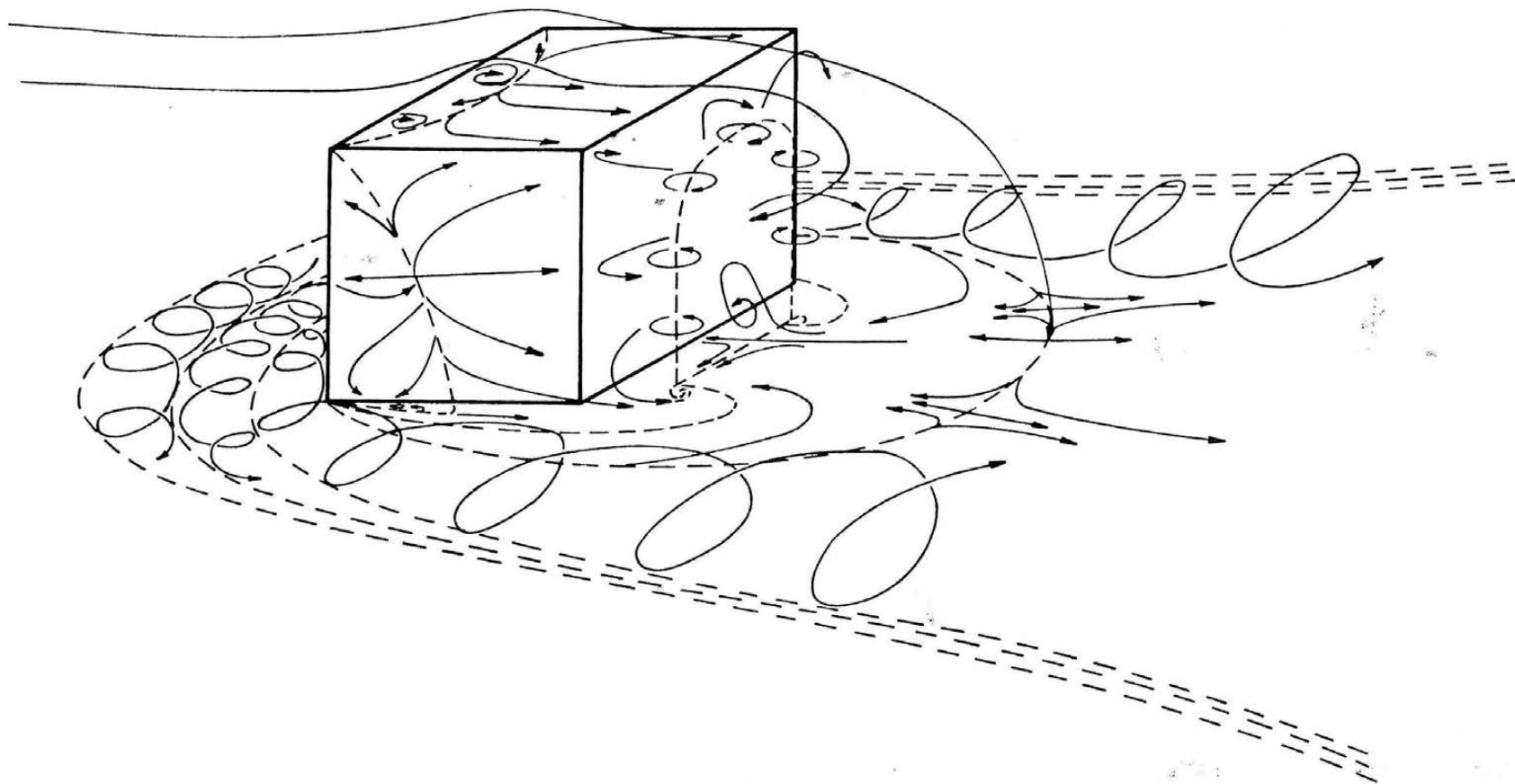


Figure 2.1. Flow Pattern around a Rectangular Block (Woo, 1976)

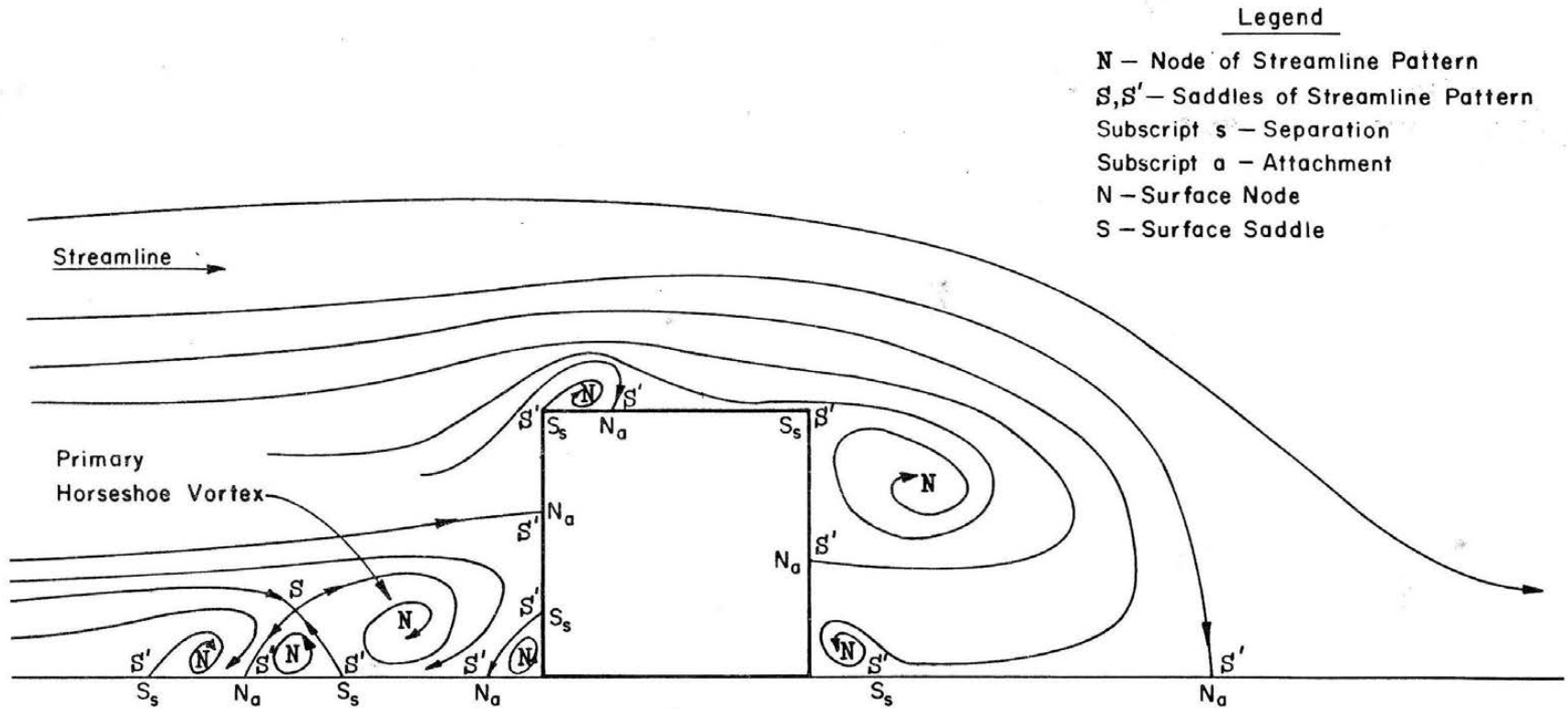


Figure 2.2. Streamlines in the Flow on the Centerline for a Rectangular Block (Woo, 1976)

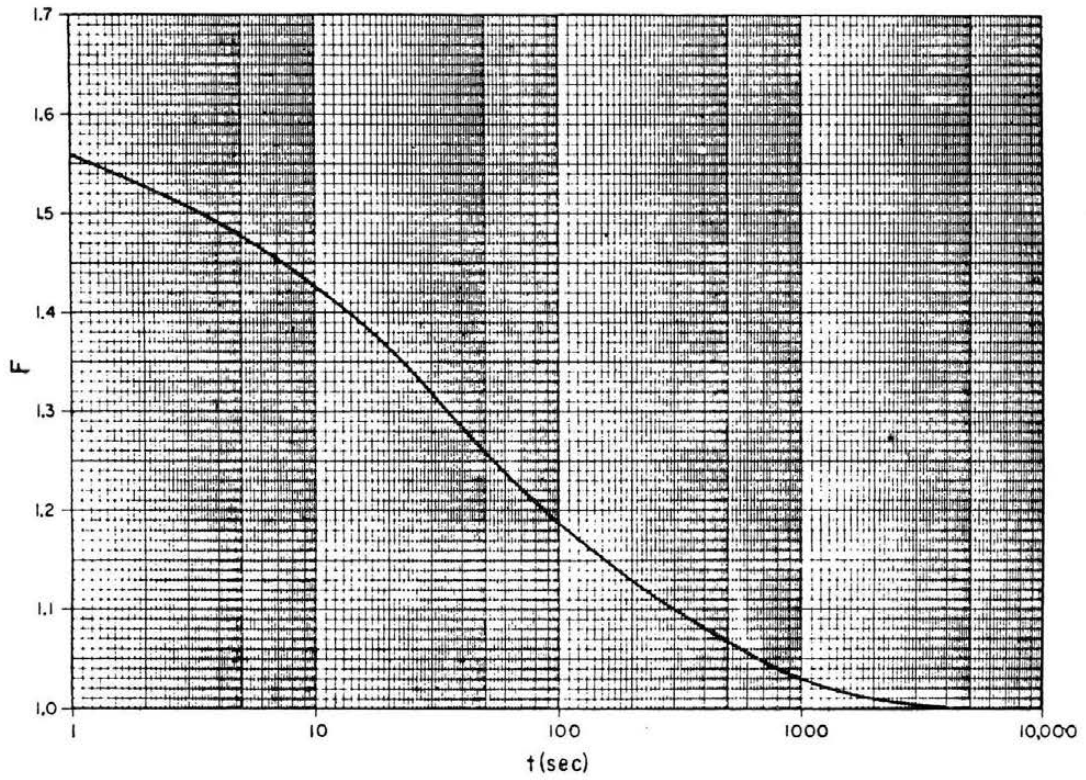


Figure 3.1. Ratio of Probable Maximum Speed Averaged over Period ( $t$ ) to that Averaged over One Hour (Vellozzi and Cohen, 1968)

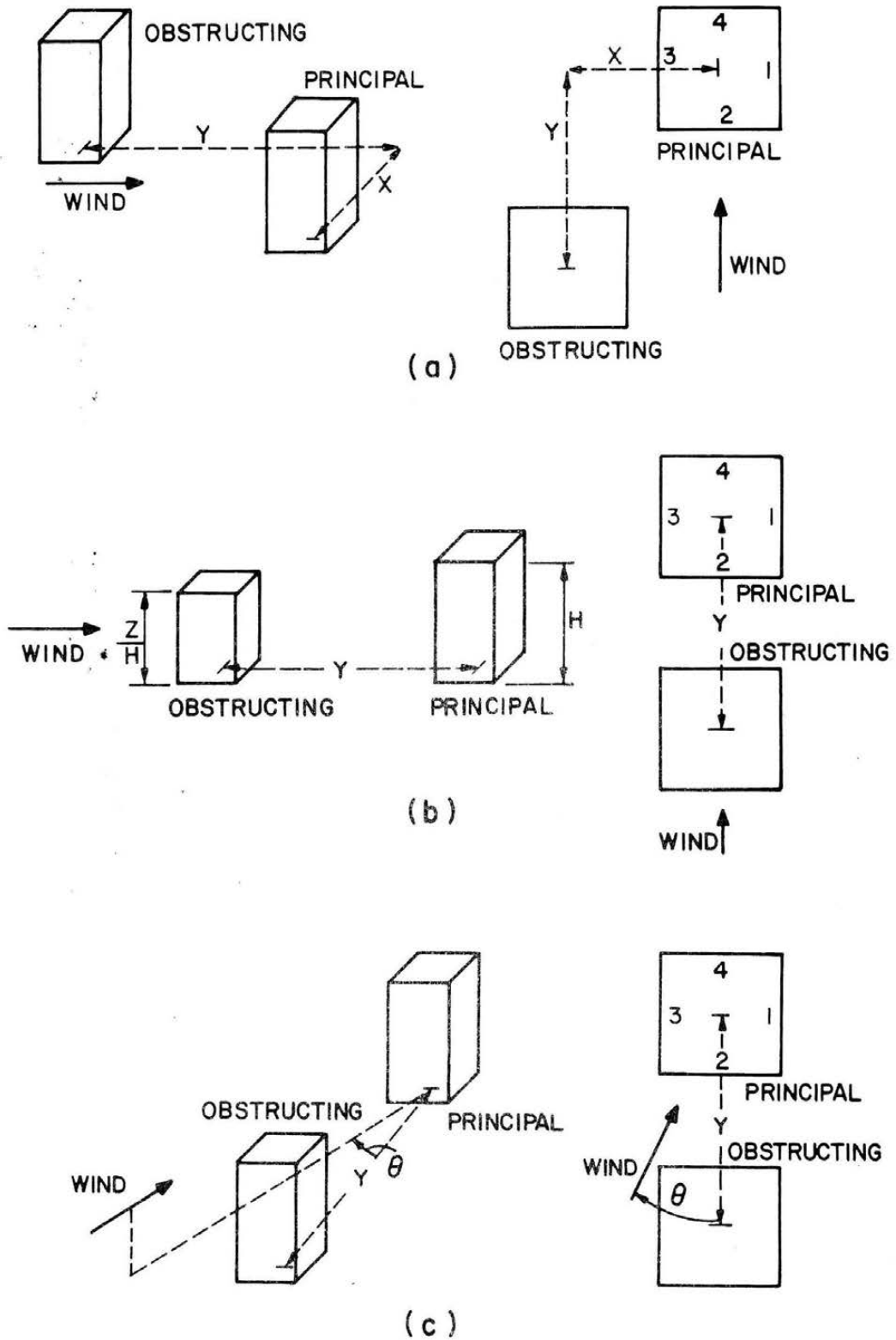
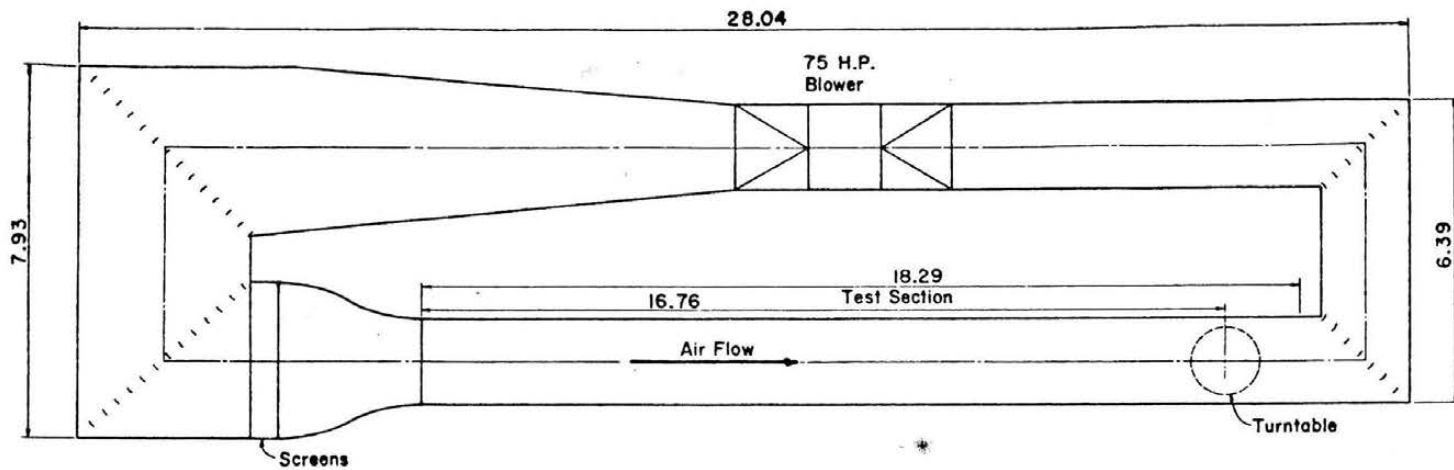
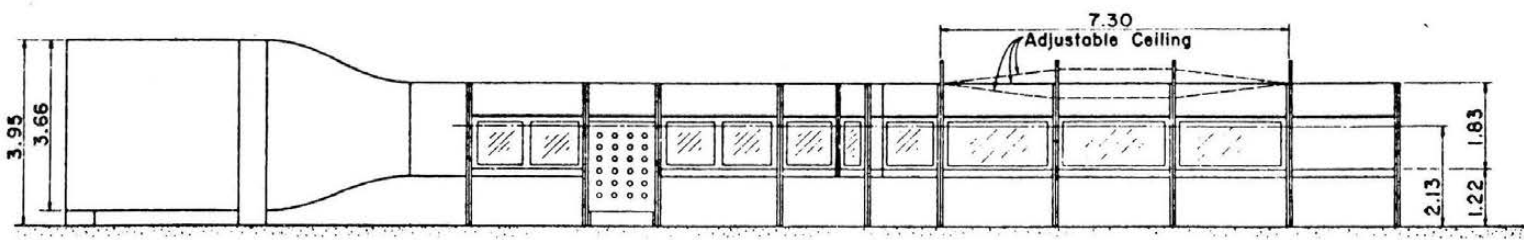
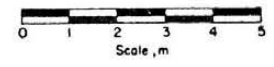


Figure 4.1. Building Configurations



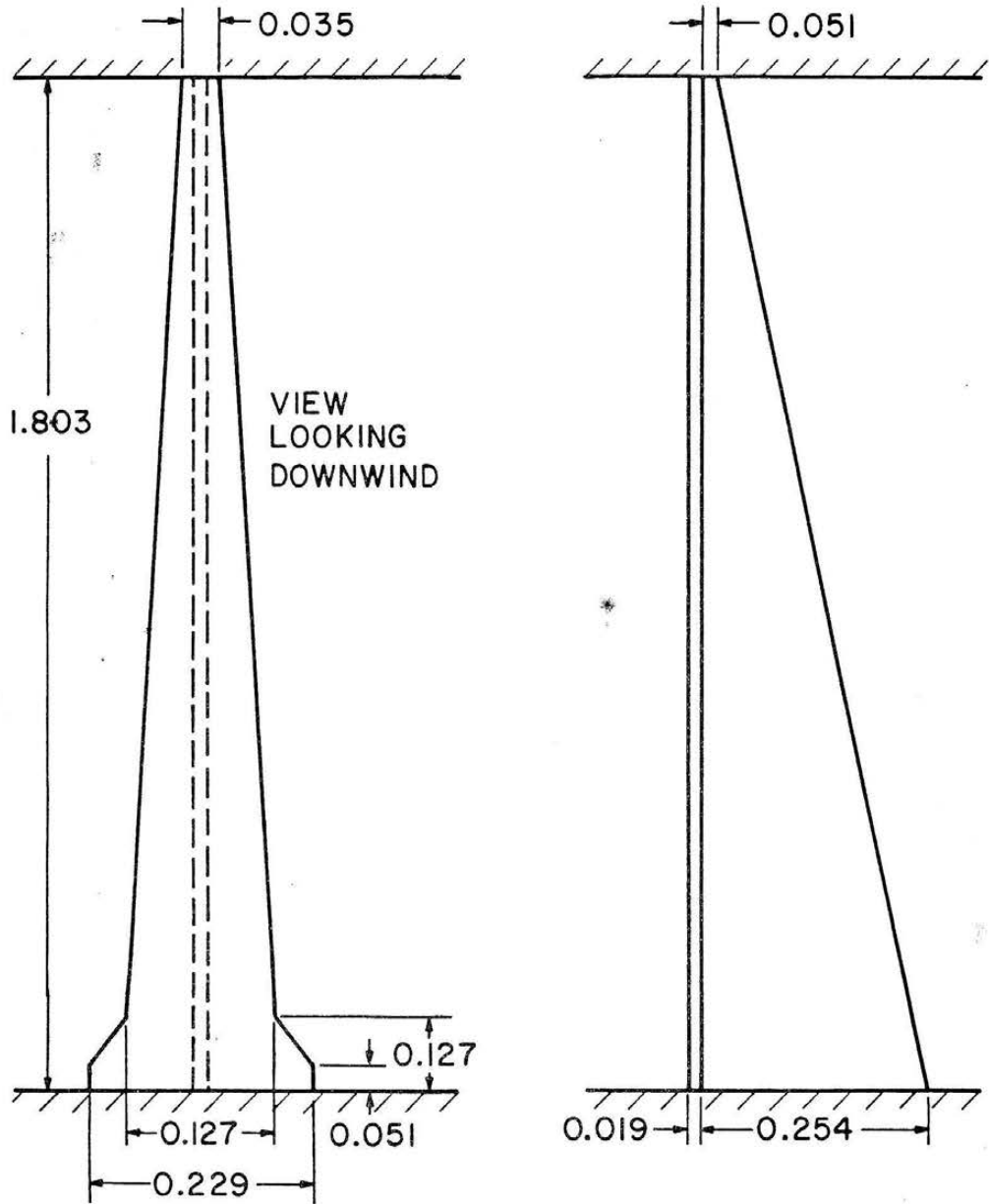
PLAN



All Dimensions in m

ELEVATION

Figure 4.2. Industrial Aerodynamics Wind Tunnel, Fluid Dynamics and Diffusion Laboratory, Colorado State University



ALL DIMENSIONS IN METERS  
DRAWING NOT TO SCALE

Figure 4.3. Spire Geometry

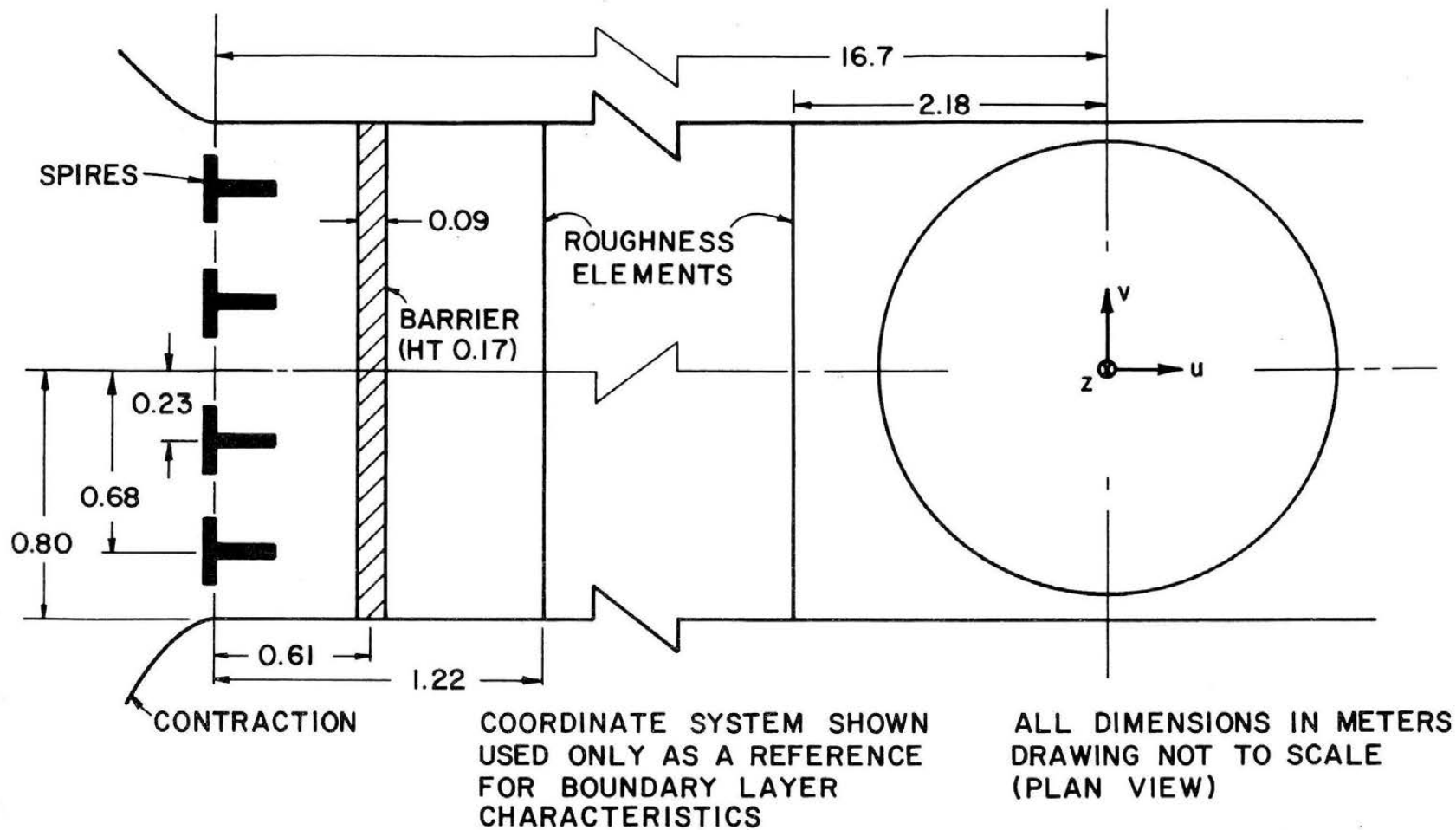
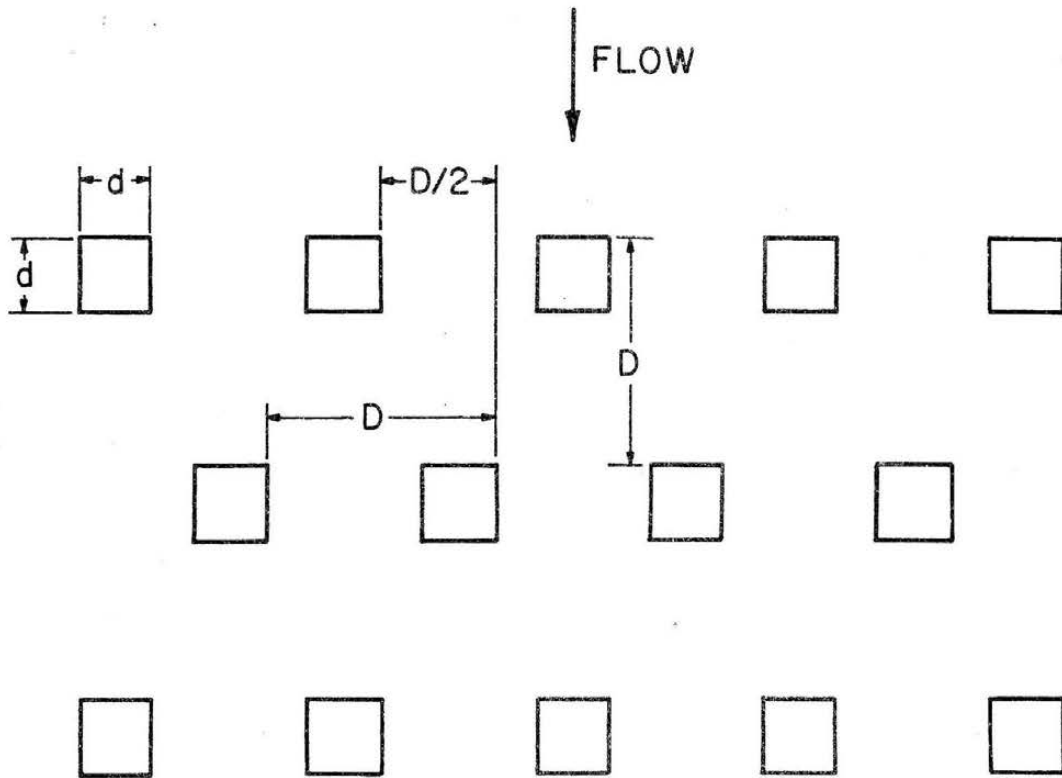


Figure 4.4. Wind Tunnel Arrangement



INDIVIDUAL BLOCKS ARE CUBES

BOUNDARY LAYER	$D$ (m)	$d$ (m)	$d_r$ (m)
2	0.075	0.025	0.84

$$D/d = 3.0$$

Figure 4.5. Roughness Configurations

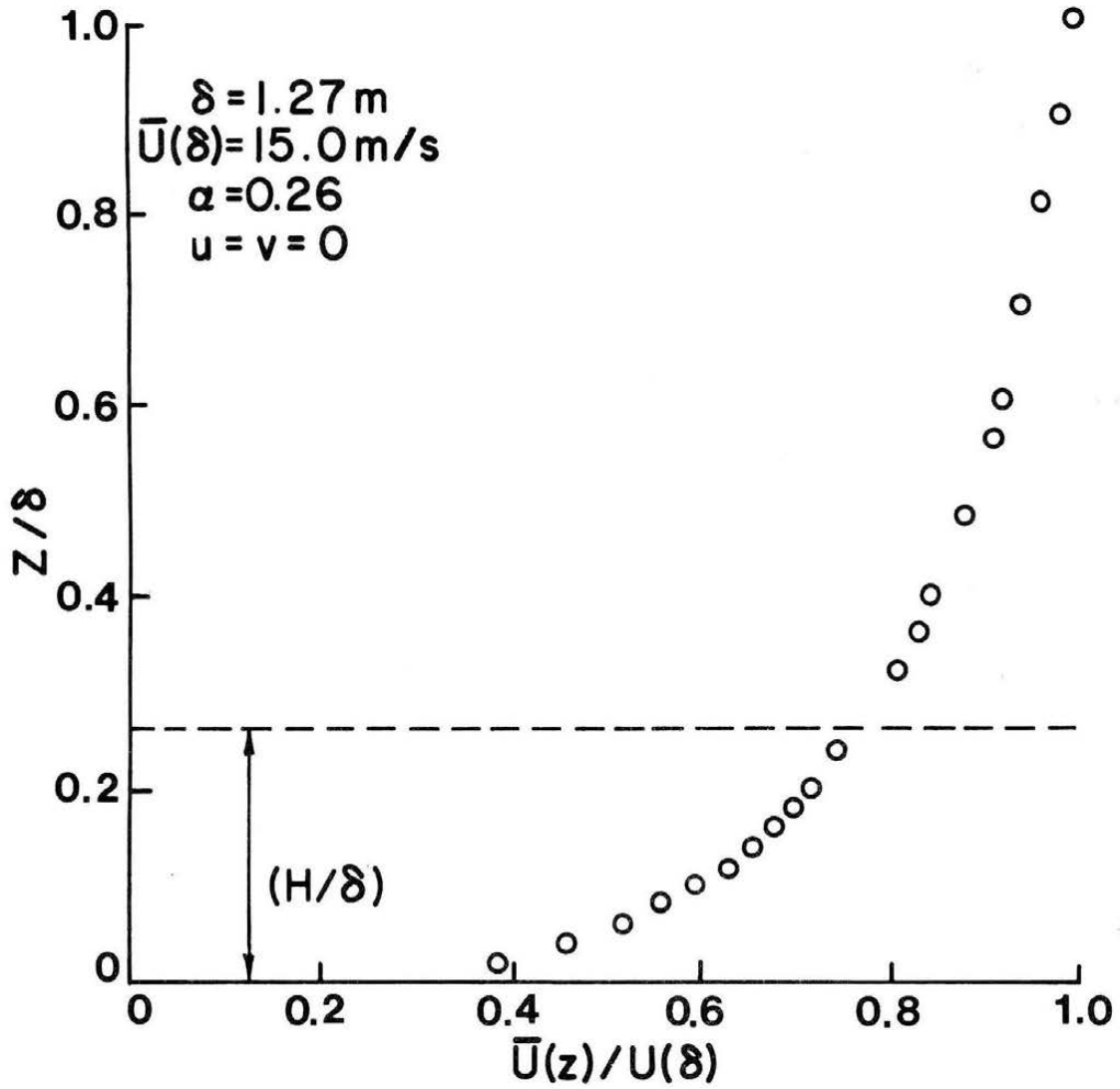


Figure 4.6. Mean Velocity Profile (B. L. "2," Akins, 1976)

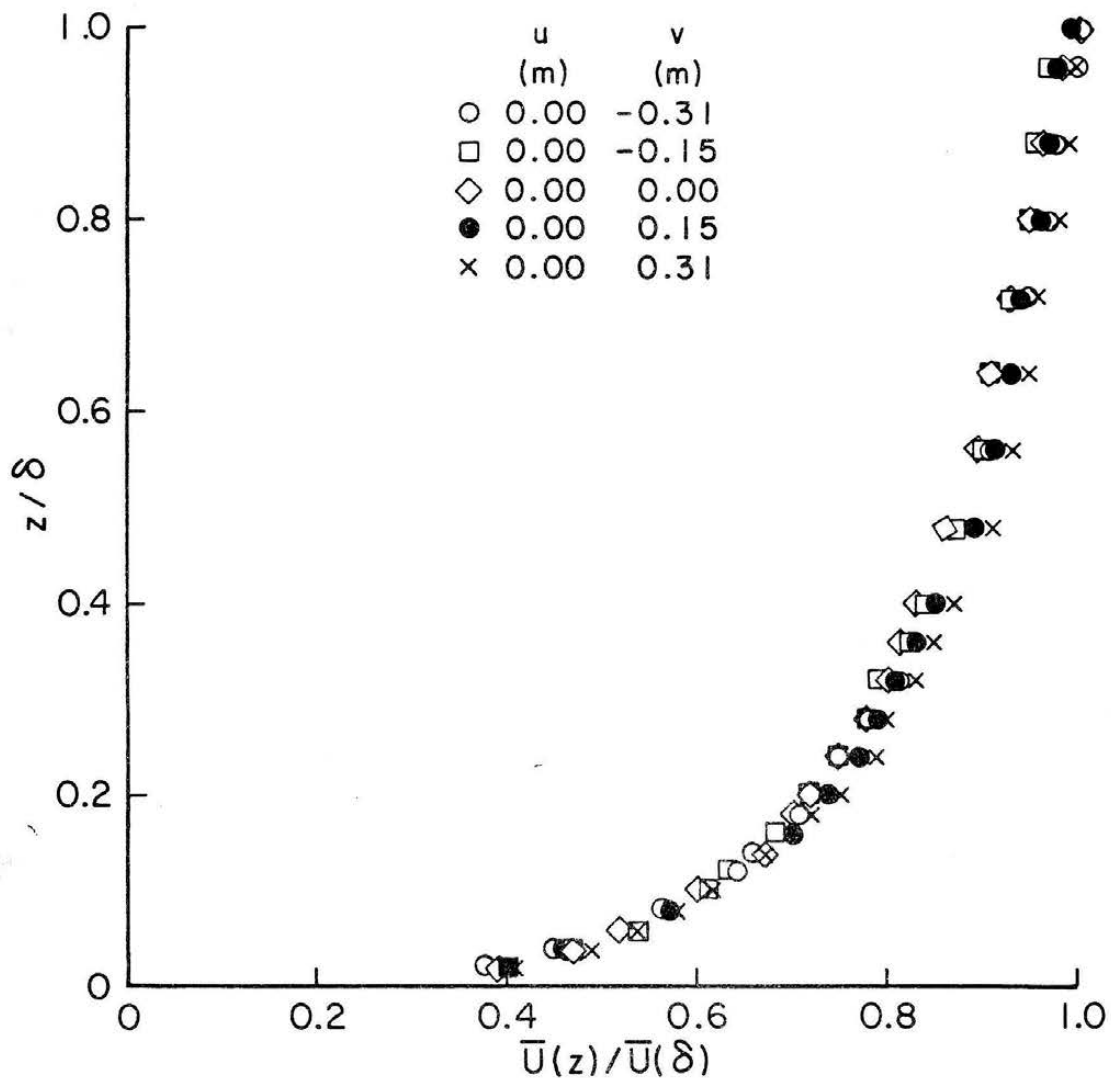


Figure 4.7. Lateral Variation of Mean Velocity Profile  
(B. L. "2," Akins, 1976)

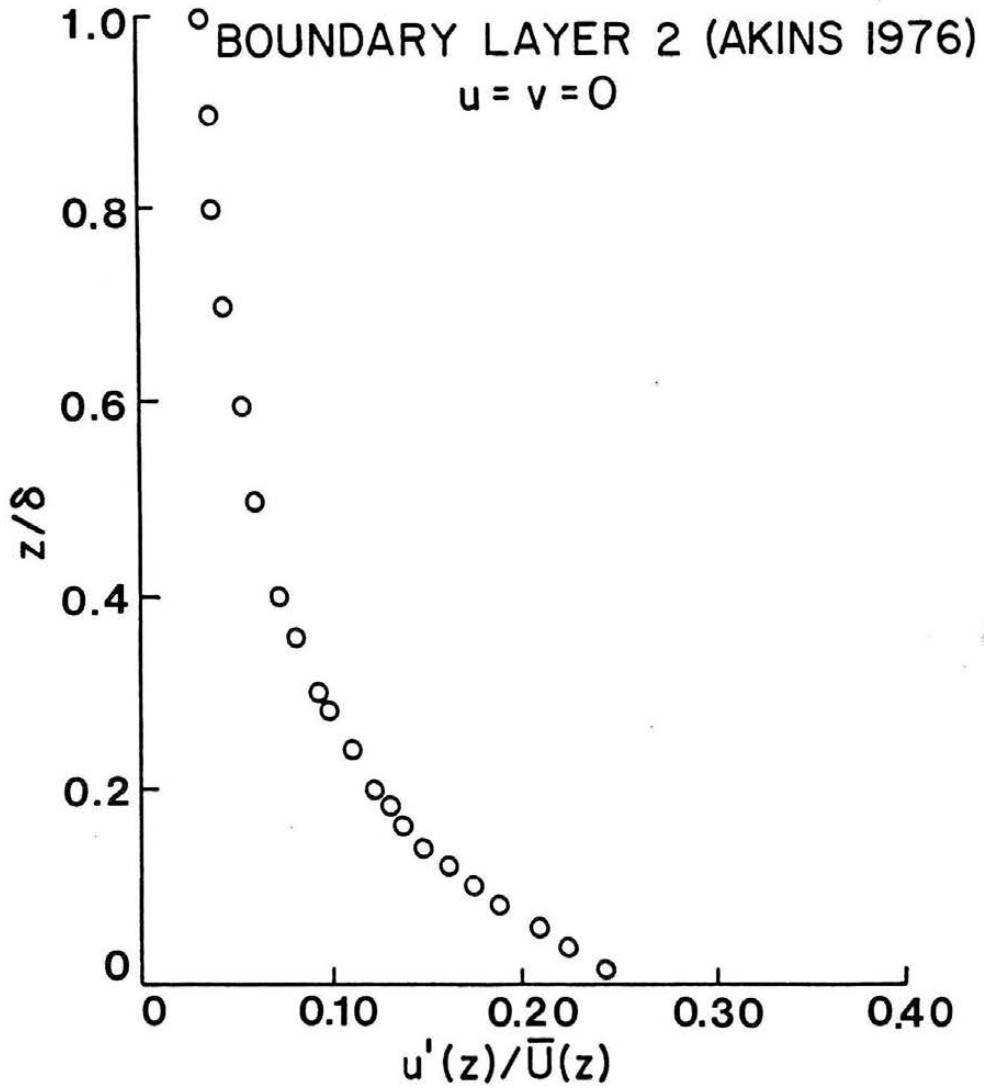


Figure 4.8a. Local Longitudinal Turbulence Intensity

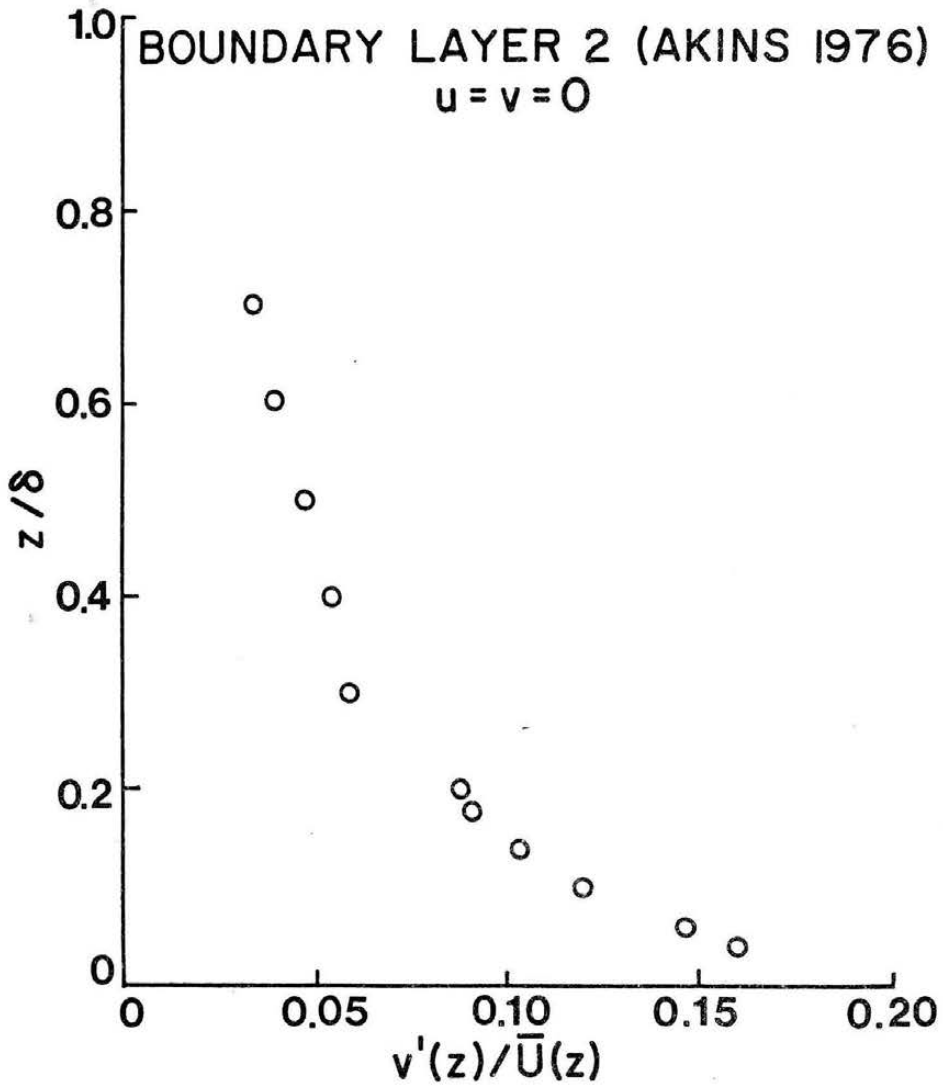


Figure 4.8b. Local Lateral Turbulence Intensity

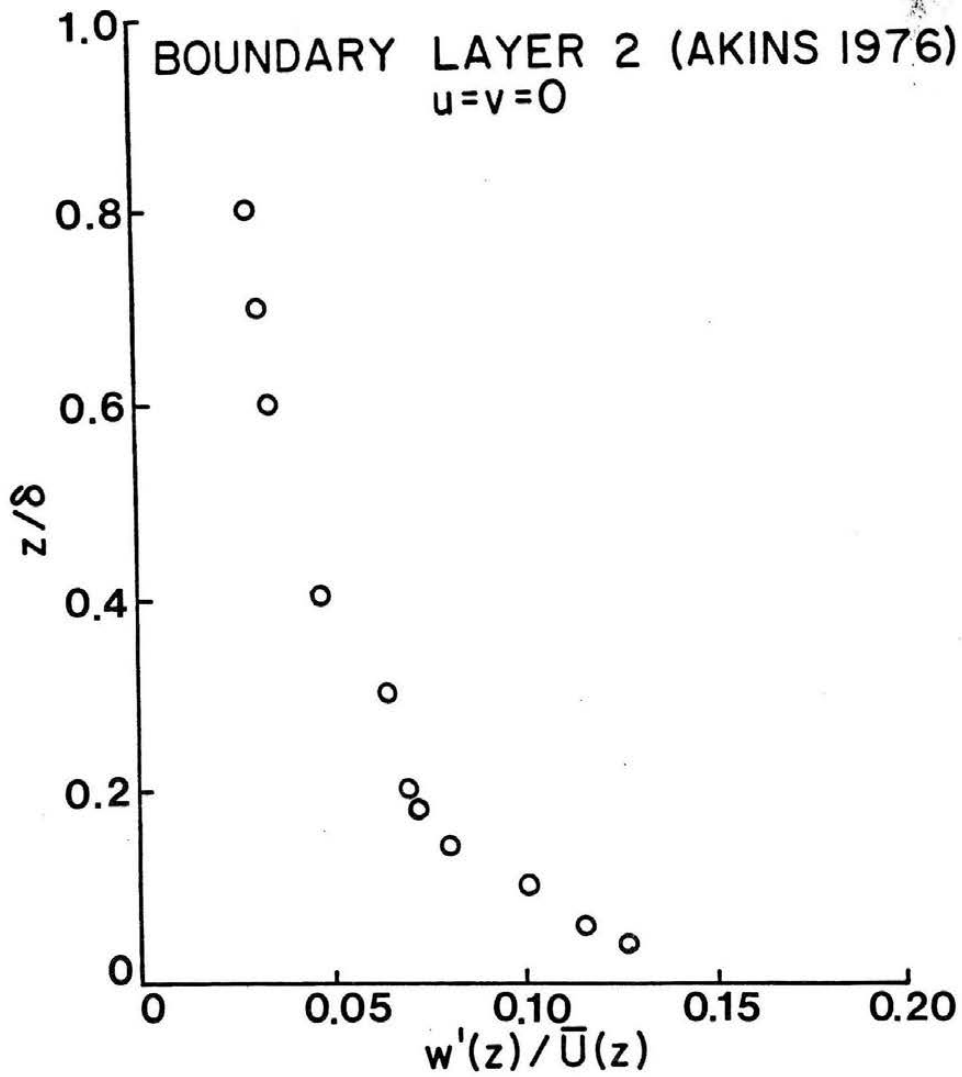


Figure 4.8c. Local Vertical Turbulence Intensity

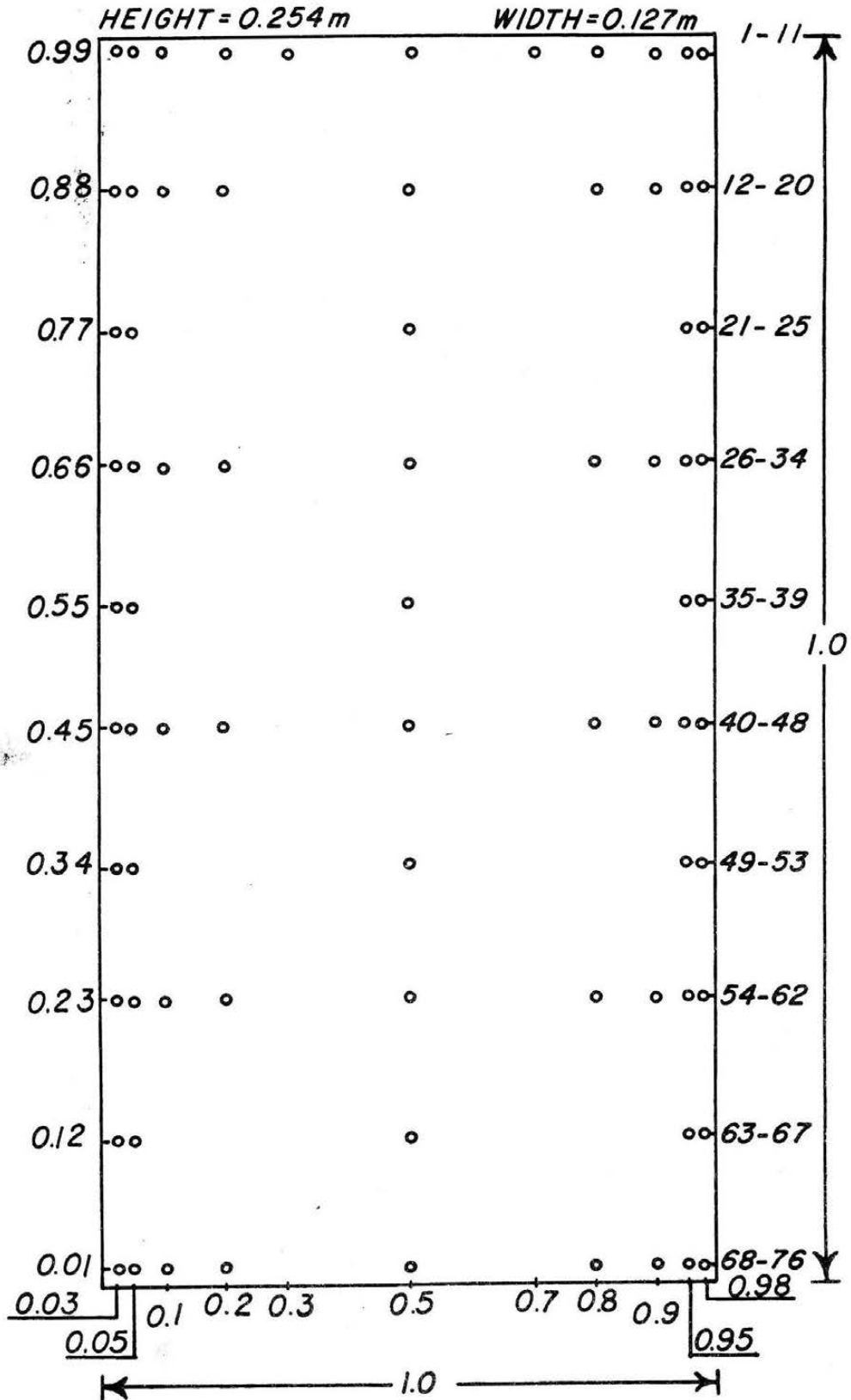


Figure 4.9. Pressure Tap Spacing

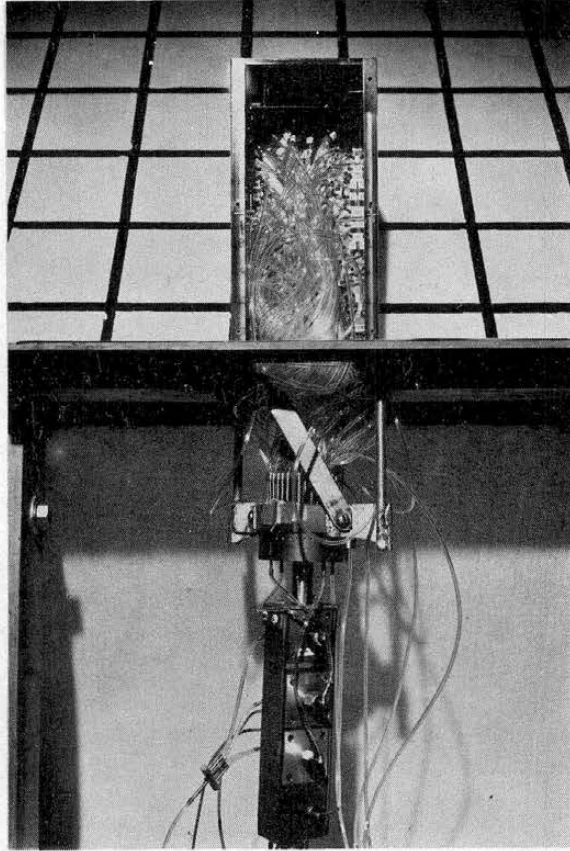


Figure 4.10. Principal Building Showing Pressure Valve and Transducers

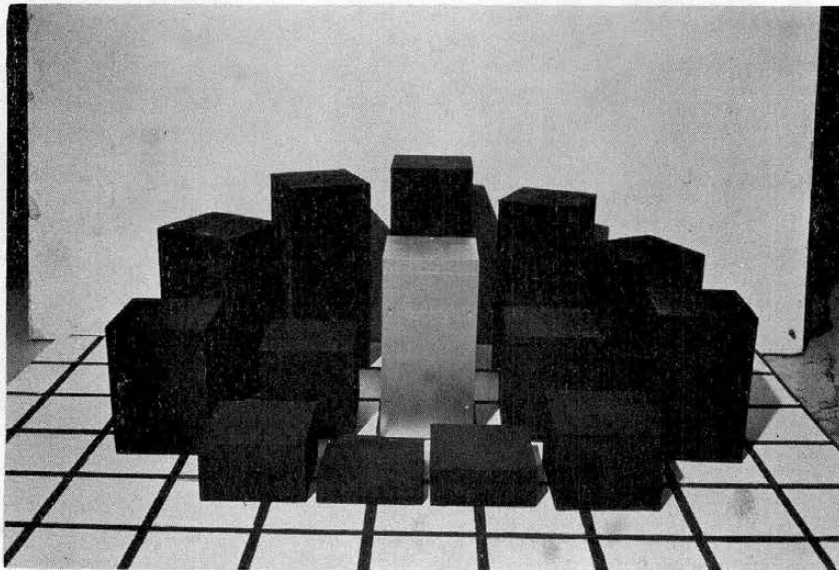


Figure 4.11. Obstructing Buildings and Principal Building

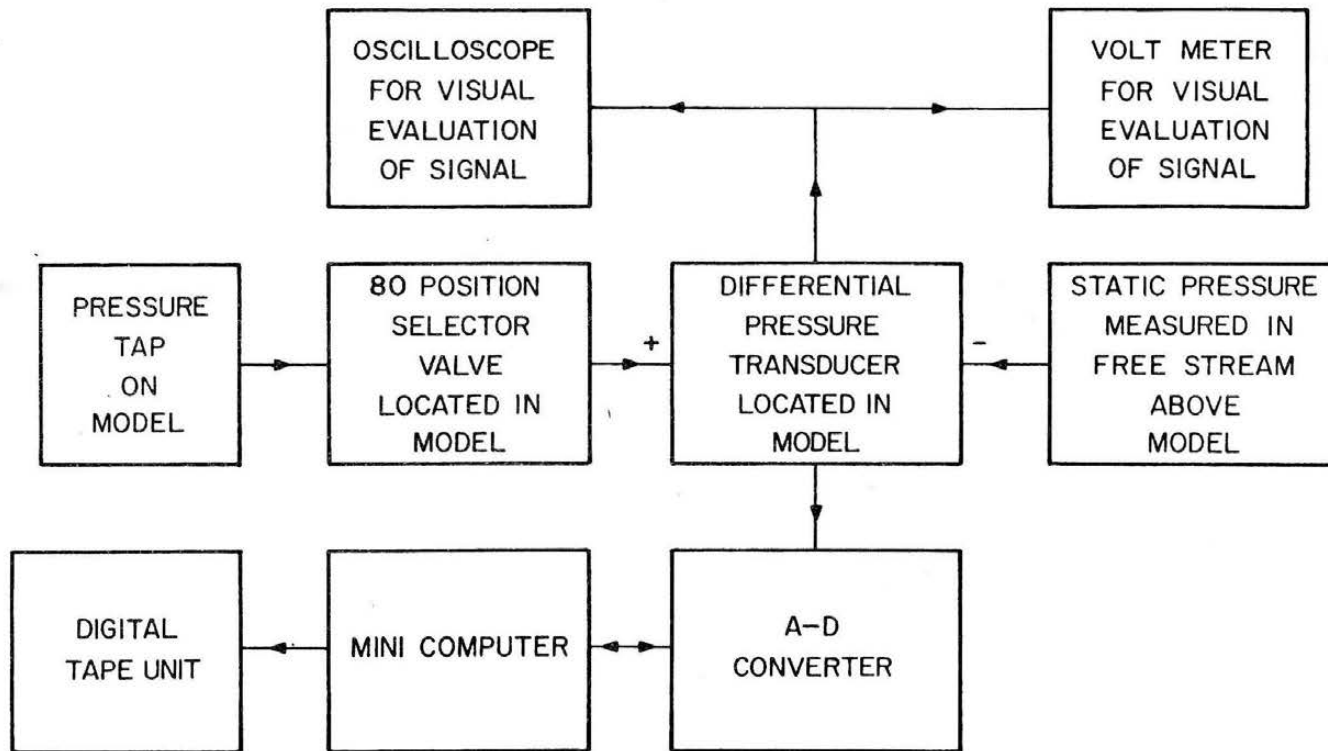


Figure 4.12. Schematic of Data Acquisition System

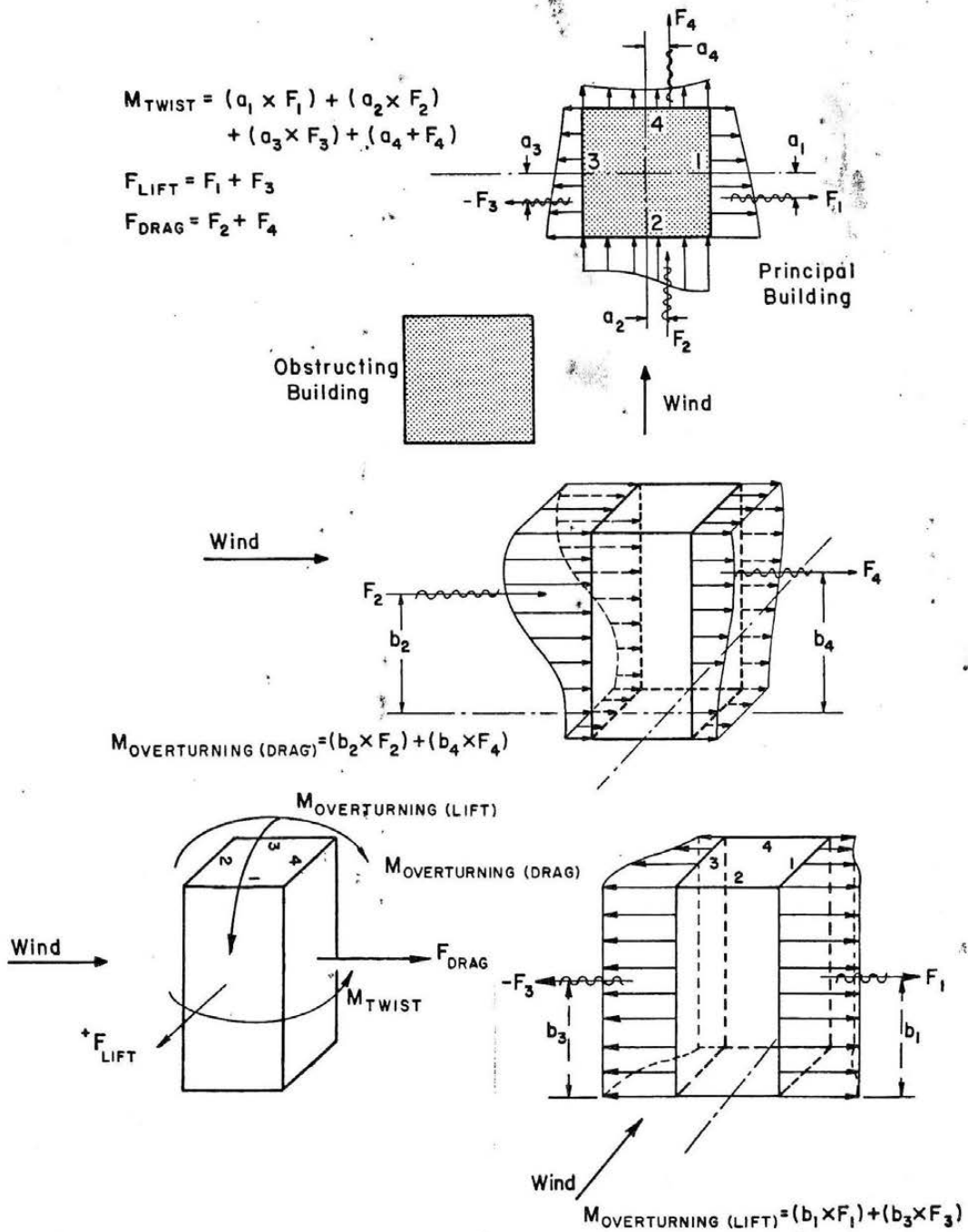


Figure 4.13. Forces and Moments

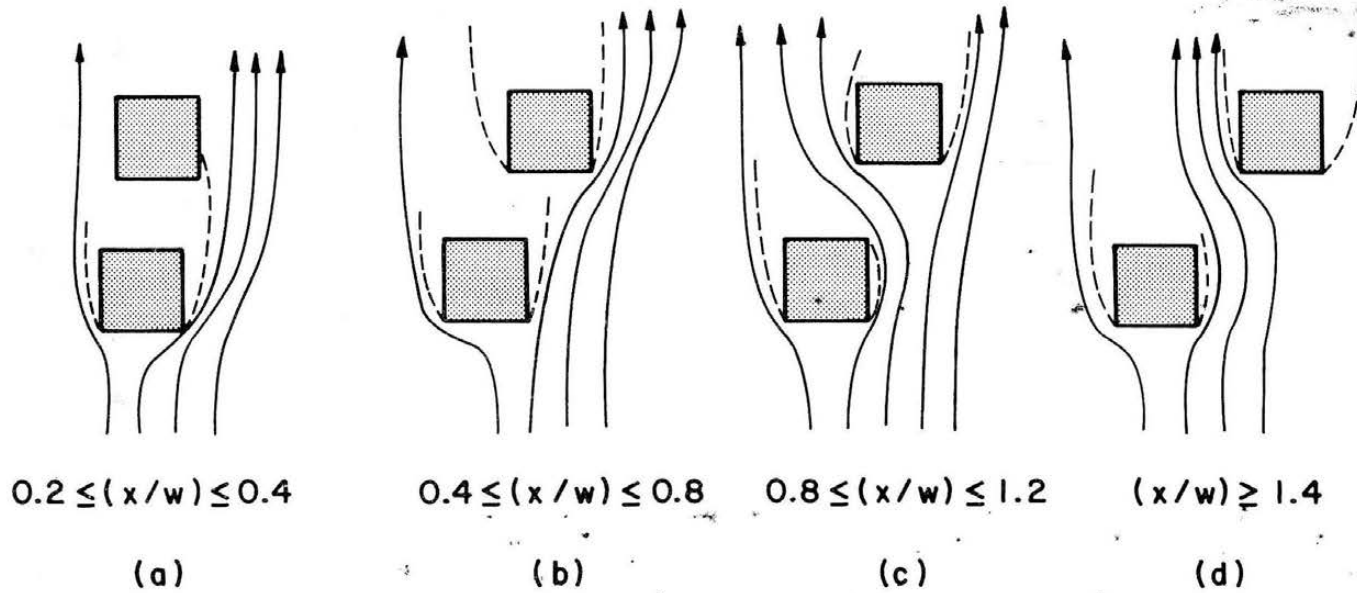


Figure 5.1. Effect of Varying Obstructing Building Placement in the Lateral Direction (Streamlines in the Flow)

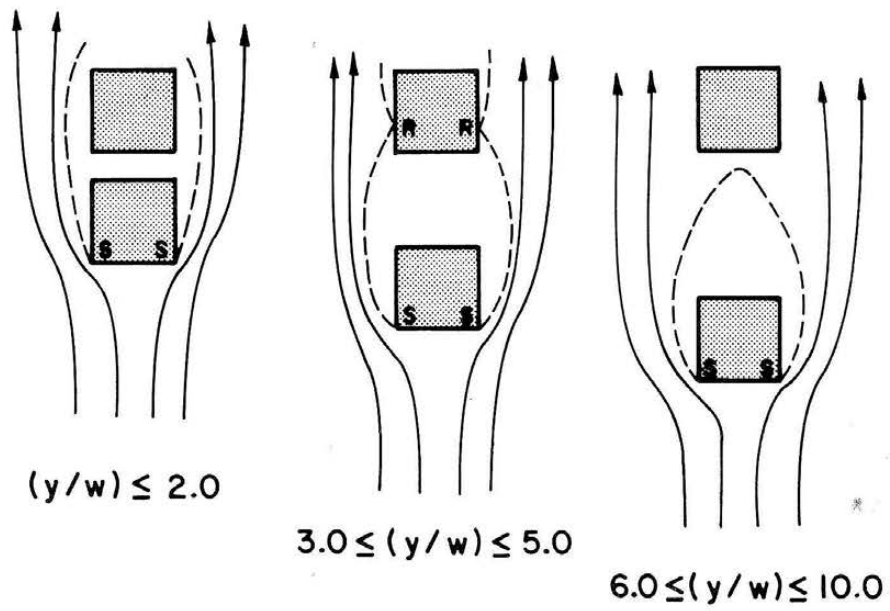
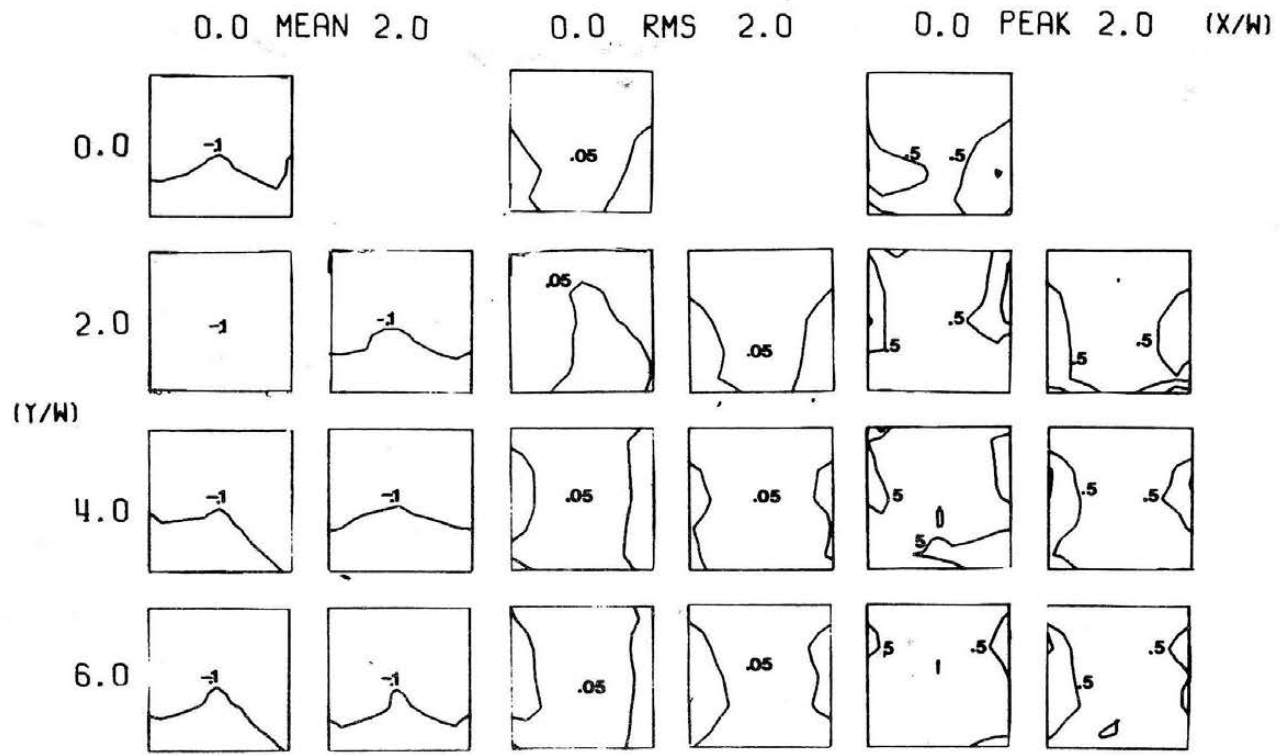


Figure 5.2. Effect of Varying Obstructing Building Placement in the Longitudinal Direction (Streamlines in the Flow)



WIND LOAD INTERACTION ON AN ADJACENT BUILDING

PRESSURE COEFFICIENTS      SIDE 4

Figure 5.3. Pressure Coefficients for Side 4

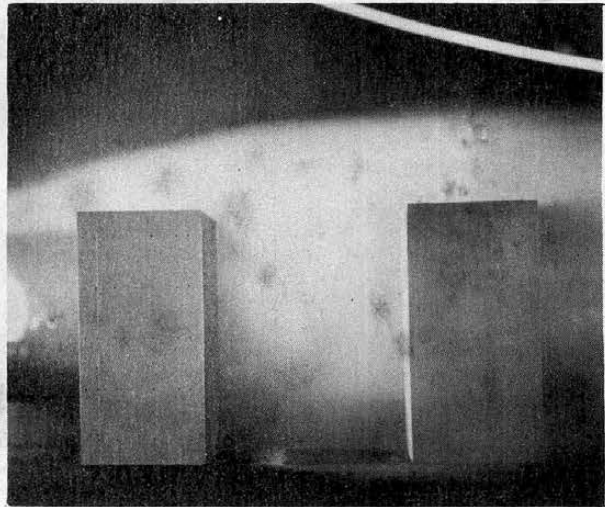
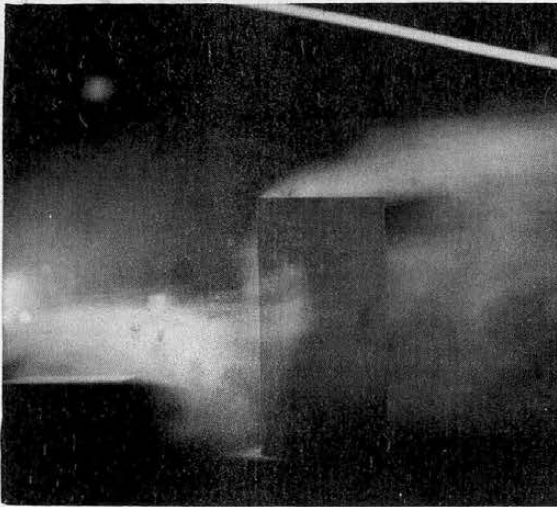
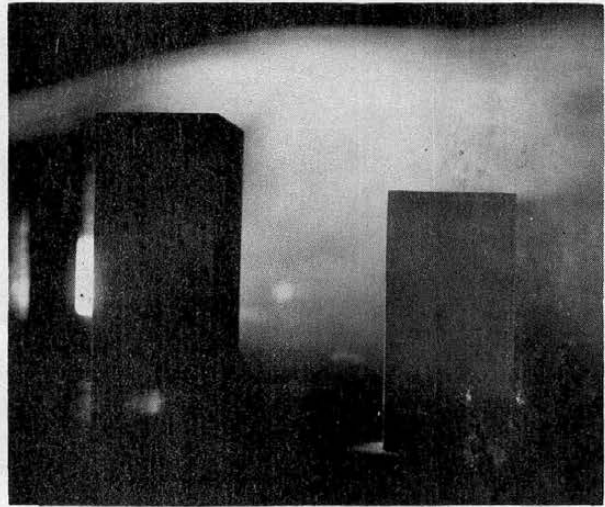
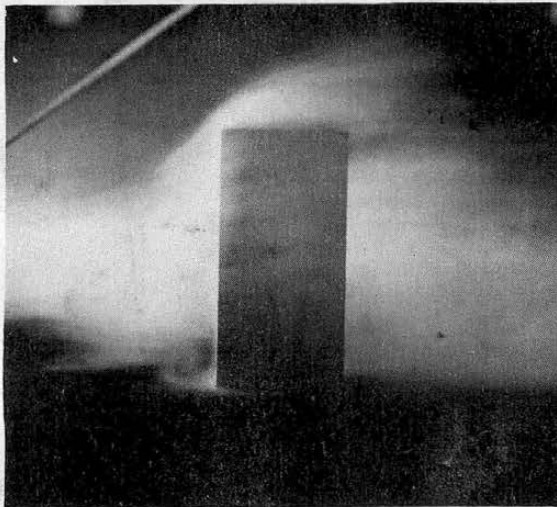
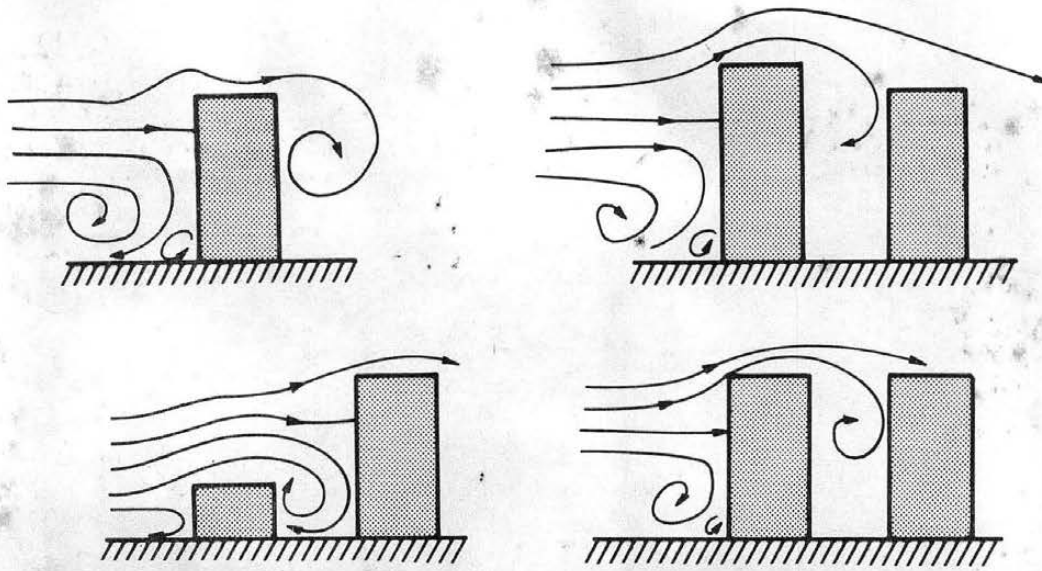


Figure 5.4. Effect of Varying Obstructing Building Height (Streamlines in the Flow and Smoke Visualization)

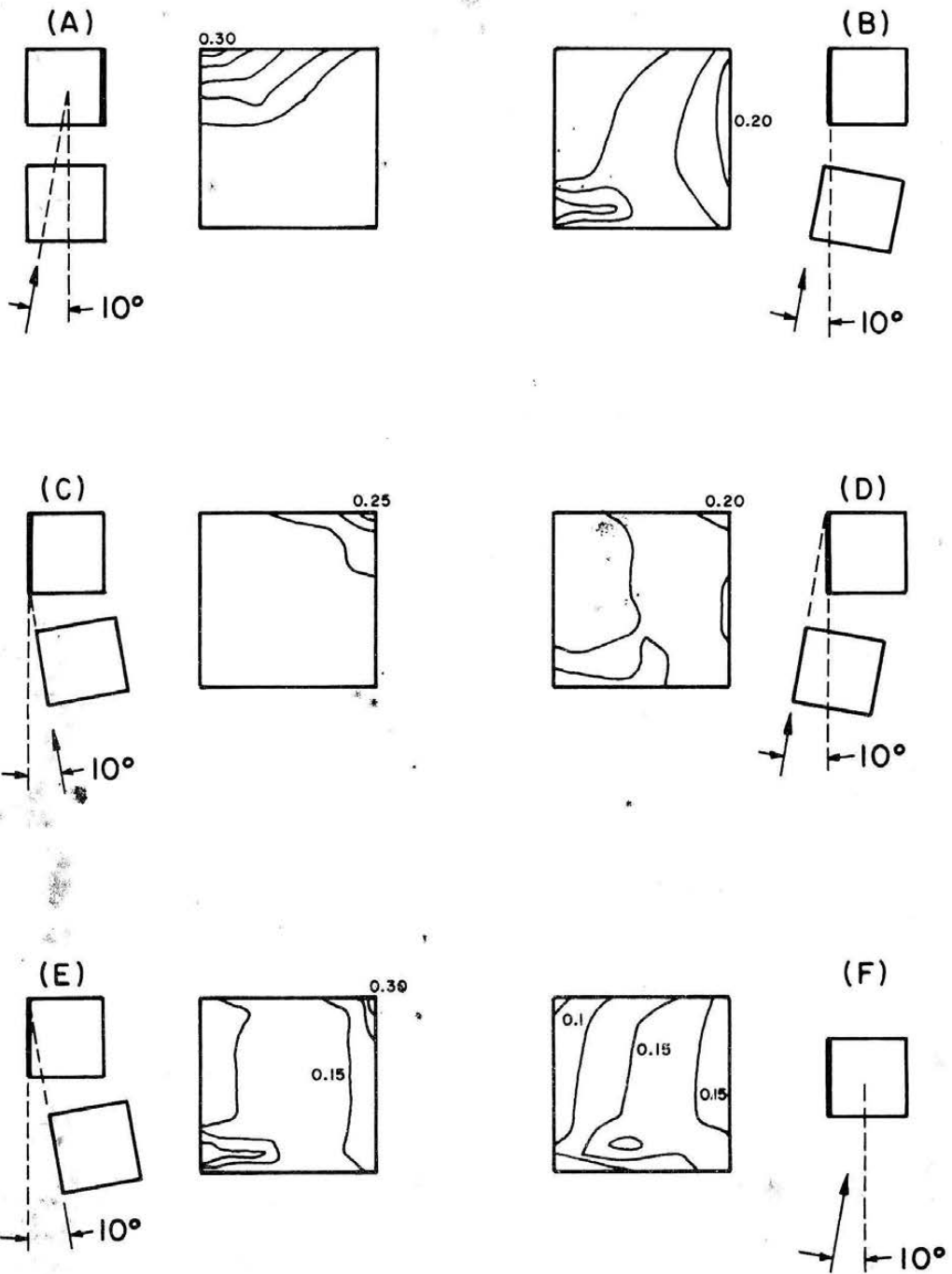
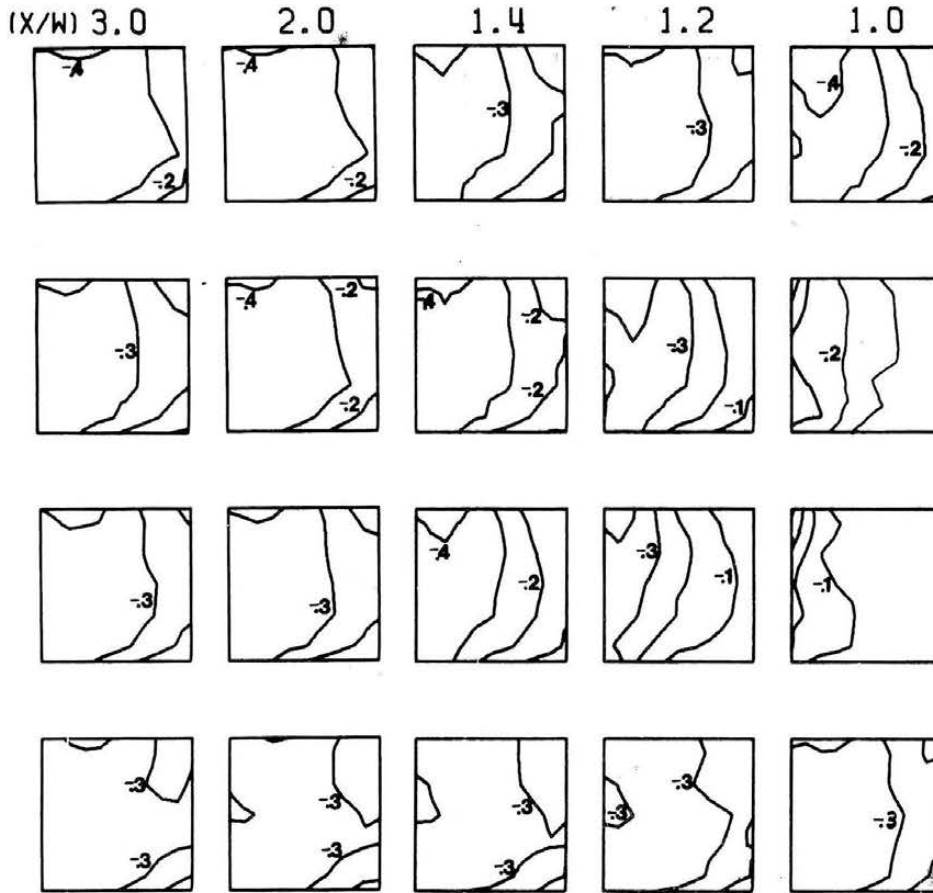


Figure 5.5. RMS Pressure Distribution for Small Changes in Approach Wind Configurations



WIND LOAD INTERACTION ON ADJACENT BUILDINGS  
 MEAN PRESSURE COEFFICIENTS  
 SIDE 1



Figure 5.6a. Mean Pressure Coefficients, Set A, Side 1

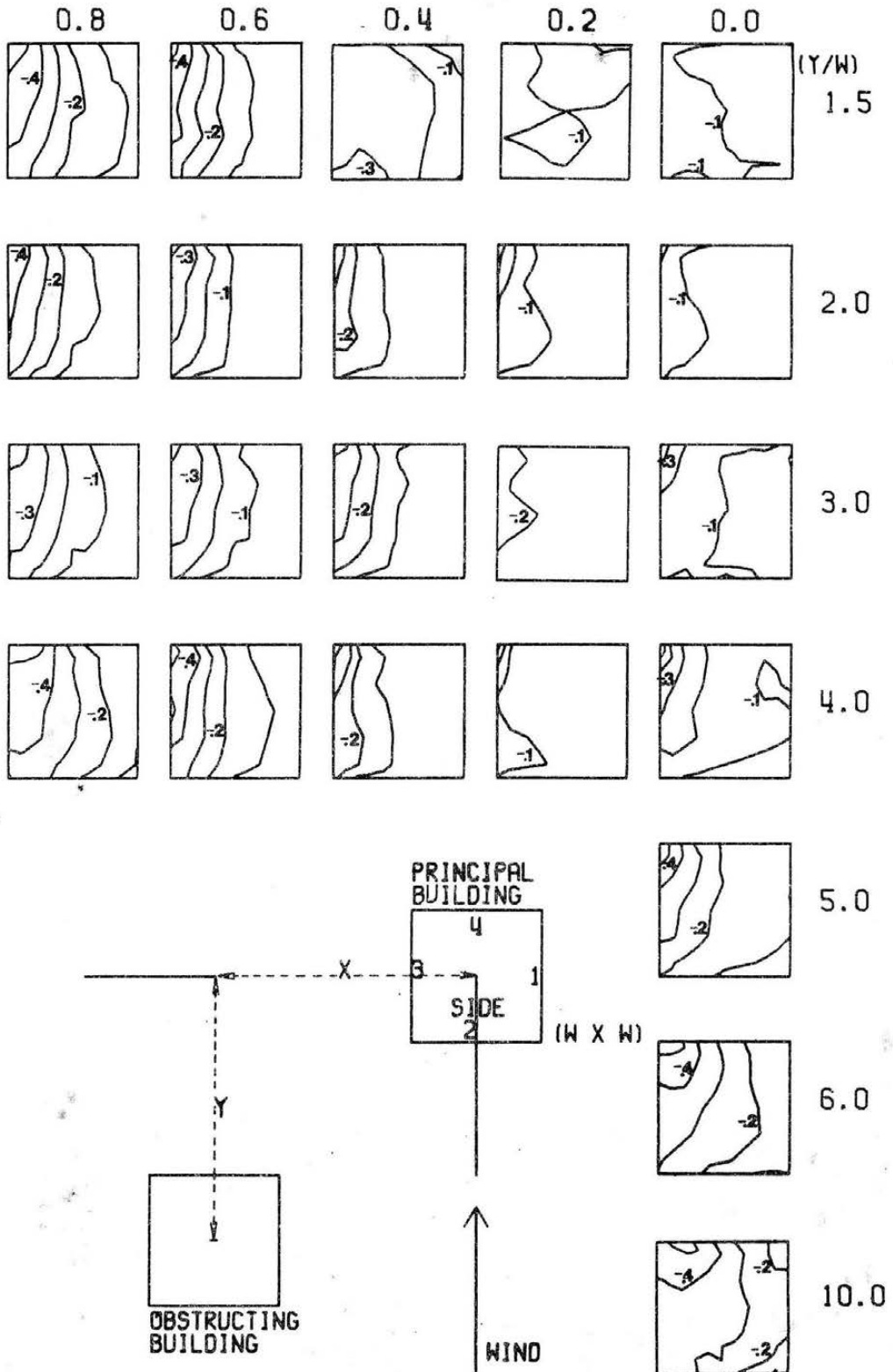
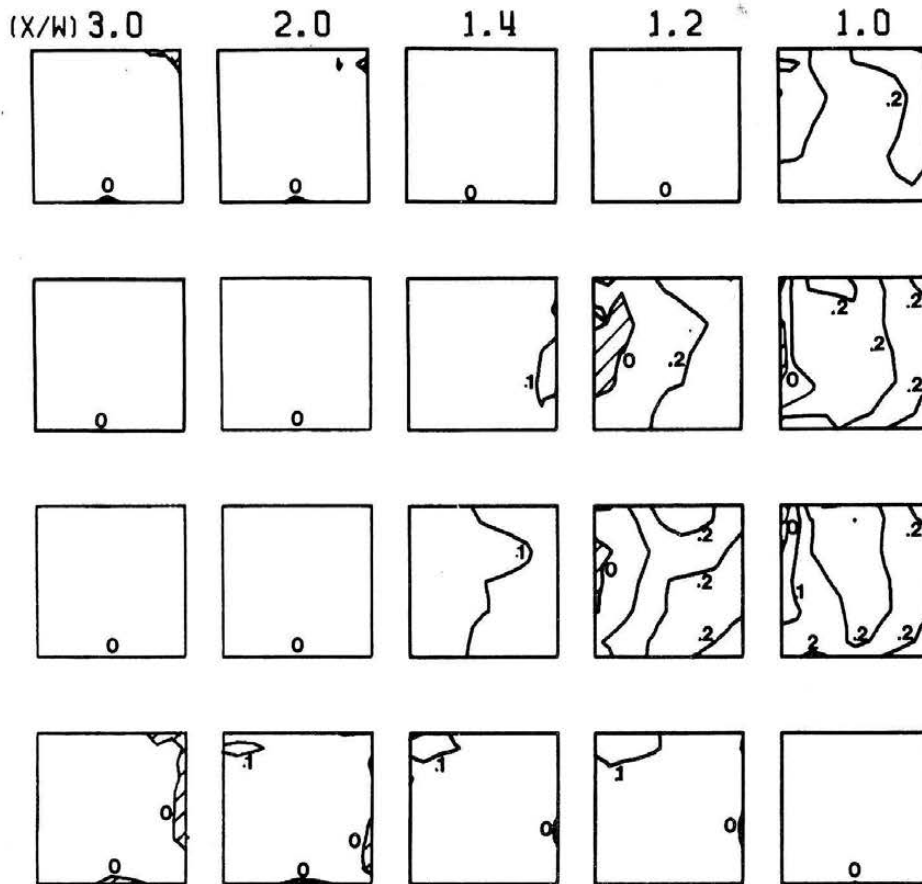


Figure 5.6a (continued)



ADVERSE (-) AND BENEFICIAL (+) WIND LOADING  
 MEAN PRESSURE COEFFICIENTS  
 SIDE 1



Figure 5.6b. Mean Pressure Effects, Set A, Side 1

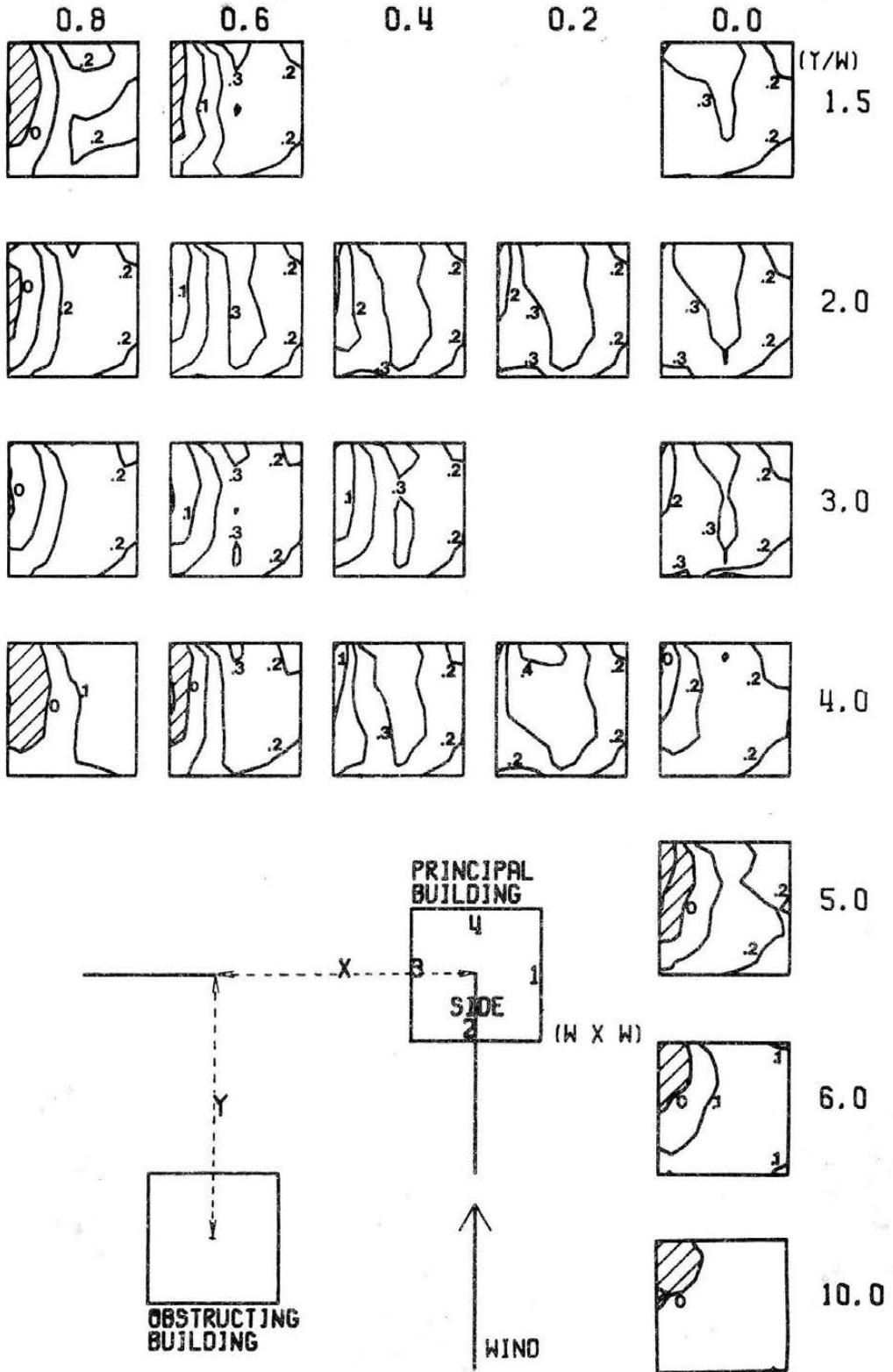
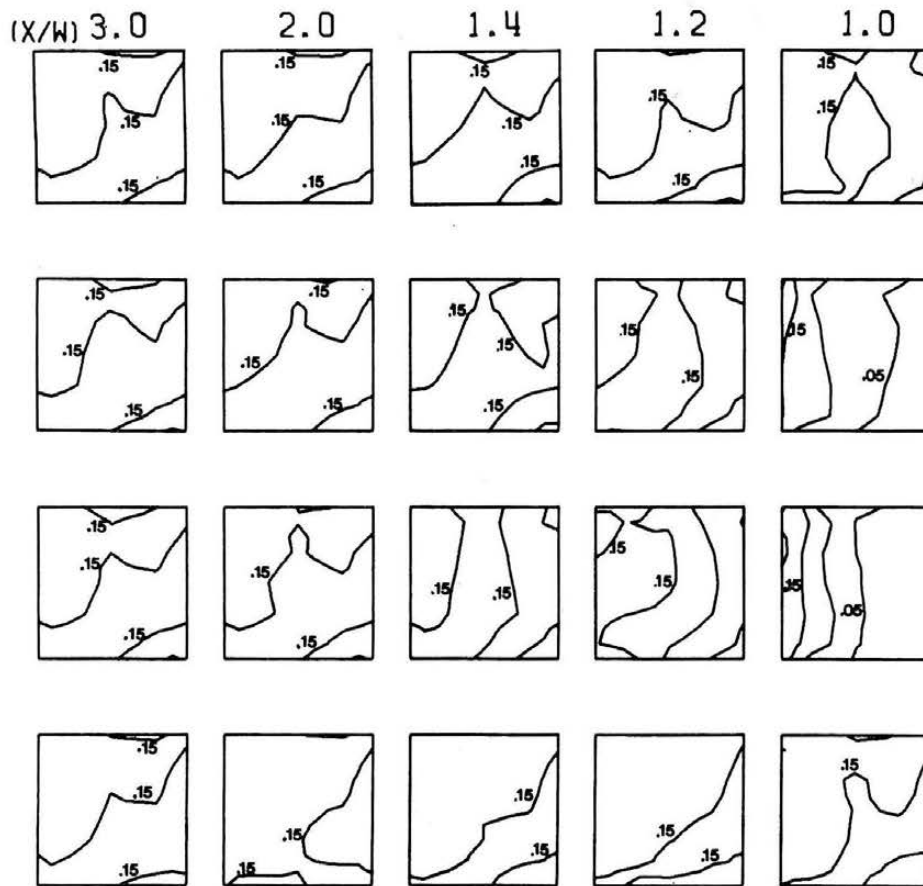


Figure 5.6b (continued)



WIND LOAD INTERACTION ON ADJACENT BUILDINGS  
 RMS PRESSURE COEFFICIENTS  
 SIDE 1

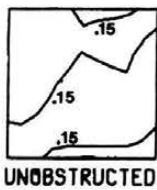


Figure 5.6c. RMS Pressure Coefficients, Set A, Side 1

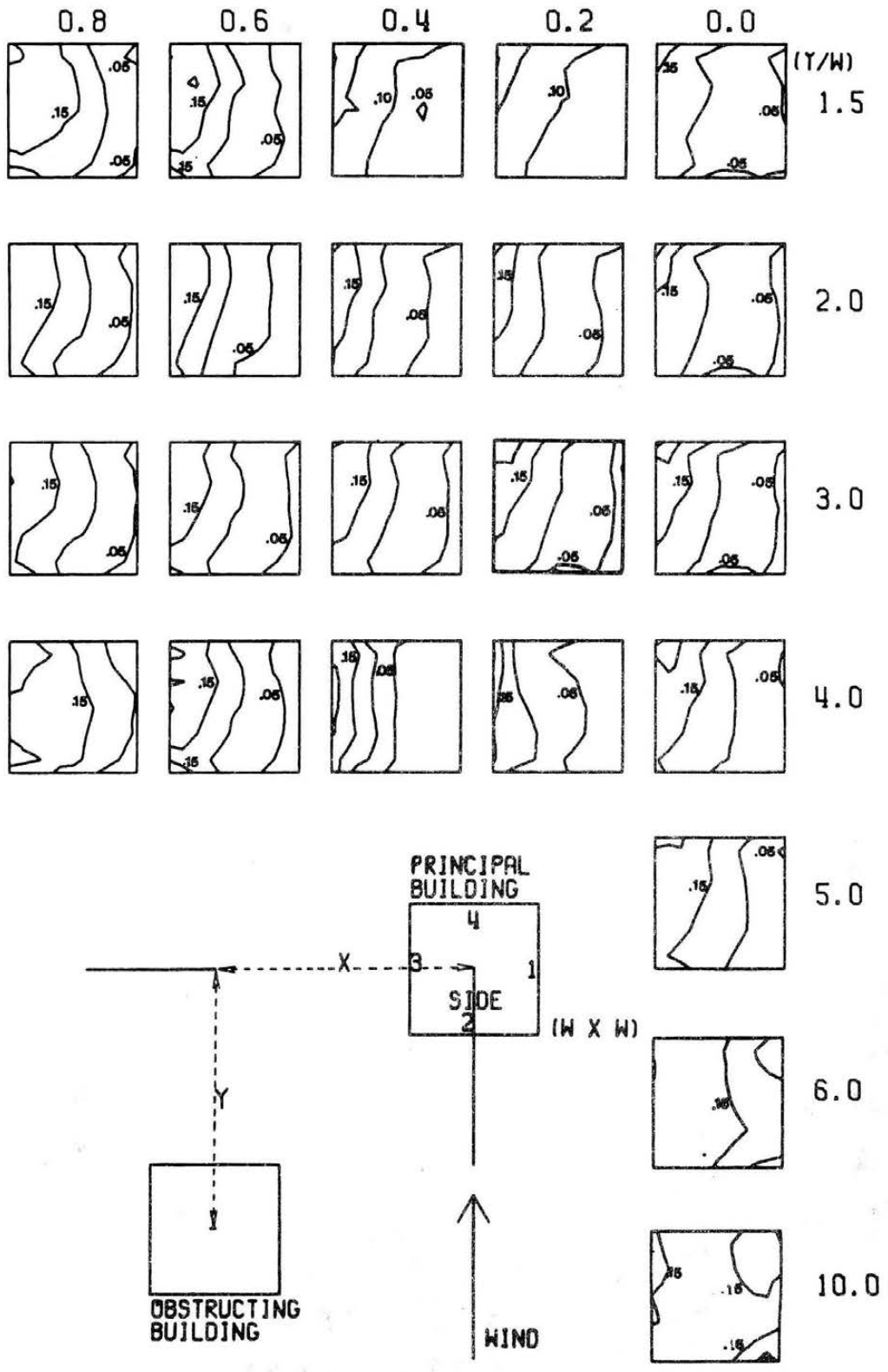
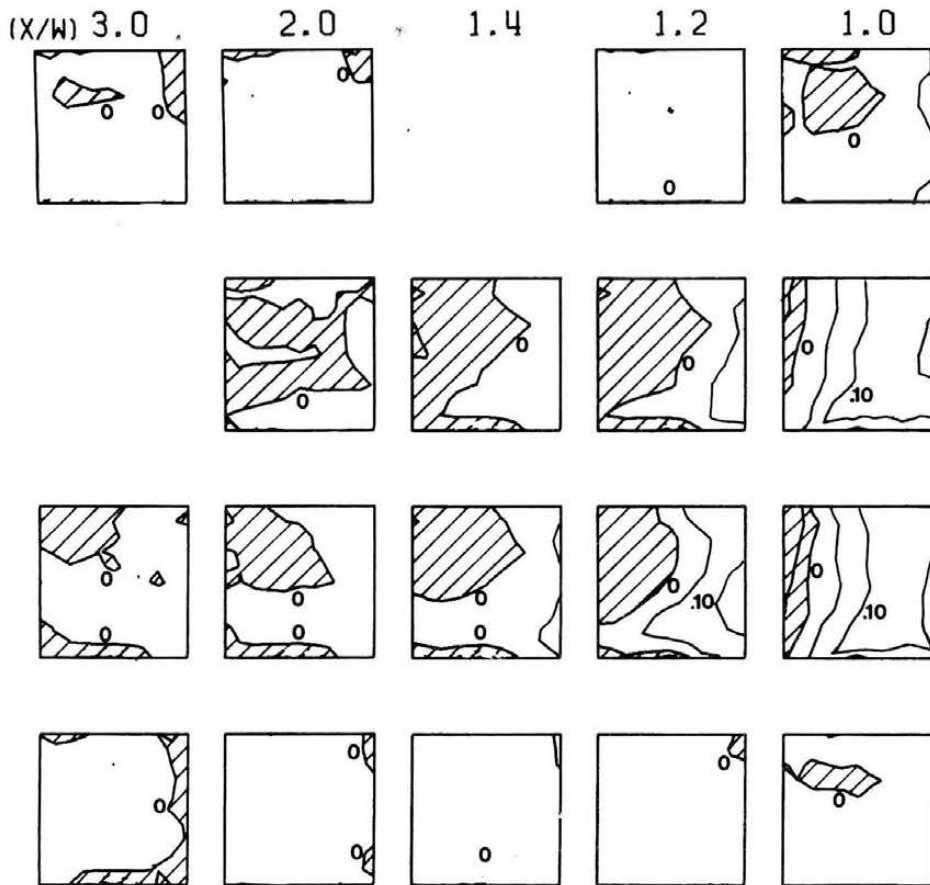


Figure 5.6c (continued)



ADVERSE (-) AND BENEFICIAL (+) WIND LOADING  
RMS PRESSURE COEFFICIENTS  
SIDE 1

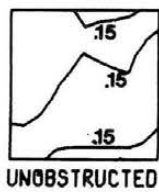


Figure 5.6d. RMS Pressure Effects, Set A, Side 1

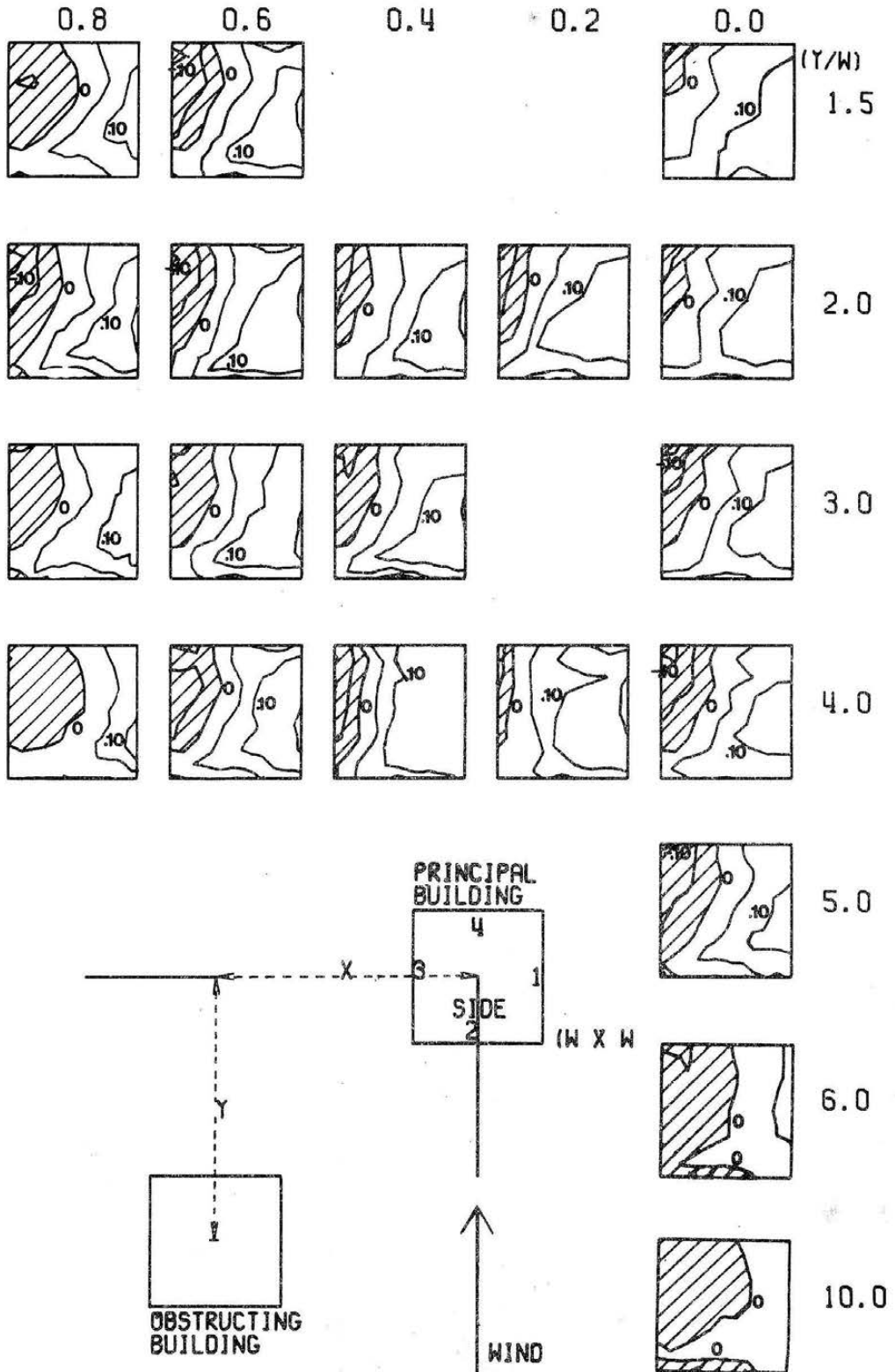
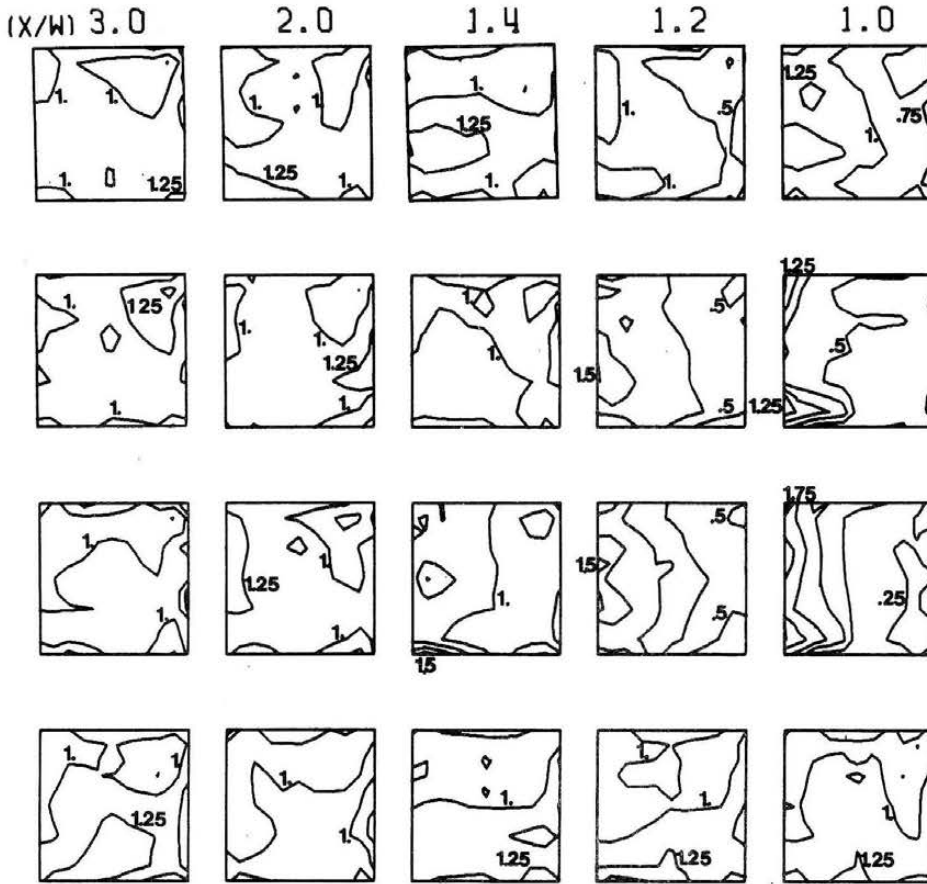


Figure 5.6d (continued)



WIND LOAD INTERACTION ON ADJACENT BUILDINGS  
 PEAK PRESSURE COEFFICIENTS  
 SIDE 1

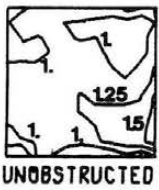
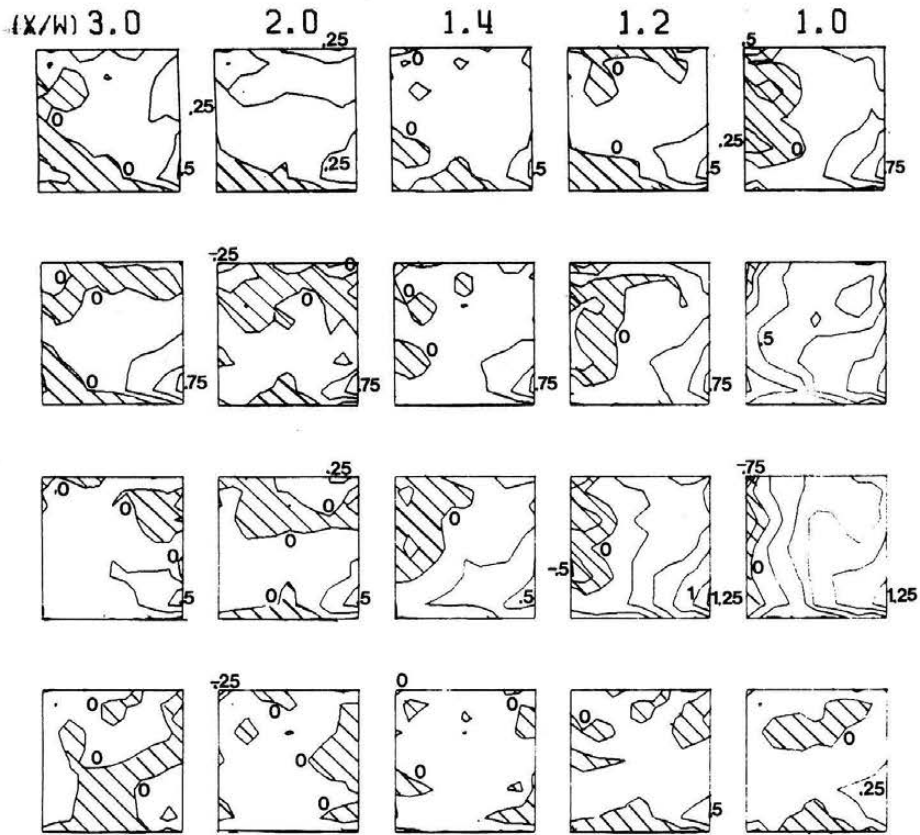


Figure 5.6e. Peak Pressure Coefficients, Set A, Side 1





ADVERSE (-) AND BENEFICIAL (+) WIND LOADING  
 PEAK PRESSURE COEFFICIENTS  
 SIDE 1

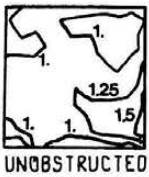


Figure 5.6f. Peak Pressure Effects, Set A, Side 1

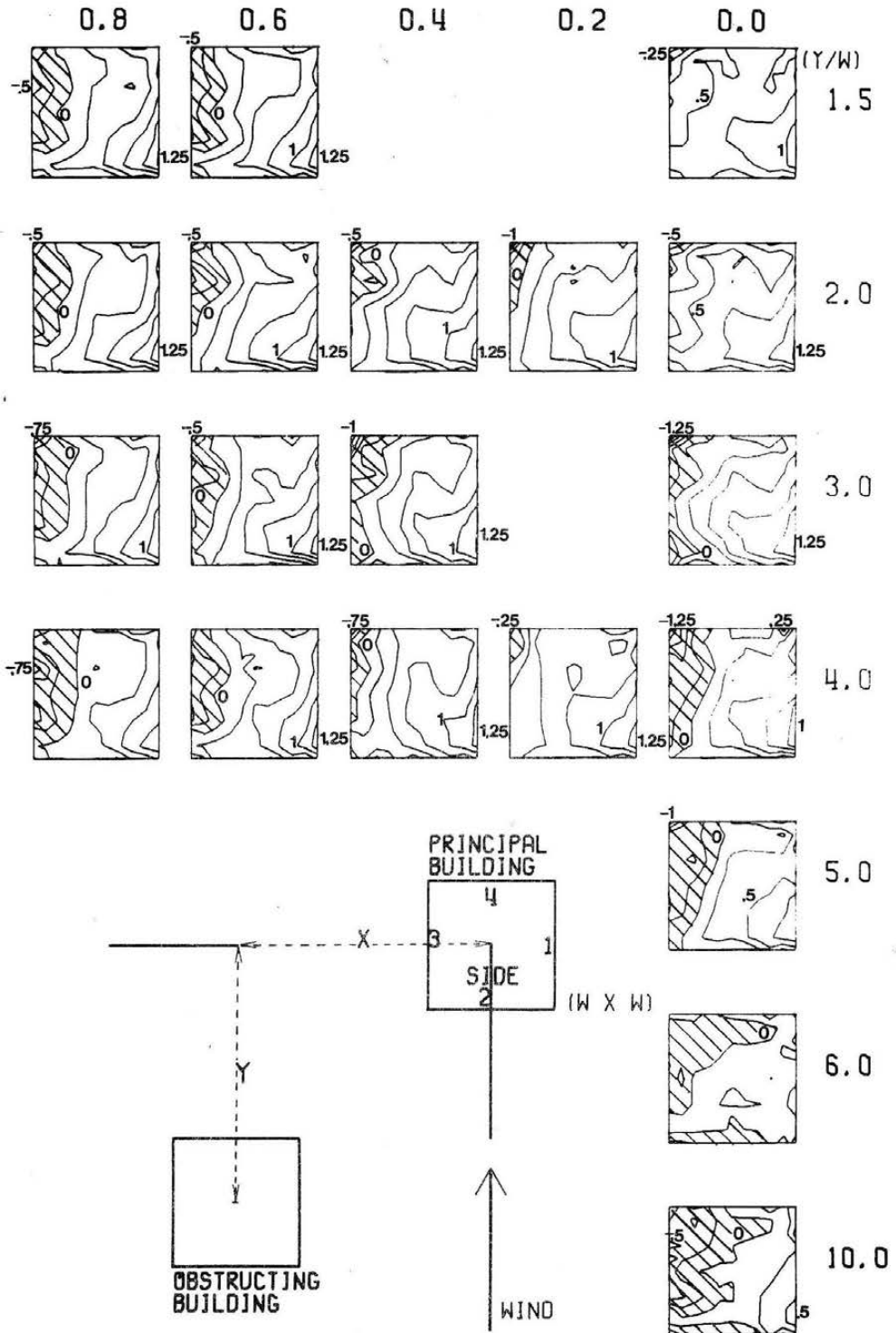
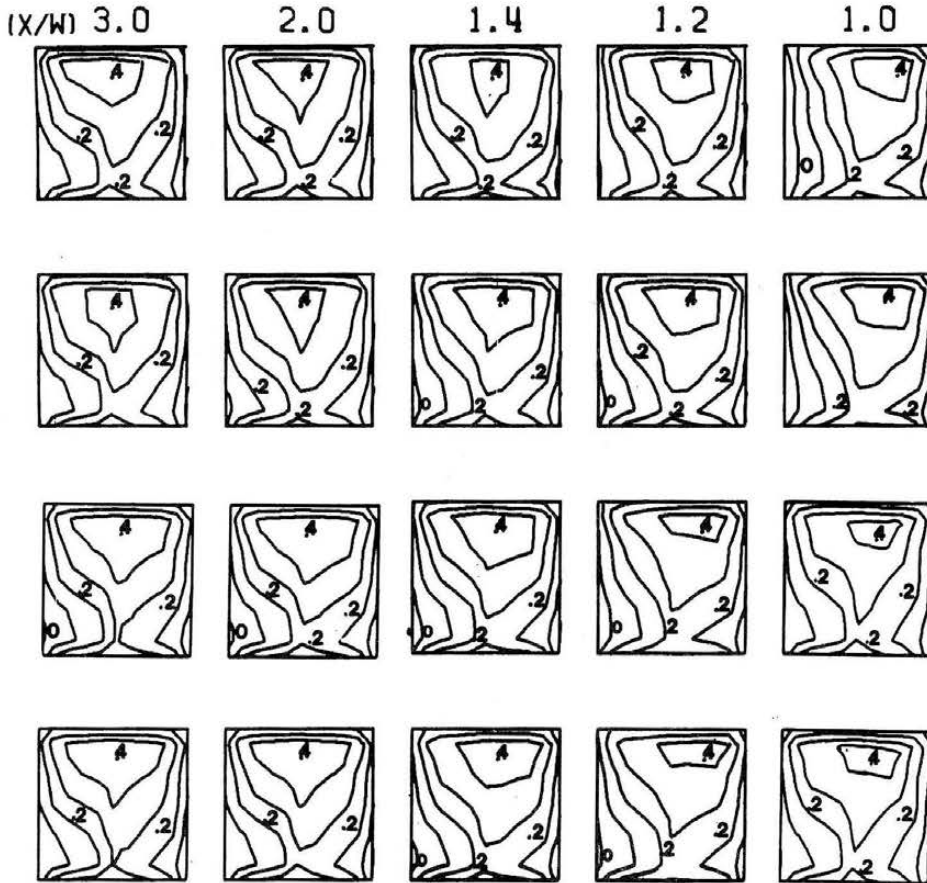


Figure 5.6f (continued)



WIND LOAD INTERACTION ON ADJACENT BUILDINGS  
 MEAN PRESSURE COEFFICIENTS  
 SIDE 2



Figure 5.7a. Mean Coefficients, Set A, Side 2

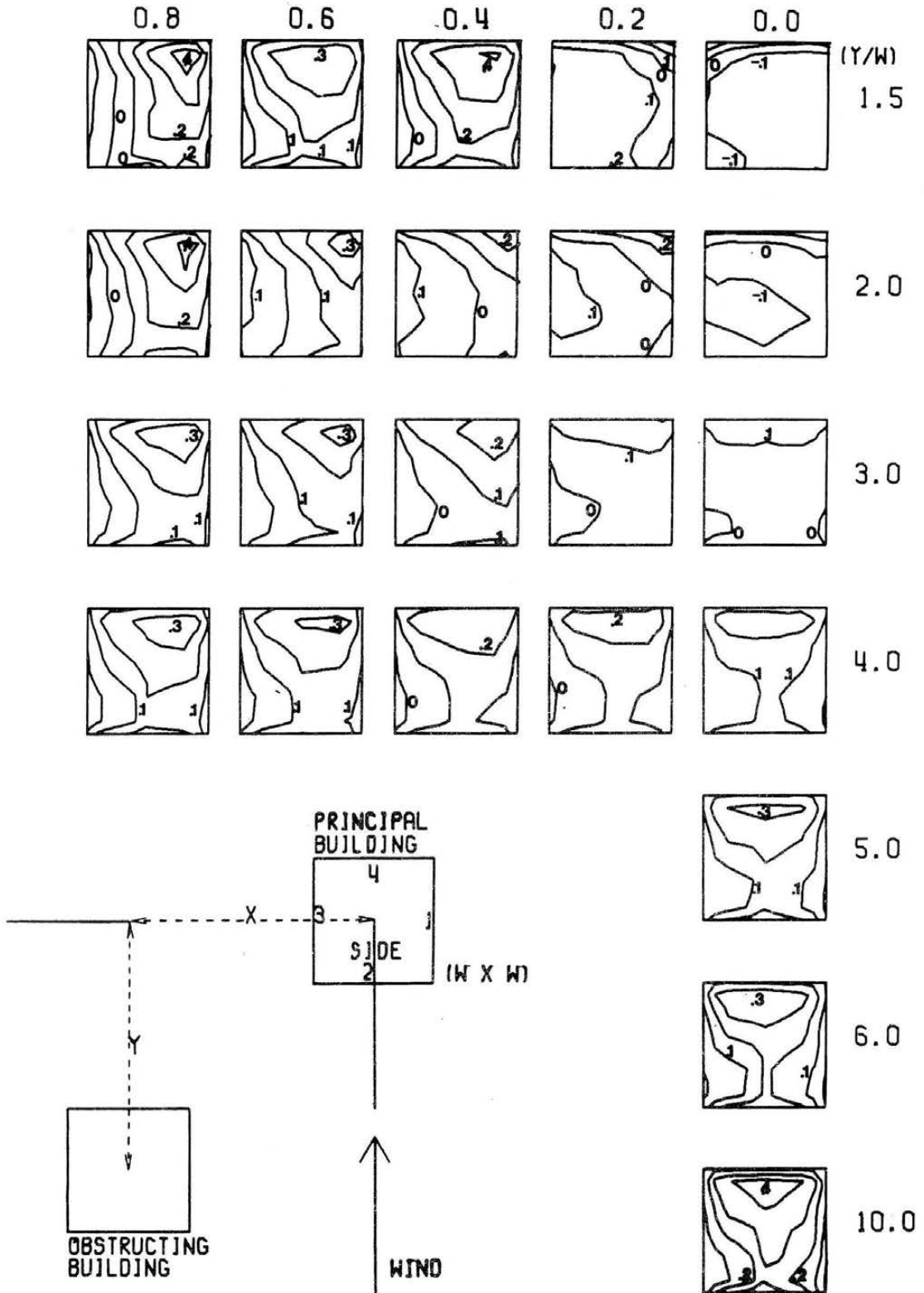
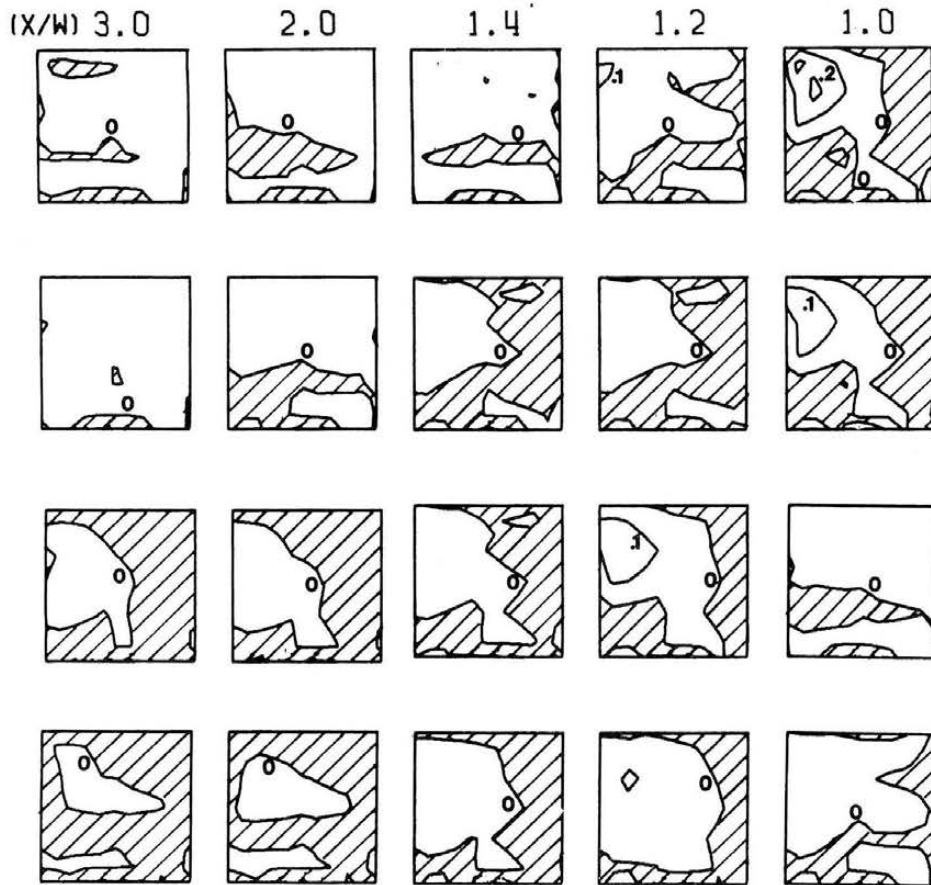


Figure 5.7a (continued)



ADVERSE (↖) AND BENEFICIAL (+) WIND LOADING  
 MEAN PRESSURE COEFFICIENTS  
 SIDE 2



Figure 5.7b. Mean Pressure Effects, Set A, Side 2

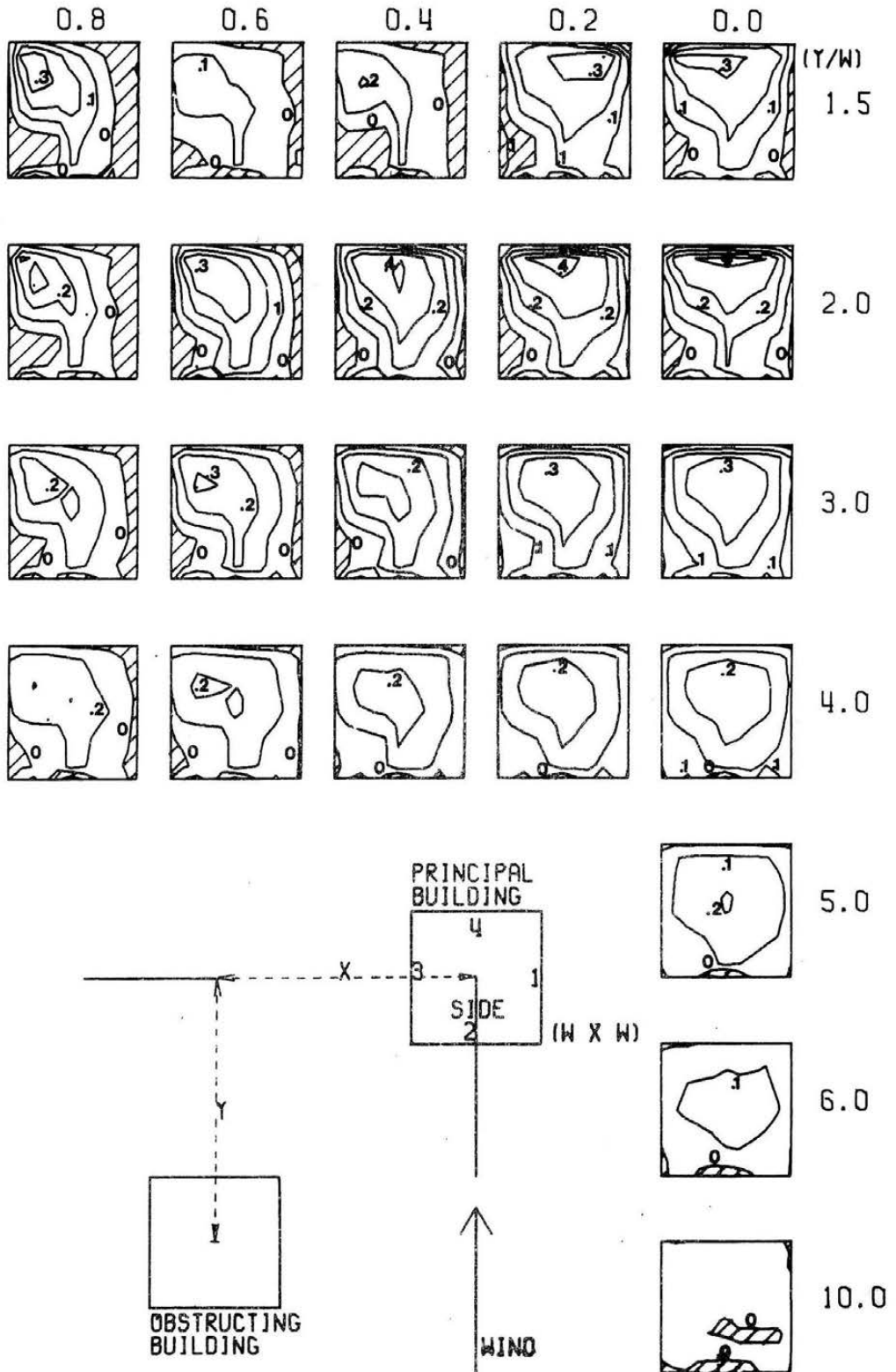
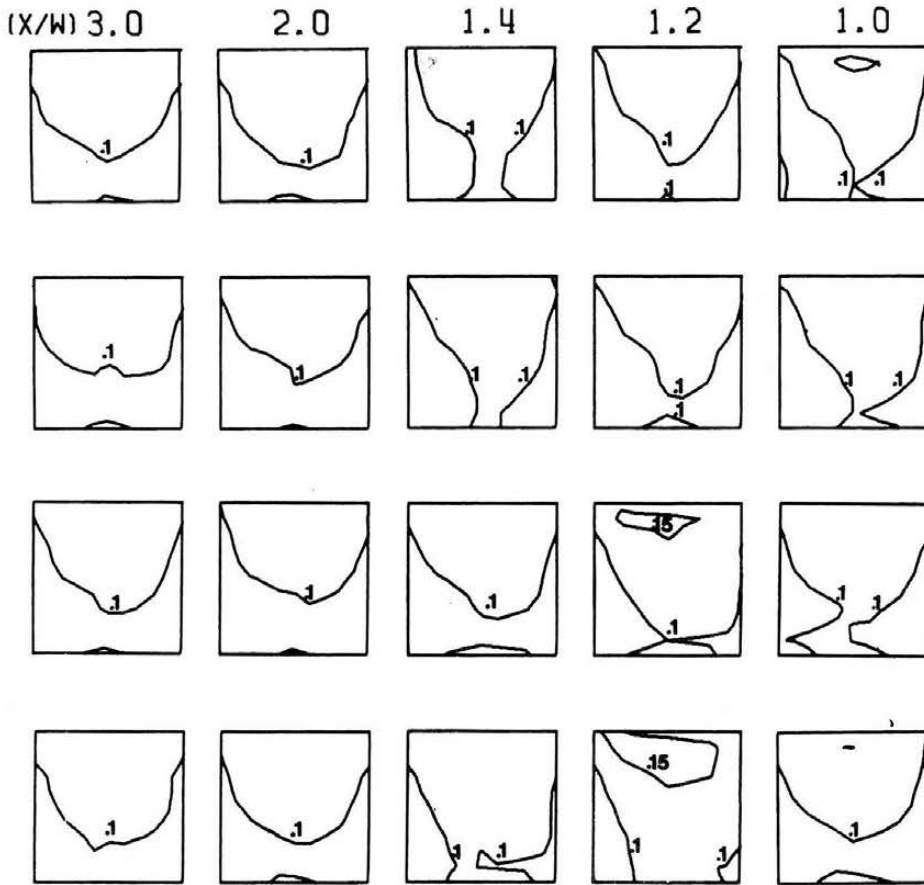


Figure 5.7b (continued)



WIND LOAD INTERACTION ON ADJACENT BUILDINGS  
 RMS PRESSURE COEFFICIENTS  
 SIDE 2

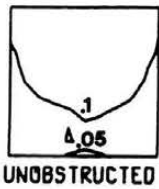


Figure 5.7c. RMS Pressure Coefficients, Set A, Side 2

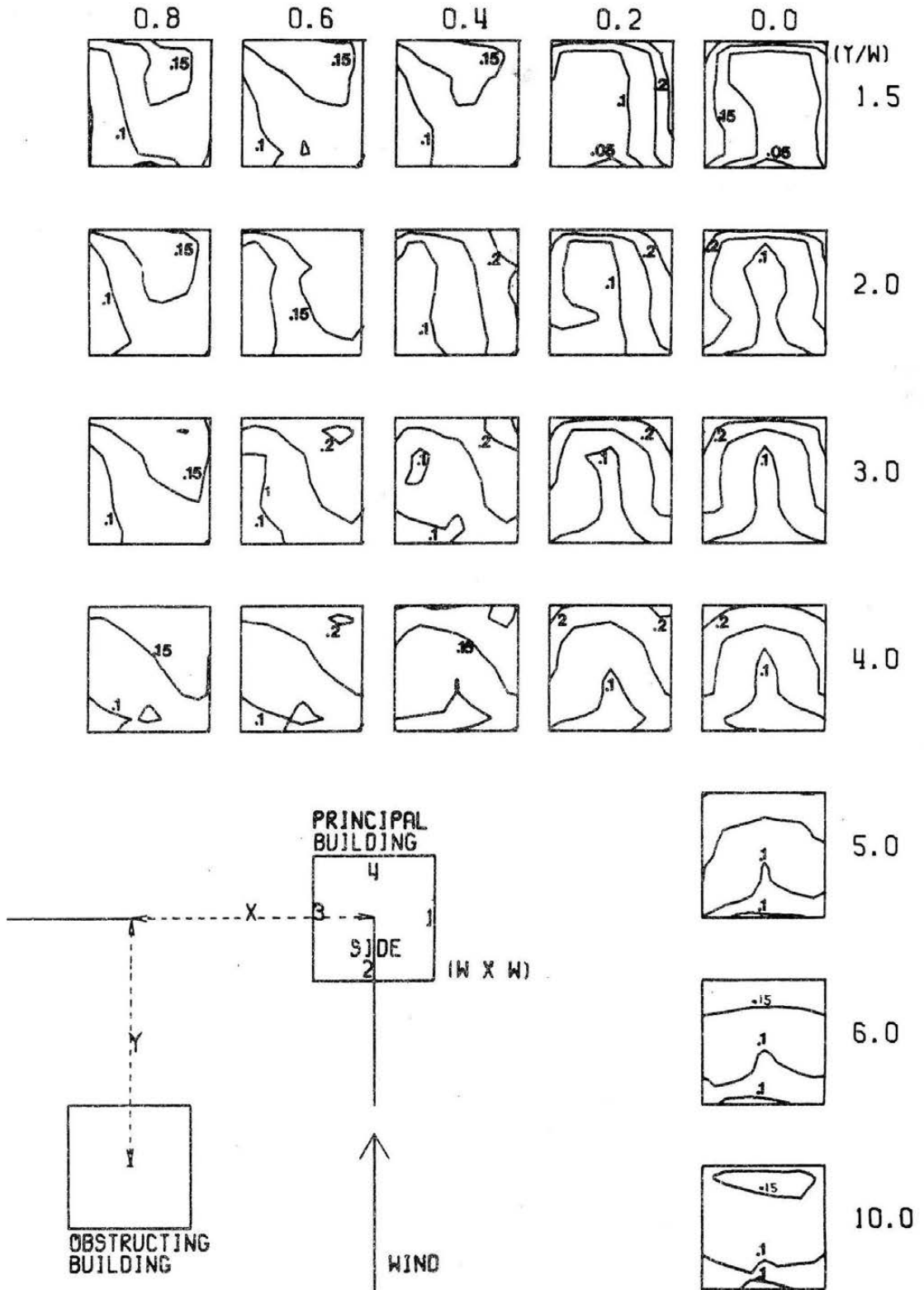
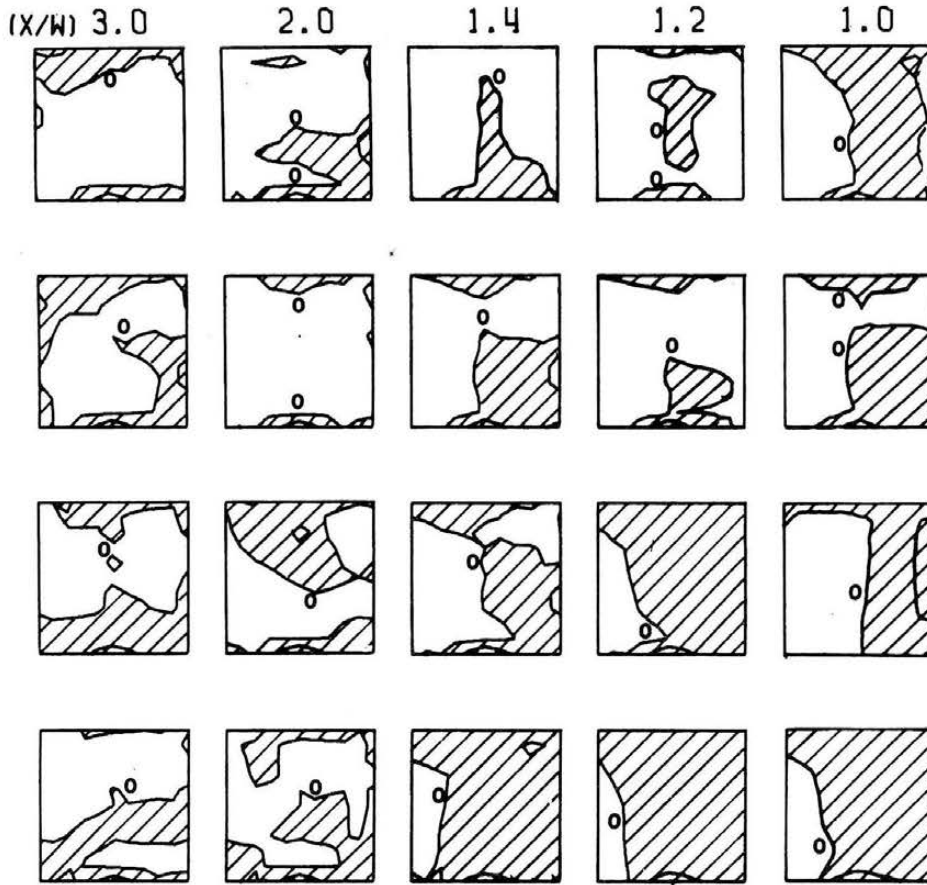


Figure 5.7c (continued)



ADVERSE ( $\ominus$ ) AND BENEFICIAL ( $\oplus$ ) WIND LOADING  
 RMS PRESSURE COEFFICIENTS  
 SIDE 2

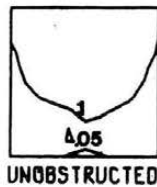


Figure 5.7d. RMS Pressure Effects, Set A, Side 2

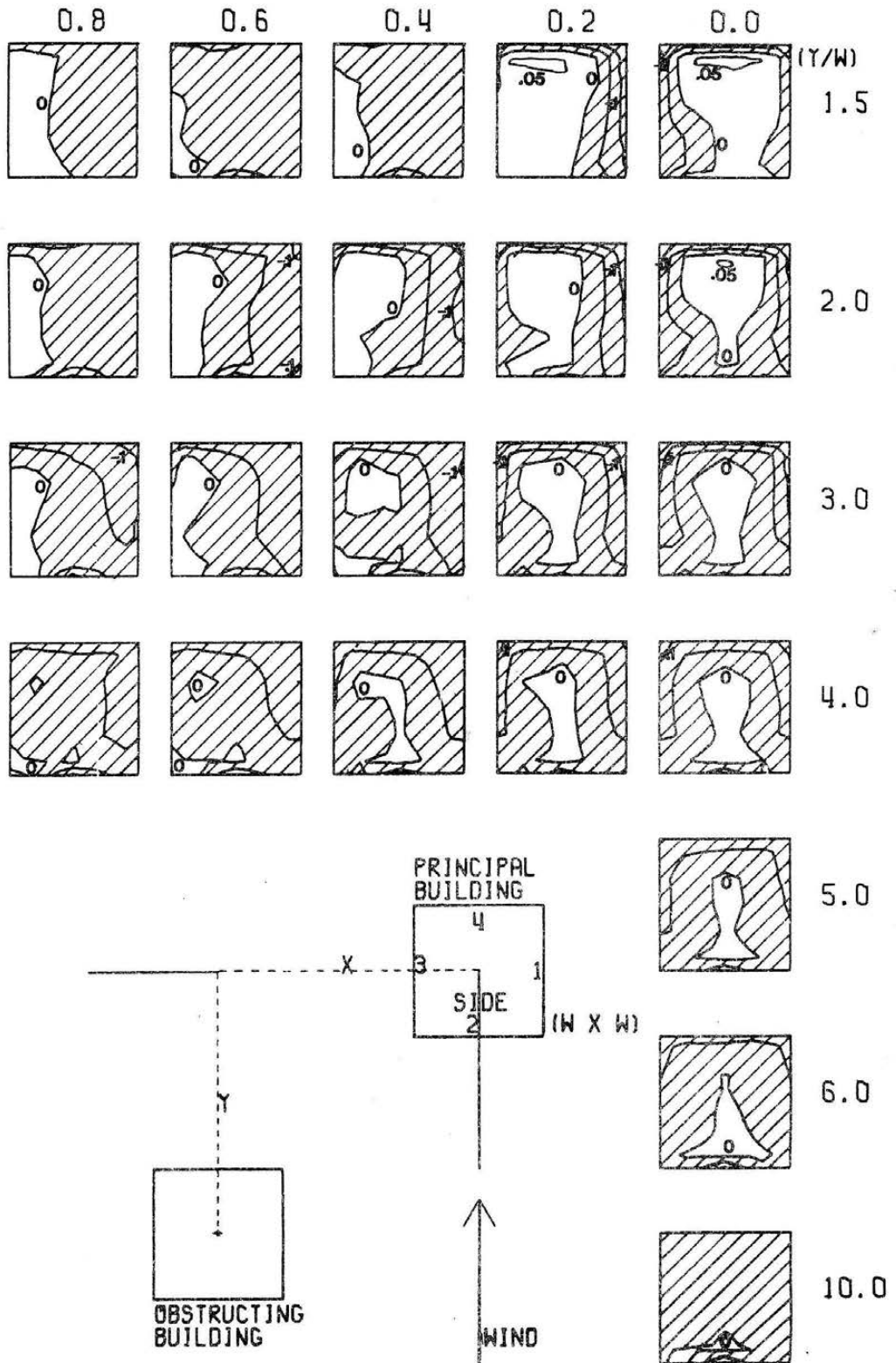
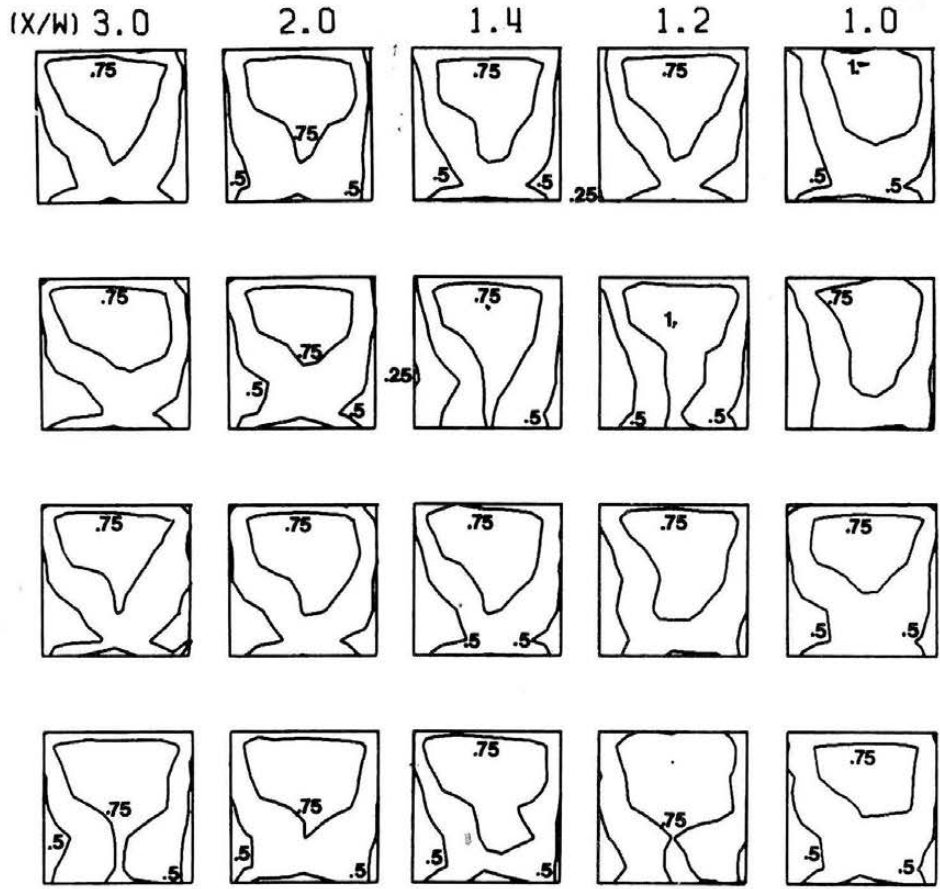


Figure 5.7d (continued)



WIND LOAD INTERACTION ON ADJACENT BUILDINGS  
 PEAK PRESSURE COEFFICIENTS  
 SIDE 2



Figure 5.7e. Peak Pressure Coefficients, Set A, Side 2

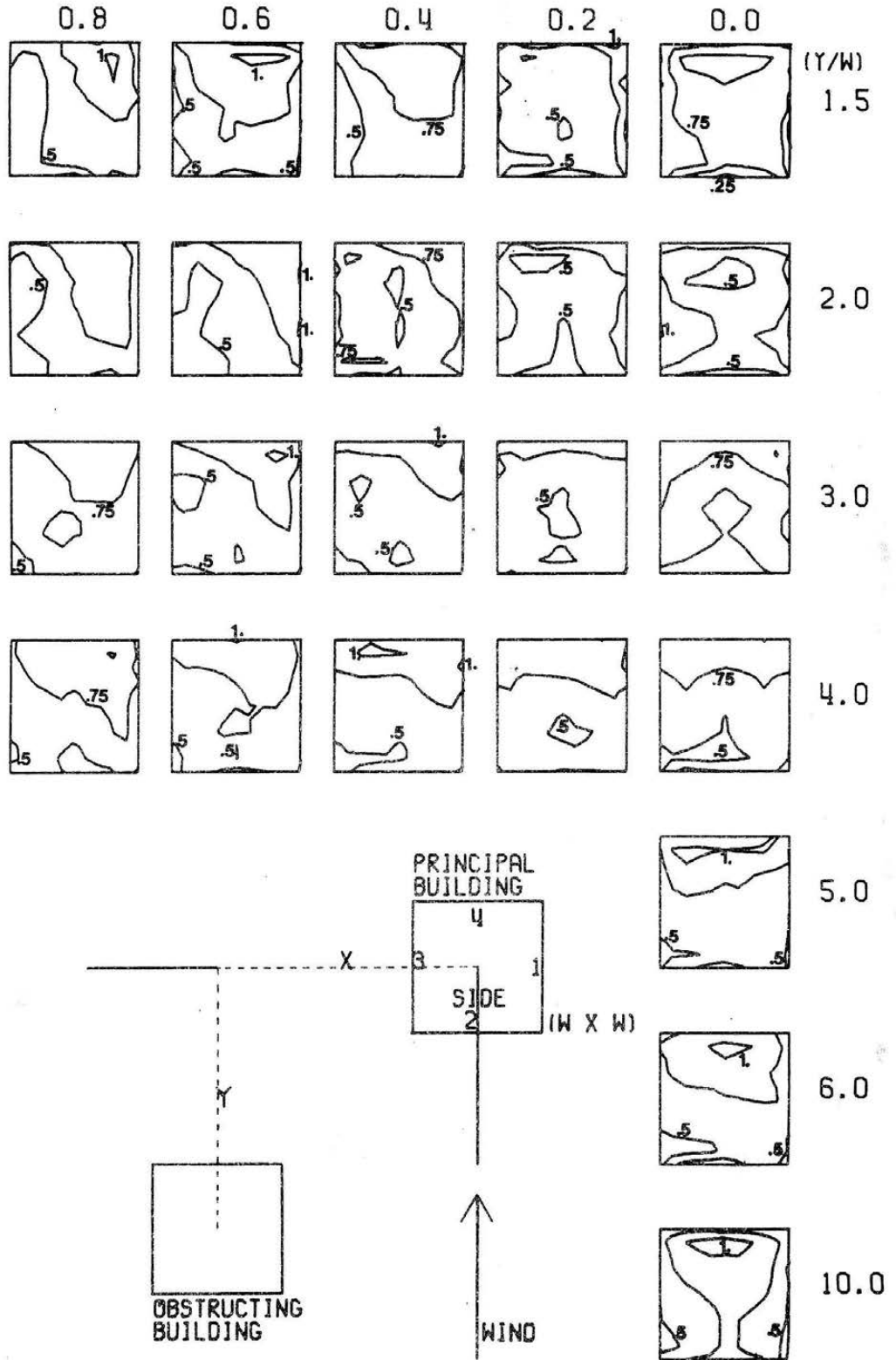
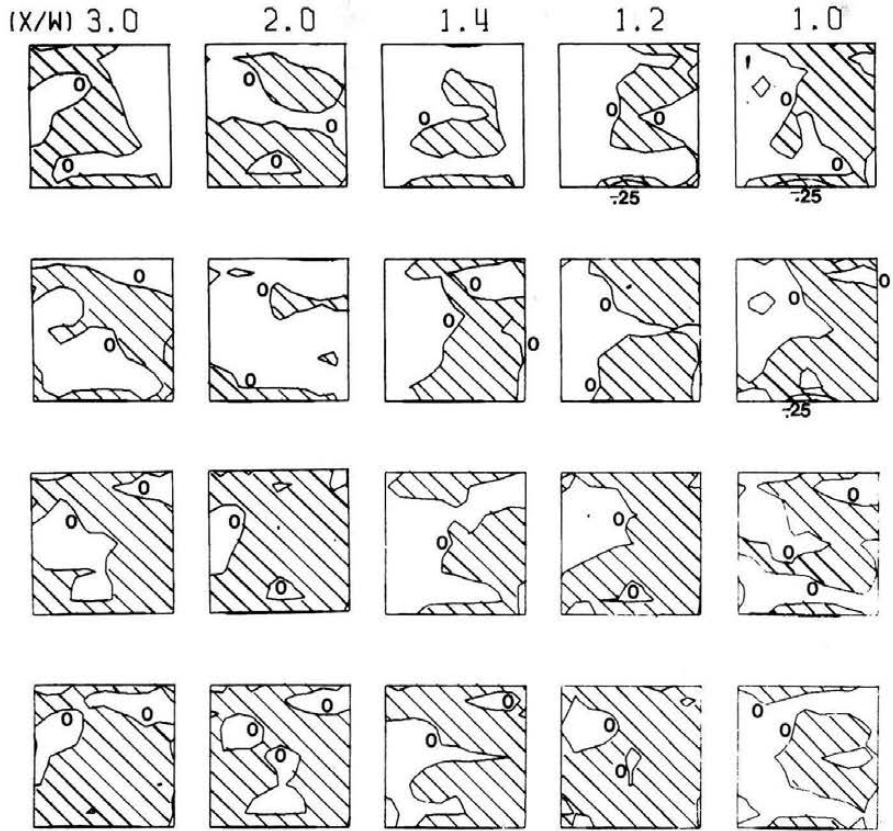


Figure 5.7e (continued)



ADVERSE (≡) AND BENEFICIAL (+) WIND LOADING  
 PEAK PRESSURE COEFFICIENTS  
 SIDE 2

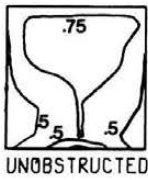


Figure 5.7f. Peak Pressure Effects, Set A, Side 2

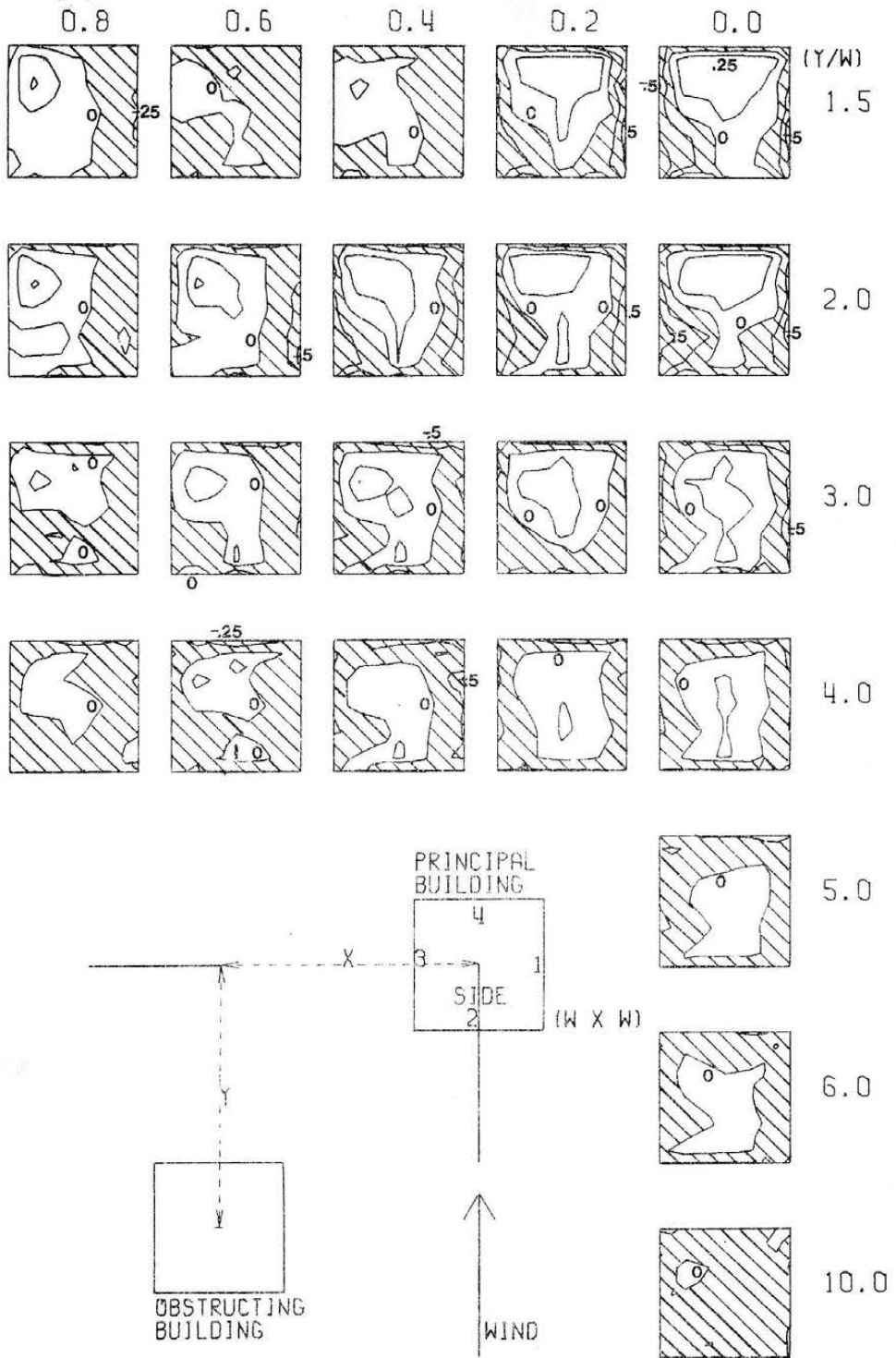
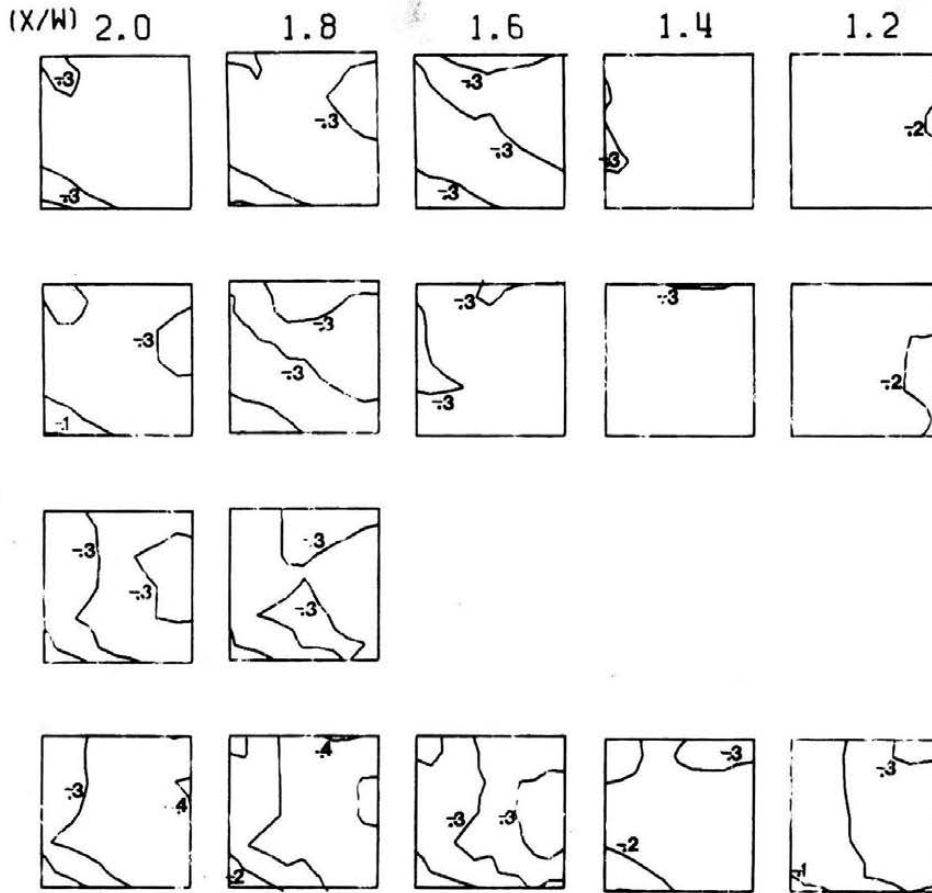


Figure 5.7f (continued)



WIND LOAD INTERACTION ON ADJACENT BUILDINGS  
 MEAN PRESSURE COEFFICIENTS  
 SIDE 3



Figure 5.8a. Mean Pressure Coefficients, Set A, Side 3

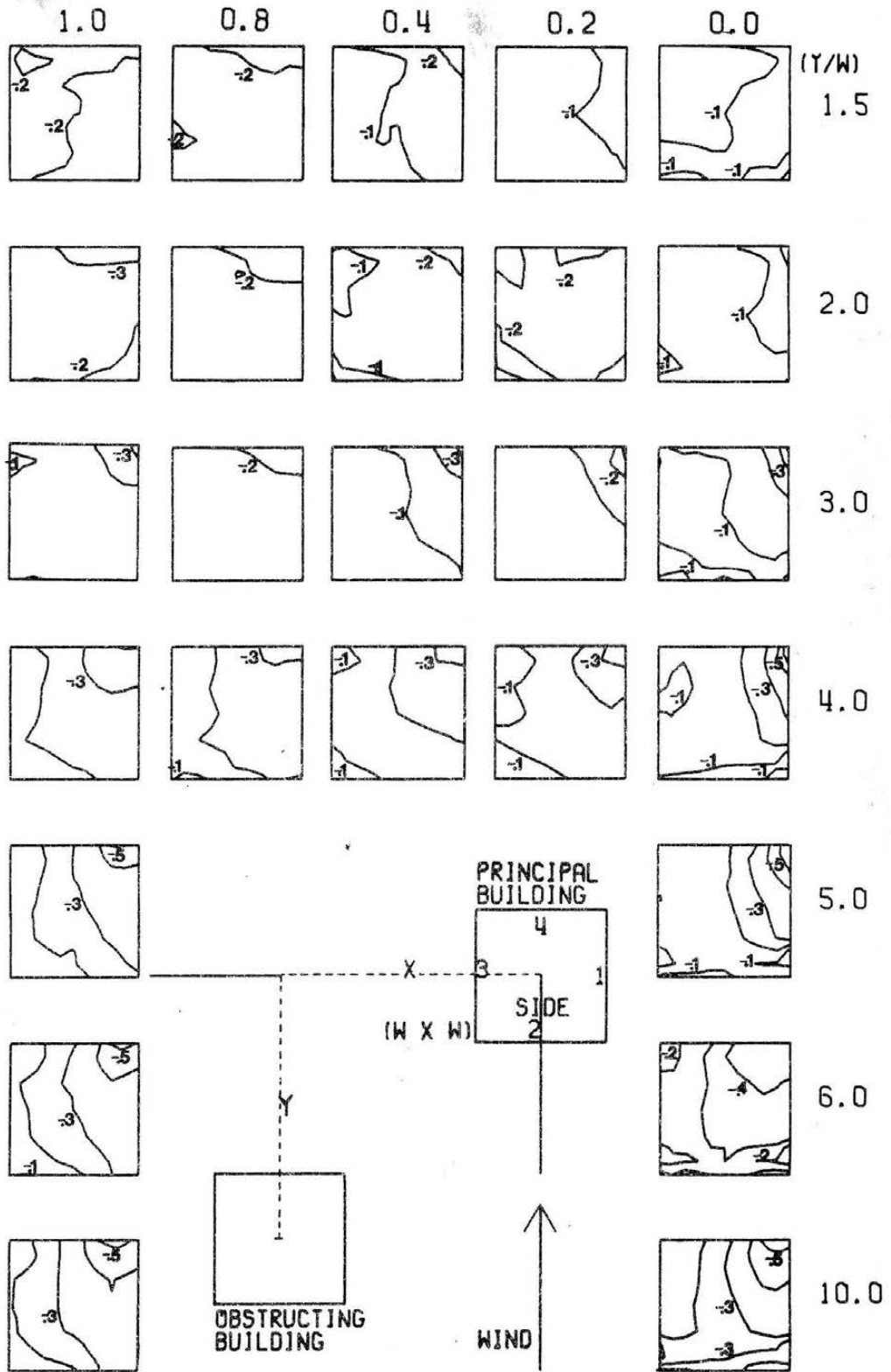
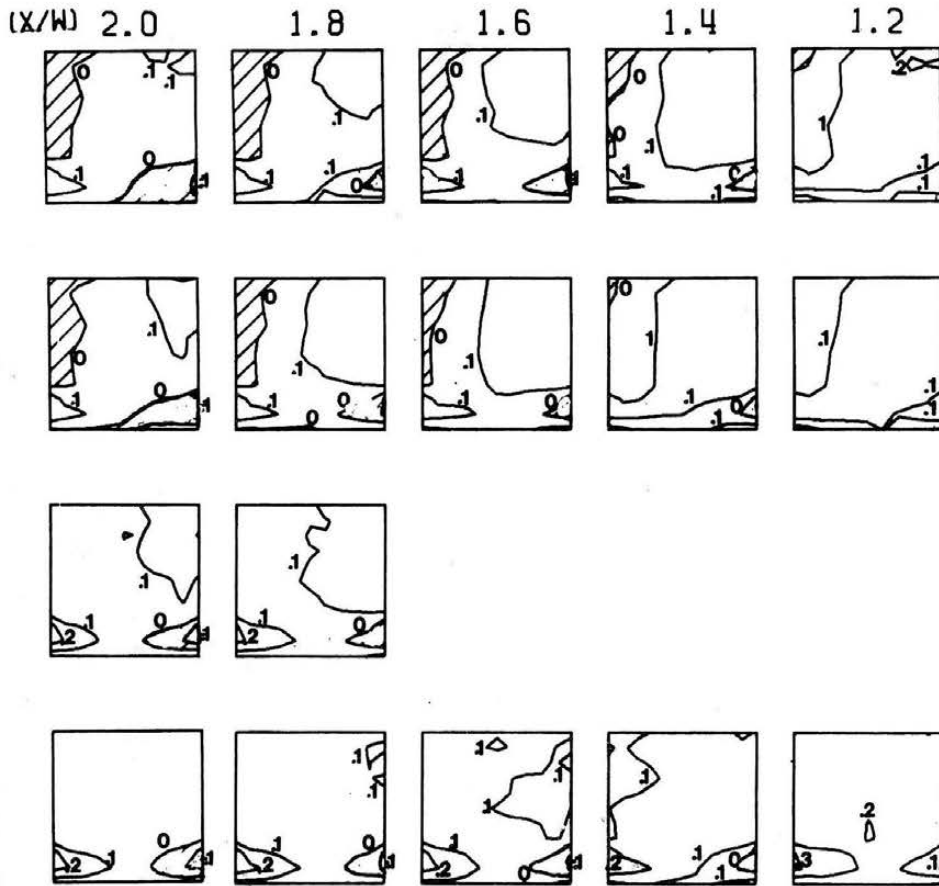


Figure 5.8a (continued)



ADVERSE (-) AND BENEFICIAL (+) WIND LOADING  
 MEAN PRESSURE COEFFICIENTS  
 SIDE 3



Figure 5.8b. Mean Pressure Effects, Set A, Side 3

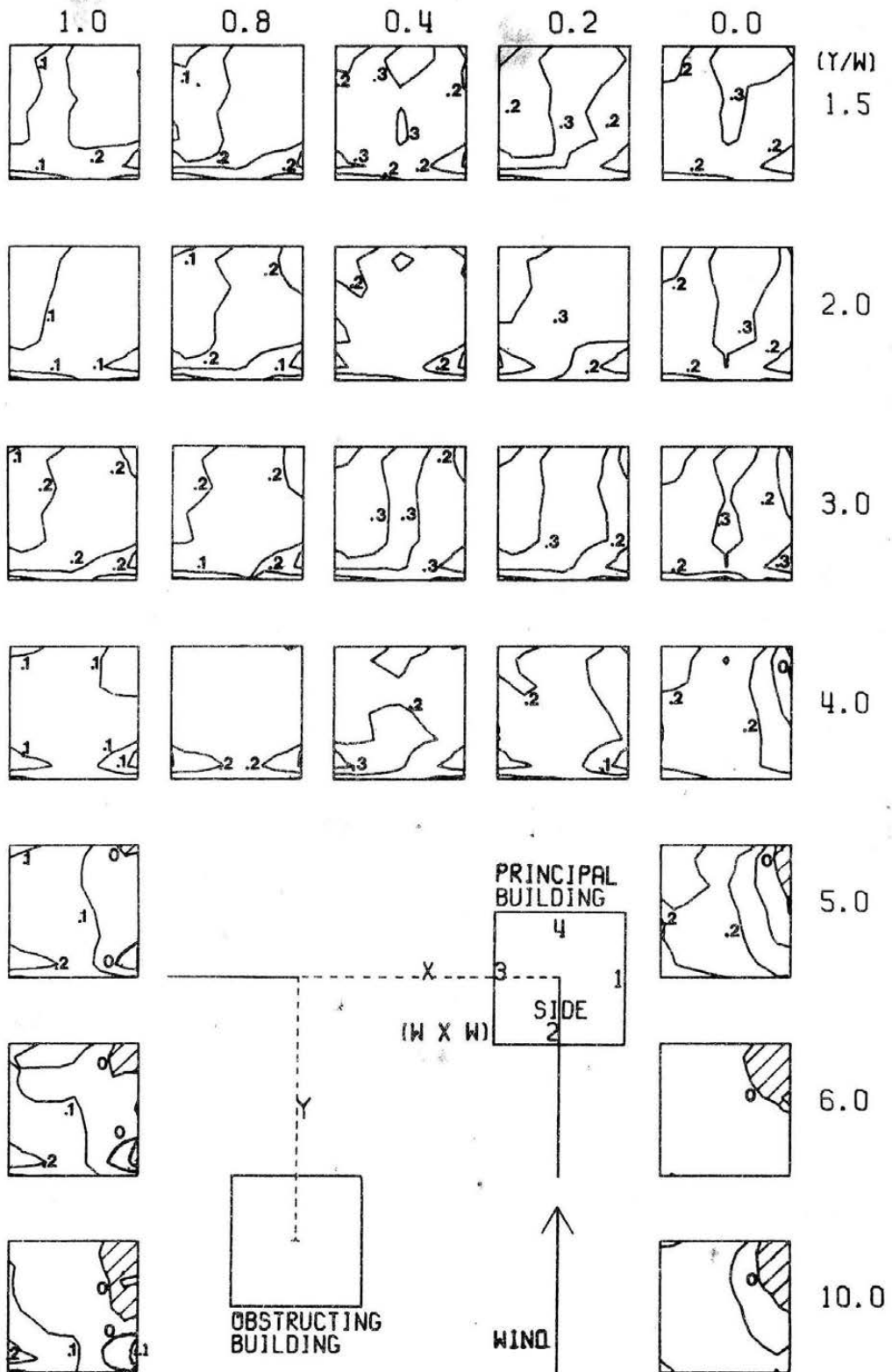
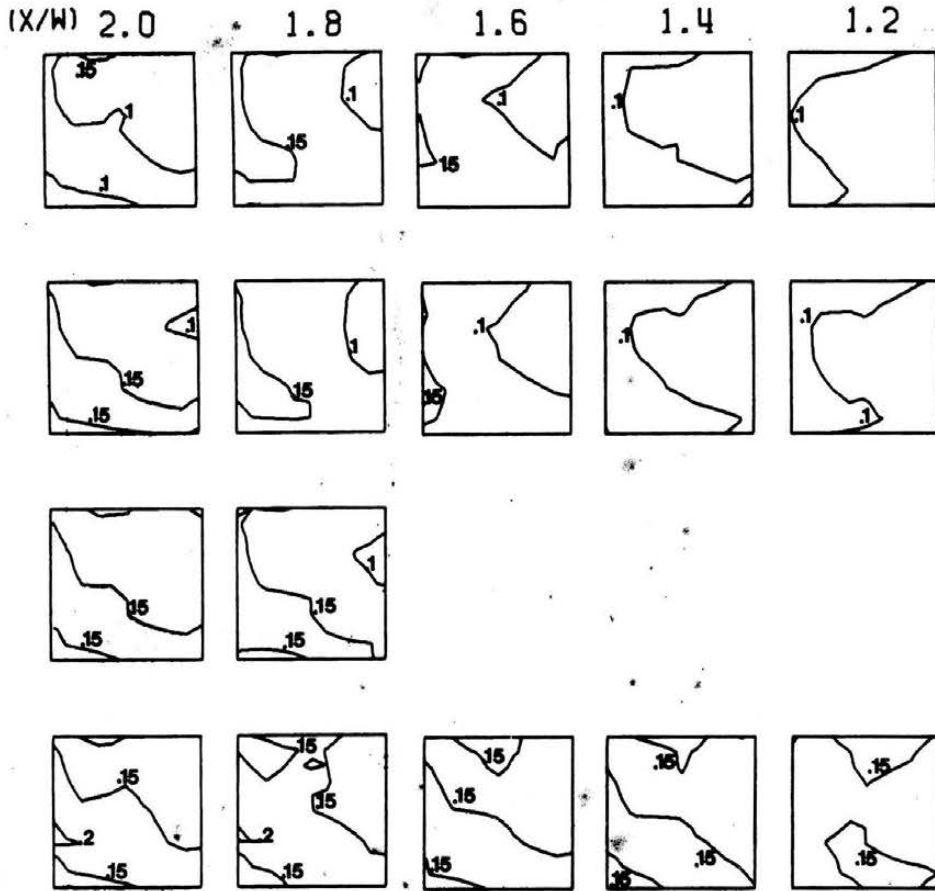


Figure 5.8b (continued)



WIND LOAD INTERACTION ON ADJACENT BUILDINGS  
 RMS PRESSURE COEFFICIENTS  
 SIDE 3

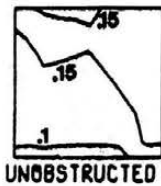


Figure 5.8c. RMS Pressure Coefficients, Set A, Side 3

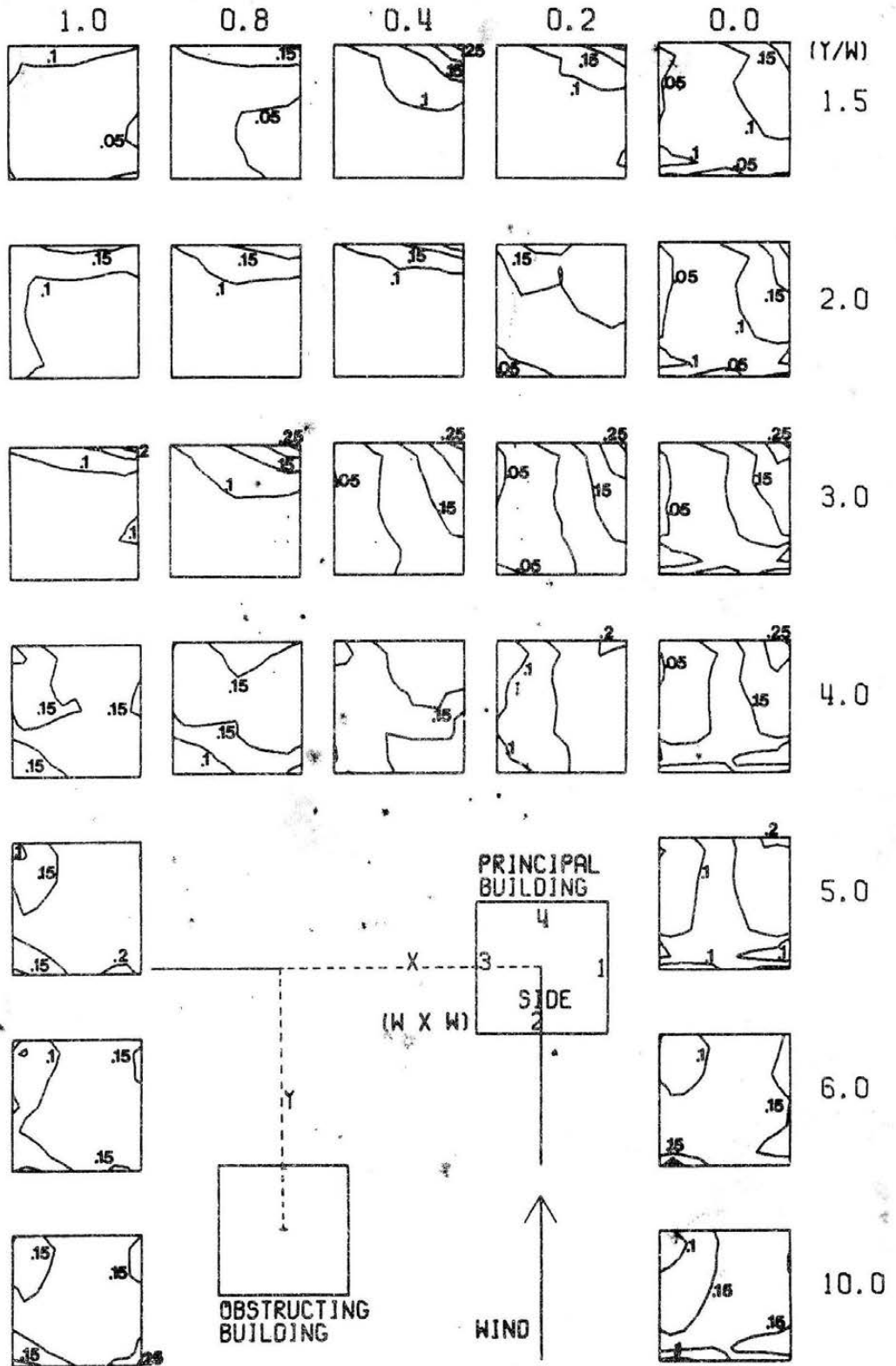
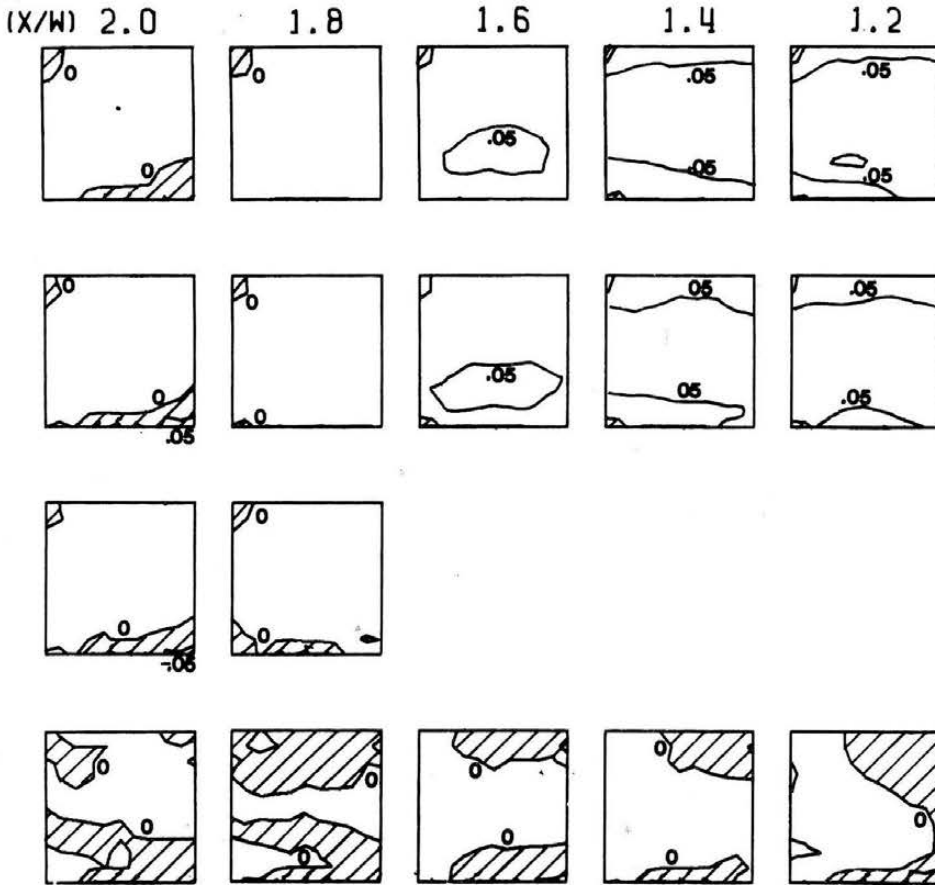


Figure 5.8c (continued)



ADVERSE (-) AND BENEFICIAL (+) WIND LOADING  
 RMS PRESSURE COEFFICIENTS  
 SIDE 3

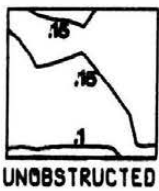


Figure 5.8d. RMS Pressure Effects, Set A, Side 3

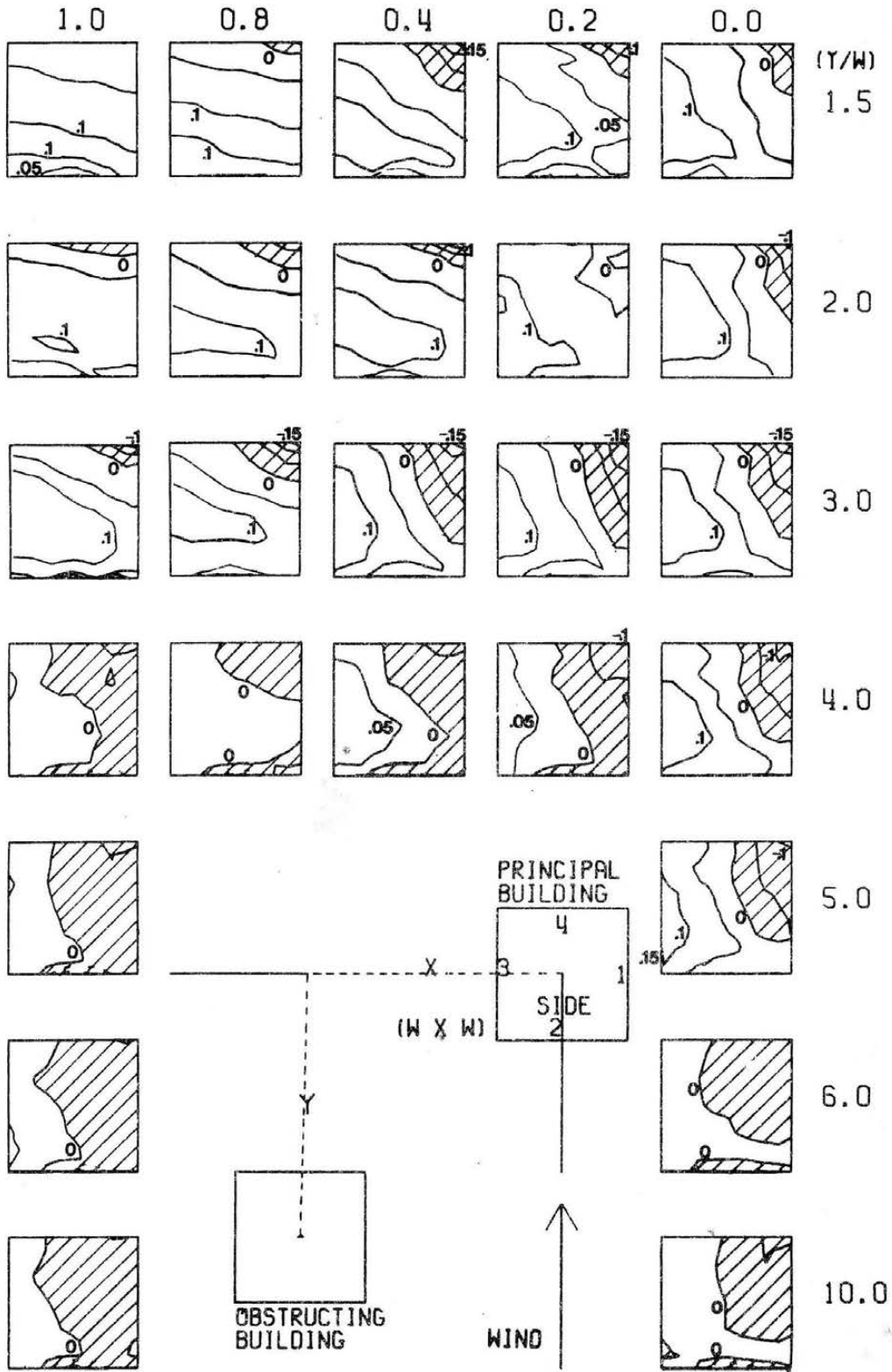
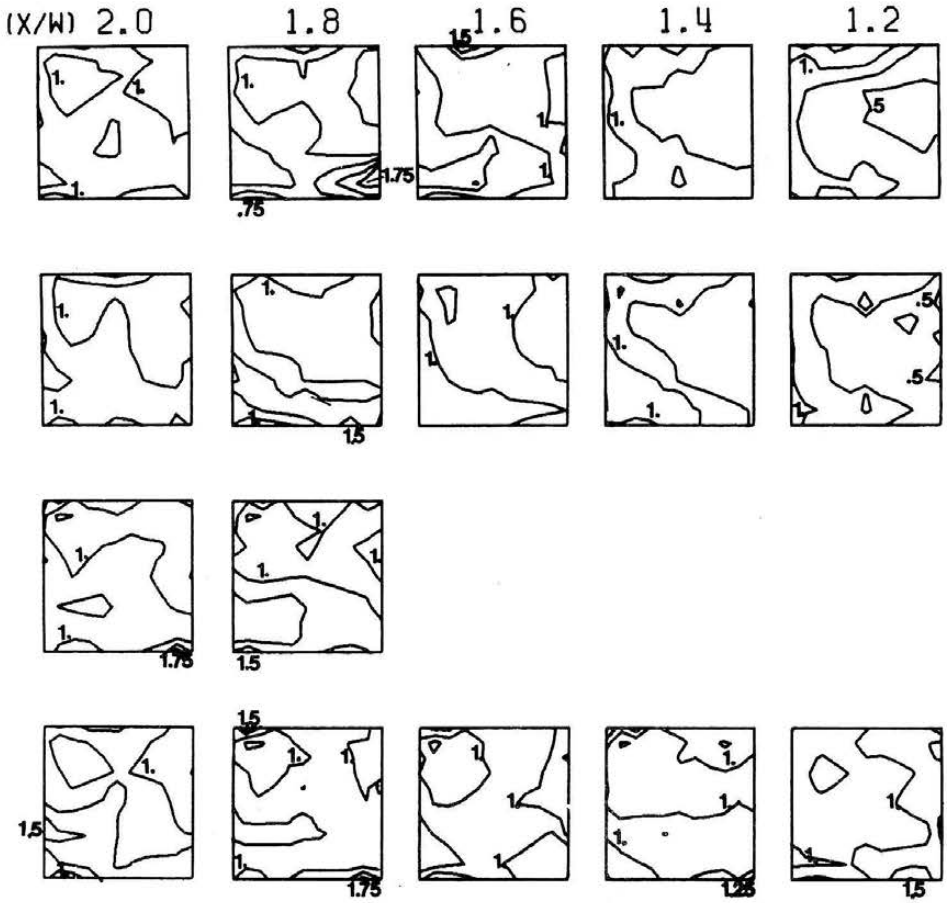


Figure 5.8d (continued)



WIND LOAD INTERACTION ON ADJACENT BUILDINGS  
 PEAK PRESSURE COEFFICIENTS  
 SIDE 3

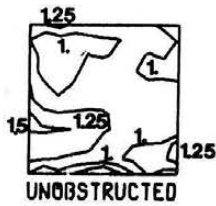


Figure 5.8e. Peak Pressure Coefficients, Set A, Side 3

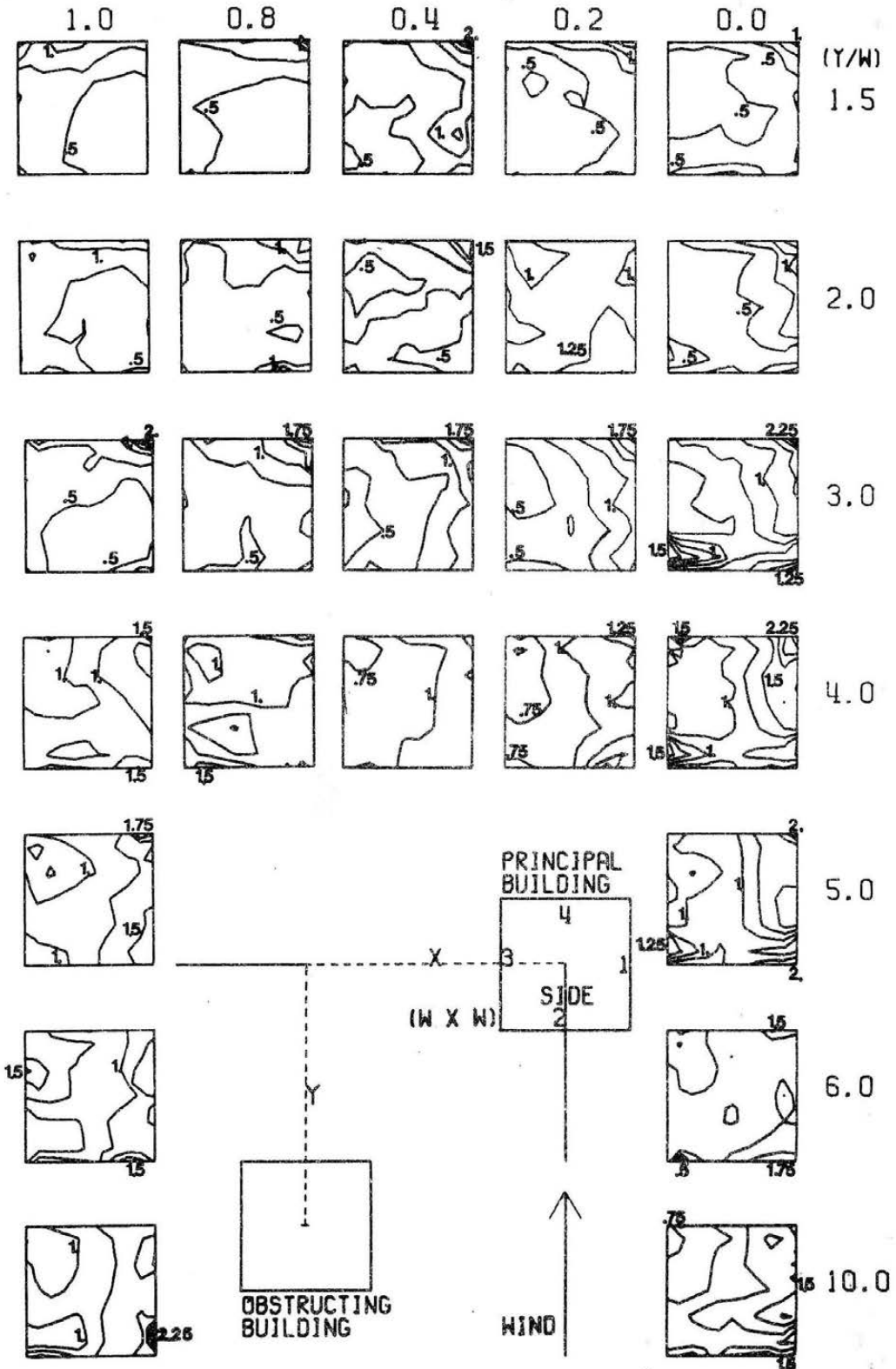
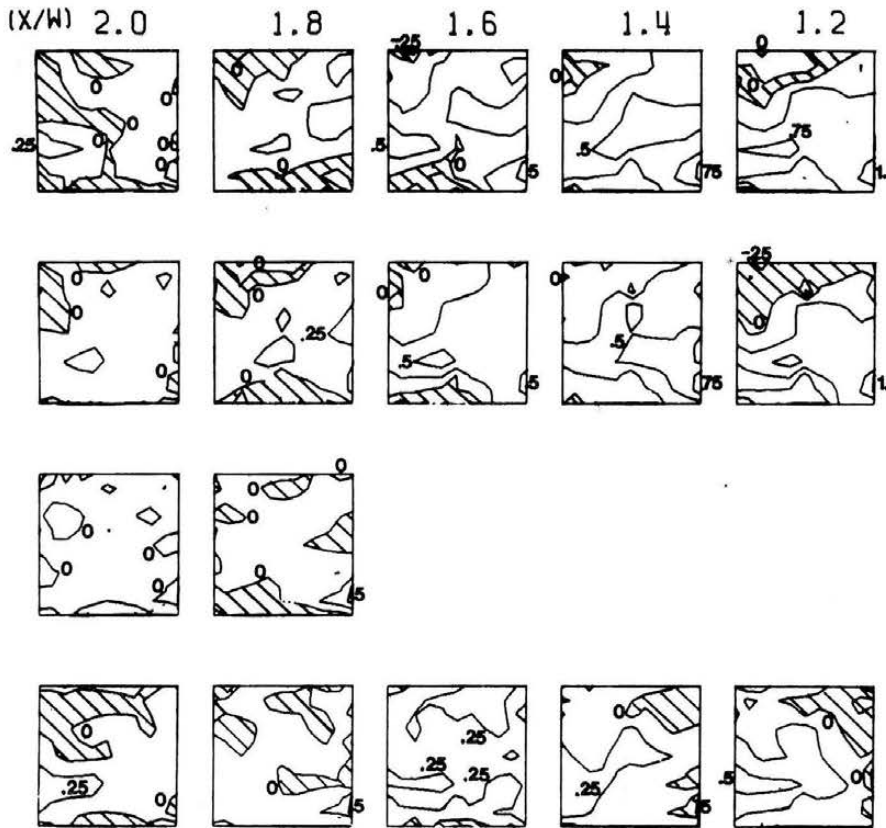


Figure 5.8e (continued)



ADVERSE (-) AND BENEFICIAL (+) WIND LOADING  
 PEAK PRESSURE COEFFICIENTS  
 SIDE 3



Figure 5.8f. Peak Pressure Effects, Set A, Side 3

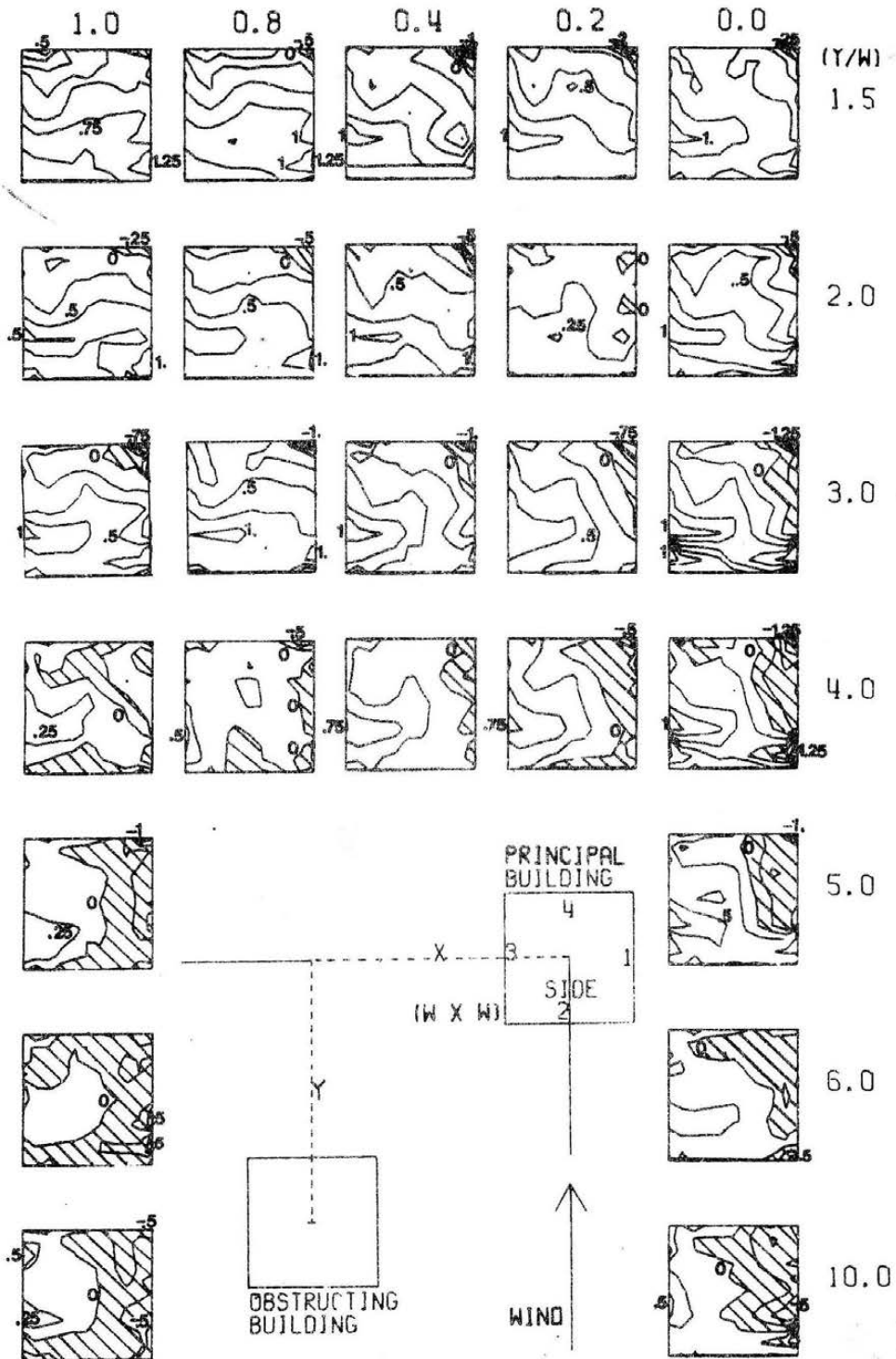
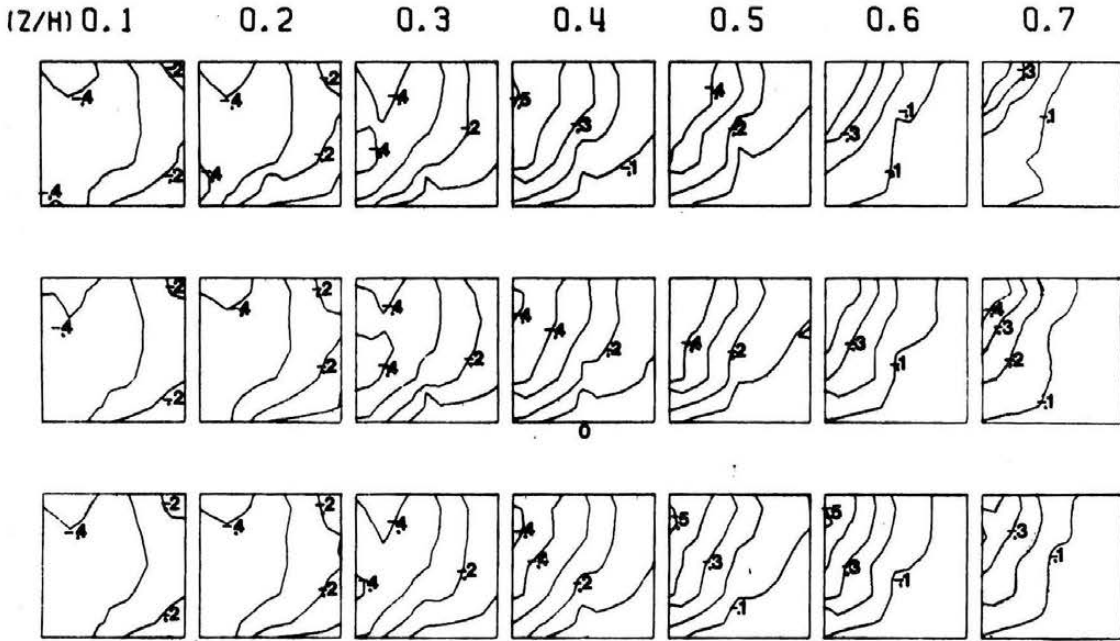


Figure 5.8f (continued)



WIND LOAD INTERACTION ON AN ADJACENT BUILDING

MEAN PRESSURE COEFFICIENTS

SIDE 1



Figure 5.9a. Mean Pressure Coefficients, Set B, Side 1

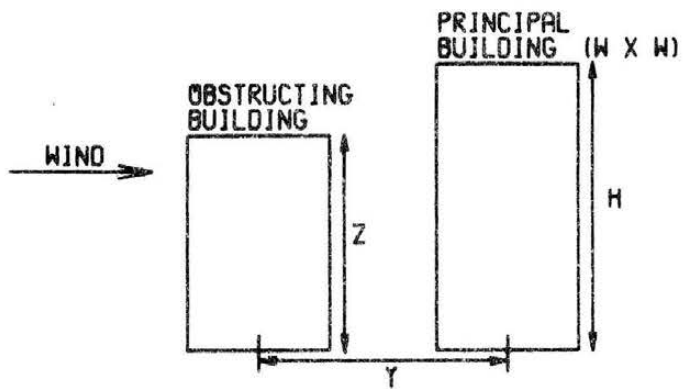
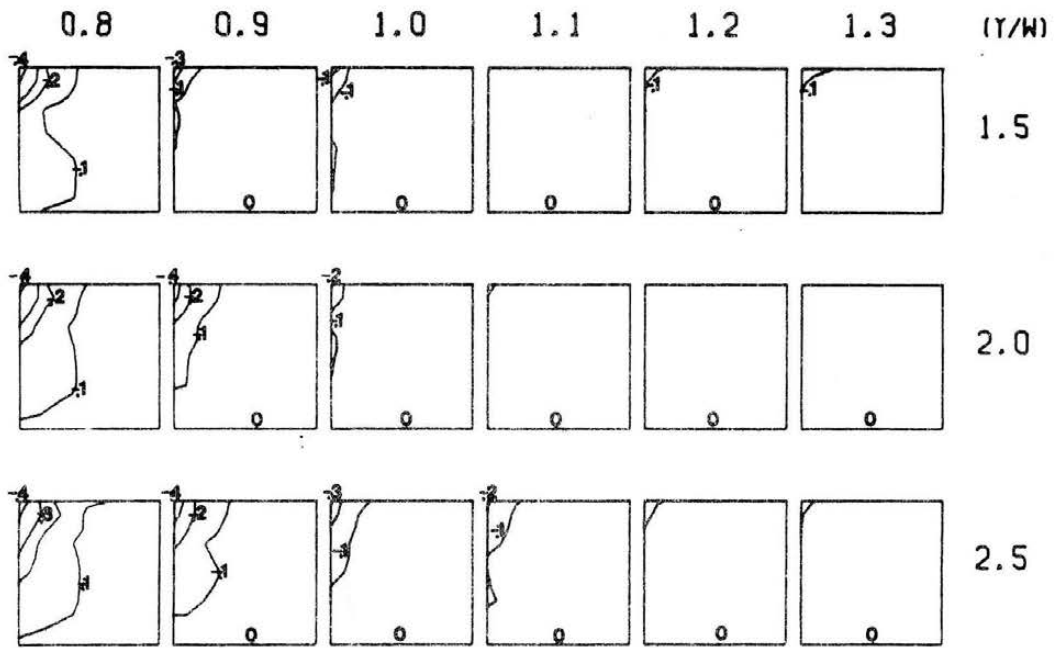
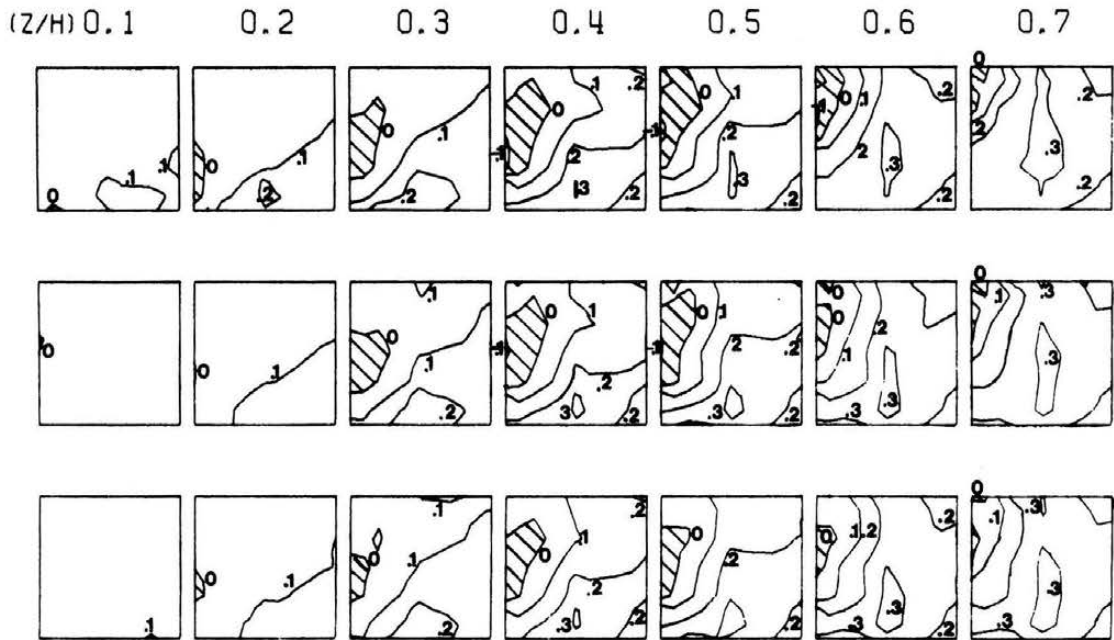


Figure 5.9a (continued)



ADVERSE (↔) AND BENEFICIAL (+) WIND LOADING  
 MEAN PRESSURE COEFFICIENTS  
 SIDE 1



Figure 5.9b. Mean Pressure Effects, Set B, Side 1

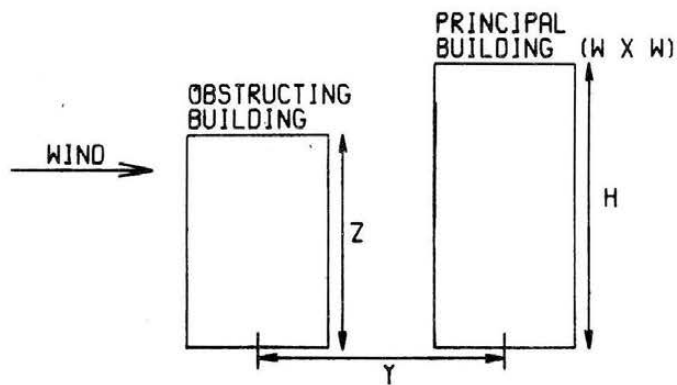
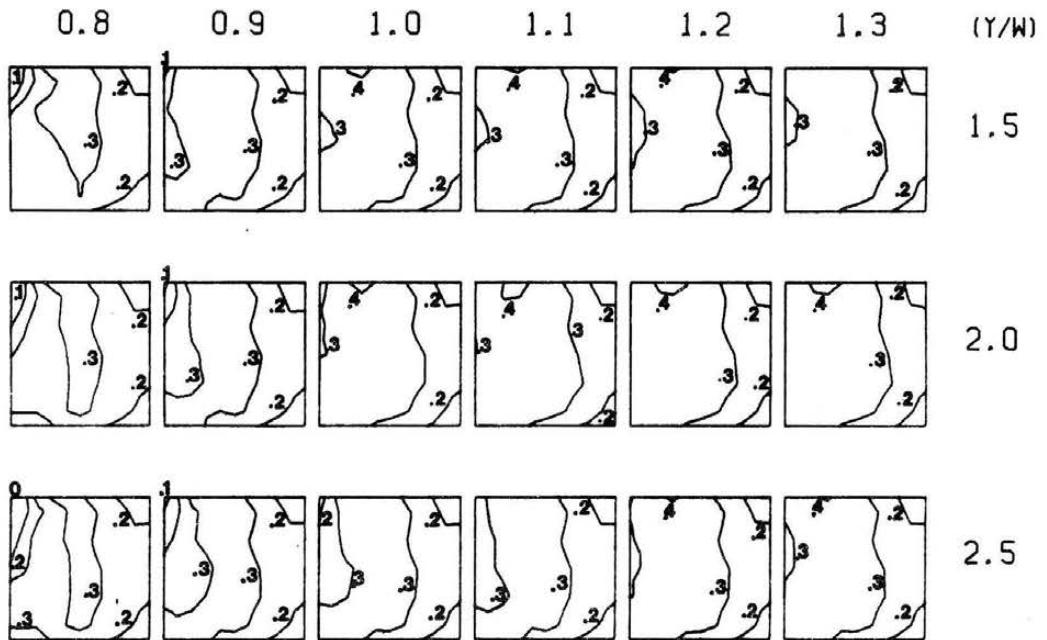
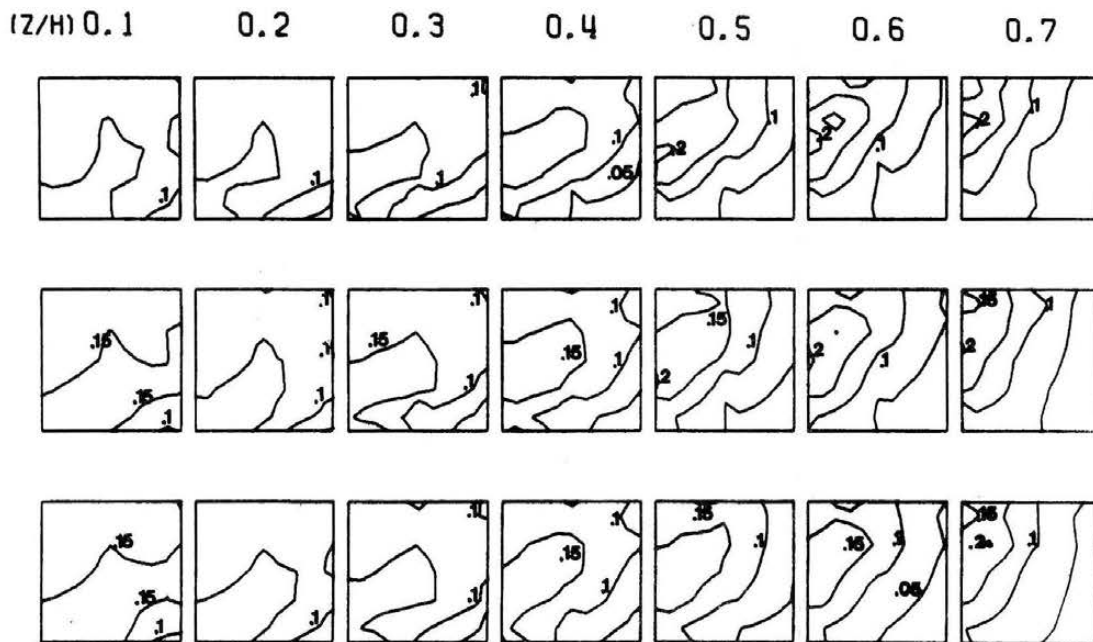


Figure 5.9b (continued)



WIND LOAD INTERACTION ON AN ADJACENT BUILDING  
 RMS PRESSURE COEFFICIENTS  
 SIDE 1

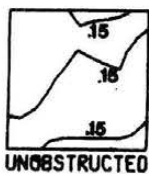


Figure 5.9c. RMS Pressure Coefficients, Set B, Side 1

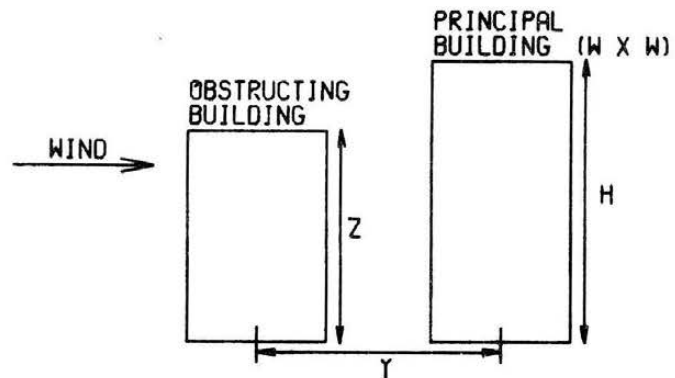
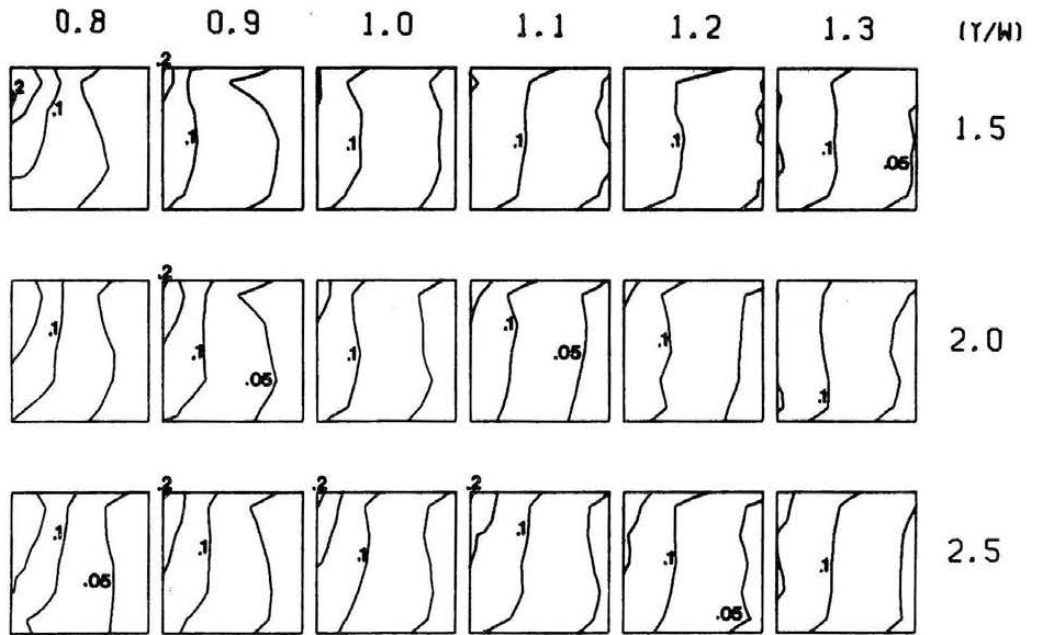
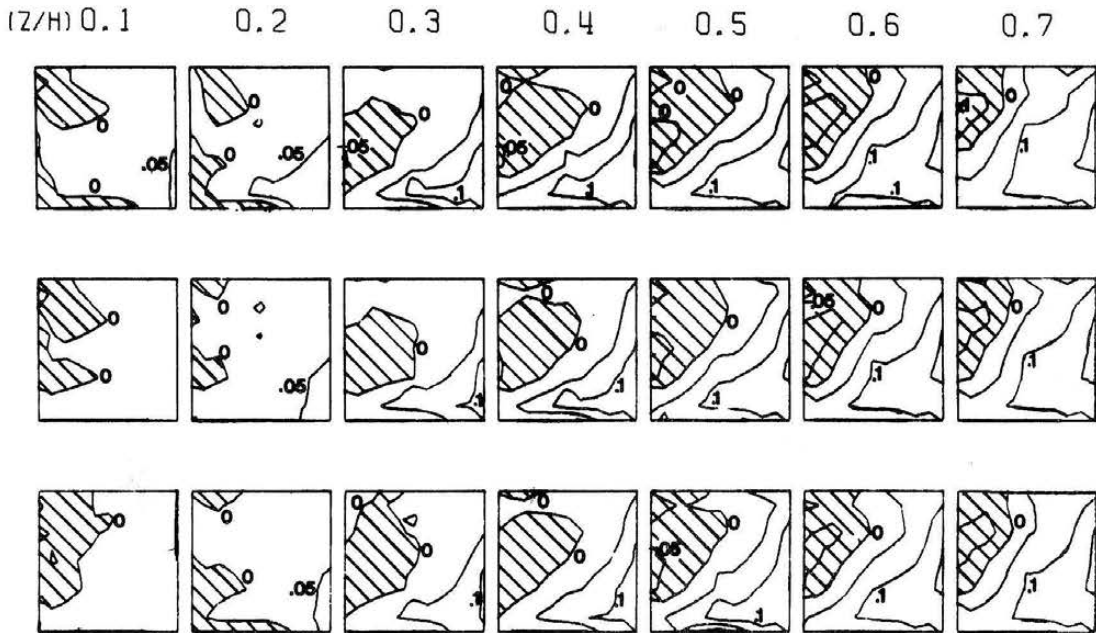


Figure 5.9c (continued)



ADVERSE (hatched) AND BENEFICIAL (+) WIND LOADING  
 RMS PRESSURE COEFFICIENTS  
 SIDE 1

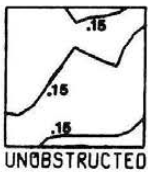


Figure 5.9d. RMS Pressure Effects, Set B, Side 1

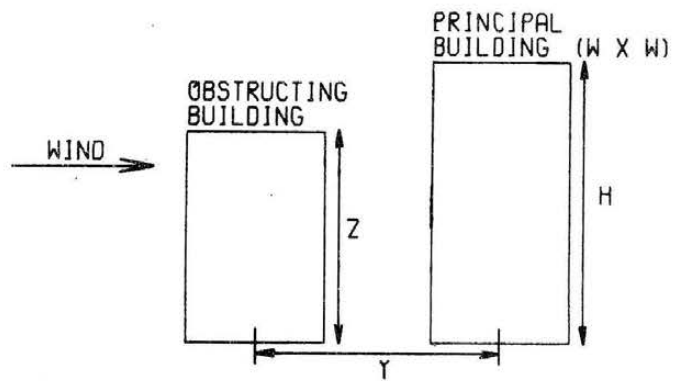
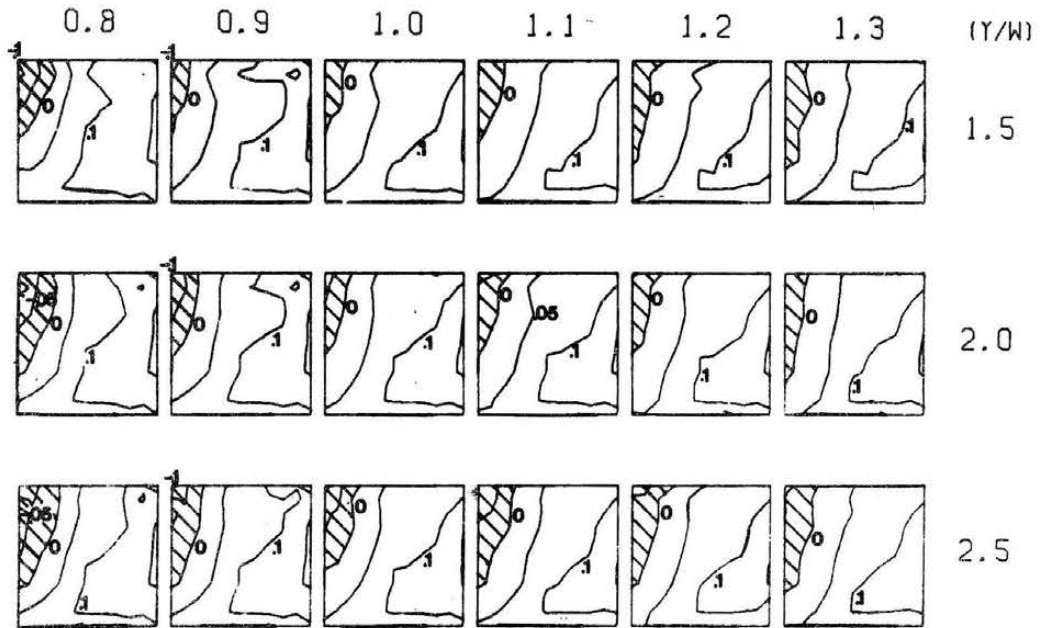
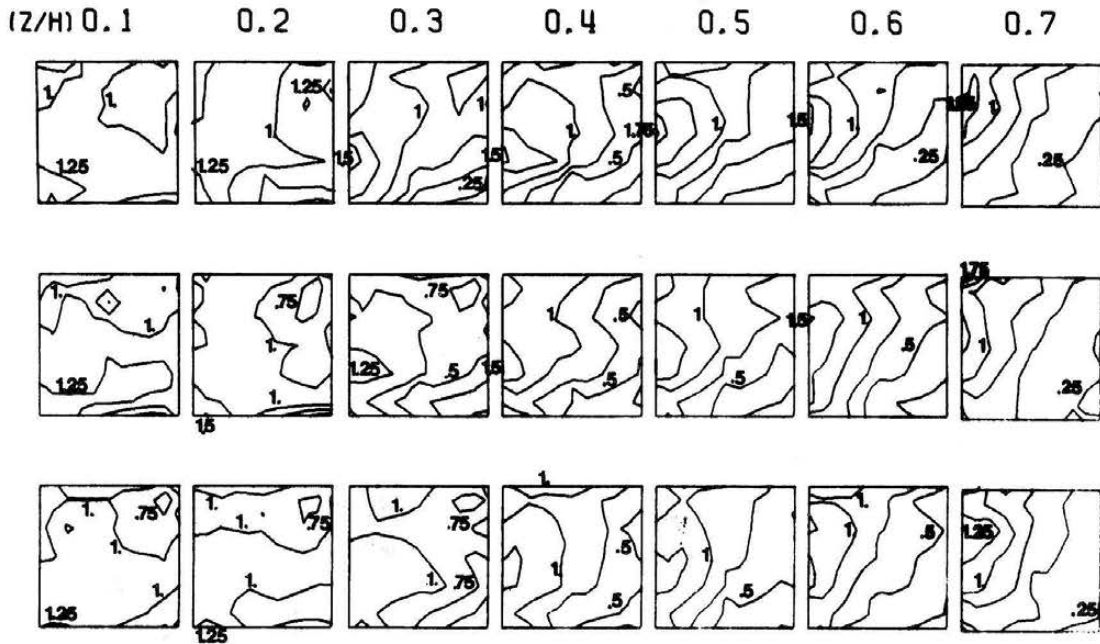


Figure 5.9d (continued)



WIND LOAD INTERACTION ON AN ADJACENT BUILDING  
 PEAK PRESSURE COEFFICIENTS  
 SIDE 1

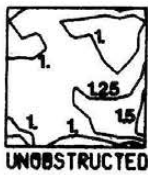


Figure 5.9e. Peak Pressure Coefficients, Set B, Side 1

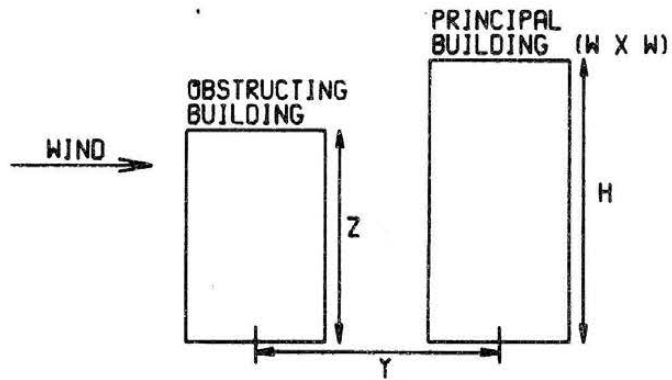
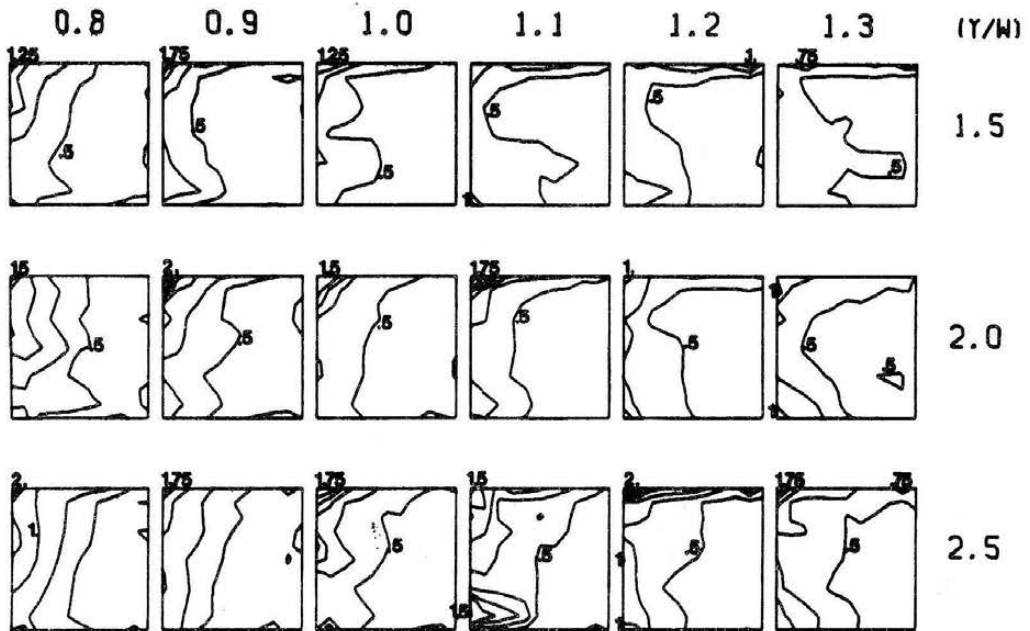
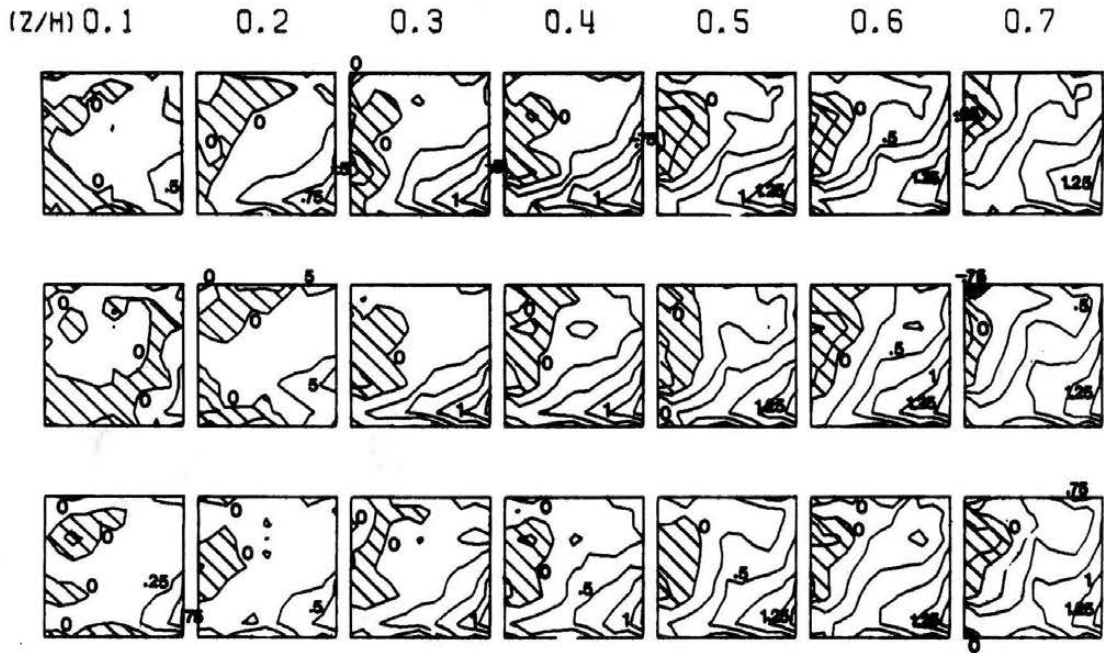


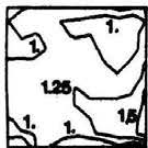
Figure 5.9e (continued)



ADVERSE (↖) AND BENEFICIAL (+) WIND LOADING

PEAK PRESSURE COEFFICIENTS

SIDE 1



UNOBSTRUCTED

Figure 5.9f. Peak Pressure Effects, Set B, Side 1

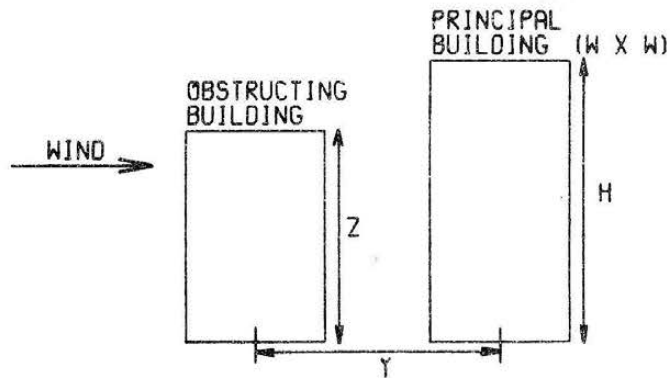
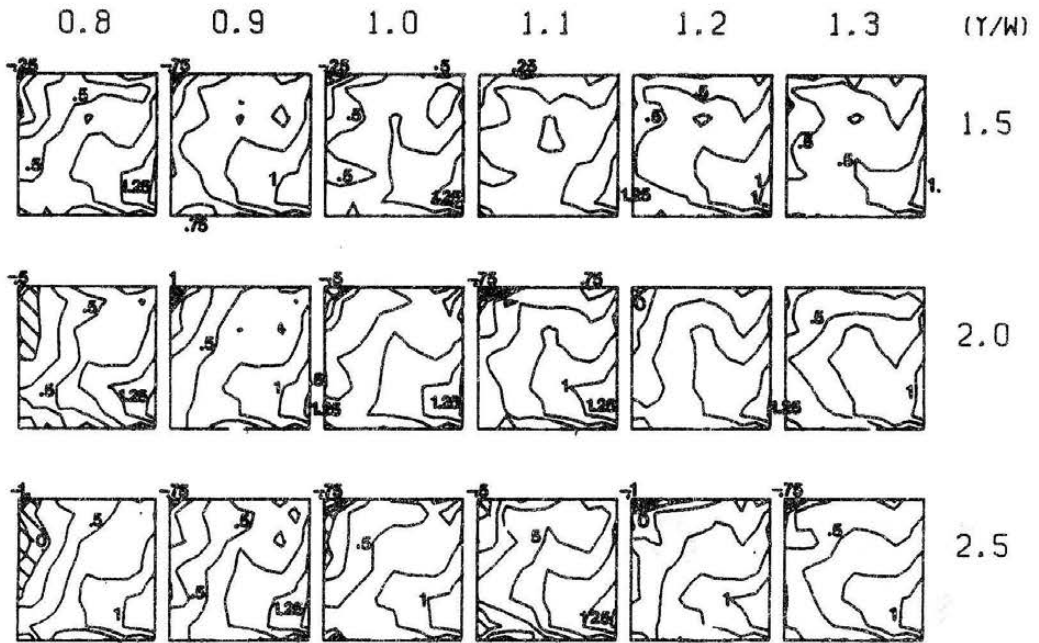
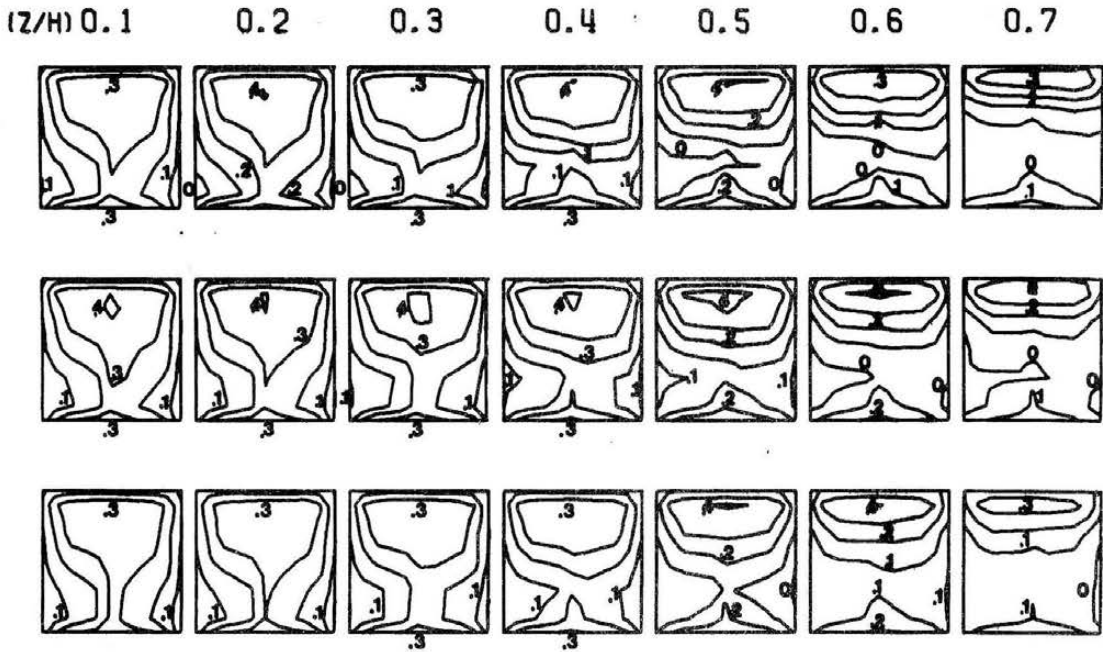


Figure 5.9f (continued)



WIND LOAD INTERACTION ON AN ADJACENT BUILDING

MEAN PRESSURE COEFFICIENTS

SIDE 2



Figure 5.10a. Mean Pressure Coefficients, Set B, Side 2

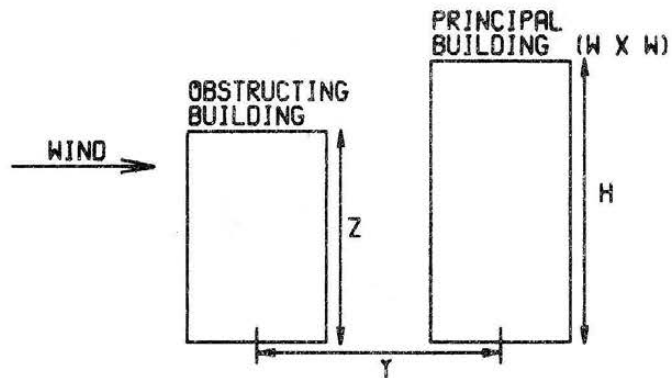
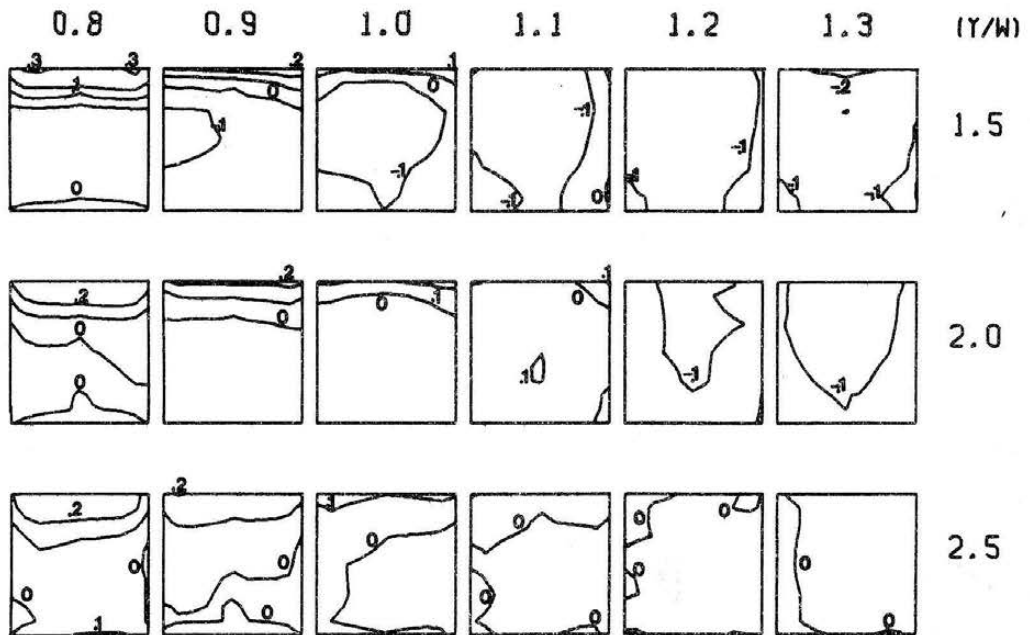
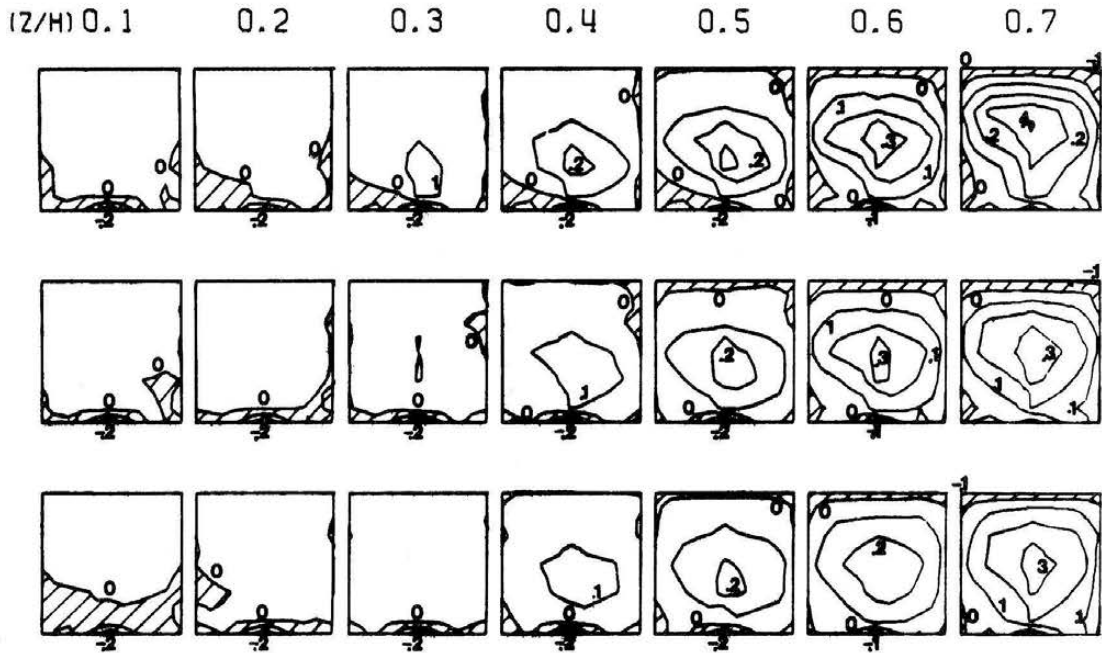


Figure 5.10a (continued)



ADVERSE (↖) AND BENEFICIAL (+) WIND LOADING

MEAN PRESSURE COEFFICIENTS

SIDE 2



Figure 5.10b. Mean Pressure Effects, Set B, Side 2

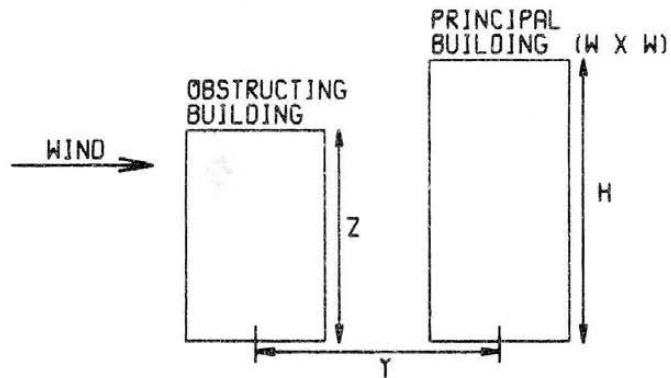
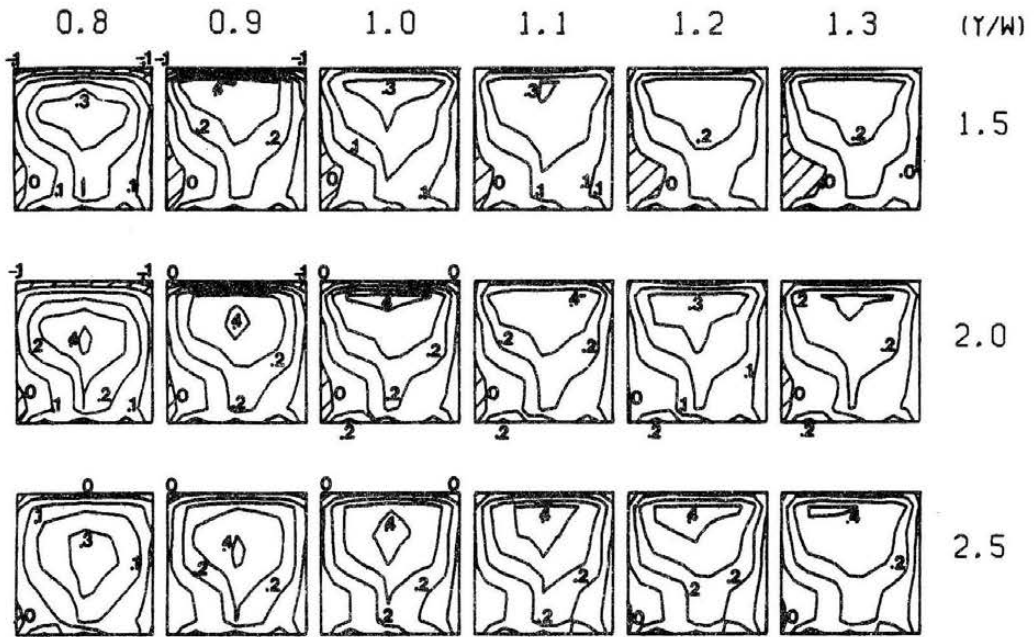
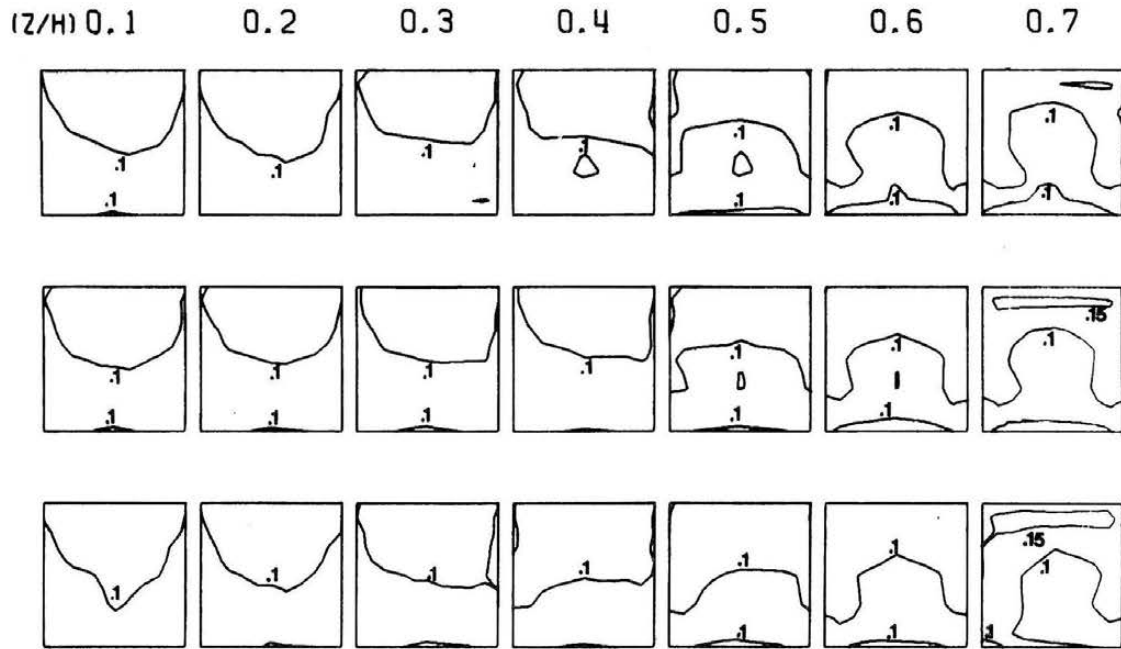


Figure 5.10b (continued)



WIND LOAD INTERACTION ON AN ADJACENT BUILDING

RMS PRESSURE COEFFICIENTS

SIDE 2

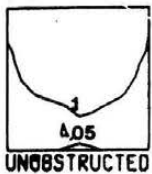


Figure 5.10c. RMS Pressure Coefficients, Set B, Side 2

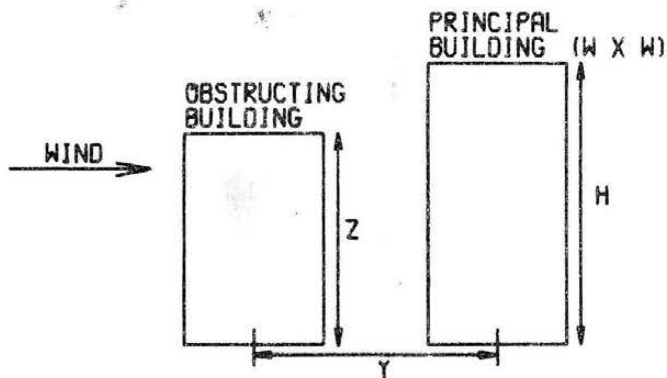
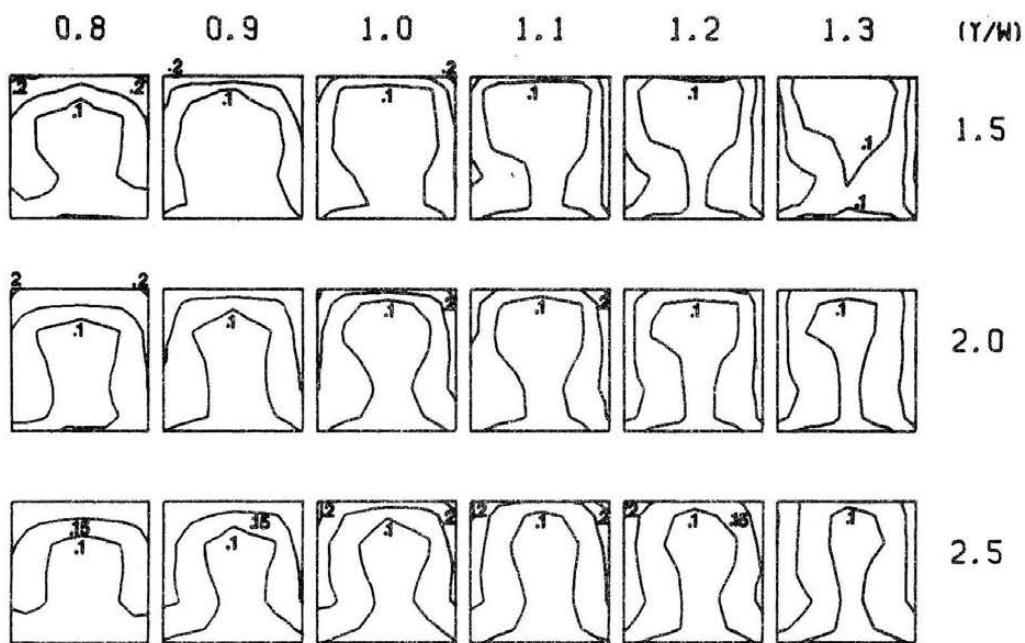
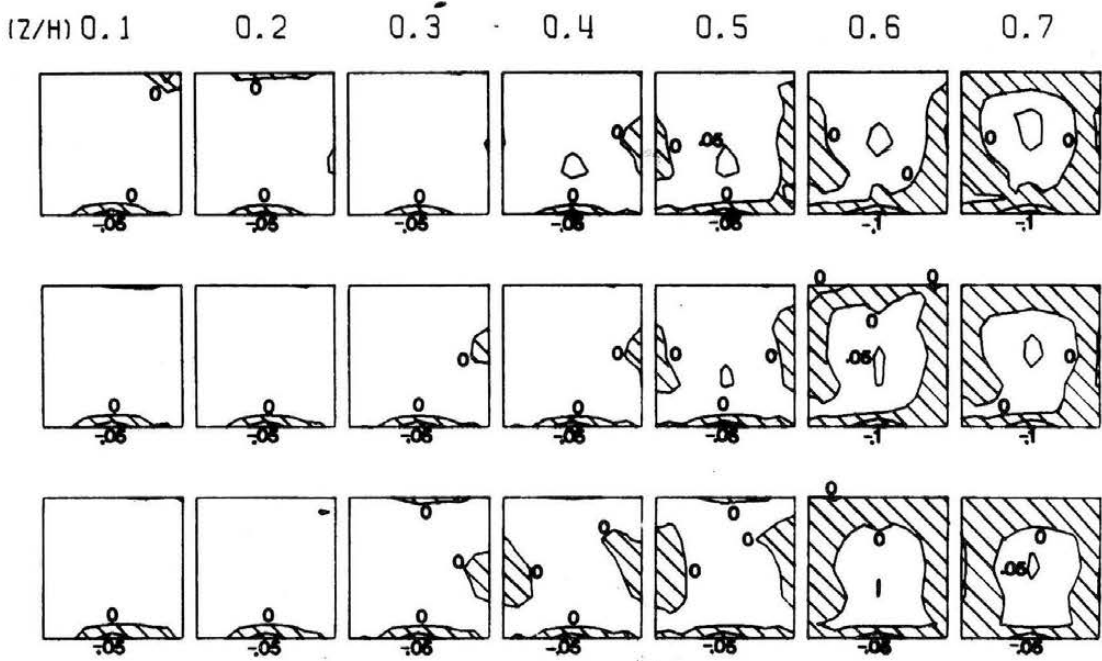


Figure 5.10c (continued)



ADVERSE (↔) AND BENEFICIAL (+) WIND LOADING\*  
 RMS PRESSURE COEFFICIENTS  
 SIDE 2

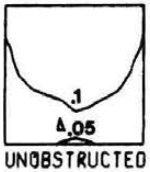


Figure 5.10d. RMS Pressure Effects, Set B, Side 2

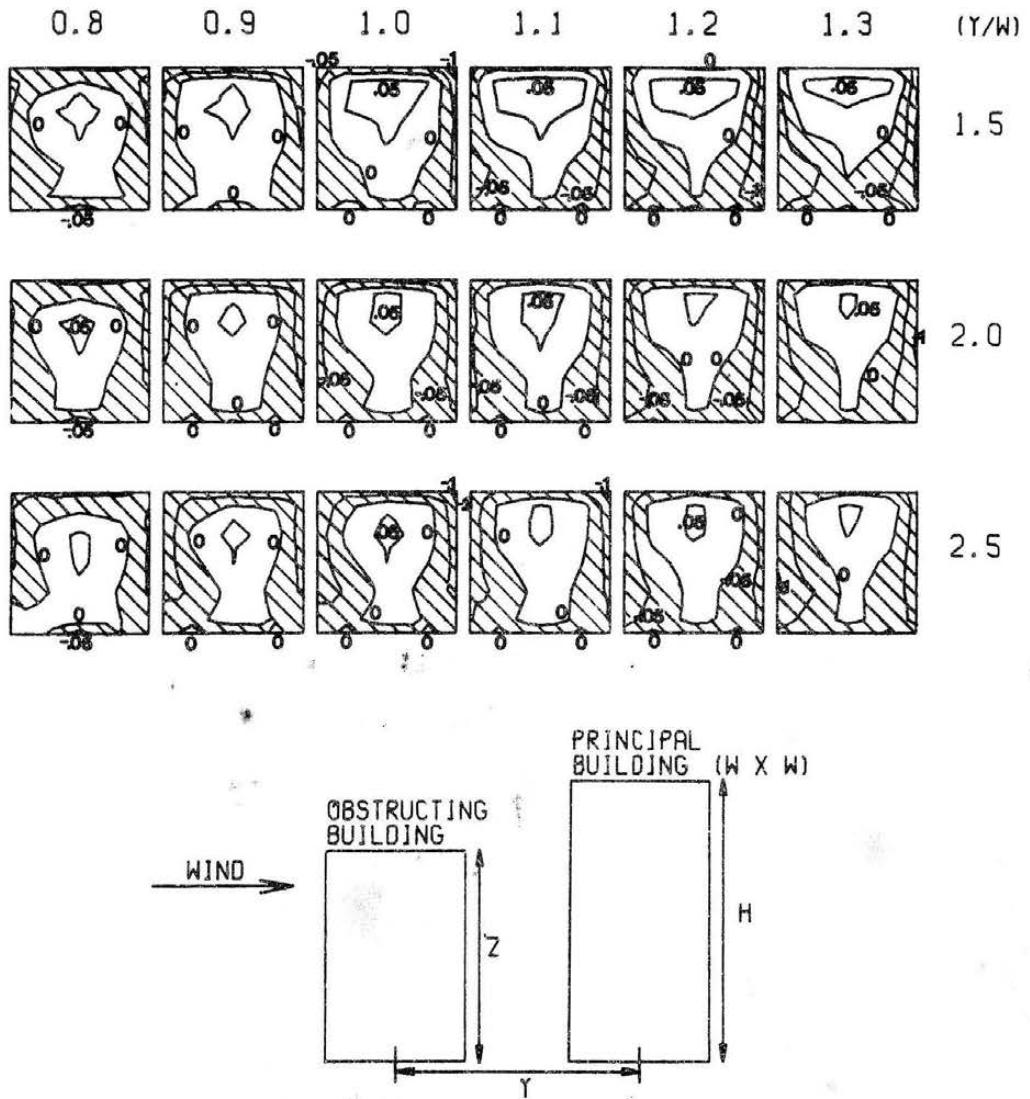
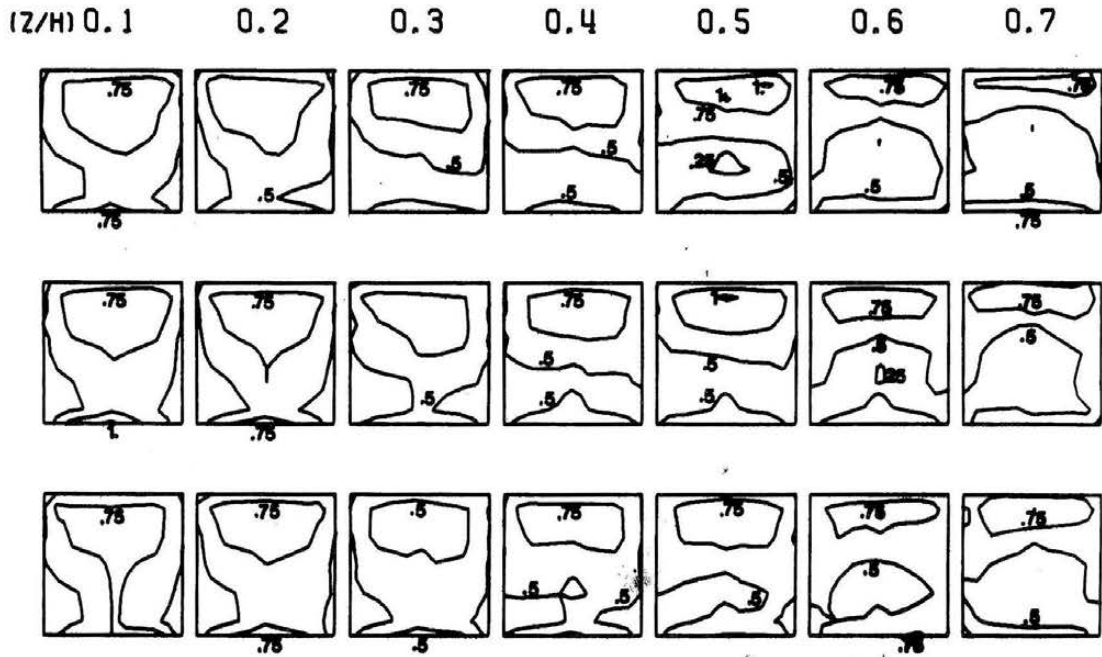


Figure 5.10d (continued)



WIND LOAD INTERACTION ON AN ADJACENT BUILDING  
 PEAK PRESSURE COEFFICIENTS  
 SIDE 2



Figure 5.10e. Peak Pressure Coefficients, Set B, Side 2

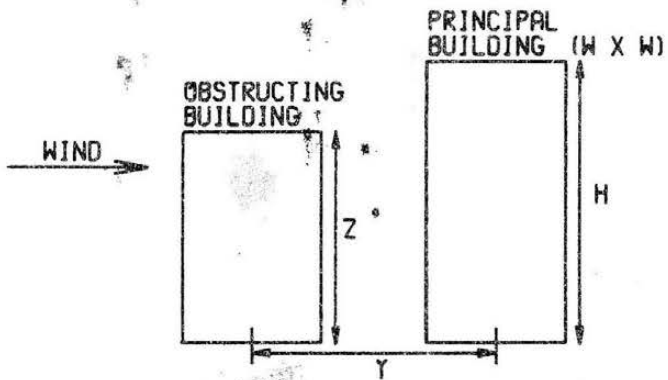
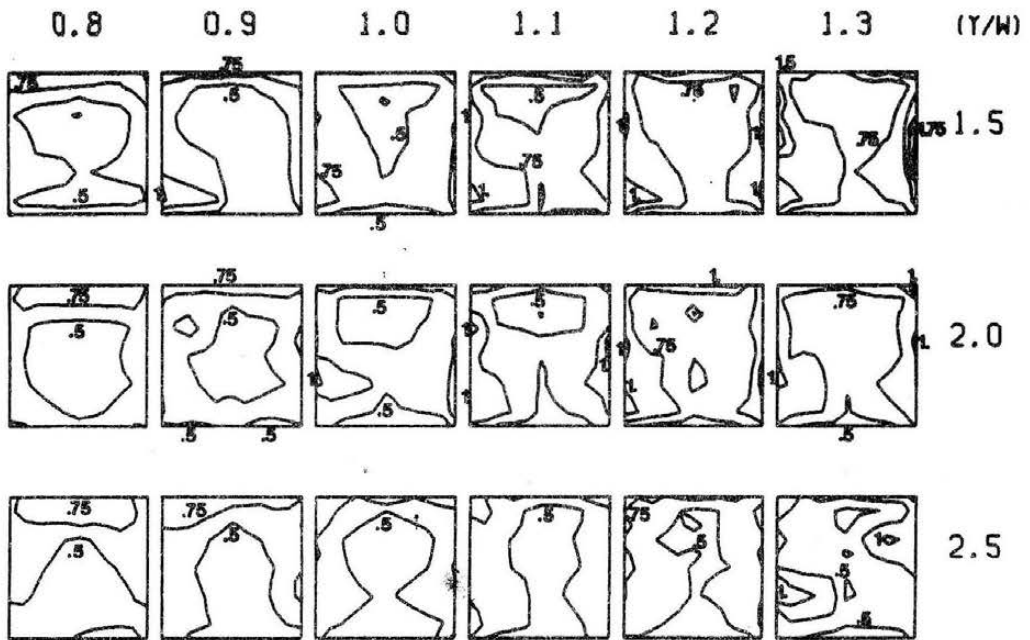
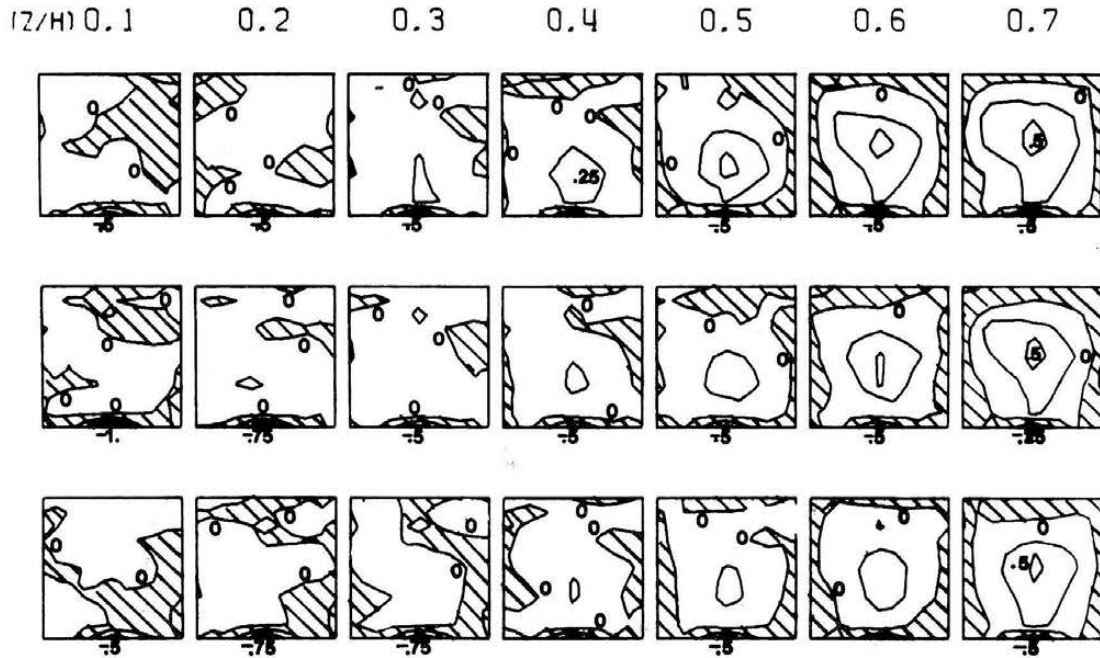


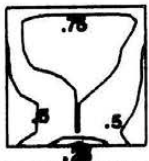
Figure 5.10e (continued)



ADVERSE (-) AND BENEFICIAL (+) WIND LOADING

PEAK PRESSURE COEFFICIENTS

SIDE 2



UNOBSTRUCTED

Figure 5.10f. Peak Pressure Effects, Set B, Side 2

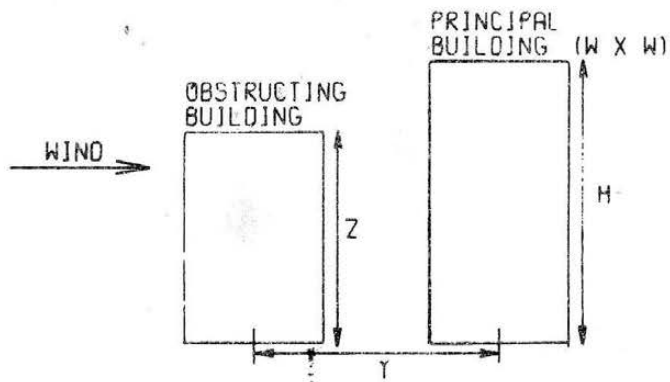
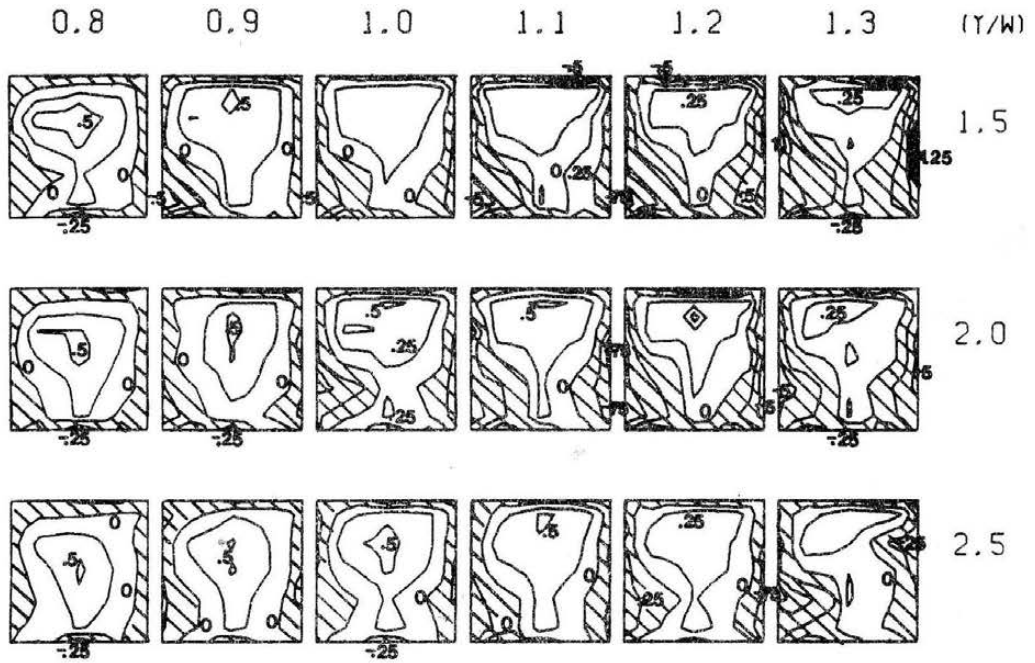


Figure 5.10f (continued)

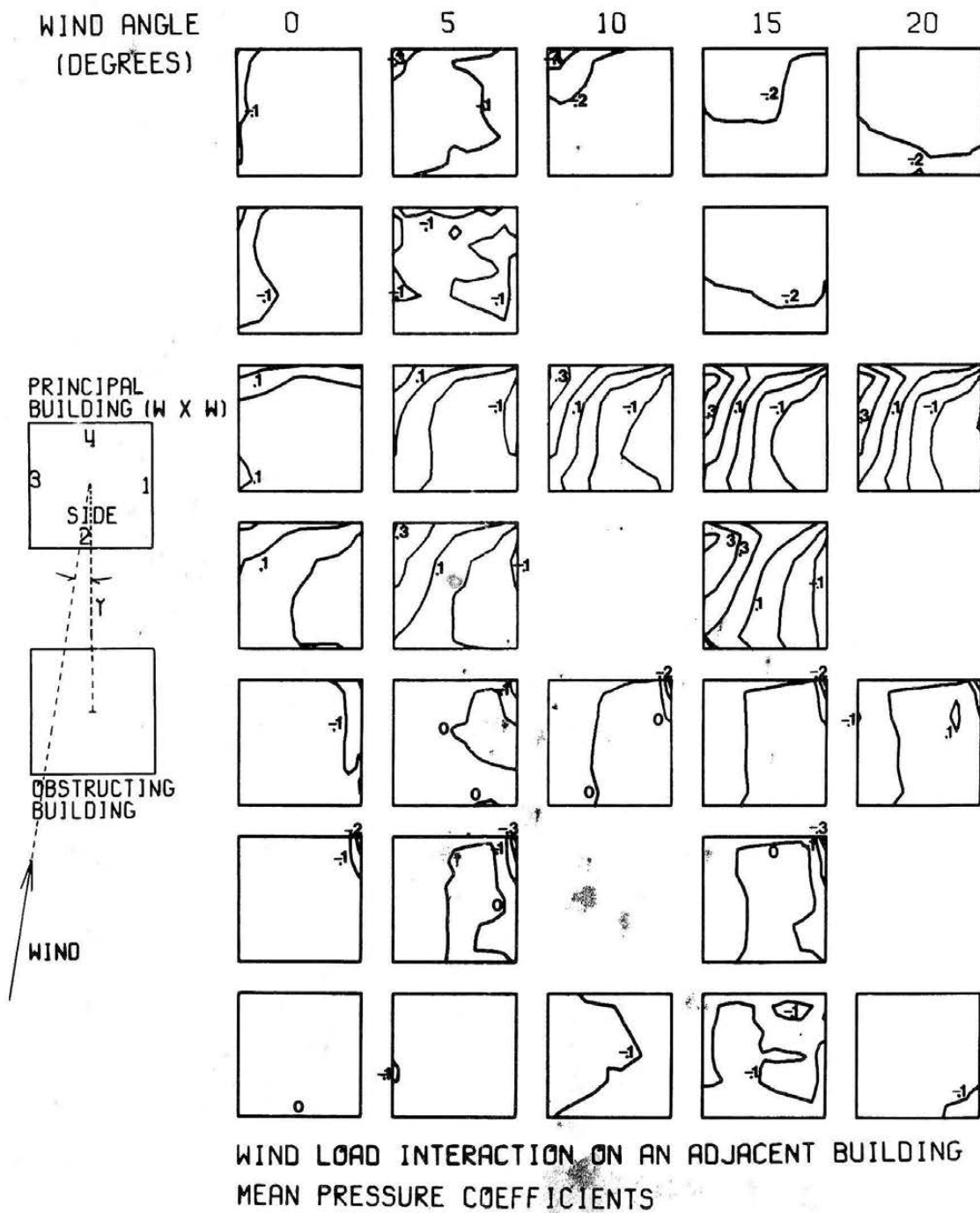


Figure 5.11a. Mean Pressure Coefficients, Set C

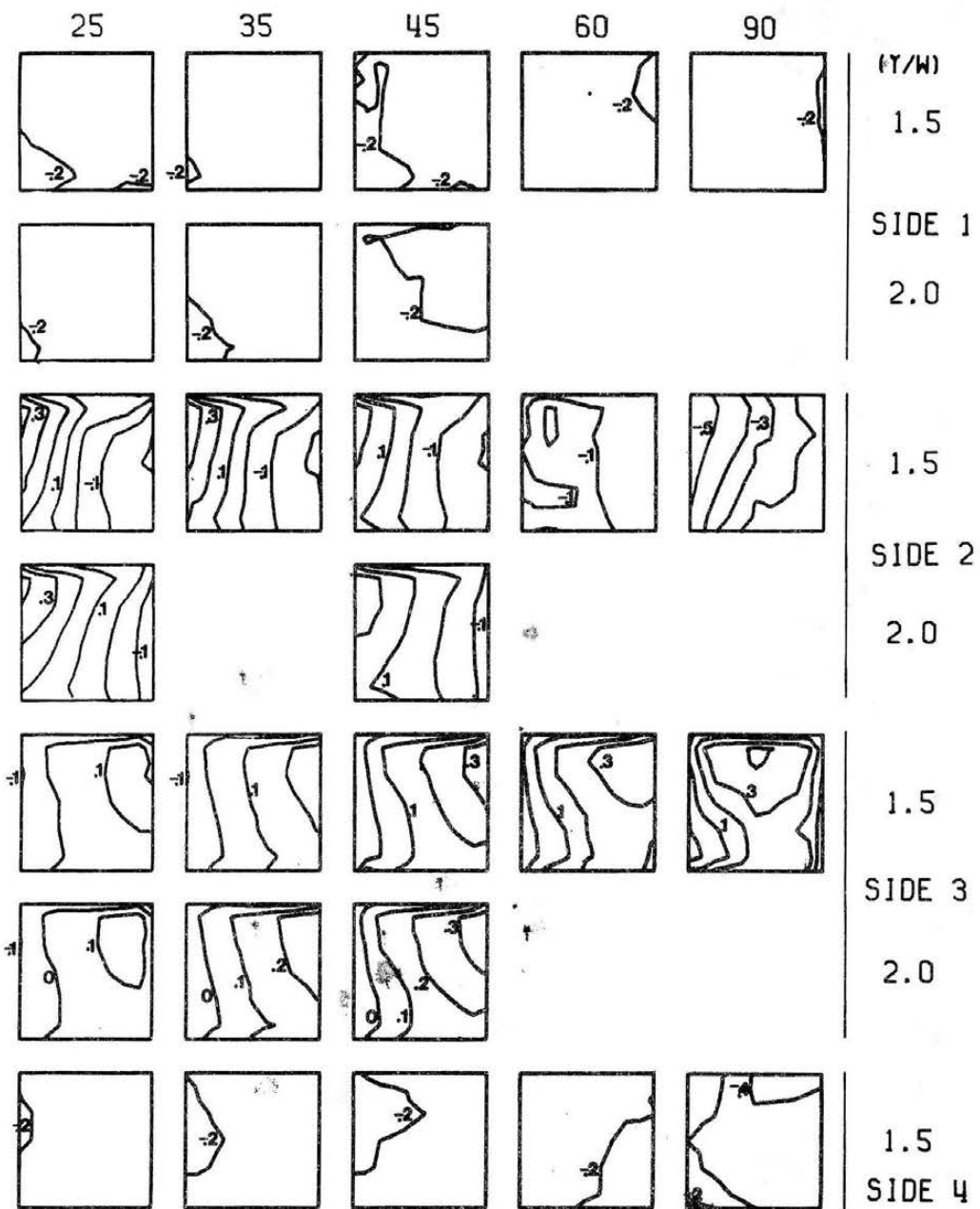


Figure 5.11a (continued)

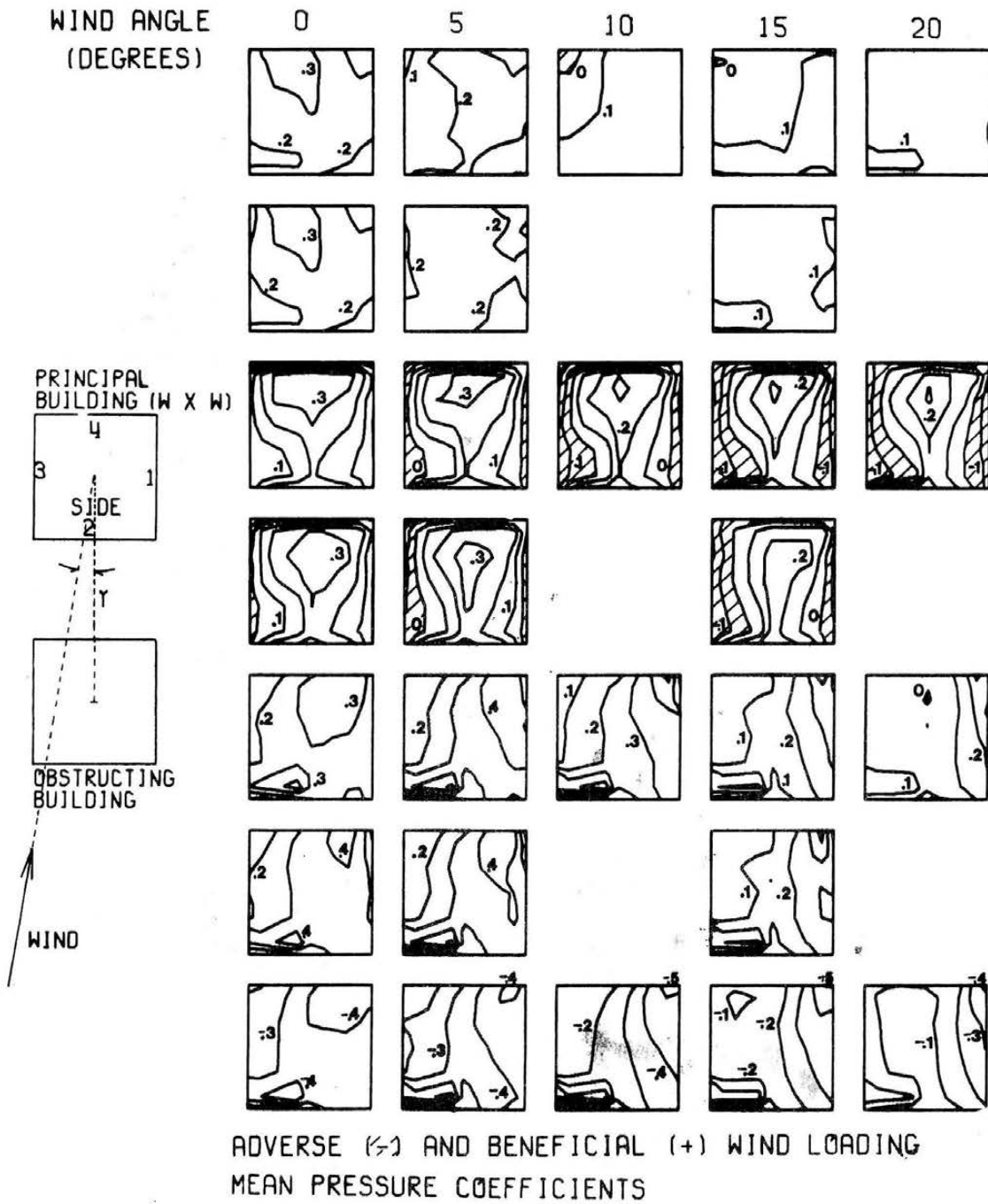


Figure 5.11b. Mean Pressure Effects, Set C

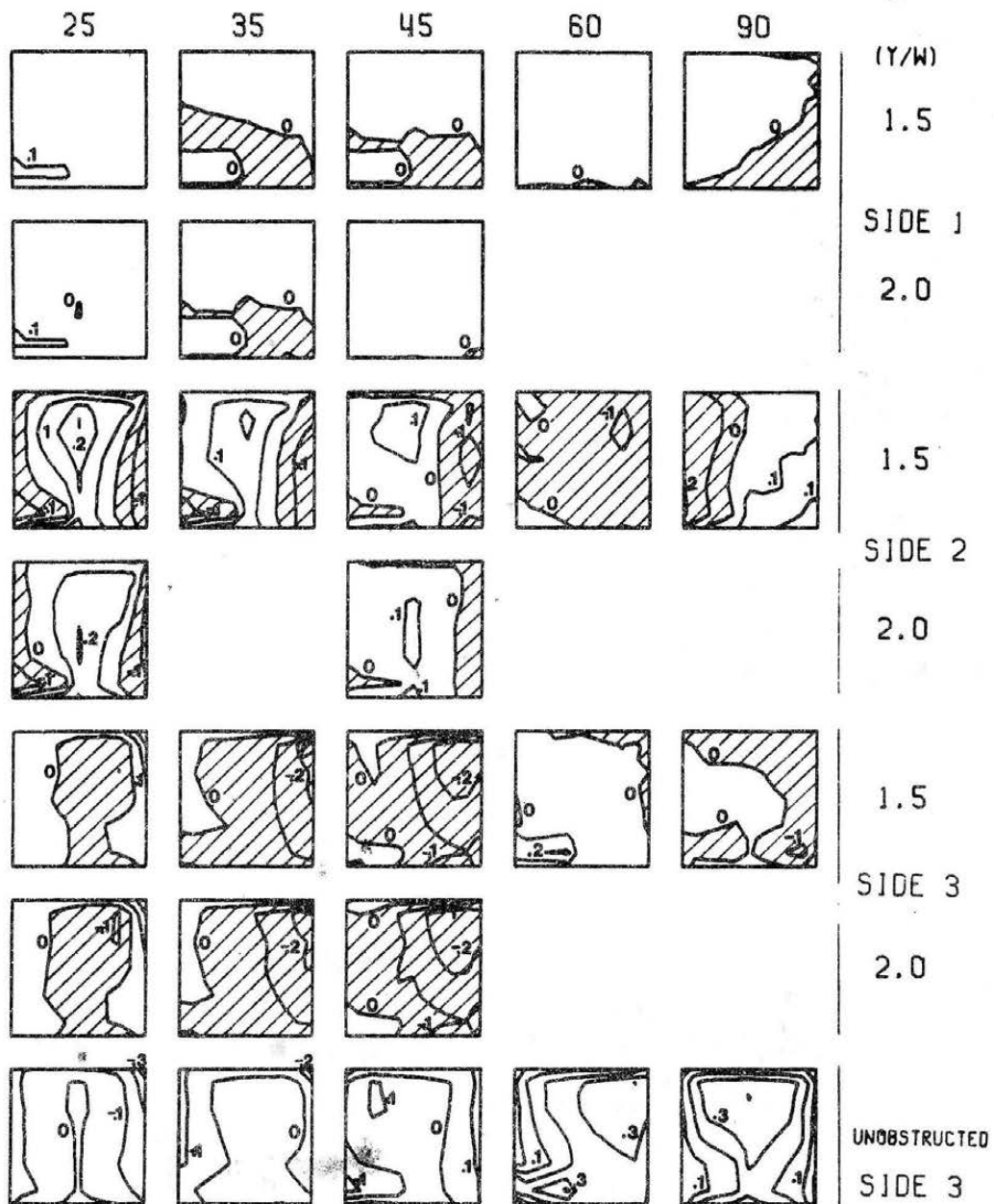
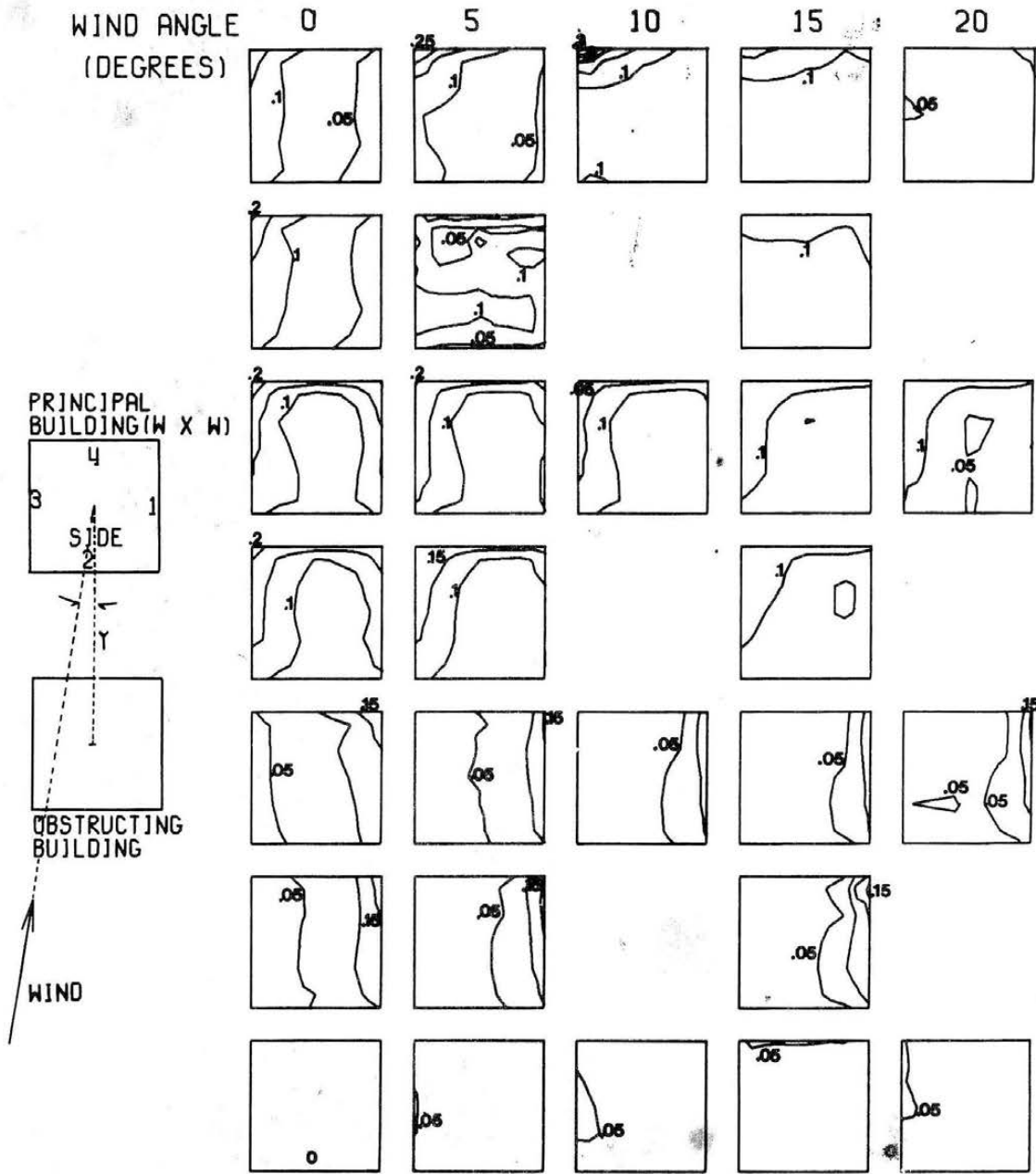


Figure 5.11b (continued)



WIND LOAD INTERACTION ON AN ADJACENT BUILDING  
RMS PRESSURE COEFFICIENTS

Figure 5.11c. RMS Pressure Coefficients, Set C

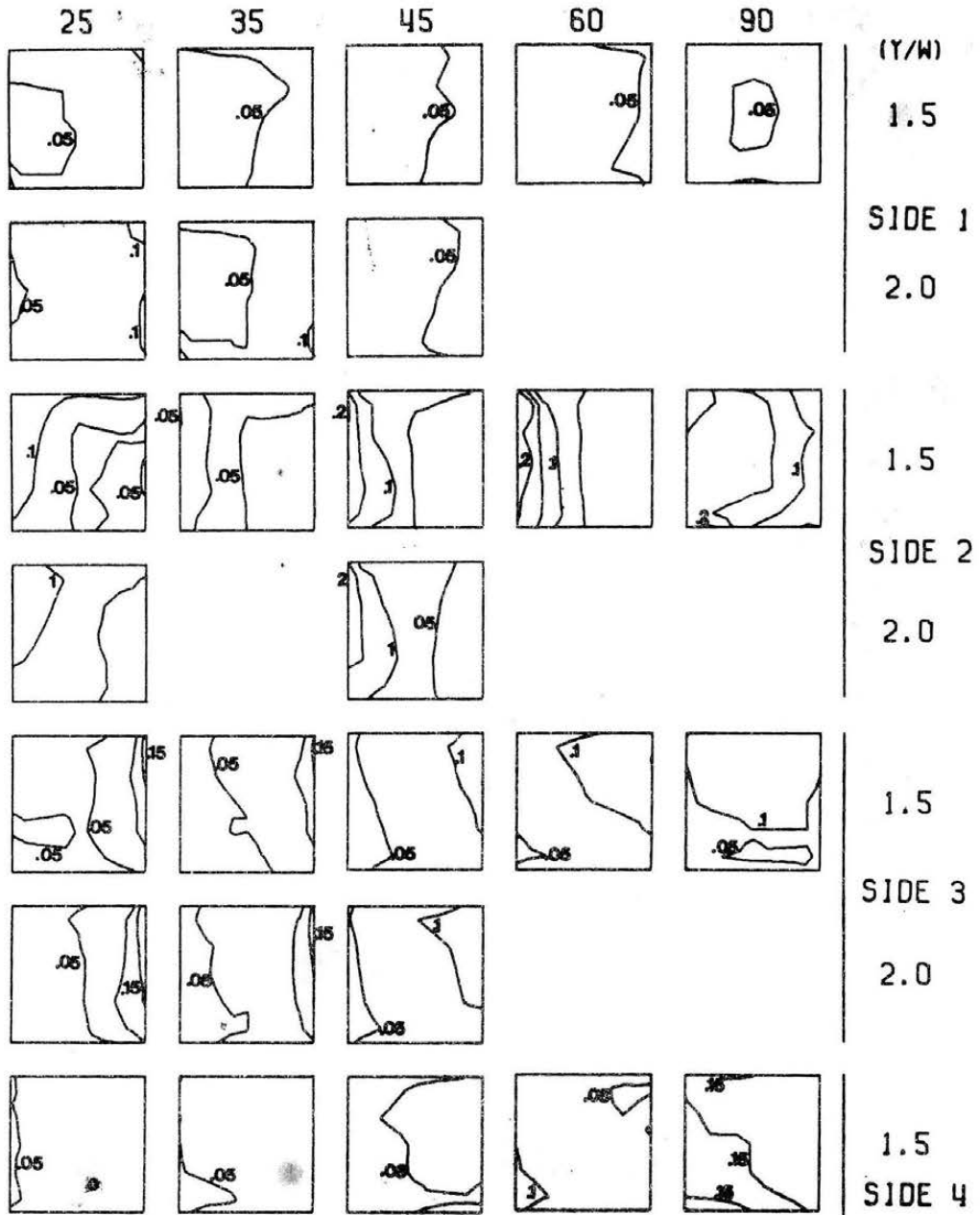


Figure 5.11c (continued)

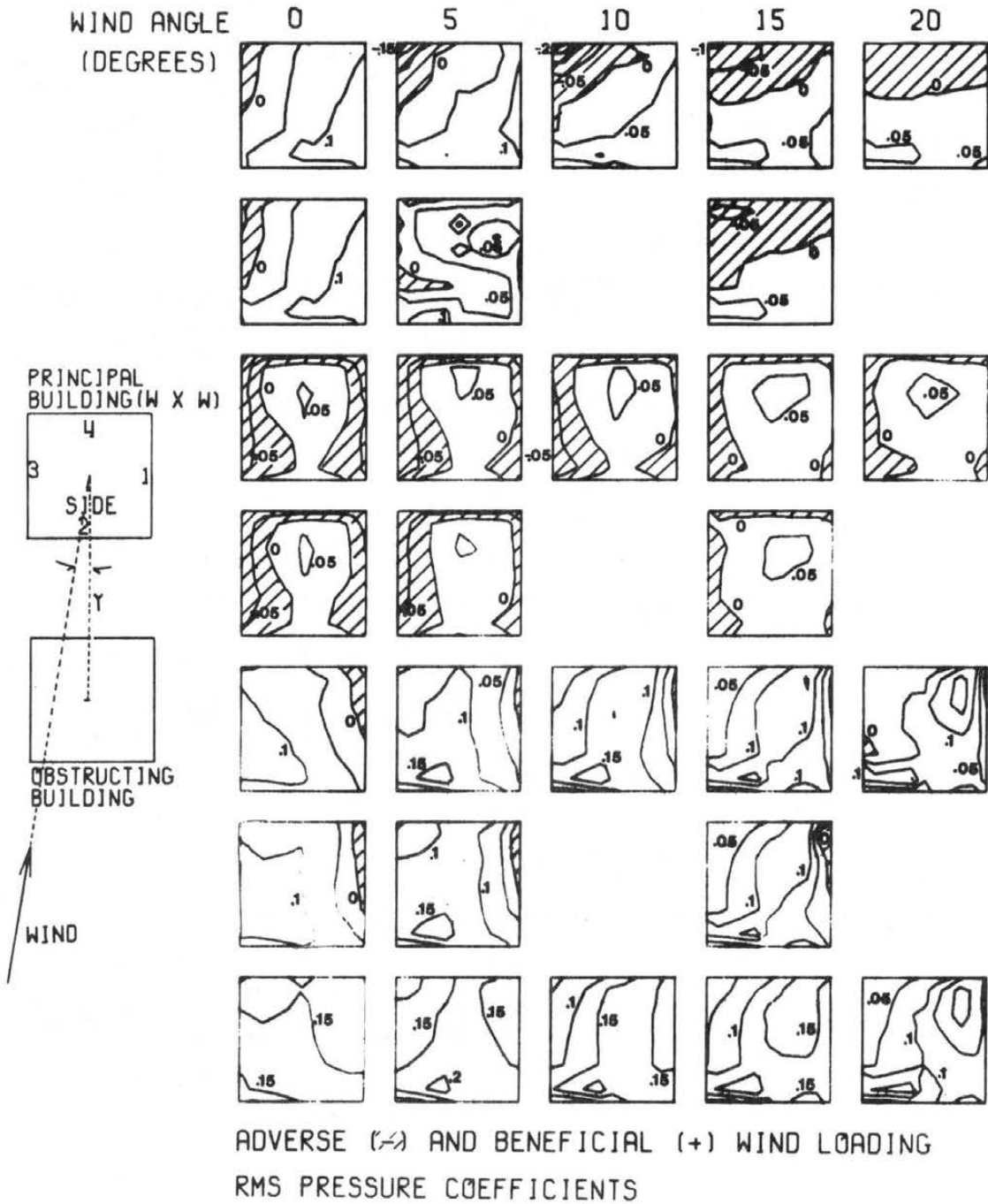


Figure 5.11d. RMS Pressure Effects, Set C

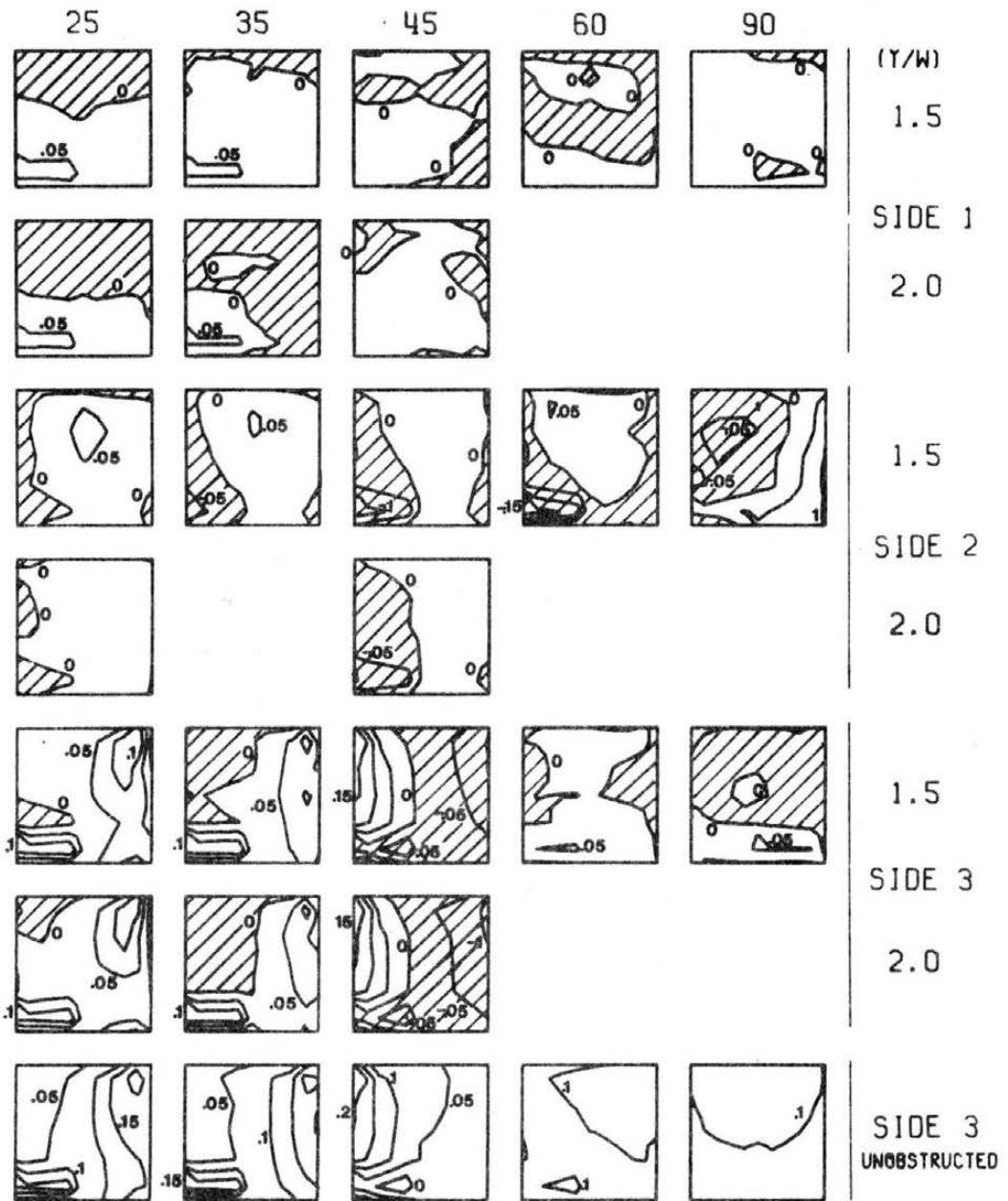


Figure 5.11d (continued)

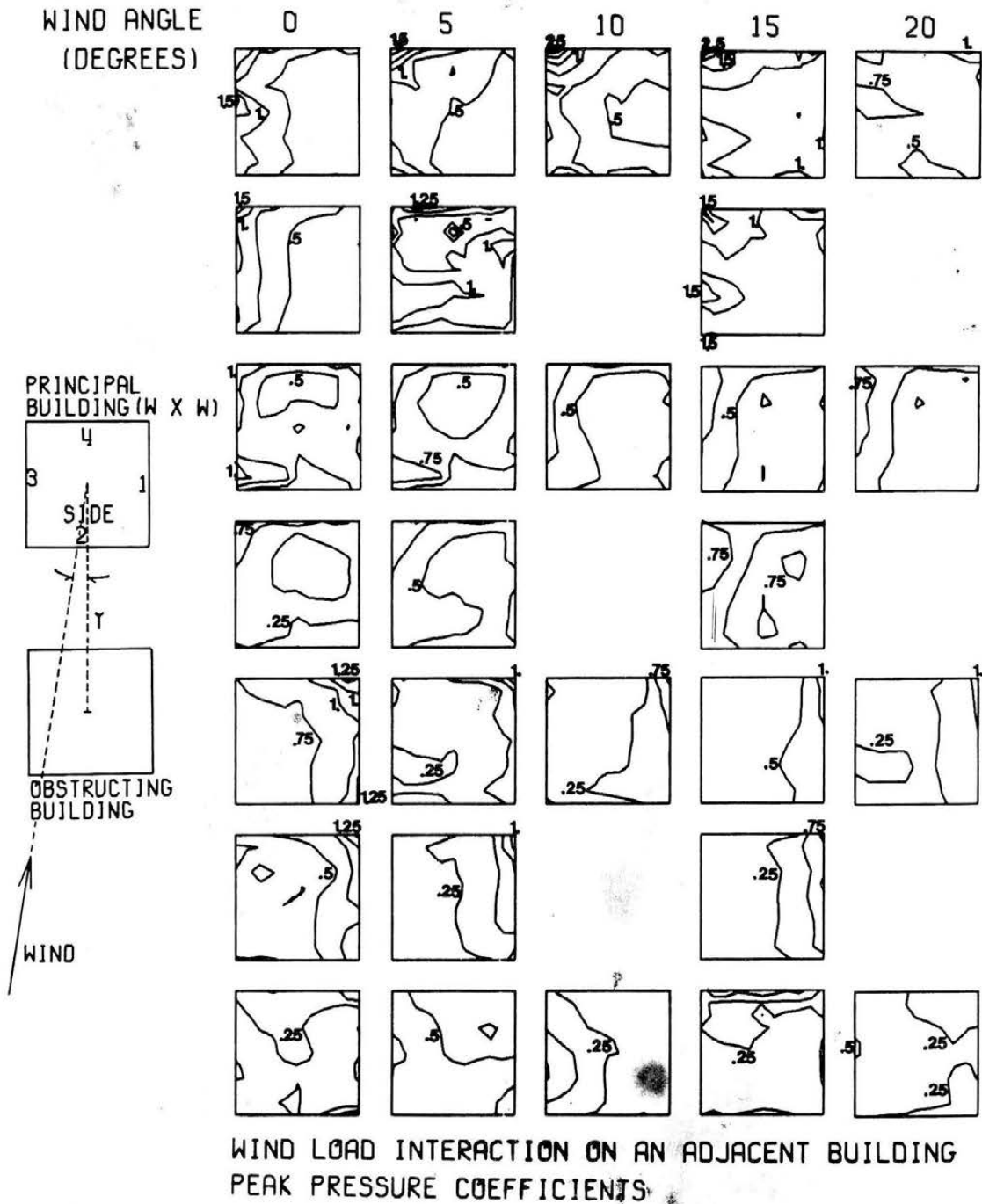


Figure 5.11e. Peak Pressure Coefficients, Set C

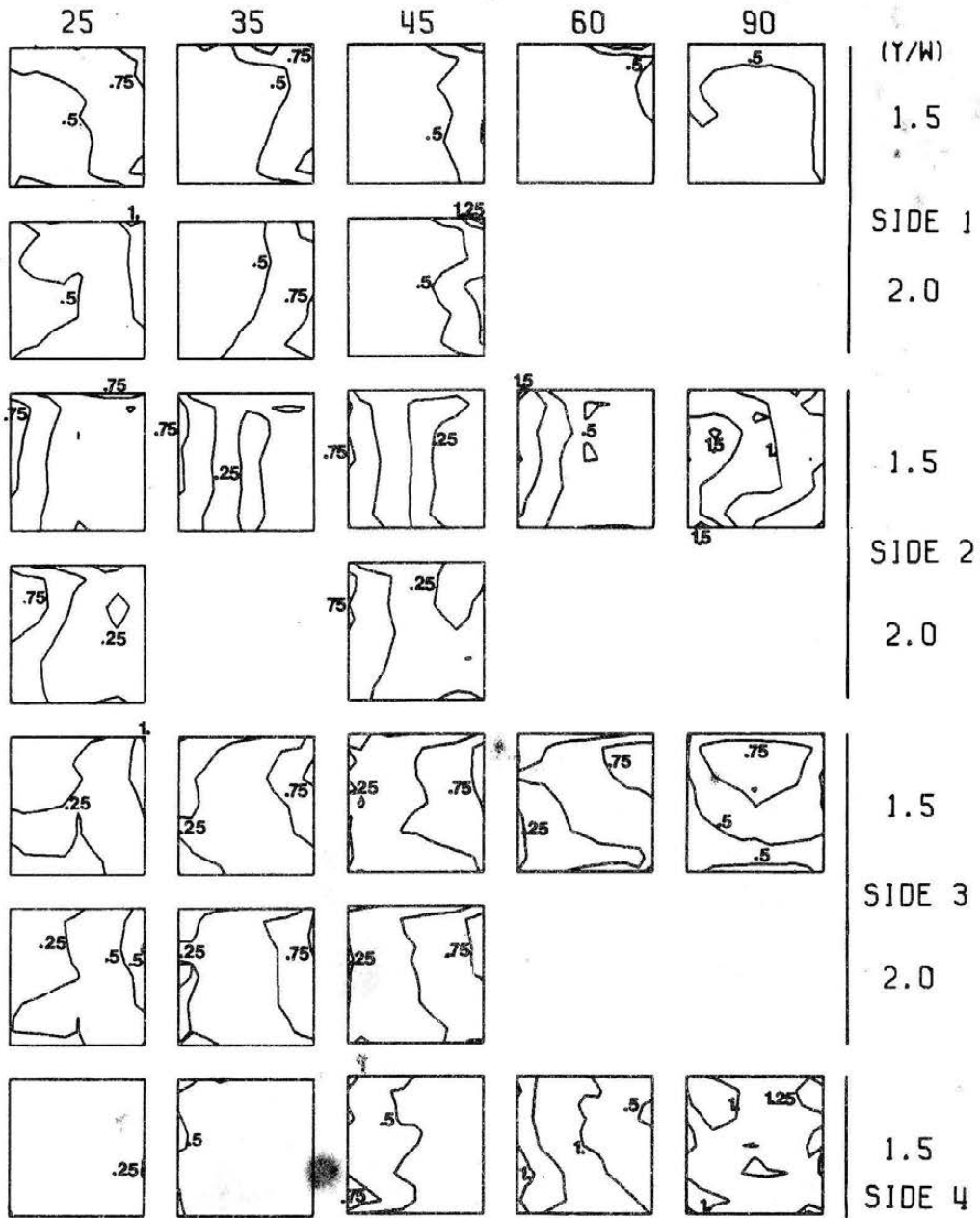


Figure 5.11e (continued)

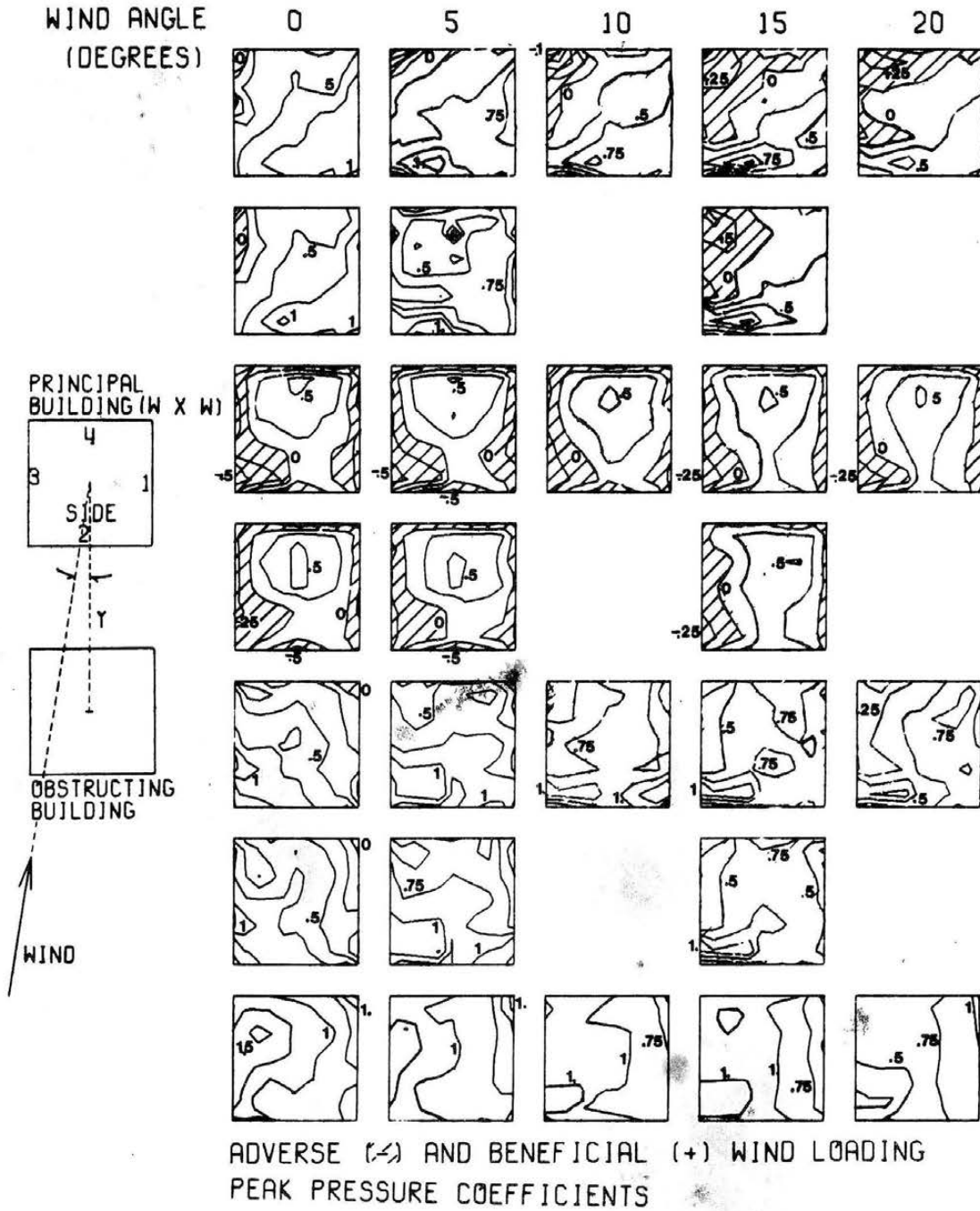


Figure 5.11f. Peak Pressure Effects, Set C

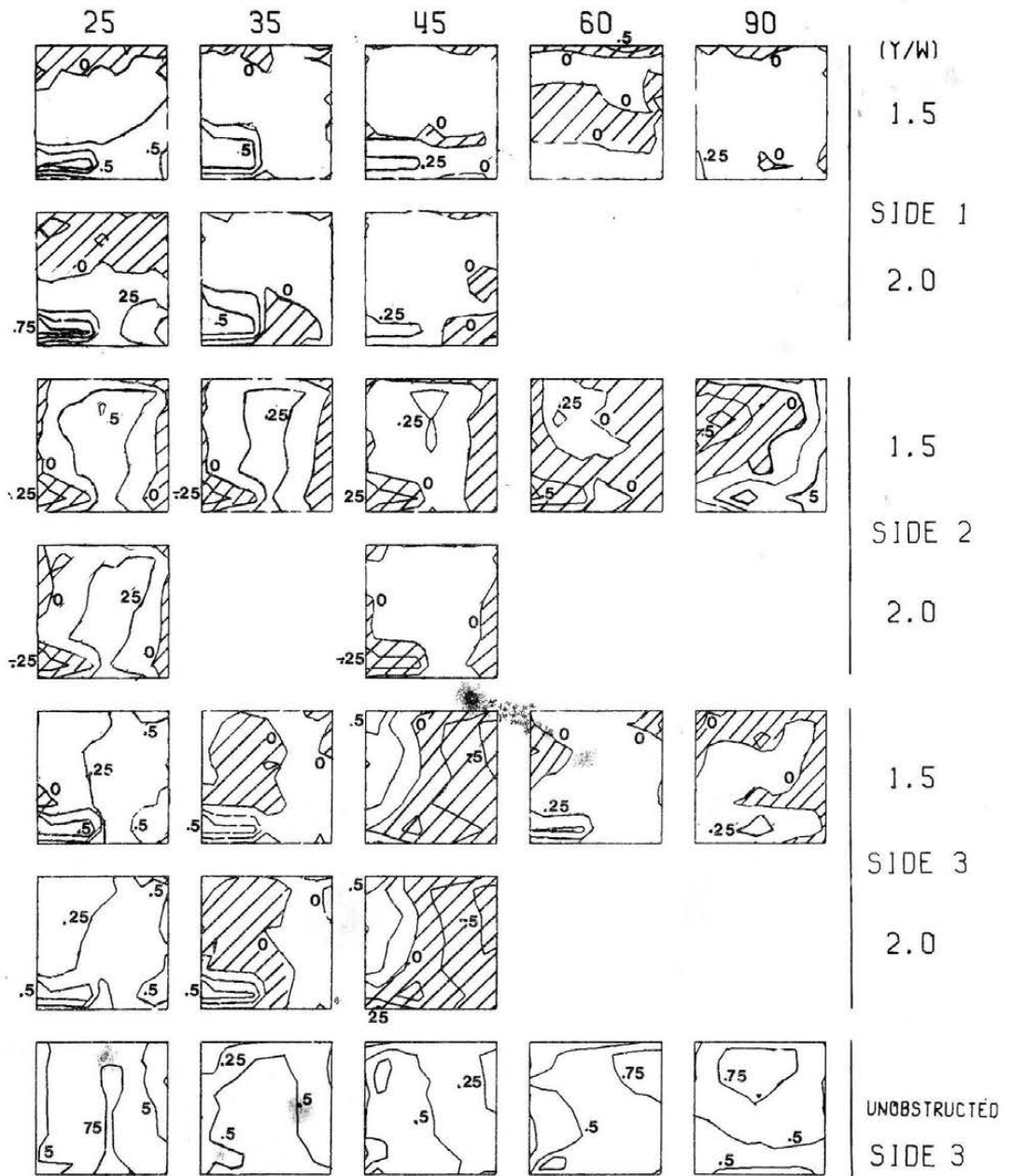


Figure 5.11f (continued)

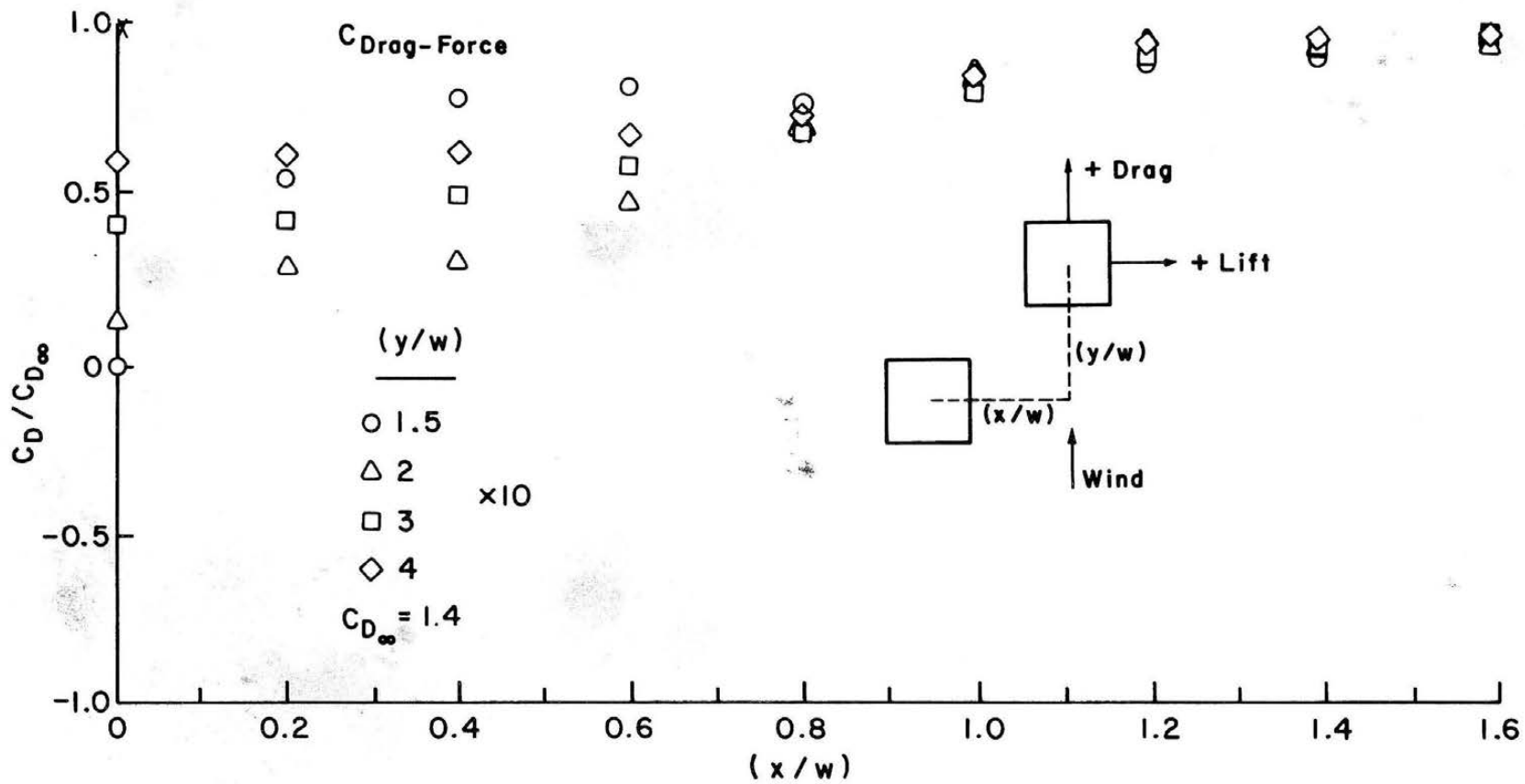


Figure 5.12a.  $C_{\text{DRAG-FORCE}}$ : Set A

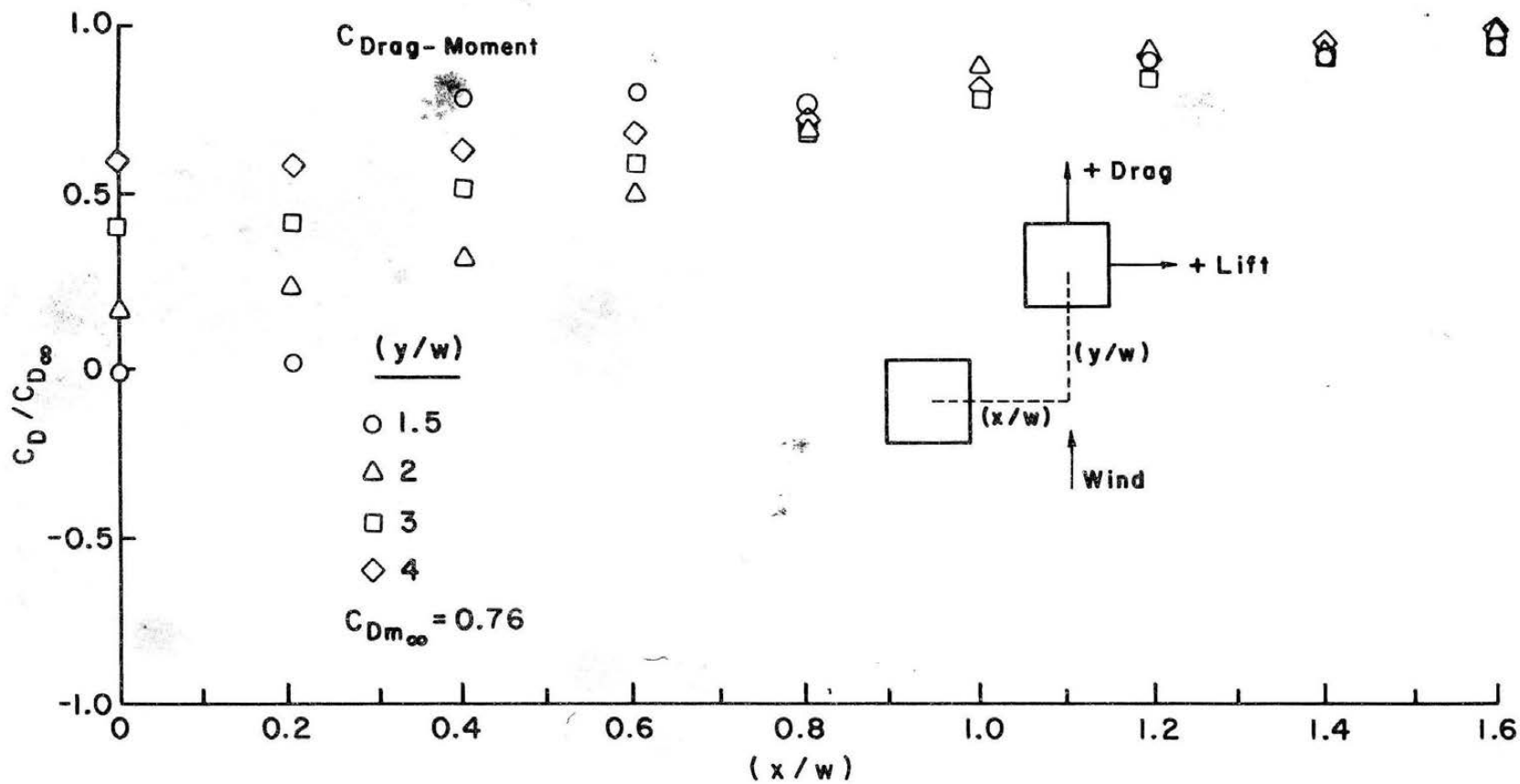


Figure 5.12b.  $C_{\text{DRAG-MOMENT}}$ : Set A

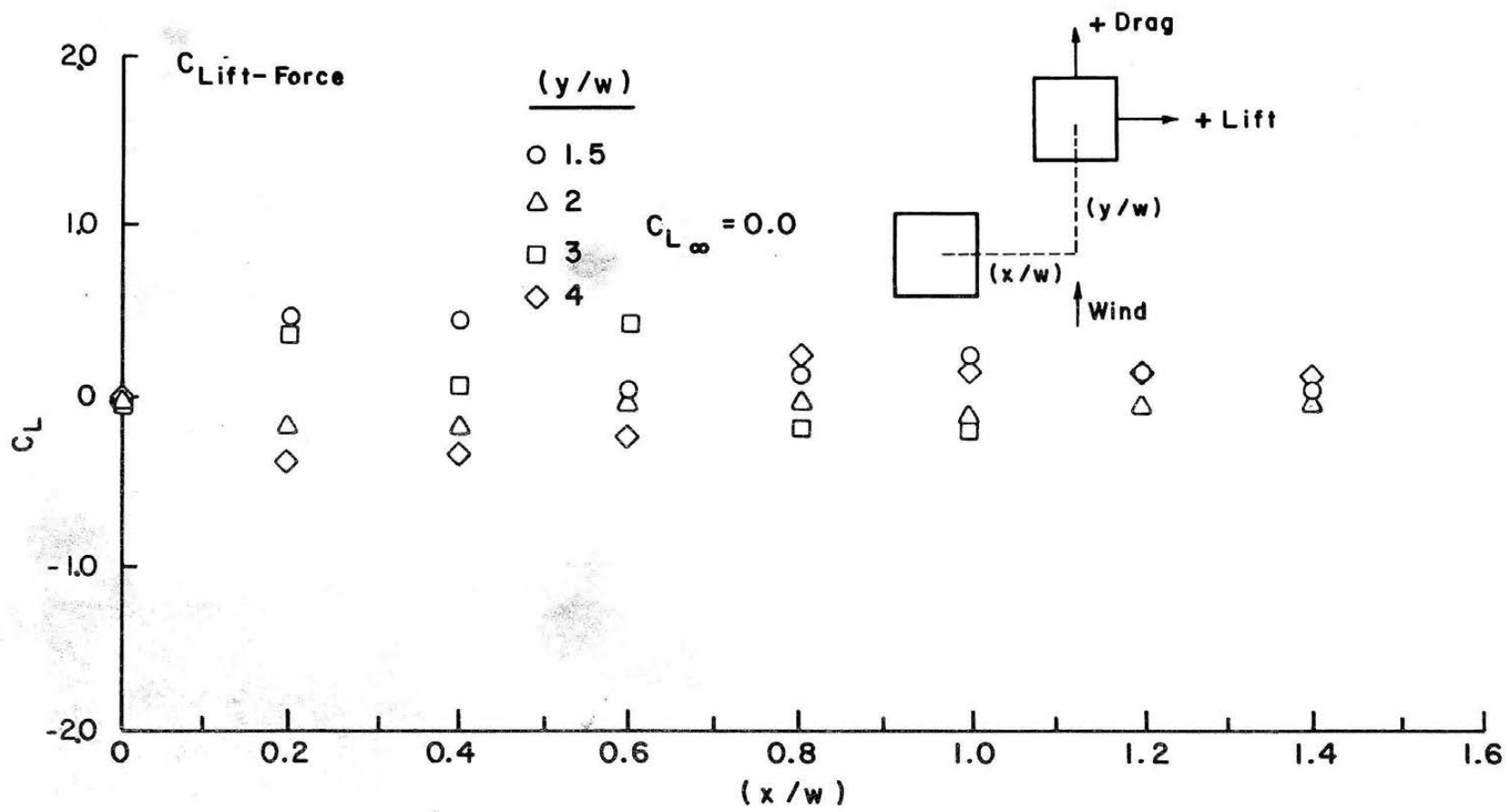


Figure 5.12c.  $C_{LIFT-FORCE}$ : Set A

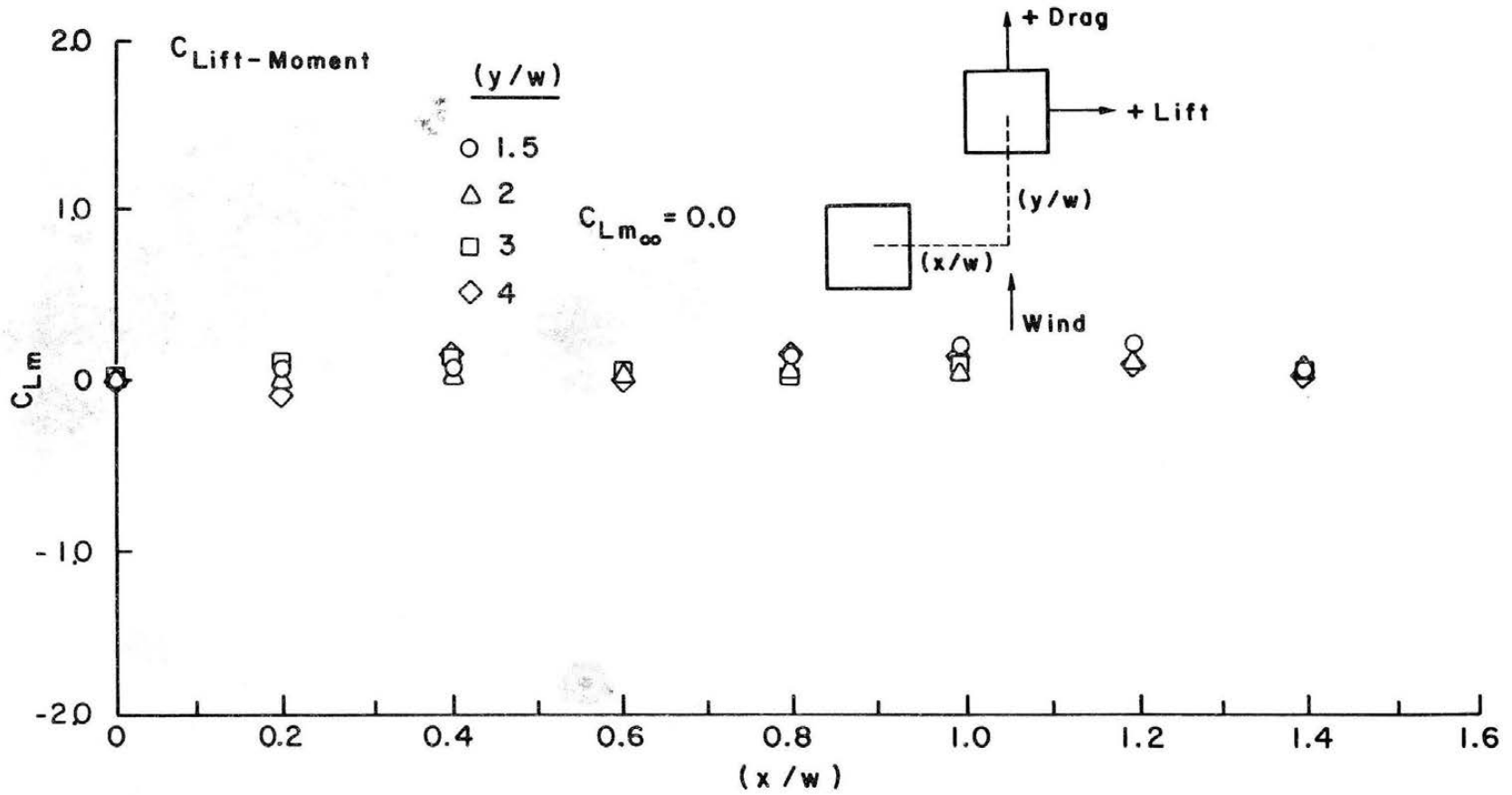


Figure 5.12d.  $C_{LIFT-MOMENT}$ : Set A

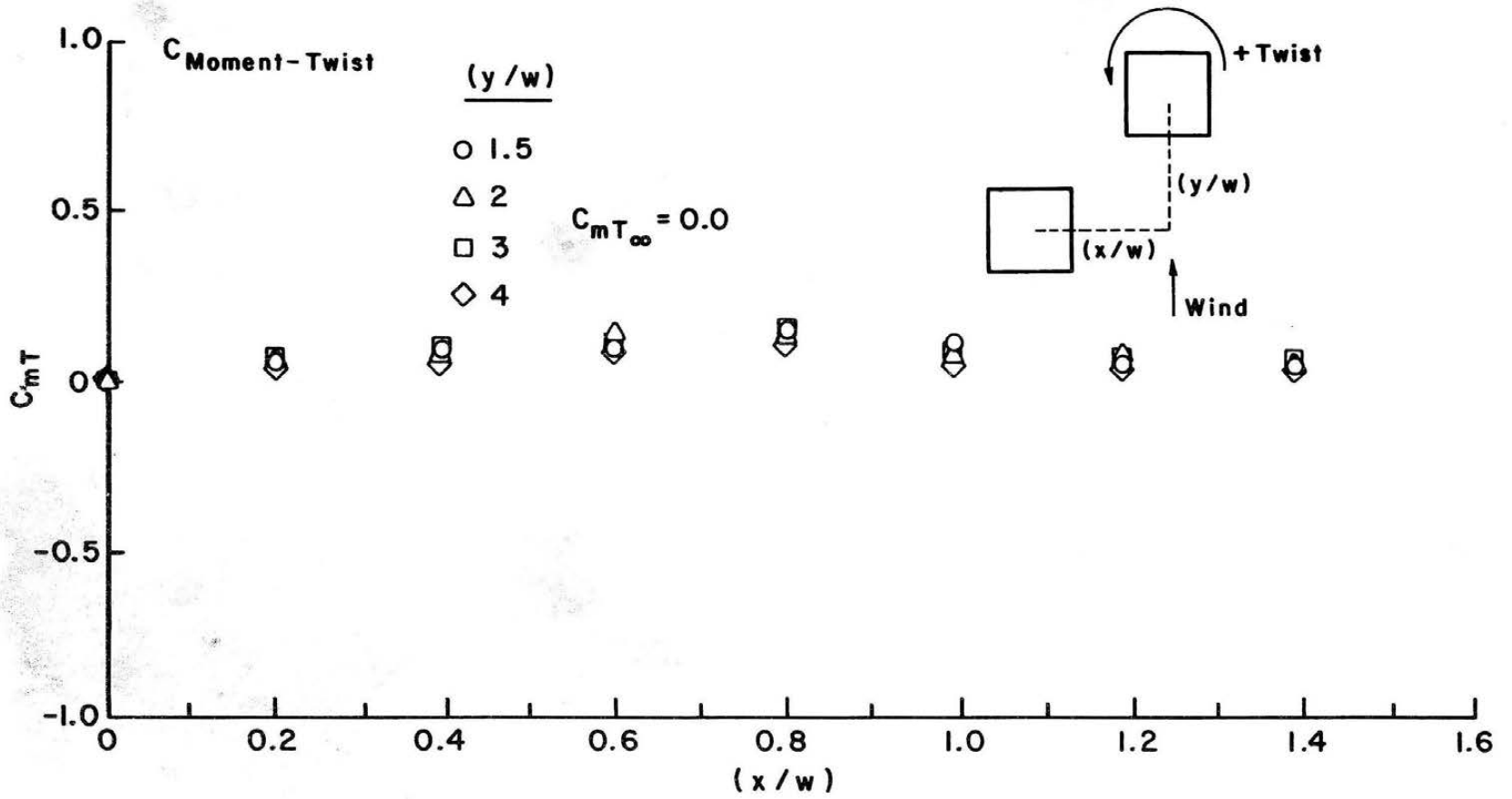


Figure 5.12e.  $C_{\text{MOMENT-TWIST}}$ : Set A

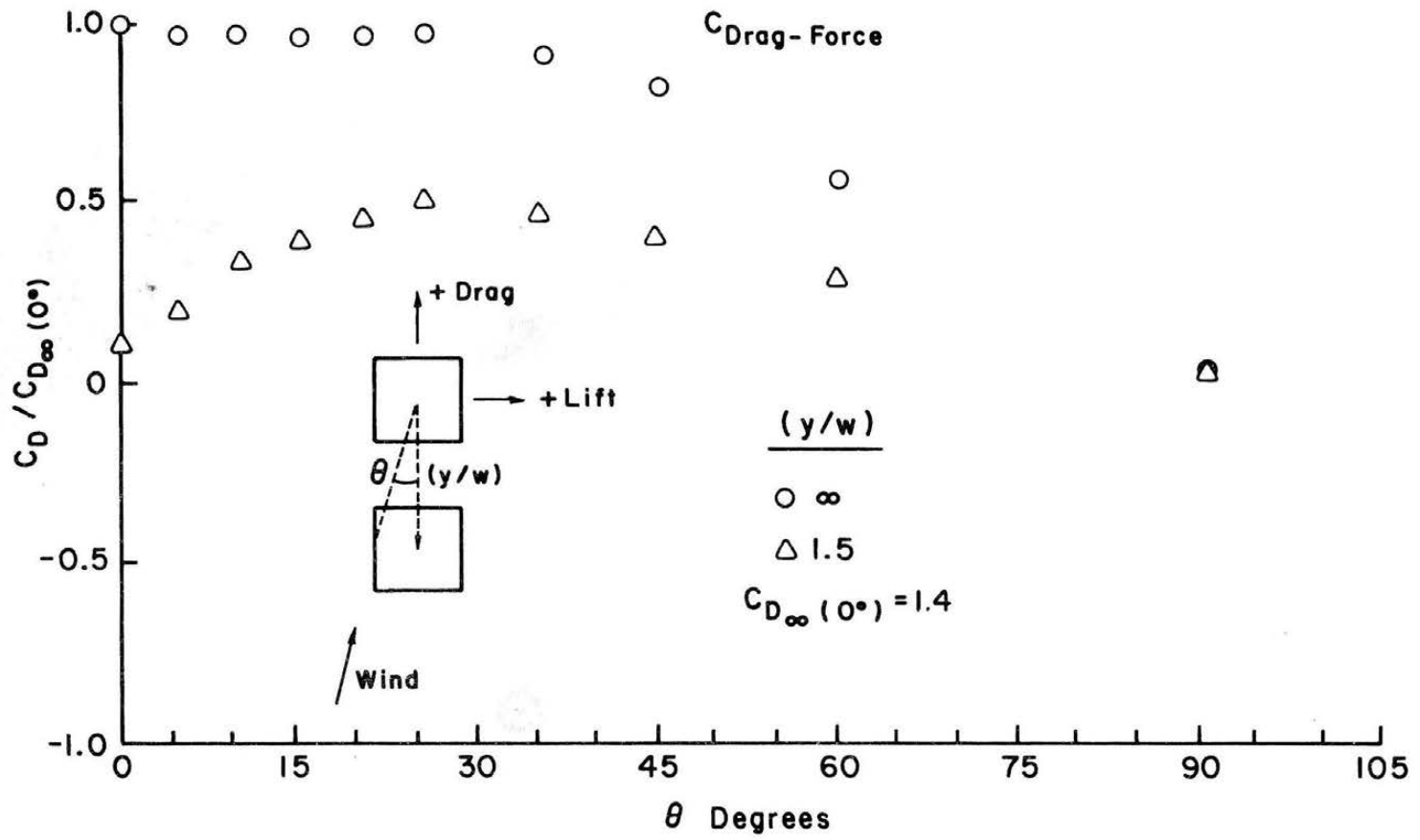


Figure 5.13a.  $C_{D_{\text{DRAG-FORCE}}}$ : Set C

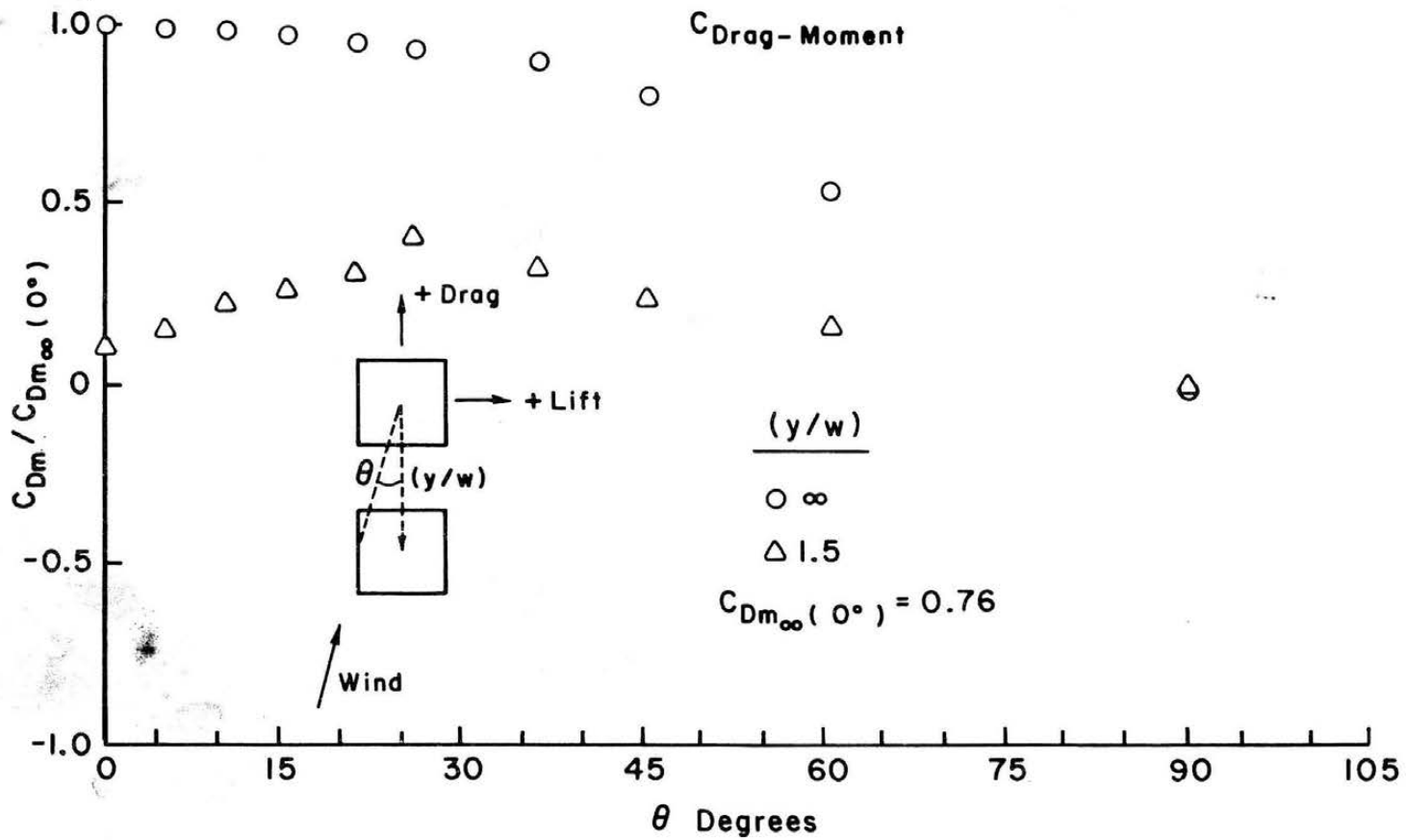


Figure 5.13b.  $C_{\text{DRAG-MOMENT}}$ : Set C

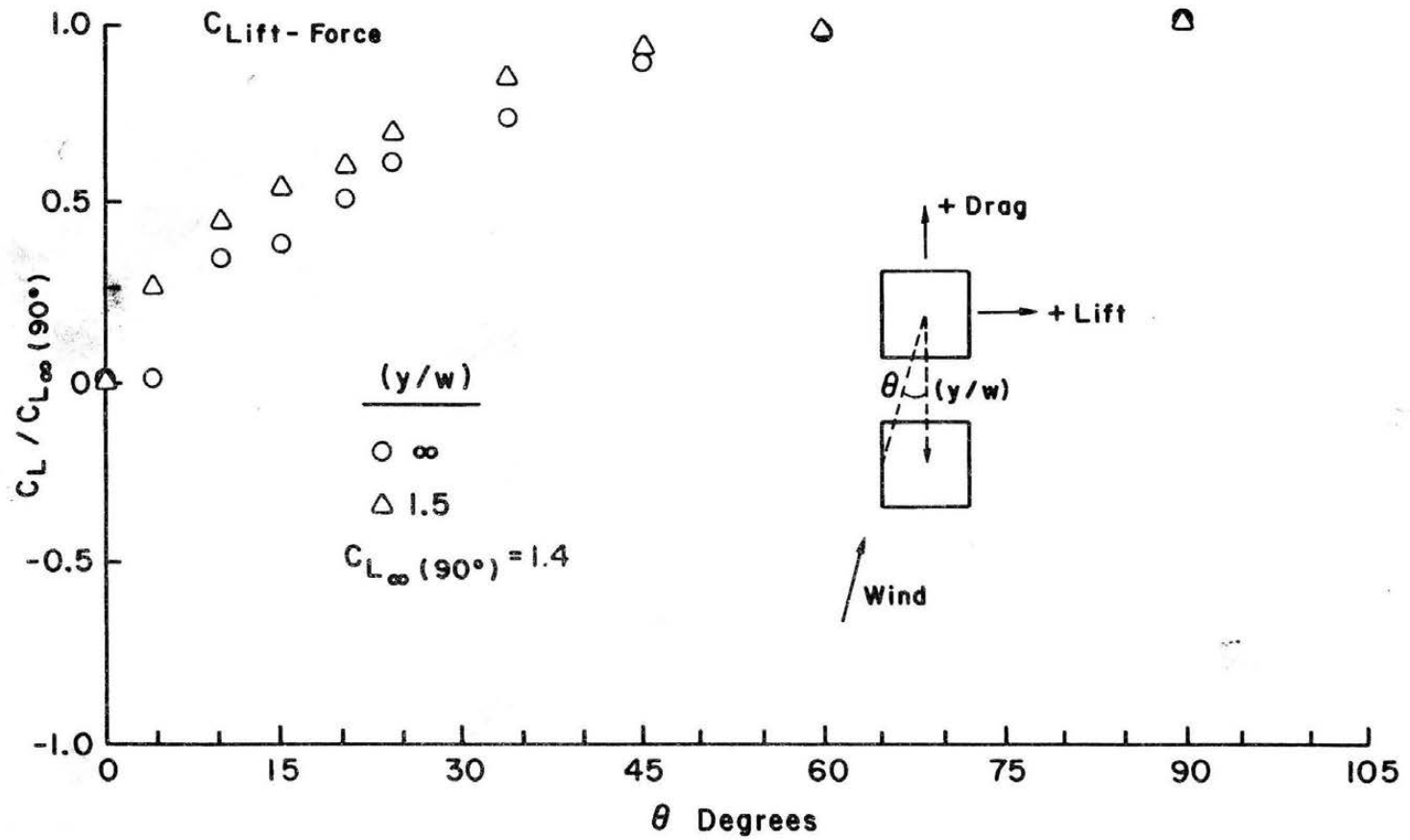


Figure 5.13c.  $C_{LIFT-FORCE}$ : Set C

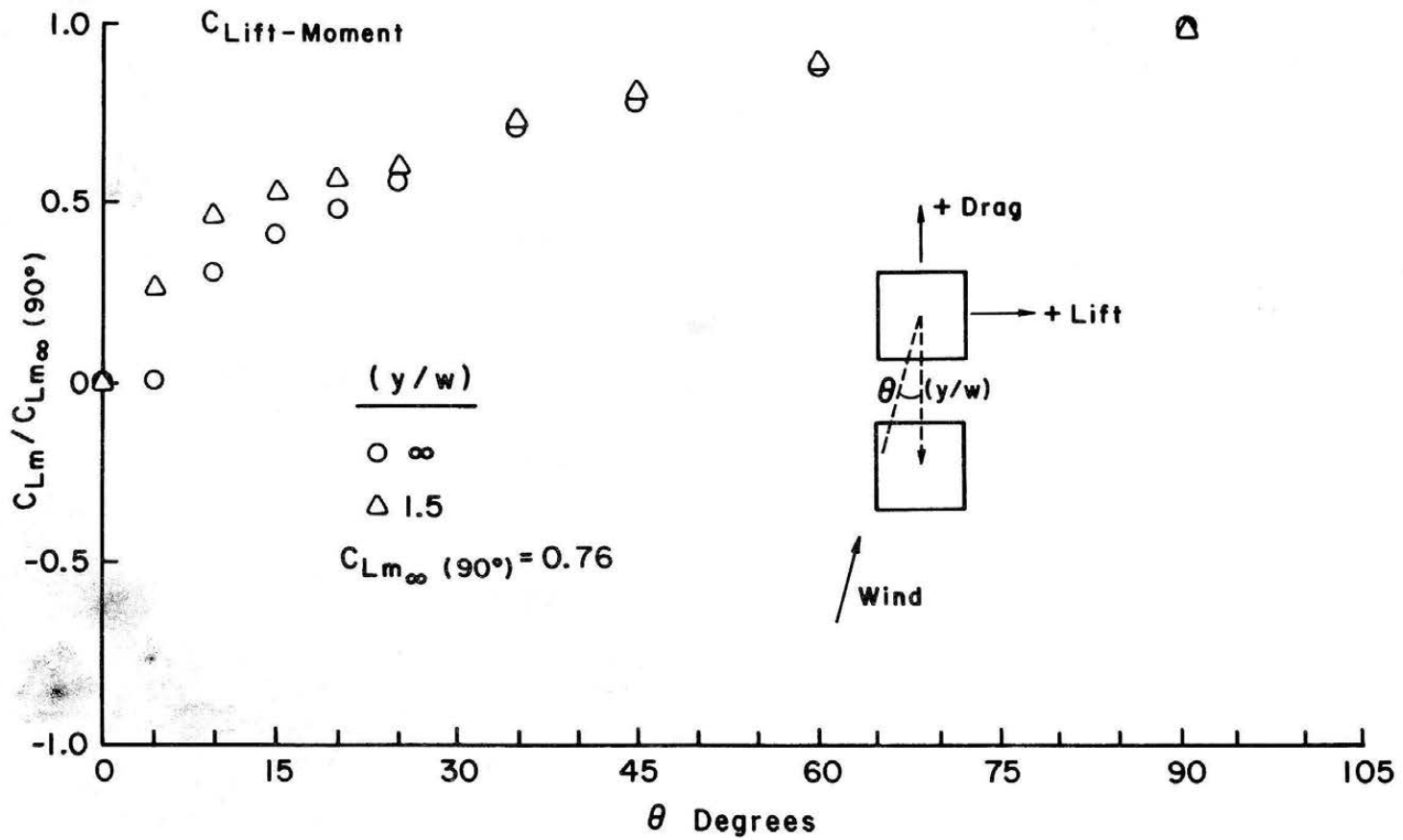


Figure 5.13d.  $C_{LIFT-MOMENT}$ : Set C

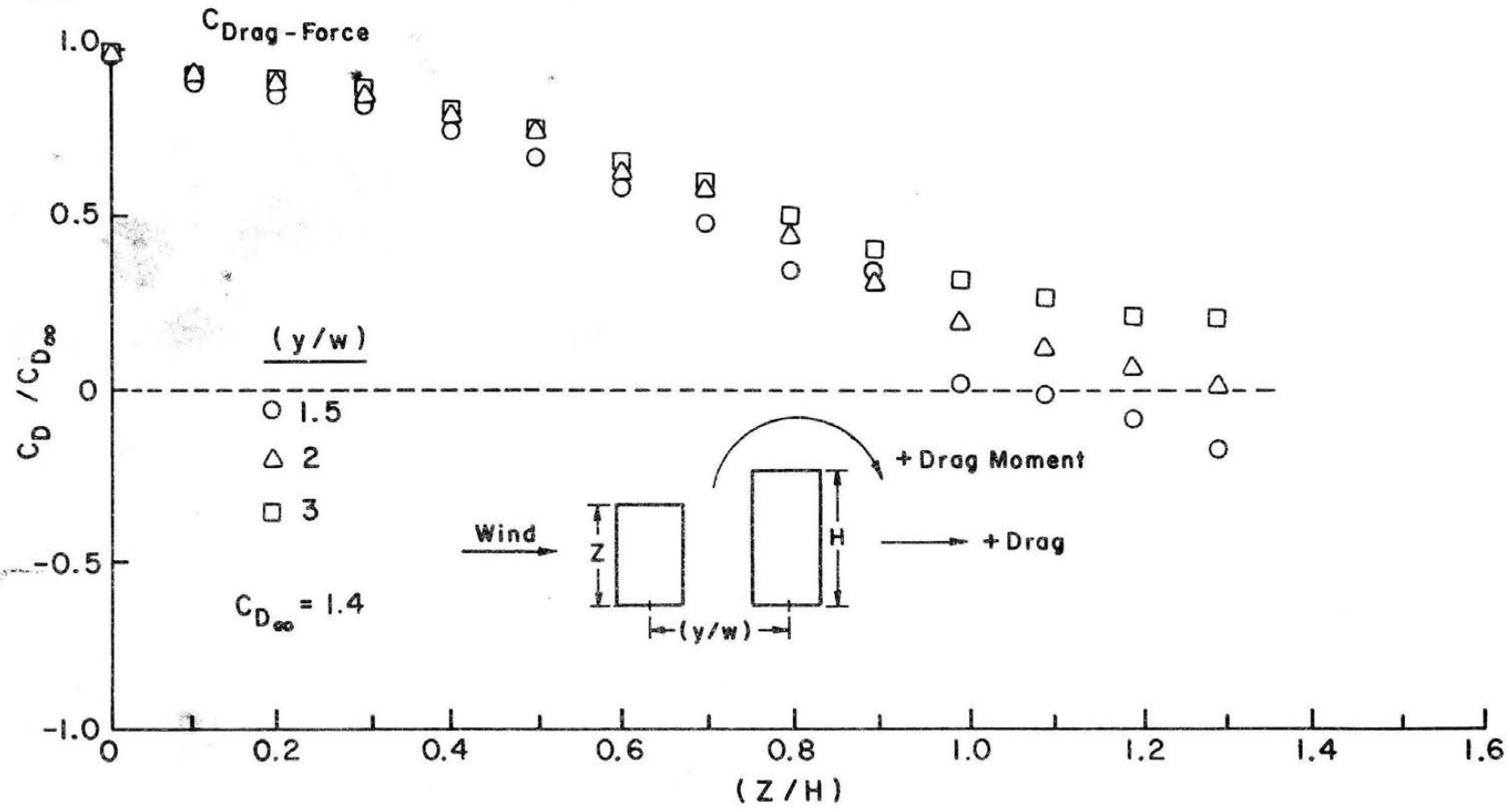


Figure 5.14a.  $C_{D_{\text{DRAG-FORCE}}}$ : Set B

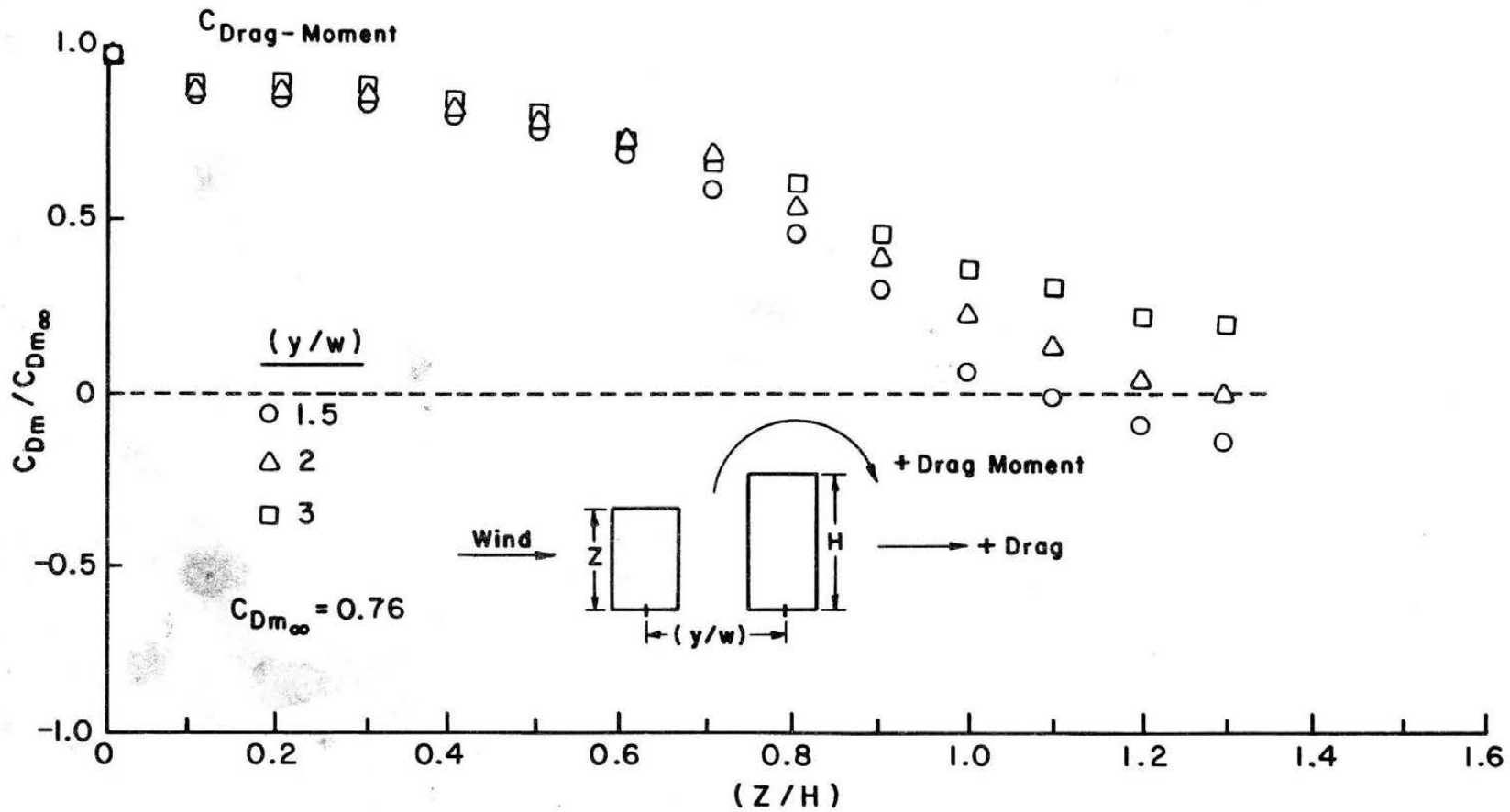


Figure 5.14b.  $C_{DRAG-MOMENT}$ : Set B

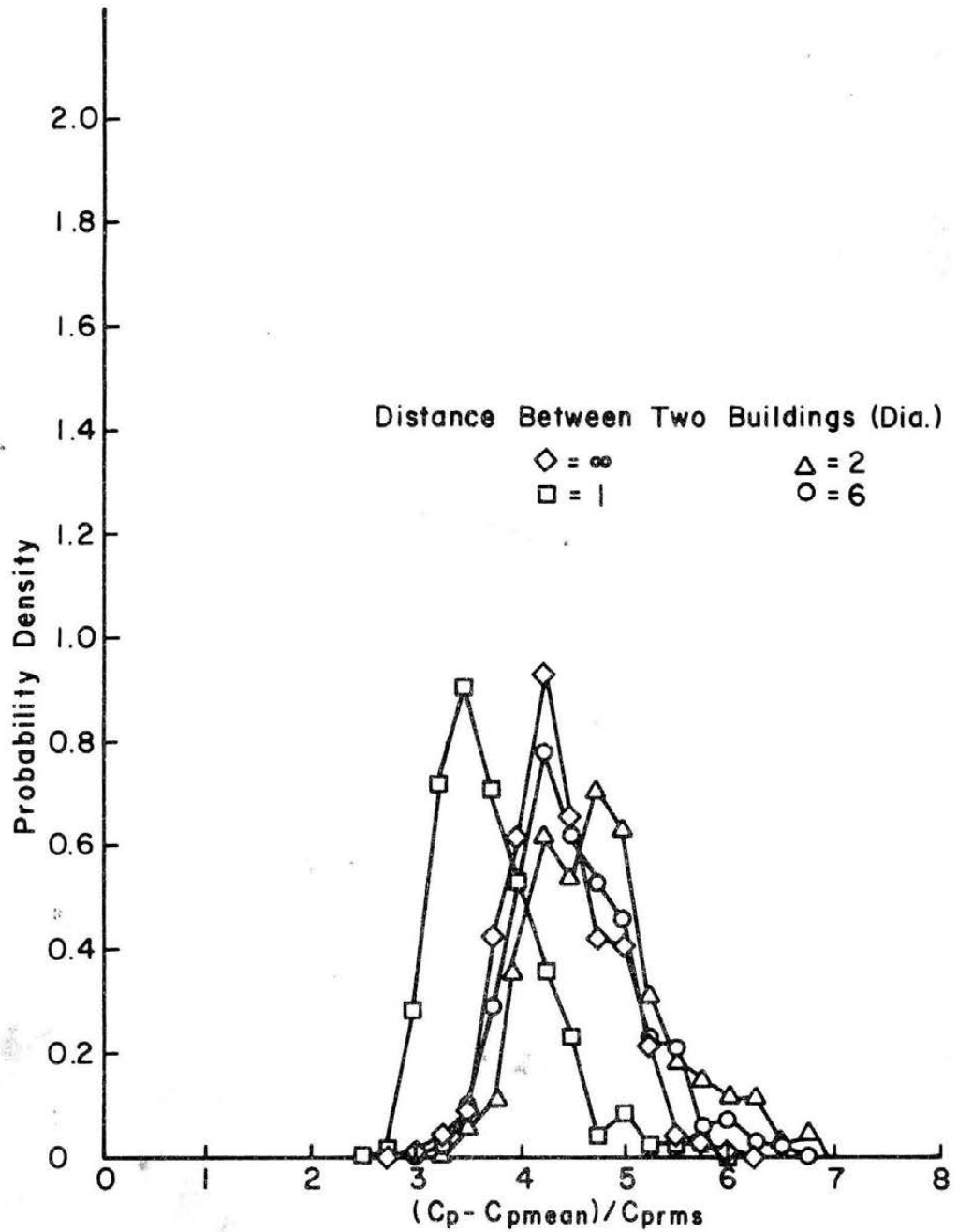


Figure 5.15. Probability Distribution of Peak Positive Pressure--  
Tap 244--350 Points

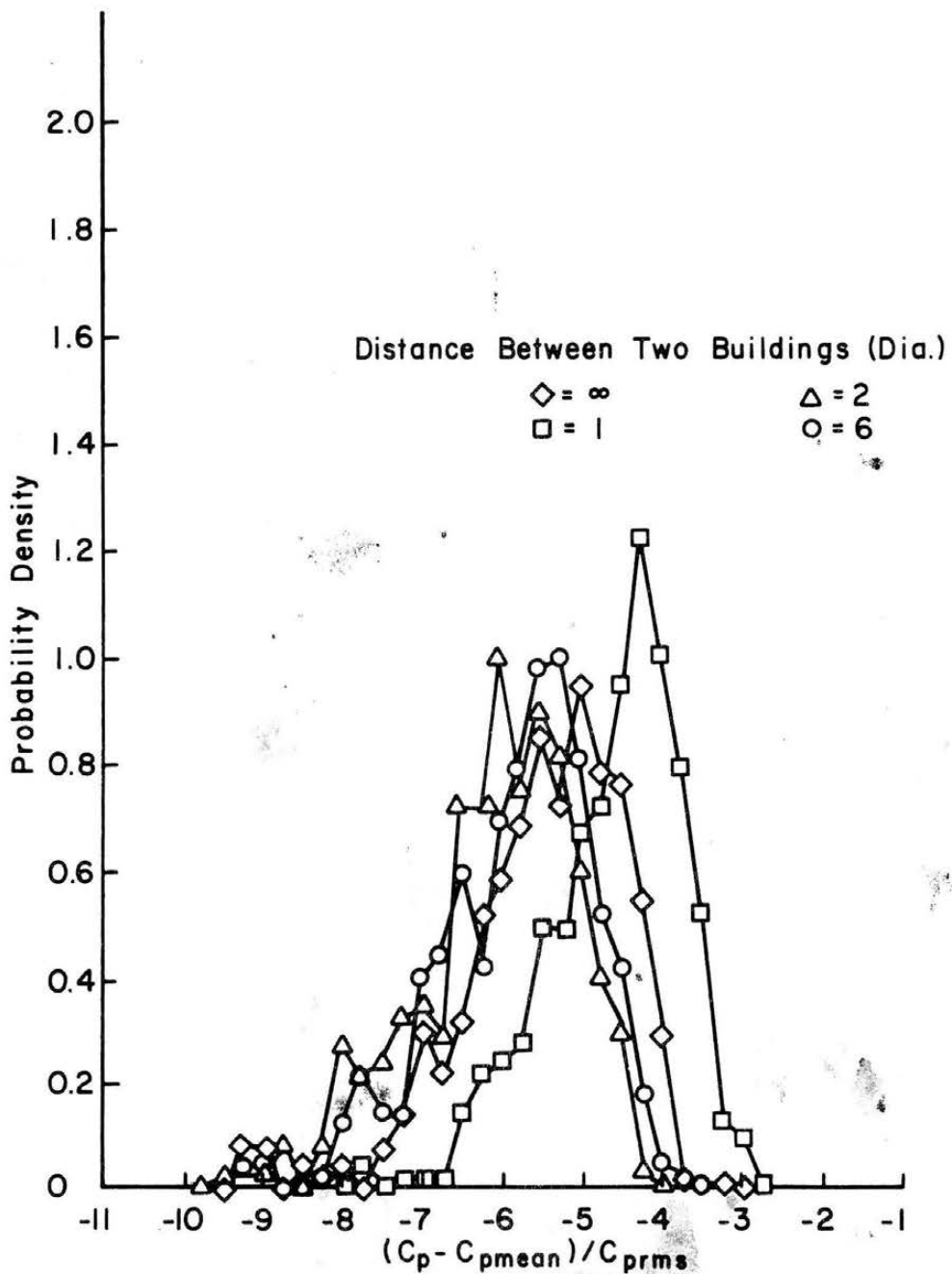


Figure 5.16. Probability Distribution of Peak Negative Pressure-- Tap 141--350 Points

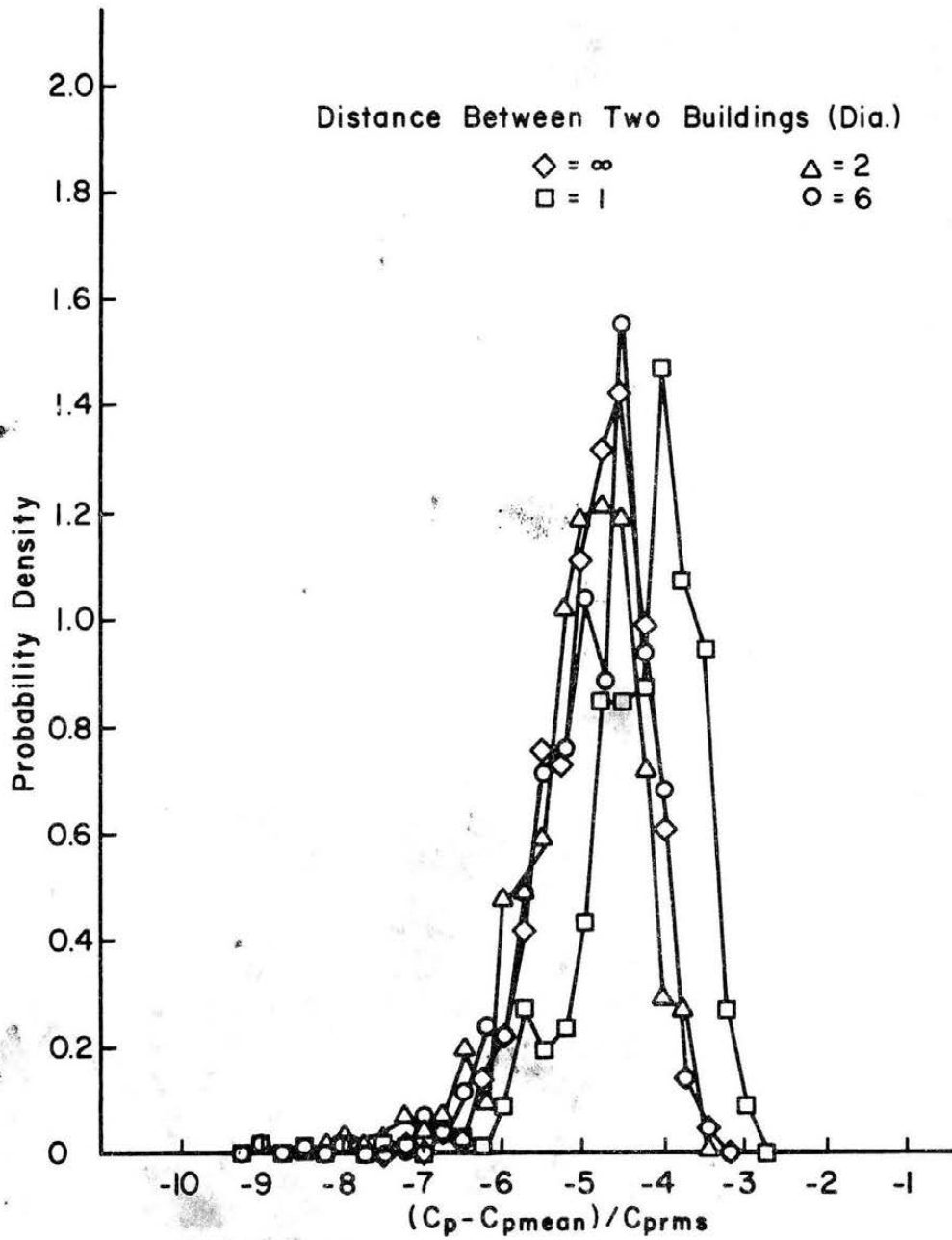


Figure 5.17. Probability Distribution of Peak Negative Pressure, Tap 144

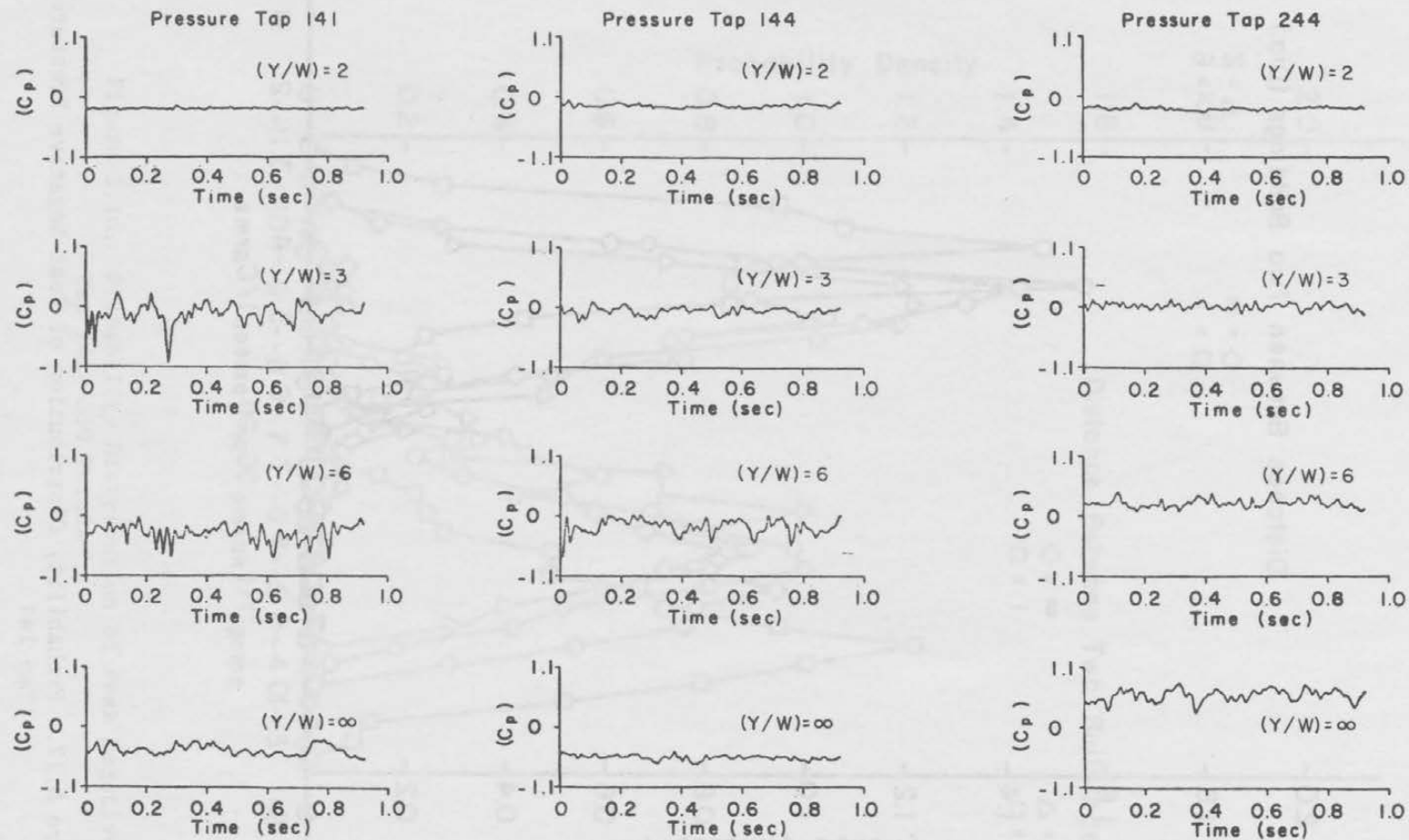


Figure 5.18. One Second Continuous Pressure Samples, Taps 141, 144, 244

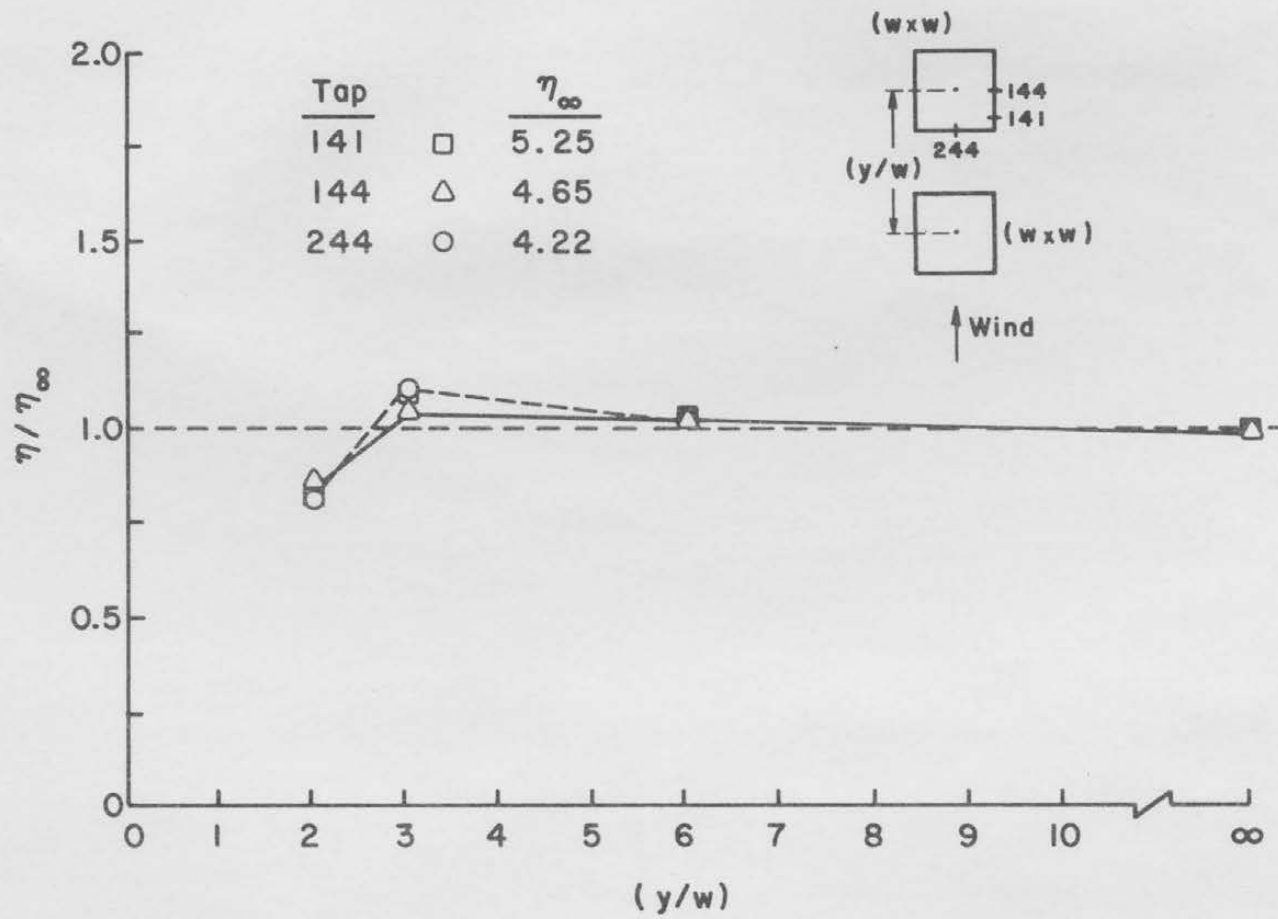


Figure 5.19.  $(\eta/\eta_\infty)$  versus Distance between Buildings